MycoKeys 91: 1–23 (2022)
doi: 10.3897/mycokeys.91.84803
https://mycokeys.pensoft.net

RESEARCH ARTICLE

A peer-reviewed open-access journal
MycoKeys
Launched to accelerate biodiversity research

Morphological and phylogenetic analyses reveal two new species and a new record of *Phyllosticta* (Botryosphaeriales, Phyllostictaceae) from Hainan, China

Zhaoxue Zhang[1,2], Xiaoyong Liu[1], Xiuguo Zhang[1], Zhe Meng[1]

1 *College of Life Sciences, Shandong Normal University, Jinan, 250358, China* **2** *Shandong Provincial Key Laboratory for Biology of Vegetable Diseases and Insect Pests, College of Plant Protection, Shandong Agricultural University, Taian, 271018, China*

Corresponding author: Zhe Meng (zmeng@sdnu.edu.cn)

Academic editor: Huzefa Raja | Received 3 April 2022 | Accepted 12 June 2022 | Published 4 July 2022

Citation: Zhang Z, Liu X, Zhang X, Meng Z (2022) Morphological and phylogenetic analyses reveal two new species and a new record of *Phyllosticta* (Botryosphaeriales, Phyllostictaceae) from Hainan, China. MycoKeys 91: 1–23. https://doi.org/10.3897/mycokeys.91.84803

Abstract

The fungal genus *Phyllosticta* has been reported from all around the world and accommodates numerous pathogenic and endophytic species isolated from a wide range of plant hosts. Based on multilocus phylogenies from a combined dataset of genes encoding internal transcribed spacer (ITS), large subunit of ribosomal RNA (LSU rDNA), translation elongation factor 1 alpha (TEF1α), actin (ACT) and glycerol-3-phosphate dehydrogenase (GPDH), in conjunction with morphological characteristics, we describe two new species *P. oblongifoliae* **sp. nov.** and *P. pterospermi* **sp. nov.**, as well as a new Chinese record *P. capitalensis*. Their similarity and dissimilarity to morphologically-allied and phylogenetically-related species are also annotated and discussed.

Keywords

multigene phylogeny, new species, taxonomy

Introduction

Phyllosticta Pers. was introduced by Persoon (1818) and *P. convallariae* Pers. was designated as the type species (Donk 1968). Since *Phyllosticta* is distinct from other genera in that family, Seaver (1922) treated it in the family Phyllostictaceae Fr. of the or-

der Phyllostictales. Nevertheless, *Phyllosticta* was accommodated in the family Botryosphaeriaceae Theiss. & Syd. (in Botryosphaeriales C.L. Schoch et al.) in several major studies (e.g. Crous et al. 2006; Schoch et al. 2006; Liu et al. 2012). However, the phylogenetic analyses by Wikee et al. (2013a) allocated *Phyllosticta* in a clade sister to Botryosphaeriaceae. As a result, the genus is currently accepted in the family Phyllostictaceae, in the order Botryosphaeriales.

A total of 3,213 names are documented for *Phyllosticta* in the Index Fungorum (accessed on 31 March 2022) (Hongsanan et al. 2020; Wijayawardene et al. 2020). However, many of these names have been synonymised (van der Aa and Vanev 2002). Currently, 1499 species are accepted in the genus (Bánki et al. 2022). The majority of the *Phyllosticta* species are known to infect a broad range of hosts and cause plant diseases, such as leaf and fruit spots (Wikee et al. 2013a; Zhou et al. 2015; Lin et al. 2017). Van der Aa (1973) revised this genus and established his own morphological criteria, i.e. aseptate pycnidia and hyaline conidia that are usually covered by a mucoid layer and bear a single apical appendage. According to these criteria, van der Aa and Vanev (2002) re-classified *Phyllosticta* and accepted 190 species. Other species were recombined into *Asteromella* Pass. & Thüm., *Diaporthe* Fuckel, *Guignardia* Viala & Ravaz, *Leptodothiorella* Höhn. and *Phoma* Sacc. A rare tropical species from the Brazilian Cerrado, *P. xylopiae-sericeae* Furlan. & Dianese, although morphologically well documented (Furlanetto and Dianese 1998), remains to be molecularly characterised. Recently, DNA sequencing of orthologous genes has greatly improved our knowledge of fungal phylogeny. Since van der Aa and Vanev (2002), several studies have shown that phylogenetic analyses can help delineate species in *Phyllosticta* (Baayen et al. 2002; Wulandari et al. 2009; Glienke et al. 2011; Wikee et al. 2011). More recently, new species of *Phyllosticta* have been increasingly described, based on a combination of molecular data and morphological features (Su and Cai 2012; Wang et al. 2012, 2013; Wong et al. 2012; Zhang et al. 2012, 2013; Wikee et al. 2013a; Wulandari et al. 2013; Crous et al. 2014, 2015, 2016, 2017, 2018, 2019, 2021; Zhou et al. 2015; Guarnaccia et al. 2017; Lin et al. 2017; Hattori et al. 2020; Norphanphoun et al. 2020). Norphanphoun et al. (2020) assembled all species denoted as *Phyllosticta* in GenBank, analysing a comprehensive dataset of five loci and consequently proposing six species complexes, viz. *P. capitalensis* species complex, *P. concentrica* species complex, *P. cruenta* species complex, *P. owaniana* species complex, *P. rhodorae* species complex and *P. vaccinii* species complex.

Hainan Province (18°10'–20°10'N, 108°37'–111°05'E) is an island in southern China, with an annual mean temperature of 22–27 °C and an annual precipitation of 1000–2600 mm. Bawangling National Forest Park is located in the southwest of Hainan, with a typical tropical rainforest climate. Fungi associated with leaf spots were collected from *Rhapis excelsa*, *Garcinia oblongifolia* and *Pterospermum heterophyllum*. Using sequences of five gene loci, which include the internal transcribed spacer of ribosomal RNA (ITS rDNA), large subunit of ribosomal RNA (LSU rDNA), translation elongation factor 1 alpha (TEF1α), actin (ACT) and glycerol-3-phosphate dehydrogenase (GPDH). We also incorporated their morphology and

then identified these fungi as three species of the *P. capitalensis* species complex, including two new species, as well as a species new to China, based on morphology and phylogenetic analyses.

Materials and methods

Isolation and morphological studies

Leaves of *Rhapis excelsa*, *Garcinia oblongifolia* and *Pterospermum heterophyllum* showing necrotic spots were collected at the Bawangling National Forest Park, Hainan Province, China. Isolates were obtained using a tissue isolation method (Jiang et al. 2021). Fragments (5 × 5 mm) were taken from the margin of leaf lesions, surface-sterilised by immersing consecutively in 75% ethanol solution for 1 min, 5% sodium hypochlorite solution for 30 s and then rinsed in sterile distilled water for 1 min (Jiang et al. 2021). The sterilised fragments were dried with sterilised paper towels and placed on potato dextrose agar (PDA: 200 g potato, 20 g dextrose, 20 g agar, 1000 ml distilled water, pH 7.0) and incubated at 25 °C for 2–4 days. Subsequently, portions of agar with fungal mycelium from the periphery of the colonies were transferred into new PDA plates and photographed on the 7th and 15th days by a digital camera (Canon Powershot G7X). An inoculum of the purified colonies was placed on 2% malt extract agar (MEA:20 g malt extract, 20 g soy peptone, 15 g agar, 1000 ml distilled water, pH 5.6) and incubated under continuous near-UV light at room temperature to promote sporulation (Braun et al. 2018). Micromorphological characters were observed using an Olympus SZX10 stereomicroscope and Olympus BX53 microscope, all fitted with an Olympus DP80 high-definition colour digital camera to photodocument fungal structures. All fungal strains were stored in 10% sterilised glycerine at 4 °C for further studies. Structural measurements were taken using the Digimizer software (https://www.digimizer.com/), with thirty measurements taken for each character. The holotype specimens were deposited in the Herbarium of Plant Pathology, Shandong Agricultural University (HSAUP). Ex-holotype living cultures were deposited in the Shandong Agricultural University Culture Collection (SAUCC). Taxonomic information of the new taxa was submitted to MycoBank (http://www.mycobank.org).

DNA extraction and sequencing

Genomic DNA was extracted from fungal mycelia grown on PDA, using a modified cetyltrimethylammonium bromide (CTAB) protocol as described in Guo et al. (2000). The internal transcribed spacer region (ITS) with intervening 5.8S rRNA gene, large subunit of rRNA gene (LSU), translation elongation factor 1-alpha gene (*tef1*), actin gene (ACT) and glyceraldehyde-3-phosphate dehydrogenase gene (GPDH) were amplified and sequenced by using the primer pairs ITS5/ITS4 (White et al. 1990),

LROR/LR5 (White et al. 1990), EF1-728F/EF2 (O'Donnell et al. 1998; Carbone and Kohn 1999), ACT-512F/ACT-783R (Carbone and Kohn 1999) and Gpd1-LM/Gpd2-LM (Myllys et al. 2002), respectively.

PCR was performed using an Eppendorf Master Thermocycler (Hamburg, Germany). Amplification reactions were carried out in a 25 µl reaction volume, which contained 12.5 µl 2×Green Taq Mix (Vazyme, Nanjing, China), 1 µl of each forward and reverse primer (10 µM stock; Biosune, Shanghai, China), 1 µl template genomic DNA (approximately 10 ng/µl) and 9.5 µl distilled deionised water. PCR parameters were as follows: 94 °C for 5 min; 35 cycles of denaturation at 94 °C for 30 s, annealing at a suitable temperature for 50 s and extension at 72 °C for 1 min; and a final elongation step at 72 °C for 10 min. The suitable annealing temperatures for the genes were 55 °C for ITS, 51 °C for LSU, 52 °C for ACT, 48 °C for *tef1* and 52 °C for GPDH, respectively. PCR products were checked through a 1% agarose gel electrophoresis, stained with GelRed and visualised by a UV light. Sequencing was performed bi-directionally by Biosune Company Limited (Shanghai, China). Consensus sequences were obtained using MEGA v. 7.0 (Kumar et al. 2016). All sequences generated in this study were deposited in GenBank (Table 1).

Phylogenetic analyses

The generated consensus sequences were subjected to BLAST searches to identify closely-related sequences in the NCBI's GenBank nucleotide database (Zhang et al. 2000). For phylogenetic inferences, based on ITS-LSU-*tef1*-ACT-GPDH sequences, a subset of sequences from the alignments of Norphanphoun et al. (2020) was used as the backbone. Newly-generated sequences in this study were aligned with related sequences retrieved from GenBank (Table 1) using MAFFT 7 online tool with the Auto strategy (Katoh et al. 2019; http://mafft.cbrc.jp/alignment/server/). To establish the identity of the isolates at species level, phylogenetic analyses were first performed for each locus individually and then all loci were concatenated together for a unified analysis (ITS-LSU-*tef1*-ACT-GPDH).

Phylogenetic analyses were carried out with Maximum Likelihood (ML) and Bayesian Inference (BI) algorithms. The best evolutionary model for each partition was determined using MrModelTest v. 2.3 (Nylander 2004) and incorporated into the BI analyses. ML and BI run on the CIPRES Science Gateway portal (https://www.phylo.org/; Miller et al. 2012) using RAxML-HPC2 on XSEDE v. 8.2.12 (Stamatakis 2014) and MrBayes on XSEDE v. 3.2.7a (Huelsenbeck and Ronquist 2001; Ronquist and Huelsenbeck 2003; Ronquist et al. 2012), respectively. Default parameters were used for the ML analyses and the rapid bootstrapping with the automatic halt option was set for the BI analyses. Bayesian Inference included four parallel runs of 10,000,000 generations, with the stop rule option and a sampling frequency of 1,000 generations. Burn-in fraction was set to 0.25 and posterior probabilities (PP) were determined from the remaining trees. All resultant trees were plotted using FigTree v. 1.4.4 (http://tree.bio.ed.ac.uk/software/figtree) and the layout of the trees was edited in Adobe Illustrator CC 2019.

Table 1. Species and GenBank accession numbers of DNA sequences used in this study.

Species[1]	Voucher[2]	Host/Substrate	Country	GenBank accession number				
				ITS	LSU	*tef1*	ACT	GPDH
Phyllosticta acaciigena	CPC 28295 *	*Acacia suaveolens*	Australia	KY173433	KY173523	–	KY173570	–
P. aloeicola	CPC 21020 *	*Aloe ferox*	South Africa	KF154280	KF206214	KF289193	KF289311	KF289124
	CPC 21021	*Aloe ferox*	South Africa	KF154281	KF206213	KF289194	KF289312	KF289125
P. ardisiicola	NBRC 102261 *	*Ardisia crenata*	Japan	AB454274	AB454274	–	AB704216	–
P. aristolochiicola	BRIP 53316 *	*Aristolochia acuminata*	Australia	JX486129	–	–	–	–
P. azevinhi	MUCC0088	*Ilex pedunculosa*	Japan	AB454302	AB454302	–	AB704226	–
P. beaumarisii	CBS 535.87	*Muehlenbekia adpressa*	Australia	AY042927	KF306229	KF289170	KF306232	KF289074
P. brazillianiae	LGMF 330 *	*Mangifera indica*	Brazil	JF343572	KF206217	JF343593	JF343656	JF343758
	LGMF 333	*Mangifera indica*	Brazil	JF343574	KF206216	JF343595	JF343658	JF343760
P. camelliae	MUCC0059	*Camellia japonica*	Japan	AB454290	AB454290		AB704223	
P. capitalensis	CBS 128856 *	*Stanhopea graveolens*	Brazil	JF261465	KF206255	JF261507	KF289289	JF343776
	CBS 226.77	*Baccaurea ramiflora*	Brazil	FJ538336	KF206289	FJ538394	FJ538452	JF343718
	CBS 356.52	*Paphiopedilum callosum*	Germany	FJ538342	KF206300	FJ538400	FJ538458	KF289087
	CBS 100175	*Ilex* sp.	Not given	FJ538320	KF206327	FJ538378	FJ538436	JF343699
	CBS 101228	*Citrus* sp.	Brazil	FJ538319	KF206325	FJ538377	FJ538435	KF289086
	CBS 114751	*Nephelium lappaceum*	Hawaii	EU167584	EU167584	FJ538407	FJ538465	KF289088
	CBS 115047	*Vaccinium* sp.	New Zealand	FJ538323	KF206318	FJ538381	FJ538439	KF289077
	CBS 115049	*Aspidosperma polyneuron*	Brazil	FJ538324	KF206317	FJ538382	FJ538440	KF289084
	CBS 117118	*Bowdichia nitida*	Brazil	FJ538339	JQ743603	FJ538397	FJ538455	KF289090
	CBS 120428	*Musa acuminata*	Indonesia	JN692544	KF206315	JN692532	JN692520	JN692509
	CBS 123373	*Sansevieria* sp.	Netherlands	FJ538341	JQ743604	FJ538399	FJ538457	JF343703
	CPC 13987	*Protea repens*	Portugal	KF206183	KF206281	KF289176	KF289263	KF289083
	CPC 16592	*Citrus limon*	Argentina	KF206187	KF206270	KF289273	KF289178	KF289092
	CPC 17468	*Cymbidium* sp.	Brazil	KF206188	KF206259	KF289189	KF289284	KF289120
	CPC 20256	*Ophiopogon japonicus*	Thailand	KC291337	KF206247	KC342557	KC342534	KF289089
	CPC 20257	*Ficus benjamina*	Thailand	KC291338	KF206246	KC342558	KC342535	KF289099
	LGMF219	*Citrus sinensis*	Brazil	KF206202	KF206220	JF261490	KF289306	JF343737
	LGMF220	*Citrus sinensis*	Brazil	KF206203	KF206219	JF261488	KF289307	JF343735
	LGMF222	*Citrus sinensis*	Brazil	KF206204	KF206218	JF261492	KF289308	JF343739
	SAUCC210144	***Rhapis excelsa***	**China**	**OM571175**	**OM571179**	**OM640045**	**OM640047**	**OM640049**
	SAUCC210148	***Rhapis excelsa***	**China**	**OM571176**	**OM571180**	**OM640046**	**OM640048**	**OM640050**
P. carochlae	CGMCC 3.17317 *	*Caryota ochlandra*	China	KJ847422	–	KJ847444	KJ847430	KJ847438
	CGMCC 3.17318	*Caryota ochlandra*	China	KJ847423	–	KJ847445	KJ847431	KJ847439
P. cavendishii	BRIP 554196 *	*Musa* cv. Formosana	Taiwan	JQ743562	–	KF009743	KF014080	–
	BRIP 58008	*Banana*	Australia	KC988365	–	KF009742	KF014071	–
P. cordylinophila	CPC 20261 *	*Cordyline fruticosa*	Thailand	KF170287	KF206242	KF289172	KF289295	KF289076
	CPC 20277	*Cordyline fruticosa*	Thailand	KF170288	KF206228	KF289171	KF289301	KF289075
P. eugeniae	CBS 445.82	*Eugenia aromatica*	Indonesia	AY042926	KF206288	KF289208	KF289246	KF289139
P. fallopiae	MUCC0113 *	*Fallopia japonica*	Japan	AB454307	AB454307	–	–	–
P. harai	MUCC0043	*Aucuba japonica*	Japan	AB454281	AB454281	–	AB704219	–
P. hubeiensis	CGMCC 3.14986 *	*Viburnum odoratissimim*	China	JX025037	–	JX025042	JX025032	JX025027
	CGMCC 3.14987	*Viburnum odoratissimim*	China	JX025038	–	JX025043	JX025033	JX025028
P. ilicis-aquifolii	CGMCC 3.14358 *	*Ilex aquifolium*	China	JN692538	–	JN692526	JN692514	–
	CGMCC 3.14359	*Ilex aquifolium*	China	JN692539	–	JN692527	JN692515	–
P. maculata	CPC 18347 *	*Musa* cv. Goly-goly pot-pot	Australia	JQ743570	–	KF009700	KF014016	–
	BRIP 46622	*Musa* cv. Goly-goly pot-pot	Australia	JQ743567	–	KF009692	KF014013	–
P. mangiferae	IMI 260.576 *	*Mangifera indica*	India	JF261459	KF206222	JF261501	JF343641	JF343748
	CPC 20260	Arecaceae	Thailand	KF206193	KF206243	KF289187	KF289294	KF289114
P. mangifera-indica	MFLUCC 10–0029 *	*Mangifera indica*	Thailand	KF170305	KF206240	KF289190	KF289296	KF289121

Species[1]	Voucher[2]	Host/Substrate	Country	GenBank accession number				
				ITS	LSU	*tef1*	ACT	GPDH
P. miurae	MUCC0065	*Lindera praecox*	Japan	AB454291	AB454291	–	AB704224	–
P. musaechinensis	GZAAS6.1247	*Musa.* sp.	China	KF955294	–	KM816639	KM816627	KM816633
	GZAAS6.1384	*Musa.* sp.	China	KF955295	–	KM816640	KM816628	KM816634
P. musarum	BRIP57803	*Musa.* sp.	Malaysia	JX997138	–	KF009737	KF014055	–
	BRIP58028	*Musa.* sp.	Australia	KC988377	–	KF009738	KF014054	–
P. oblongifolae	**SAUCC210055**	***Garcinia oblongifolia***	**China**	**OM248442**	**OM232085**	**OM273890**	**OM273894**	**OM273898**
	SAUCC210054	***Garcinia oblongifolia***	**China**	**OM248443**	**OM232086**	**OM273891**	**OM273895**	**OM273899**
	SAUCC210053	***Garcinia oblongifolia***	**China**	**OM248444**	**OM232087**	**OM273892**	**OM273896**	**OM273900**
	SAUCC210052 *	***Garcinia oblongifolia***	**China**	**OM248445**	**OM232088**	**OM273893**	**OM273897**	**OM273901**
P. paracapitalensis	CPC 26517 *	*Citrus floridana*	Italy	KY855622	KY855796	KY855951	KY855677	KY855735
	CPC 26518	*Citrus floridana*	Italy	KY855623	KY855797	KY855952	KY855678	KY855736
	CPC 26700	*Citrus floridana*	Italy	KY855624	KY855798	KY855953	KY855679	KY855737
	CPC 26701	*Citrus floridana*	Italy	KY855625	KY855799	KY855954	KY855680	KY855738
	CPC 26805	*Citrus floridana*	Italy	KY855626	KY855800	KY855955	KY855681	KY855739
	CPC 26806	*Citrus floridana*	Italy	KY855627	KY855801	KY855956	KY855682	KY855740
	CPC 28120	*Citrus limon*	Spain	KY855628	KY855802	KY855957	KY855683	KY855741
P. paracapitalensis	CPC 28121	*Citrus limon*	Spain	KY855629	KY855803	KY855958	KY855684	KY855742
	CPC 28122	*Citrus limon*	Spain	KY855630	KY855804	KY855959	KY855685	KY855743
	CPC 28123	*Citrus limon*	Spain	KY855631	KY855805	KY855960	KY855686	KY855744
	CPC 28127	*Citrus limon*	Spain	KY855632	KY855806	KY855961	KY855687	KY855745
	CPC 28128	*Citrus limon*	Spain	KY855633	KY855807	KY855962	KY855688	KY855746
	CPC 28129	*Citrus limon*	Spain	KY855634	KY855808	KY855963	KY855689	KY855747
P. parthenocissi	CBS 111645 *	*Parthenocissus quinquefolia*	USA	EU683672	–	JN692530	JN692518	–
P. partricuspidatae	NBRC 9466 *	*Parthenocissus tricuspidata*	Japan	KJ847424	–	KJ847446	KJ847432	KJ847440
	NBRC 9757	*Parthenocissus tricuspidata*	Japan	KJ847425	–	KJ847447	KJ847433	KJ847441
P. philoprina	CBS 587.69	*Ilex aquifolium*	Spain	KF154278	KF206297	KF289206	KF289250	KF289137
	CBS 616.72	*Ilex aquifolium*	Germany	KF154279	KF206296	KF289205	KF289251	KF289136
P. pterospermi	**SAUCC210104** *	***Pterospermum heterophyllum***	**China**	**OM249954**	**OM249956**	**OM273902**	**OM273904**	**OM273906**
	SAUCC210406	***Pterospermum heterophyllum***	**China**	**OM249955**	**OM249957**	**OM273903**	**OM273905**	**OM273907**
P. rhizophorae	NCYUCC 19–0352 *	*Rhizophora stylosa*	Taiwan	MT360030	MT360039	–	MT363248	MT363250
	NCYUCC 19–0358	*Rhizophora stylosa*	Taiwan	MT360031	MT360040	–	MT363249	MT363251
P. schimae	CGMCC 3.14354 *	*Schima superba*	China	JN692534	–	JN692522	JN692510	JN692506
P. schimicola	CGMCC 3.17319 *	*Schima superba*	China	KJ847426	–	KJ847448	KJ847434	KJ854895
	CGMCC 3.17320	*Schima superba*	China	KJ847427	–	KJ847449	KJ847435	KJ854896
P. styracicola	LC1642 *	*Styrax gradiflorus*	China	JX025040	–	JX025045	JX025035	JX025030
P. vitis-rotundifoliae	CGMCC 3.17321	*Vitis rotundifolia*	USA	KJ847429	–	KJ847451	KJ847437	KJ847443
	CGMCC 3.17322 *	*Vitis rotundifolia*	USA	KJ847428	–	KJ847450	KJ847436	KJ847442

[1]Newly generated sequences in this study are in bold. [2]Isolates marked with "*" are ex-type or ex-epitype strains.

Results

Phylogenetic analyses

A total of 86 isolates representing the *Phyllosticta* species were phylogenetically analysed, of which 84 isolates in the *P. capitalensis* species complex were considered as ingroup and two strains of *Phyllosticta hubeiensis* (CGMCC 3.14986, CGMCC 3.14987) in

the *P. cruenta* species complex were used as outgroup. The final alignment contained 2665 concatenated characters, viz. 1–733 (ITS), 734–1499 (LSU), 1500–1790 (*tef1*), 1791–2042 (ACT), 2043–2665 (GPDH). Of these characters, 1964 were constant, 126 were variable and parsimony-uninformative and 575 were parsimony-informative. MrModelTest recommended that the Bayesian Inference should use Dirichlet base frequencies for the ITS, LSU, *tef1*, ACT and GPDH data partitions. The GTR+I+G model was proposed for ITS, LSU and GPDH, while HKY+G for *tef1* and ACT. The MCMC analysis of the five concatenated genes was run for 1,520,000 generations, resulting in 30,402 trees. The initial 7,600 trees generated in the burn-in phase were discarded, while the remaining trees were used to calculate posterior probabilities in the majority rule consensus trees. The alignment contained a total of 876 unique site patterns (ITS: 358, LSU: 69, *tef1*: 170, ACT: 137, GPDH: 142). The topology of the ML tree confirmed the tree topology obtained from the Bayesian Inference and, therefore, only the ML tree is presented (Fig. 1). The 86 strains were assigned to 34 species, based on the five-gene phylogeny (Fig. 1). The present study revealed three species, viz. *Phyllosticta oblongifolae* sp. nov., *P. pterospermi* sp. nov. and *P. capitalensis*. The *P. oblongifolae* sp. nov. was a sister group to *P. eugeniae* (0.98/81) and the *P. pterospermi* sp. nov. was closely related to *P. mangiferae* (0.99/92).

Taxonomy

The taxa described belong in family Phyllostictaceae.

Phyllosticta oblongifoliae **Z.X. Zhang, X.Y. Liu, Z. Meng & X.G. Zhang, sp. nov.**
Fig. 2
MycoBank No: 843232

Etymology. The specific epithet "*oblongifoliae*" refers to the host plant *Garcinia oblongifolia*.

Type. China, Hainan Province: Bawangling National Forest Park, on diseased leaves of *Garcinia oblongifolia*, 19 May 2021, Z.X. Zhang (holotype, HSAUP210052; ex-type SAUCC210052).

Description. Leaf endogenic and associated with leaf spots. Asexual morph: Conidiomata pycnidial, mostly aggregated in clusters, black, erumpent. In MEA culture exuding colourless to opaque conidial masses within 10 days or longer. Pycnidial wall multilayered, textura angularis, brown to dark brown, up to 30 μm thick; inner walls hyaline. Conidiophores indistinct, often reduced to conidiogenous cells. Conidiogenous cells terminal, subcylindrical, ampulliform, hyaline, smooth, 9.0–14.0 × 2.5–4.5 μm. Conidia 8.0–13.0 × 6.0–8.0 μm, mean ± SD = 10.0 ± 1.3 × 7.2 ± 0.5 μm, hyaline, aseptate, thin and smooth walled, coarsely guttulate or with a single large central guttule, ovoid, ampulliform, ellipsoidal to subglobose, enclosed in a thin mucoid sheath, 1.0–2.0 μm thick and bearing a hyaline, apical mucoid appendage, 3.0–8.5 × 1.0–1.5 μm, flexible, unbranched, tapering towards an acutely rounded tip.

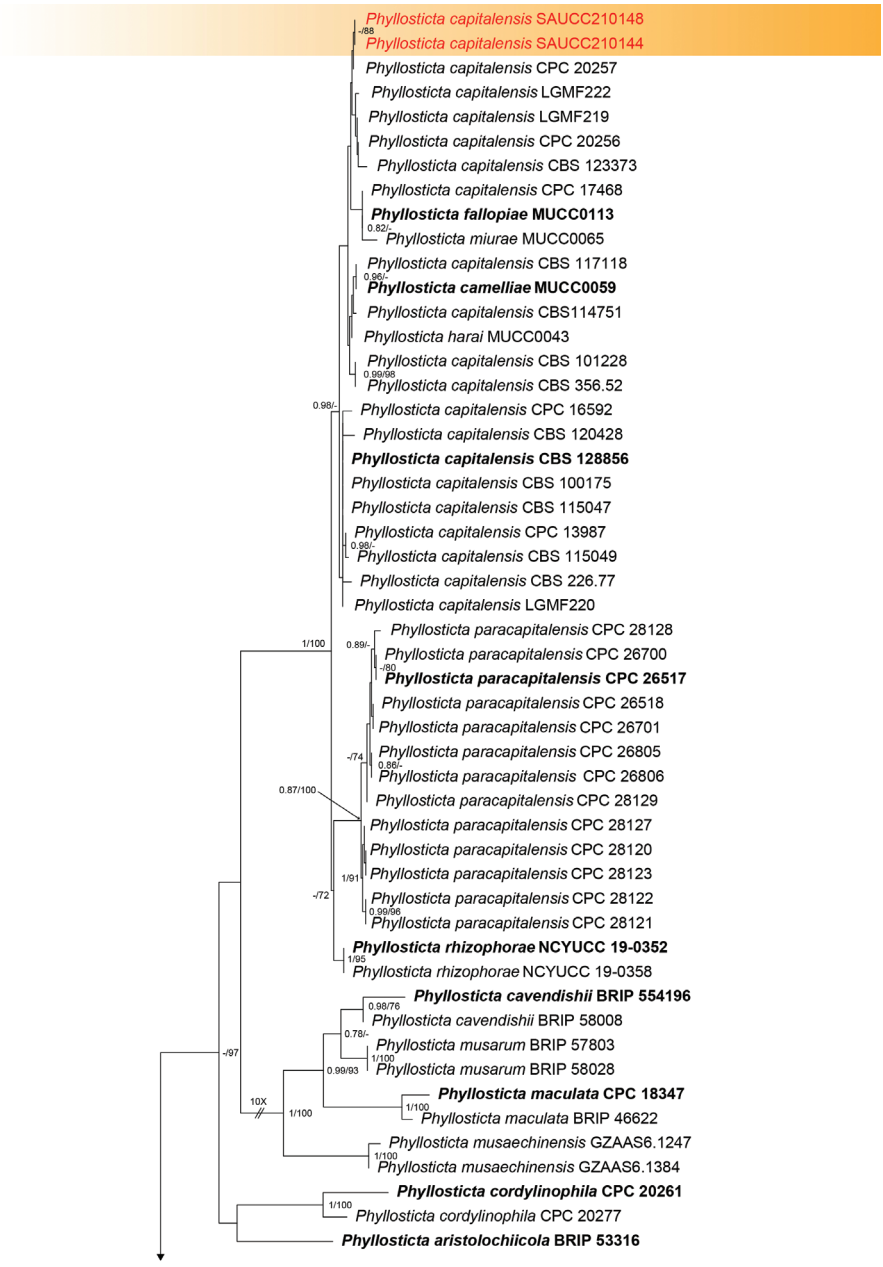

Figure 1. Phylogram of the *Phyllosticta capitalensis* species complex, based on a concatenated ITS, LSU, *tef1*, ACT and GPDH sequence alignment, with *Phyllosticta hubeiensis* (CGMCC 3.14986, CGMCC 3.14987) of the *P. cruenta* species complex serving as outgroup. Bayesian Inference posterior probabilities and Maximum Likelihood bootstrap support values above 0.70 and 70% are shown at the first and second position, respectively. Ex-type cultures are indicated in bold face. Strains obtained in the current study are in red. Some branches are shortened for layout purposes – these are indicated by two diagonal lines with the number of times. The bar at the left-bottom represents substitutions per site.

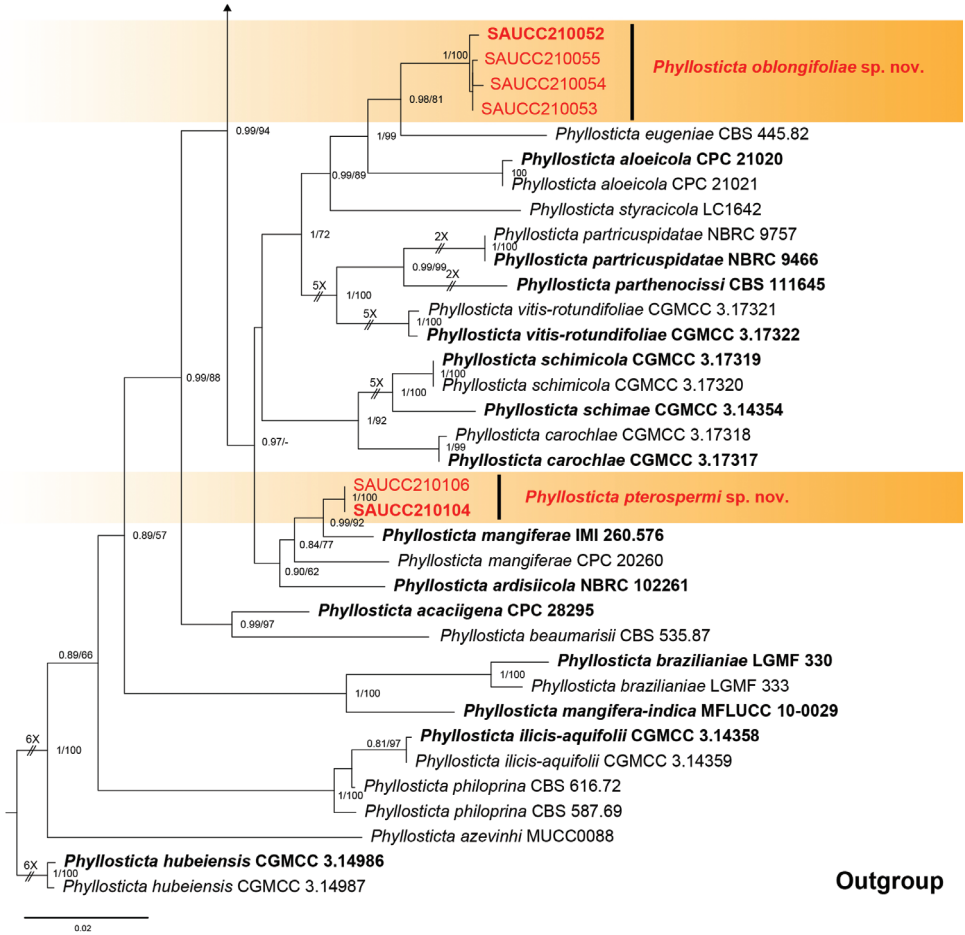

Figure 1. Continued.

Culture characteristics. Colonies on PDA occupying an entire 90 mm Petri dish in 14 days at 25 °C in darkness, with a growth rate of 6.0–6.5 mm/day, greenish-black in obverse and reverse. Colonies on MEA 82–86 mm in diameter after 14 days at 25 °C in darkness, with a growth rate of 5.7–6.2 mm/day, undulate at edge, white to grey white in obverse and reverse, with moderate aerial mycelia on the surface, with black, gregarious conidiomata.

Additional specimens examined. China, Hainan Province: Bawangling National Forest Park, on diseased leaves of *Garcinia oblongifolia*, 19 May 2021, Z.X. Zhang, HSAUP210053, living culture SAUCC210053; on diseased leaves of *Garcinia oblongifolia*, 19 May 2021, Z.X. Zhang, paratype HSAUP210054, ex-paratype living culture SAUCC210054; on diseased leaves of *Garcinia oblongifolia*, 19 May 2021, Z.X. Zhang, paratype HSAUP210055, ex-paratype living culture SAUCC210055.

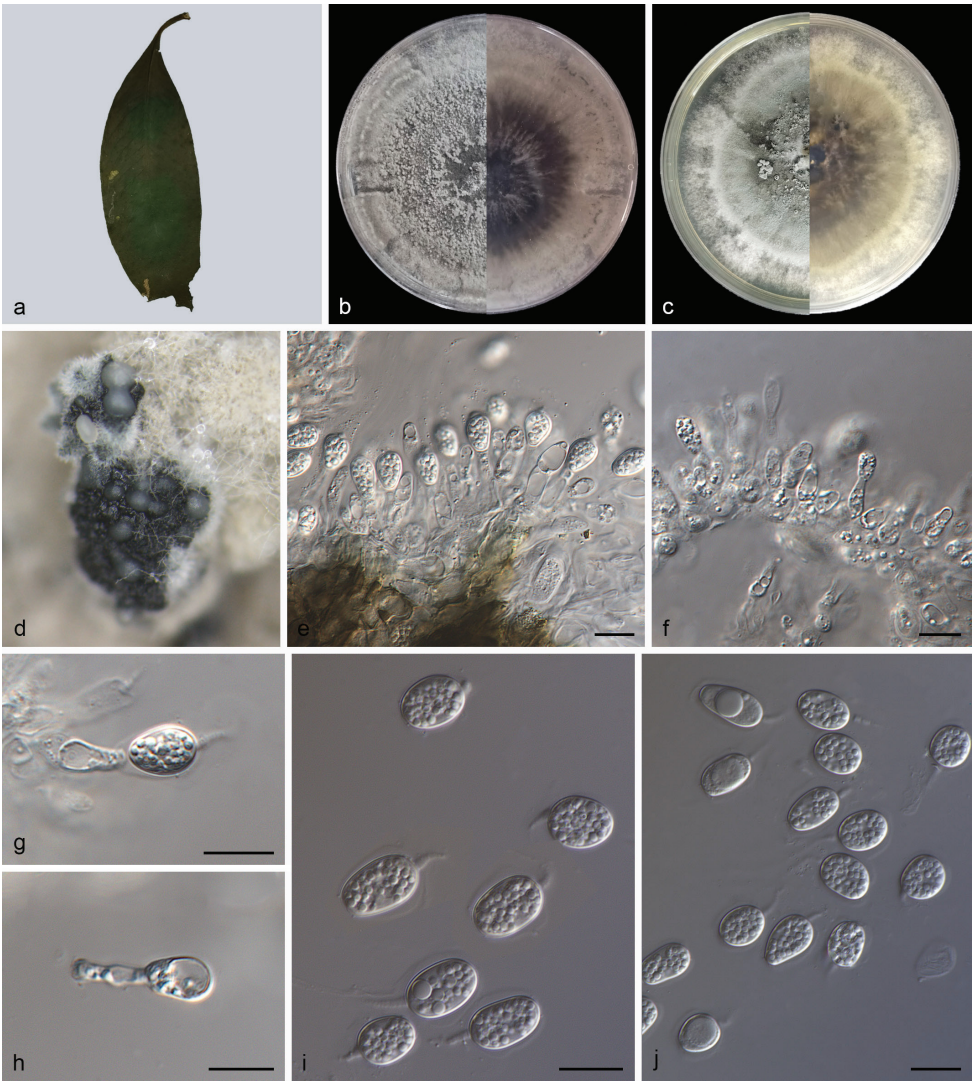

Figure 2. *Phyllosticta oblongifoliae* (SAUCC210052) **a** diseased leaf of *Garcinia oblongifolia* **b, c** colonies (left-above, right-reverse) after 15 days on PDA (**b**) and MEA (**c**) **d** conidiomata **e–h** conidiogenous cells with conidia **i–j** conidia. Scale bars: 10 μm (**e–j**).

Notes. *Phyllosticta oblongifoliae* is introduced, based on the multi-locus phylogenetic analysis as the strain clustered into a well-supported clade (Fig. 1; 1.00/100), which is closely related to *Phyllosticta ugeniae* (0.98/81), but distinguished, based on molecular data, ITS, LSU, *tef1*, ACT and GPDH loci by 57 nucleotide differences in the concatenated alignment. Morphologically, *P. oblongifoliae* (SAUCC210052) differs from *P. ugeniae* (CBS 445.82) in its shorter and wider conidia (8.0–13.0 × 6.0–8.0 vs. 9.6–16.8 × 4.8–6.0 μm) (Wikee et al. 2013a). Therefore, we establish this fungus as a novel species (Jeewon and Hyde 2016).

Phyllosticta pterospermi **Z.X. Zhang, X.Y. Liu, Z. Meng & X.G. Zhang, sp. nov.**
Fig. 3
MycoBank No: 843233

Type. China, Hainan Province: Bawangling National Forest Park, on diseased leaves of *Pterospermum heterophyllum*, 19 May 2021, Z.X. Zhang (holotype, HSAUP210104; ex-holotype living culture SAUCC210104).

Etymology. The specific epithet "*pterospermi*" refers to the genus name of the host plant *Pterospermum heterophyllum*.

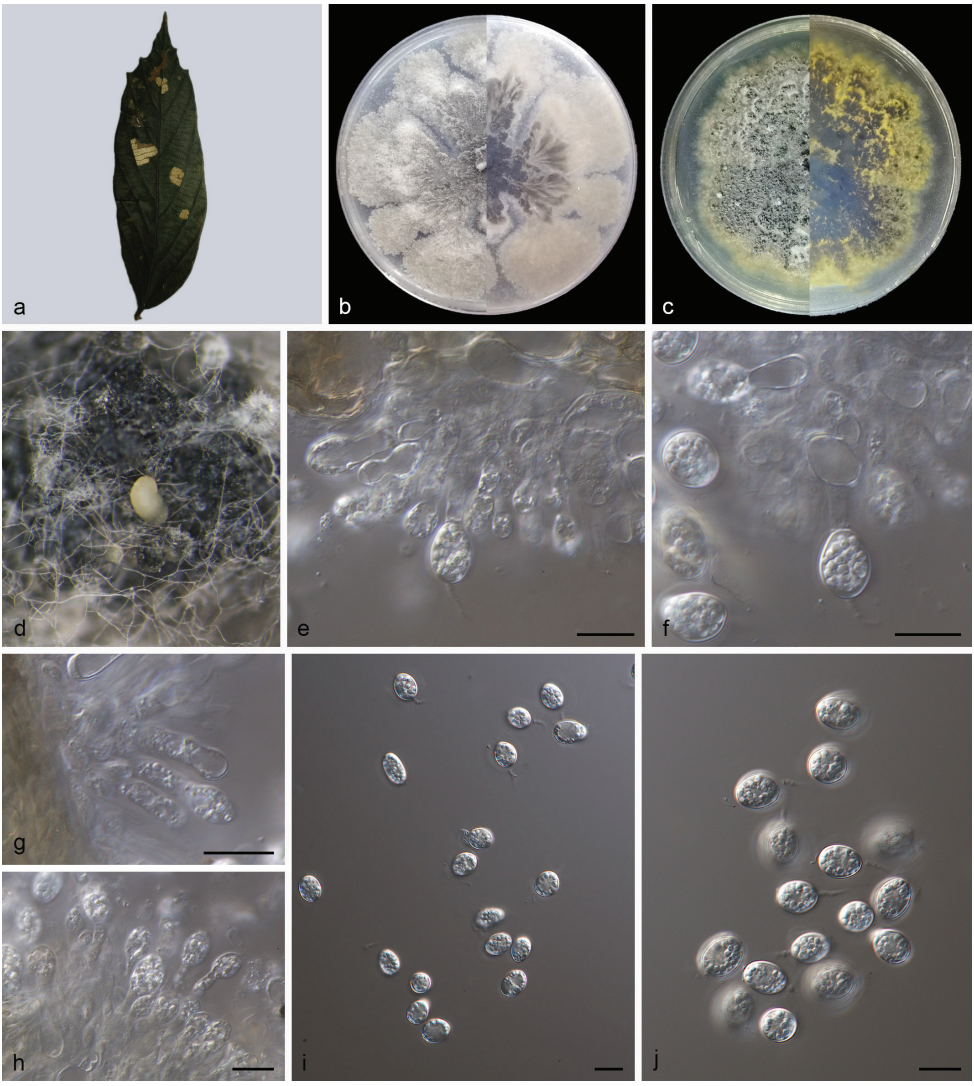

Figure 3. *Phyllosticta pterospermi* (holotype SAUCC210104) **a** diseased leaf of *Pterospermum heterophyllum* **b, c** colonies (left-above, right-reverse) after 15 days on PDA (**b**) and MEA (**c**) **d** conidiomata **e–h** conidiogenous cells with conidia **i–j** conidia. Scale bars: 10 μm (**e–j**).

Description. Leaf endogenic and associated with leaf spots. Asexual morph: Conidiomata pycnidial, mostly aggregated in clusters, black, erumpent. On MEA, pycnidia exudes yellow conidial masses, within 15 days or longer. Pycnidial walls multilayered, textura angularis, brown, up to 30 μm thick; inner walls of hyaline. Conidiophores indistinct, often reduced to conidiogenous cells. Conidiogenous cells, cylindrical, hyaline, smooth, 7.5–11.0 × 2.5–4.5 μm. Conidia 8.0–12.0 × 4.5–8.5 μm, mean ± SD = 9.8 ± 0.9 × 7.3 ± 0.7 μm, hyaline, aseptate, thin and smooth-walled, coarsely guttulate or with a single large central guttule, obovoid, ellipsoidal to subglobose, enclosed in a thin mucoid sheath, 1.0–2.0 μm thick and bearing a hyaline, apical mucoid appendage, 4.0–6.8 × 1.5–3.0 μm, flexible, unbranched, tapering towards an acutely rounded tip.

Culture characteristics. Colonies on PDA 80–90 mm in diameter after 14 days at 25 °C in darkness, with a growth rate of 5.7–6.5 mm/day, undulate at edge, grey white to greyish-green in obverse and reverse. Colonies on MEA 82–86 mm in diameter after 14 days at 25 °C in darkness, with a growth rate of 5.8–6.2 mm/day, undulate at edge, grey white to yellow in obverse and reverse, with moderate aerial mycelia on the surface, with black, gregarious conidiomata.

Additional specimen examined. China, Hainan Province: Bawangling National Forest Park, on diseased leaves of *Pterospermum heterophyllum*. 19 May 2021, Z.X. Zhang, paratype HSAUP210106, ex-paratype living culture SAUCC210106.

Notes. Two isolates from leaf spots of *Pterospermum heterophyllum* phylogenetically clustered into a well-supported clade (1.00/100), which is closely related to *P. ardisiicola* (0.90/62) and *P. mangiferae* (0.99/91; Fig. 1). However, *P. pterospermi* differs from *P. ardisiicola* by 30 nucleotides (13/603 in ITS, 3/553 in LSU and 14/248 ACT) and from *P. mangiferae* by 29 nucleotides (7/567 in ITS, 2/763 in LSU, 3/215 in *tef1*, 3/226 in ACT and 14/643 in GPDH). In morphology, they are distinguished by hosts and conidial size (8.0–12.0 × 4.5–8.5 μm in *P. pterospermi* vs. 7.0–11.0 × 5.0–7.5 μm in *P. ardisiicola* vs. 10.0–12.0 × 6.0–7.0 μm in *P. mangiferae*). Furthermore, *P. pterospermi* differs from *P. ardisiicola* and *P. mangiferae* by wider conidiogenous cells (7.5–11.0 × 2.5–4.5 μm vs. 5.0–12.5 × 1.2–2.5 μm) and from *P. mangiferae* in having longer conidiogenous cells (7.5–11.0 × 2.5–4.5 μm vs. 6.0–10.0 × 3.0–4.0 μm) (Motohashi et al. 2008; Glienke et al. 2011). Therefore, we establish this strain as *P. pterospermi* sp. nov. (Jeewon and Hyde 2016).

Phyllosticta capitalensis Henn., Hedwigia 48: 13. 1908

Fig. 4

Description. Leaf endogenic and associated with leaf spots. Asexual morph: Conidiomata pycnidial, mostly aggregated in clusters, black, erumpent. In MEA, cultures exuded colourless to opaque conidial masses, appeared on pycnidia after 10 days or longer. Pycnidial walls of multilayered, textura angularis, brown to dark brown, up to 35 μm thick; inner walls hyaline. Conidiophores subcylindrical to ampulliform, frequently reduced to conidiogenous cells or branching from a basal supporting cell, coated in mucoid layer, 8.0–14.0 × 3.0–5.0 μm. Conidiogenous cells terminal, subcylindrical to

ampulliform, hyaline, smooth, 8.0–11.0 × 3.0–4.5 μm. Conidia 9.0–12.5 × 5.0–7.0 μm, mean ± SD = 10.6 ± 0.9 × 6.2 ± 0.5 μm, solitary, hyaline, aseptate, thin and smooth walled, coarsely guttulate or with a single large central guttule, ovoid, ampulliform, ellipsoidal to subglobose, enclosed in a thin mucoid sheath, 1.3–2.7 μm thick and bearing a hyaline, apical mucoid appendage, 3.0–8.5 × 1.0–1.5 μm, flexible, unbranched, tapering towards an acutely rounded tip. Spermatia hyaline, smooth, guttulate to granular, bacilliform, 6.0–8.2 × 1.3–2.0 μm, occurring in conidioma with conidia. Sexual morph: Ascomata shape and wall like those of the conidiomata. Asci bitunicate, hyaline, clavate to broadly fusoid-ellipsoid, with visible apical chamber, 2 μm diam., 45–85 × 9–13 μm. Ascospores bi- to multiseriate, hyaline, smooth, granular to guttulate, aseptate, straight, rarely curved, widest in the middle, limoniform with obtuse ends, 15–18 × 6–7 μm.

Culture characteristics. Colonies on PDA occupying an entire 90 mm Petri dish in 14 days at 25 °C in darkness, with a growth rate of 6.0–6.5 mm/day, greenish-black in obverse and reverse. Colonies on MEA 82–86 mm in diameter after 14 days at 25 °C in darkness, with a growth rate of 5.7–6.2 mm/day, undulate at edge, white to grey white in obverse and reverse, with moderate aerial mycelia on the surface, with black, gregarious conidiomata.

Specimens examined. China, Hainan Province: Bawangling National Forest Park, on diseased leaves of *Rhapis excelsa* (Thunb.) Henry ex Rehd, 19 May 2021, Z.X. Zhang, HSAUP210144, living culture SAUCC210144; on diseased leaves of *Rhapis excelsa*. 19 May 2021, Z.X. Zhang, HSAUP210148, living culture SAUCC210148.

Notes. Based on morphological features, Hennings (1908) described *Phyllosticta capitalensis* and Glienke et al. (2011) added molecular data. The holotype (CBS 128856) of *P. capitalensis* was collected from *Stanhopea graveolens* (Glienke et al. 2011). In our current study, two isolates (SAUCC210144, SAUCC210148), collected from diseased leaves of *Rhapis excelsa*, cluster in the *P. capitalensis* clade (Fig. 1). Although four other species are also in this clade, we consider these two isolates as *P. capitalensis*, based on their morphological characters, such as granular to guttulate ascospores (15–18 × 6–7 vs. 15–17 × 5–6 μm), subcylindrical to ampullate conidiogenous cells (8.0–11.0 × 3.0–4.5 vs. 7–10 × 3–5 μm), ellipsoidal to subglobose conidia (9–12.5 × 5–7 vs. 11–12 × 6–7 μm) and hyaline, apical mucoid appendages (3–8.5 × 1–1.5 vs. 6–8 × 1–1.5 μm).

Discussion

Compared to other parts of China, species richness is highly diverse in Hainan Province, especially in Bawangling National Forest Park, which has a typical tropical rainforest climate. The environment favours growth of unusual microbial species. Historically, *Phyllosticta* species have been identified by morphology and host association. However, overlapping morphology makes it difficult to pinpoint homologous characters and, consequently, traditional identification of *Phyllosticta* species has long been a complicated

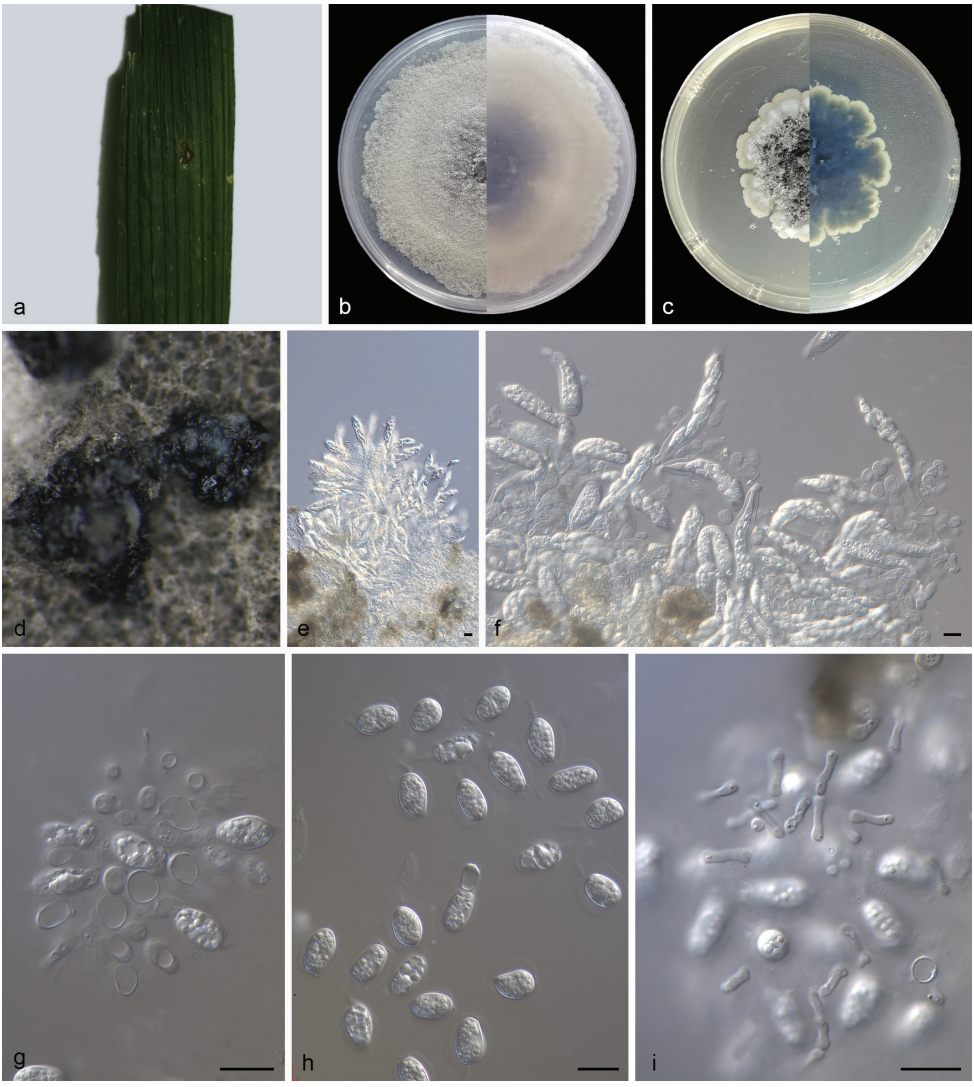

Figure 4. *Phyllosticta capitalensis* (holotype SAUCC210144) **a** diseased leaf of *Rhapis excelsa* **b, c** colonies (left-above, right-reverse) after 15 days on PDA (**b**) and MEA (**c**) **d** conidiomata **e** asci and ascospores **f** asci, ascospores and conidia **g** conidiogenous cells with conidia **h** conidia **i** spermatia. Scale bars: 10 μm (**e–i**).

endeavour (Norphanphoun et al. 2020). This issue has led to confusion in the taxonomy of *Phyllosticta*. Molecular phylogenetics has promoted species delimitation and species complex determination (Baayen et al. 2002; Okane et al. 2003; Motohashi et al. 2009; Wulandari et al. 2009; Glienke et al. 2011; Wikee et al. 2012). Norphanphoun et al. (2020) introduced six species complexes in *Phyllosticta*, based on five gene loci encoding the internal transcribed spacer of ribosomal RNA (ITS rDNA), large subunit of ribosomal RNA (LSU rDNA), translation elongation factor 1 alpha (TEF1α), actin (ACT)

and glycerol-3-phosphate dehydrogenase (GPDH). Amongst these, the *P. capitalensis* species complex consisted of 28 cryptic species, *P. acaciigena*, *P. aloeicola*, *P. ardisiicola*, *P. aristolochiicola*, *P. azevinhi*, *P. beaumarisii*, *P. brazilianiae*, *P. capitalensis*, *P. carochlae*, *P. cavendishii*, *P. cordylinophila*, *P. eugeniae*, *P. fallopiae*, *P. ilicis-aquifolii*, *P. maculata*, *P. mangiferae*, *P. mangifera-indicae*, *P. musaechinensis*, *P. musarum*, *P. paracapitalensis*, *P. parthenocissi*, *P. partricuspidatae*, *P. philoprina*, *P. rhizophorae*, *P. schimae*, *P. schimicola*, *P. styracicola* and *P. vitis-rotundifoliae*. In this study, we focus our analyses on the *P. capitalensis* species complex and report two new species and one new Chinese record.

Multilocus phylogeny, as well as morphological characters observed in culture, described and illustrated herein eight isolates of *Phyllosticta* species from three host genera, which contributed knowledge to the diversity of *Phyllosticta* species in Hainan, China. Two new species are proposed: *P. oblongifoliae* sp. nov. and *P. pterospermi* sp. nov. This is the first time we report *Phyllosticta* species from *Pterospermum heterophyllum* (Sterculiaceae). In a recent study, *Allophoma pterospermicola* was reported as pathogenic to *Pterospermum* (Marin-Felix et al. 2019). In reality, the number of phytopathogenic fungi from the *Pterospermum* host is inherently small. The known species *Phyllosticta capitalensis* (synonym *Guignardia mangiferae*; Baayen et al. 2002) was described multiple times from *Stanhopea graveolens* (Orchidaceae) in Brazil (Glienke et al. 2011). In this study, we describe and illustrate *Phyllosticta capitalensis* again. Each of these species show typical morphological characteristics of *Phyllosticta*, i.e. conidia with mucilaginous sheaths and an apical appendage (van der Aa 1973).

Phyllosticta capitalensis is a cosmopolitan endophytic species reported in more than 300 host records in Fungal Databases (https://nt.ars-grin.gov/fungaldatabases/index.cfm) (Okane et al. 2001, 2003; Baayen et al. 2002; Glienke et al. 2011; Wikee et al. 2013b; Wu et al. 2014; Zhang et al. 2015; Tran et al. 2019; Hattori et al. 2020). As a weak pathogen, *P. capitalensis* causes leaf spots on tea (*Camellia sinensis*), oil palm (*Elaeis guineensis*), *Ricinus communis* and black spot disease on *Psidium guajava* (Cheng et al. 2019; Nasehi et al. 2019; Liao et al. 2020; Tang et al. 2020).

Acknowledgements

This work was jointly supported by the National Natural Science Foundation of China (nos. 31900014, U2002203, 31750001)

References

Baayen RP, Bonants P, Verkley G, Carroll GC, van der Aa HA, de Weerdt M, van Brouwershaven IR, Schutte GC, Maccheroni Jr W, Glienke de Blanco C, Azevedo JL (2002) Nonpathogenic isolates of the citrus black spot fungus, *Guignardia citricarpa*, identified as a cosmopolitan endophyte of woody plants, *G. mangiferae* (*Phyllosticta capitalensis*). Phytopathology 92(5): 464–477. https://doi.org/10.1094/PHYTO.2002.92.5.464

Bánki O, Roskov Y, Döring M, Ower G, Vandepitte L, Hobern D, Remsen D, Schalk P, DeWalt RE, Keping M, Miller J, Orrell T, Aalbu R, Adlard R, Adriaenssens EM, Aedo C, Aescht E, Akkari N, Alfenas-Zerbini P (2022) Catalogue of Life Checklist (Version 2022-03-21). Catalogue of Life. https://doi.org/10.48580/dfpd

Braun U, Nakashima C, Crous PW, Groenewald JZ, Moreno-Rico O, Rooney-Latham S, Blomquist CL, Haas J, Marmolejo J (2018) Phylogeny and taxonomy of the genus *Tubakia* s. lat. Fungal Systematics and Evolution 1(1): 41–99. https://doi.org/10.3114/fuse.2018.01.04

Carbone I, Kohn LM (1999) A method for designing primer sets for speciation studies in filamentous ascomycetes. Mycologia 91(3): 553–556. https://doi.org/10.1080/00275514.1999.12061051

Cheng LL, Thangaraj K, Deng C, Deng WW, Zhang ZZ (2019) *Phyllosticta capitalensis* causes leaf spot on tea plant (*Camellia sinensis*) in China. Plant Disease 103(11): e2964. https://doi.org/10.1094/PDIS-04-19-0768-PDN

Crous PW, Slippers B, Wingfield MJ, Rheeder J, Marasas WFO, Philips AJL, Alves A, Burgess T, Barber P, Groenewald JZ (2006) Phylogenetic lineages in the Botryosphaeriaceae. Studies in Mycology 55: 235–253. https://doi.org/10.3114/sim.55.1.235

Crous PW, Wingfield MJ, Schumacher RK, Summerell BA, Giraldo A, Gené J, Guarro J, Wanasinghe DN, Hyde KD, Camporesi E, Garethjones EB, Thambugala KM, Malysheva EF, Malysheva VF, Acharya K, Álvarez J, Alvarado P, Assefa A, Barnes CW, Bartlett JS, Blanchette RA, Burgess TI, Carlavilla JR, Coetzee MPA, Damm U, Decock CA, Denbreeÿen A, Devries B, Dutta AK, Holdom DG, Rooney-Latham S, Manjón JL, Marincowitz S, Mirabolfathy M, Moreno G, Nakashima C, Papizadeh M, Shahzadehfazeli SA, Amoozegar MA, Romberg MK, Shivas RG, Stalpers JA, Stielow B, Stukely MJC, Swart WJ, Tan YP, Vanderbank M, Wood AR, Zhang Y, Groenewald JZ (2014) Fungal Planet description sheets: 281–319. Persoonia 33(1): 212–289. https://doi.org/10.3767/003158514X685680

Crous PW, Wingfield MJ, Roux JJL, Richardson DM, Strasberg D, Shivas RG, Alvarado P, Edwards J, Moreno G, Sharma R, Sonawane MS, Tan YP, Altés A, Barasubiye T, Barnes CW, Blanchette RA, Boertmann D, Bogo A, Carlavilla JR, Cheewangkoon R, Daniel R, de Beer ZW, Yáñez-Morales MJ, Duong TA, Fernández-Vicente J, Geering ADW, Guest DI, Held BW, Heykoop M, Hubka V, Ismail AM, Kajale SC, Khemmuk W, Kolařík M, Kurli R, Lebeuf R, Lévesque CA, Lombard L, Magista D, Manjón JL, Marincowitz S, Mohedano JM, Nováková A, Oberlies NH, Otto EC, Paguigan ND, Pascoe IG, Pérez-Butrón JL, Perrone G, Rahi P, Raja HA, Rintoul T, Sanhueza RMV, Scarlett K, Shouche YS, Shuttleworth LA, Taylor PWJ, Thorn RG, Vawdrey LL, Solano-Vidal R, Voitk A, Wong PTW, Wood AR, Zamora JC, Groenewald JZ (2015) Fungal Planet description sheets: 371–399. Persoonia 35(1): 264–327. https://doi.org/10.3767/003158515X690269

Crous PW, Wingfield MJ, Burgess TI, St J, Hardy GE, Crane C, Barrett S, Cano-Lira JF, Leroux JJ, Thangavel R, Guarro J, Stchigel AM, Martín MP, Alfredo DS, Barber PA, Barreto RW, Baseia IG, Cano-Canals J, Cheewangkoon R, Ferreira RJ, Gené J, Lechat C, Moreno G, Roets F, Shivas RG, Sousa JO, Tan YP, Wiederhold NP, Abell SE, Accioly T, Albizu JL, Alves JL, Antoniolli ZI, Aplin N, Araújo J, Arzanlou M, Bezerra JDP, Bouchara JP, Carlavilla JR, Castillo A, Castroagudín VL, Ceresini PC, Claridge GF, Coelho G, Coimbra

VRM, Costa LA, da cunha KC, da silva SS, Daniel R, de beer ZW, Dueñas M, Edwards J, Enwistle P, Fiuza PO, Fournier J, García D, Gibertoni TB, Giraud S, Guevara-Suarez M, Gusmão LFP, Haituk S, Heykoop M, Hirooka Y, Hofmann TA, Houbraken J, Hughes DP, Kautmanová I, Koppel O, Koukol O, Larsson E, Latha KPD, Lee DH, Lisboa DO, Lisboa WS, López-Villalba Á, Maciel JLN, Manimohan P, Manjón JL, Marincowitz S, Marney TS, Meijer M, Miller AN, Olariaga I, Paiva LM, Piepenbring M, Poveda-Molero JC, Raj KNA, Raja HA, Rougeron A, Salcedo I, Samadi R, Santos TAB, Scarlett K, Seifert KA, Shuttleworth LA, Silva GA, Silva M, Siqueira JPZ, Souza-Motta C.M, Stephenson SL (2016) Fungal Planet description sheets: 469–557. Persoonia 37: 218–403. https://doi.org/10.3767/003158516X694499

Crous PW, Wingfield MJ, Burgess TI, Carnegie AJ, St J, Hardy GE, Smith D, Summerell BA, Cano-Lira JF, Guarro J, Houbraken J, Lombard L, Martín MP, Sandoval-Denis M, Alexandrova AV, Barnes CW, Baseia IG, Bezerra JDP, Guarnaccia V, May TW, Hernández-Restrepo M, Stchigel AM, Miller AN, Ordoñez ME, Abreu VP, Accioly T, Agnello C, Agustincolmán A, Albuquerque CC, Alfredo DS, Alvarado P, Araújo-Magalhães GR, Arauzo S, Atkinson T, Barili A, Barreto RW, Bezerra JL, Cabral TS, Rodríguez F Camello, Cruz RHSF, Daniëls PP, da silva BDB, de Almeida DAC, de Carvalhojúnior AA, Decock CA, Delgat L, Denman S, Dimitrov RA, Edwards J, Fedosova AG, Ferreira RJ, Firmino AL, Flores JA, García D, Gené J, Giraldo A, Góis JS, Gomes AAM, Gonçalves CM, Gouliamova DE, Groenewald M, Guéorguiev BV, Guevara-Suarez M, Gusmão LFP, Hosaka K, Hubka V, Huhndorf SM, Jadan M, Jurjevi, Kraak B, Kuera V, Kumar TKA, Kušan I, Lacerda SR, Lamlertthon S, Lisboa WS, Loizides M, Luangsa-Ard JJ, Lysková P, Maccormack WP, Macedo DM, Machado AR, Malysheva EF, Marinho P, Matoec N, Meijer M, Meši A, Mongkolsamrit S, Moreira KA, Morozova OV, Nair KU, Nakamura N, Noisripoom W, Olariaga I, Oliveira RJV, Paiva LM, Pawar P, Pereira OL, Peterson SW, Prieto M, Rodríguez-Andrade E, Rojodeblas C, Roy M, Santos ES, Sharma R, Silva GA, Souza-Motta CM, Takeuchi-Kaneko Y, Tanaka C, Thakur A, Smith MTH, Tkalec Z, Valenzuela-Lopez N, Vanderkleij P, Verbeken A, Viana MG, Wang XW, Groenewald JZ (2017) Fungal Planet description sheets: 625–715. Persoonia 39: 270–467. https://doi.org/10.3767/persoonia.2017.39.11

Crous PW, Schumacher RK, Wingfield MJ, Akulov A, Denman S, Roux J, Braun U, Burgess TI, Carnegie AJ, Váczy KZ, Guatimosim E, Schwartsburd PB, Barreto RW, Hernández-Restrepo M, Lombard L, Groenewald JZ (2018) New and interesting fungi. 1. Fungal Systematics and Evolution 1(1): 169–215. https://doi.org/10.3114/fuse.2018.01.08

Crous PW, Carnegie AJ, Wingfield MJ, Sharma R, Mughini G, Noordeloos ME, Santini A, Shouche YS, Bezerra JDP, Dima B, Guarnaccia V, Imrefi I, Jurjević Ž, Knapp DG, Kovács GM, Magistà D, Perrone G, Rämä T, Rebriev YA, Shivas RG, Singh SM, Souza-Motta CM, Thangavel R, Adhapure NN, Alexandrova AV, Alfenas AC, Alfenas RF, Alvarado P, Alves AL, Andrade DA, Andrade JP, Barbosa RN, Barili A, Barnes CW, Baseia IG, Bellanger JM, Berlanas C, Bessette AE, Bessette AR, Biketova AYu, Bomfim FS, Brandrud TE, Bransgrove K, Brito ACQ, Cano-Lira JF, Cantillo T, Cavalcanti AD, Cheewangkoon R, Chikowski RS, Conforto C, Cordeiro TRL, Craine JD, Cruz R, Damm U, de Oliveira RJV, de Souza

JT, de Souza HG, Dearnaley JDW, Dimitrov RA, Dovana F, Erhard A, Esteve-Raventós F, Félix CR, Ferisin G, Fernandes RA, Ferreira RJ, Ferro LO, Figueiredo CN, Frank JL, Freire KTLS, García D, Gené J, Gęsiorska A, Gibertoni TB, Gondra RAG, Gouliamova DE, Gramaje D, Guard F, Gusmão LFP, Haitook S, Hirooka Y, Houbraken J, Hubka V, Inamdar A, Iturriaga T, Iturrieta-González I, Jadan M, Jiang N, Justo A, Kachalkin AV, Kapitonov VI, Karadelev M, Karakehian J, Kasuya T, Kautmanová I, Kruse J, Kušan I, Kuznetsova TA, Landell MF, Larsson KH, Lee HB, Lima DX, Lira CRS, Machado AR, Madrid H, Magalhães OMC, Majerova H, Malysheva EF, Mapperson RR, Marbach PAS, Martín MP, Martín-Sanz A, Matočec N, McTaggart AR, Mello JF, Melo RFR, Mešič A, Michereff SJ, Miller AN, Minoshima A, Molinero-Ruiz L, Morozova OV, Mosoh D, Nabe M, Naik R, Nara K, Nascimento SS, Neves RP, Olariaga I, Oliveira RL, Oliveira TGL, Ono T, Ordoñez ME, de M Ottoni A, Paiva LM, Pancorbo F, Pant B, Pawłowska J, Peterson SW, Raudabaugh DB, Rodríguez-Andrade E, Rubio E, Rusevska K, Santiago ALCMA, Santos ACS, Santos C, Sazanova NA, Shah S, Sharma J, Silva BDB, Siquier JL, Sonawane MS, Stchigel AM, Svetasheva T, Tamakeaw N, Telleria MT, Tiago PV, Tian CM, Tkalčec Z, Tomashevskaya MA, Truong HH, Vecherskii MV, Visagie CM, Vizzini A, Yilmaz N, Zmitrovich IV, Zvyagina EA, Boekhout T, Kehlet T, Læssøe T, Groenewald JZ (2019) Fungal Planet description sheets: 868–950. Persoonia 39: 291–473. https://doi.org/10.3767/persoonia.2019.42.11

Crous PW, Hernández-Restrepo M, Schumacher RK, Cowan DA, Maggs-Kölling G, Marais E, Wingfield MJ, Yilmaz N, Adan OCG, Akulov A, Duarte EÁ, Berraf-Tebbal A, Bulgakov TS, Carnegie AJ, de Beer ZW, Decock C, Dijksterhuis J, Duong TA, Eichmeier A, Hien LT, Houbraken JAMP, Khanh TN, Liem NV, Lombard L, Lutzoni FM, Miadlikowska JM, Nel WJ, Pascoe IG, Roets F, Roux J, Samson RA, Shen M, Spetik M, Thangavel R, Thanh HM, Thao LD, van Nieuwenhuijzen EJ, Zhang JQ, Zhang Y, Zhao LL, Groenewald JZ (2021) New and interesting fungi. 4. Fungal Systematics and Evolution 7(1): 255–343. https://doi.org/10.3114/fuse.2021.07.13

Donk MA (1968) Report of the committee for fungi and lichen 1964–1968. Taxon 17(5): 578–581. https://doi.org/10.2307/1216075

Furlanetto C, Dianese JC (1998) Some coelomycetes from Central Brazil. Mycological Research 102(1): 19–29. https://doi.org/10.1017/S0953756297004656

Glienke C, Pereira OL, Stringari D, Fabris J, Kava-Cordeiro V, Galli-Terasawa L, Cunnington J, Shivas RG, Groenewald JZ, Crous PW (2011) Endophytic and pathogenic *Phyllosticta* species, with reference to those associated with citrus black spot. Persoonia 26(1): 47–56. https://doi.org/10.3767/003158511X569169

Guarnaccia V, Groenewald JZ, Li H, Glienke C, Carstens E, Hattingh V, Fourie PH, Crous PW (2017) First report of *Phyllosticta citricarpa* and description of two new species, *P. paracapitalensis* and *P. paracitricarpa*, from citrus in Europe. Studies in Mycology 87(1): 161–185. https://doi.org/10.1016/j.simyco.2017.05.003

Guo LD, Hyde KD, Liew ECY (2000) Identification of endophytic fungi from *Livistona chinensis* based on morphology and rDNA sequences. The New Phytologist 147(3): 617–630. https://doi.org/10.1046/j.1469-8137.2000.00716.x

Hattori Y, Motohashi K, Tanaka K, Nakashima C (2020) Taxonomical re-examination of the genus *Phyllosticta* – Parasitic fungi on Cupressaceae trees in Japan. Forest Pathology 50(5): 1–14. https://doi.org/10.1111/efp.12630

Hennings P (1908) Fungi *S. paulenses* IV a cl. *Puttmans collecti*. Hedwigia 48: e13.

Hongsanan S, Hyde KD, Phookamsak R, Wanasinghe DN, McKenzie EHC, Sarma VV, Boonmee S, Lücking R, Bhat DJ, Liu NG, Tennakoon DS, Pem D, Karunarathna A, Jiang SH, Jones EBG, Phillips AJL, Manawasinghe IS, Tibpromma S, Jayasiri SC, Sandamali DS, Jayawardena RS, Wijayawardene NN, Ekanayaka AH, Jeewon R, Lu YZ, Dissanayake AJ, Zeng XY, Luo ZL, Tian Q, Phukhamsakda C, Thambugala KM, Dai DQ, Chethana KWT, Samarakoon MC, Ertz D, Bao DF, Doilom M, Liu JK, PérezOrtega S, Suija A, Senwanna C, Wijesinghe SN, Konta S, Niranjan M, Zhang SN, Ariyawansa HA, Jiang HB, Zhang JF, Norphanphoun C, de Silva NI, Thiyagaraja V, Zhang H, Bezerra JDP, Miranda-González R, Aptroot A, Kashiwadani H, Harishchandra D, Sérusiaux E, Aluthmuhandiram JVS, Abeywickrama PD, Devadatha B, Wu HX, Moon KH, Gueidan C, Schumm F, Bundhun D, Mapook A, Monkai J, Chomnunti P, Suetrong S, Chaiwan N, Dayarathne MC, Yang J, Rathnayaka AR, Bhunjun CS, Xu JC, Zheng JS, Liu G, Feng Y, Xie N (2020) Refined families of Dothideomycetes: Dothideomycetidae and Pleosporomycetidae. Mycosphere 11(1): 1553–2107. https://doi.org/10.5943/mycosphere/11/1/13

Huelsenbeck JP, Ronquist F (2001) MRBAYES: Bayesian inference of phylogeny. Bioinformatics 17(17): 754–755. https://doi.org/10.1093/bioinformatics/17.8.754

Jeewon R, Hyde KD (2016) Establishing species boundaries and new taxa among fungi: Recommendations to resolve taxonomic ambiguities. Mycosphere 7(11): 1669–1677. https://doi.org/10.5943/mycosphere/7/11/4

Jiang N, Voglmayr H, Bian DR, Piao CG, Wang SK, Li Y (2021) Morphology and phylogeny of *Gnomoniopsis* (Gnomoniaceae, Diaporthales) from Fagaceae leaves in China. Journal of Fungi 7(10): e792. https://doi.org/10.3390/jof7100792

Katoh K, Rozewicki J, Yamada KD (2019) MAFFT online service: Multiple sequence alignment, interactive sequence choice and visualization. Briefings in Bioinformatics 20(4): 1160–1166. https://doi.org/10.1093/bib/bbx108

Kumar S, Stecher G, Tamura K (2016) MEGA7: Molecular evolutionary genetics analysis version 7.0 for bigger datasets. Molecular Biology and Evolution 33(7): 1870–1874. https://doi.org/10.1093/molbev/msw054

Liao YM, Wang ZX, Wei MC, Wang C (2020) First report of *Phyllosticta capitalensis* causing black spot disease on *Psidium guajava* in mainland China. Plant Disease 104(12): e3252. https://doi.org/10.1094/PDIS-02-20-0338-PDN

Lin S, Sun X, He W, Zhang Y (2017) Two new endophytic species of *Phyllosticta* (Phyllostictaceae, Botryosphaeriales) from southern China. Mycosphere 8(2): 1273–1288. https://doi.org/10.5943/mycosphere/8/2/11

Liu JK, Phookamsak R, Doilom M, Wikee S, Li YM, Ariyawansha H, Boonmee S, Chomnunti P, Dai DQ, Bhat JD, Romero AI, Zhuang WY, Monkai J, Jones EBG, Chukeatirote E, Zhao YC, Wang Y, Hyde KD (2012) Toward a natural classification of Botryosphaeriales. Fungal Diversity 57(1): 149–210. https://doi.org/10.1007/s13225-012-0207-4

Marin-Felix Y, Hernández-Restrepo M, Iturrieta-Gonzalez I, García D, Gené J, Groenewald JZ, Cai L, Chen Q, Quaedvlieg W, Schumacher RK, Taylor PWJ, Ambers C, Bonthond G, Edwards J, Krueger-Hadfield SA, Luangsa-ard JJ, Morton L, Moslemi A, Sandoval-Denis M, Tan YP, Thangavel R, Vaghefi N, Cheewangkoon R, Crous PW (2019) Genera

of phytopathogenic fungi: GOPHY 3. Studies in Mycology 94(1): 1–124. https://doi.org/10.1016/j.simyco.2019.05.001

Miller MA, Pfeiffer W, Schwartz T (2012) The CIPRES science gateway: enabling high-impact science for phylogenetics researchers with limited resources. In: Proceedings of the 1st Conference of the Extreme Science and Engineering Discovery Environment. Bridging from the extreme to the campus and beyond. Association for Computing Machinery, USA, 1–8. https://doi.org/10.1145/2335755.2335836

Motohashi K, Anzai K, Nakashima C (2008) Four new species of *Phyllosticta*, one new species of *Pseudocercospora*, and one new combination in *Passalora* from Japan. Mycoscience 49(2): 138–146. https://doi.org/10.1007/S10267-007-0395-Z

Motohashi K, Inaba S, Anzai K, Takamatsu S, Nakashima C (2009) Phylogenetic analyses of Japanese species of *Phyllosticta* sensu stricto. Mycoscience 50(4): 291–302. https://doi.org/10.1007/S10267-009-0487-Z

Myllys L, Stenroos S, Thell A (2002) New genes for phylogenetic studies of lichenized fungi, glyceraldehyde-3-phosphate dehydrogenase and beta-tubulin genes. Lichenologist (London, England) 34(3): 237–246. https://doi.org/10.1006/lich.2002.0390

Nasehi A, Sathyapriya H, Wong MY (2019) First report of leaf spot on oil palm caused by *Phyllosticta capitalensis* in Malaysia. Plant Disease 103(11): 2964. https://doi.org/10.1094/PDIS-04-19-0768-PDN

Norphanphoun C, Hongsanan S, Gentekaki E, Chen YJ, Kuo CH, Hyde KD (2020) Differentiation of species complexes in *Phyllosticta* enables better species resolution. Mycosphere 11(1): 2542–2628. https://doi.org/10.5943/mycosphere/11/1/16

Nylander JAA (2004) MrModelTest v. 2. Program distributed by the author. Evolutionary Biology Centre, Uppsala University.

O'Donnell K, Kistler HC, Cigelnik E, Ploetz RC (1998) Multiple evolutionary origins of the fungus causing panama disease of banana: Concordant evidence from nuclear and mitochondrial gene genealogies. Proceedings of the National Academy of Sciences of the United States of America 95(5): 2044–2049. https://doi.org/10.1073/pnas.95.5.2044

Okane I, Nakagiri A, Ito T (2001) Identity of *Guignardia* sp. inhabiting ericaceous plants. Canadian Journal of Botany 79(1): 101–109. https://doi.org/10.1139/b00-136

Okane I, Lumyong S, Ito T, Nakagiri A (2003) Extensive host range of an endophytic fungus, *Guignardia endophyllicola* (anamorph, *Phyllosticta capitalensis*). Mycoscience 44(5): 353–363. https://doi.org/10.1007/S10267-003-0128-X

Persoon CH (1818) Traité sur les champignons comestibles, contenant l'indication des espèces nuisibles; a l'histoire des champignons. Belin-Leprieur, Paris, France. https://doi.org/10.5962/bhl.title.110115

Ronquist F, Huelsenbeck JP (2003) MrBayes 3: Bayesian phylogenetic inference under mixed models. Bioinformatics 19(12): 1572–1574. https://doi.org/10.1093/bioinformatics/btg180

Ronquist F, Teslenko M, van der Mark P, Ayres DL, Darling A, Höhna S, Larget B, Liu L, Suchard MA, Huelsenbeck JP (2012) MrBayes 3.2: Efficient Bayesian phylogenetic inference and model choice across a large model space. Systematic Biology 61(3): 539–542. https://doi.org/10.1093/sysbio/sys029

Schoch CL, Shoemaker RA, Seifert KA, Hambleton S, Spatafora JW, Crous PW (2006) A multigene phylogeny of the Dothideomycetes using four nuclear loci. Mycologia 98(6): 1041–1052. https://doi.org/10.1080/15572536.2006.11832632

Seaver FJ (1922) Phyllostictaceae. North American Flora 6: 3–84.

Stamatakis A (2014) RAxML version 8: A tool for phylogenetic analysis and post-analysis of large phylogenies. Bioinformatics 30(9): 1312–1313. https://doi.org/10.1093/bioinformatics/btu033

Su YY, Cai L (2012) Polyphasic characterisation of three new *Phyllosticta* spp. Persoonia 28(1): 76–84. https://doi.org/10.3767/003158512X645334

Tang JR, Liu YL, Yin XG, Lu JN, Zhou YH (2020) First report of castor dark leaf spot caused by *Phyllosticta capitalensis* in Zhanjiang, China. Plant Disease 104(6): 1856. https://doi.org/10.1094/PDIS-11-19-2490-PDN

Tran NT, Miles AK, Dietzgen RG, Drenth A (2019) *Phyllosticta capitalensis* and *P. paracapitalensis* are endophytic fungi that show potential to inhibit pathogenic *P. citricarpa* on citrus. Australasian Plant Pathology 48(3): 281–296. https://doi.org/10.1007/s13313-019-00628-0

van der Aa HA (1973) Studies in *Phyllosticta*. Studies in Mycology 5: 1–110.

van der Aa HA, Vanev S (2002) A revision of the species described in *Phyllosticta*. Utrecht, The Netherlands: Centraalbureau voor Schimmelcultures (CBS).

Wang X, Chen G, Huang F, Zhang J, Hyde KD, Li H (2012) *Phyllosticta* species associated with citrus diseases in China. Fungal Diversity 52(1): 209–224. https://doi.org/10.1007/s13225-011-0140-y

Wang Y, Jin L, Chen XR, Lin L, Chen HG (2013) *Phyllosticta ephedricola* sp. nov. on *Ephedra intermedia*. Mycotaxon 125(1): 165–167. https://doi.org/10.5248/125.165

White T, Burns T, Lee S, Taylor J (1990) Amplification and direct sequencing of ribosomal RNA genes for phylogenetics. In: Innis MA (Ed.) PCR Protocols: A Guide to Methods and Applications. Academic Press, New York, 315–322. https://doi.org/10.1016/B978-0-12-372180-8.50042-1

Wijayawardene NN, Hyde KD, Al-Ani LKT, Tedersoo L, Haelewaters D, Rajeshkumar KC, Zhao RL, Aptroot A, Leontyev DV, Saxena RK, Tokarev YS, Dai DQ, Letcher PM, Stephenson SL, Ertz D, Lumbsch HT, Kukwa M, Issi IV, Madrid H, Phillips AJL, Selbmann L, Pfliegler WP, Horváth E, Bensch K, Kirk PM, Kolaříková K, Raja HA, Radek R, Papp V, Dima B, Ma J, Malosso E, Takamatsu S, Rambold G, Gannibal PB, Triebel D, Gautam AK, Avasthi S, Suetrong S, Timdal E, Fryar SC, Delgado G, Réblová M, Doilom M, Dolatabadi S, Pawłowska JZ, Humber RA, Kodsueb R, Sánchez-Castro I, Goto BT, Silva DKA, de Souza FA, Oehl F, da Silva GA, Silva IR, Błaszkowski J, Jobim K, Maia LC, Barbosa FR, Fiuza PO, Divakar PK, Shenoy BD, Castañeda-Ruiz RF, Somrithipol S, Lateef AA, Karunarathna SC, Tibpromma S, Mortimer PE, Wanasinghe DN, Phookamsak R, Xu J, Wang Y75, Tian F, Alvarado P, Li DW, Kušan I, Matočec N, Mešić A, Tkalčec Z, Maharachchikumbura SSN, Papizadeh M, Heredia G, Wartchow F, Bakhshi M, Boehm E, Youssef N, Hustad VP, Lawrey JD87, Santiago ALCMA, Bezerra JDP, Souza-Motta CM, Firmino AL, Tian Q, Houbraken J, Hongsanan S, Tanaka K, Dissanayake AJ, Monteiro JS, Grossart HP, Suija A, Weerakoon G, Etayo J, Tsurykau A, Vázquez V, Mungai P, Damm U, Li QR, Zhang H, Boonmee S, Lu YZ, Becerra AG, Kendrick B, Brearley FQ, Motiejūnaitė

J, Sharma B, Khare R, Gaikwad S, Wijesundara DSA, Tang LZ, He MQ, Flakus A, Rodriguez-Flakus P, Zhurbenko MP, McKenzie EHC, Stadler M, Bhat DJ, Liu JK, Raza M, Jeewon R, Nassonova ES, Prieto M, Jayalal RGU, Erdoğdu M, Yurkov A, Schnittler M, Shchepin ON, Novozhilov YK, Silva-Filho AGS, Gentekaki E, Liu P, Cavender JC, Kang Y, Mohammad S, Zhang LF, Xu RF, Li YM, Dayarathne MC, Ekanayaka AH, Wen TC, Deng CY, Pereira OL, Navathe S, Hawksworth DL, Fan XL, Dissanayake LS, Kuhnert E, Grossart HP, Thines M (2020) Outline of fungi and fungus-like taxa. Mycosphere : Journal of Fungal Biology 11(1): 1060–1456. https://doi.org/10.5943/mycosphere/11/1/8

Wikee S, Udayanga D, Crous PW, Chukeatirote E, McKenzie EHC, Bahkali AH, Dai DQ, Hyde KD (2011) *Phyllosticta* – an overview of current status of species recognition. Fungal Diversity 51(1): 43–61. https://doi.org/10.1007/s13225-011-0146-5

Wikee S, Wulandari NF, McKenzie EHC, Hyde KD (2012) *Phyllosticta ophiopogonis* sp. nov. from *Ophiopogon japonicas* (Liliaceae). Saudi Journal of Biological Sciences 19(1): 13–16. https://doi.org/10.1016/j.sjbs.2011.10.003

Wikee S, Lombard L, Nakashima C, Motohashi K, Chukeatirote E, Cheewangkoon R, McKenzie EHC, Hyde KD, Crous PW (2013a) A phylogenetic re-evaluation of *Phyllosticta* (Botryosphaeriales). Studies in Mycology 76: 1–29. https://doi.org/10.3114/sim0019

Wikee S, Lombard L, Crous PW, Nakashima C, Motohashi K, Chukeatirote E, Alias SA, McKenzie EHC, Hyde KD (2013b) *Phyllosticta capitalensis*, a widespread endophyte of plants. Fungal Diversity 60(1): 91–105. https://doi.org/10.1007/s13225-013-0235-8

Wong MH, Crous PW, Henderson J, Groenewald JZ, Drenth A (2012) *Phyllosticta* species associated with freckle disease of banana. Fungal Diversity 56(1): 173–187. https://doi.org/10.1007/s13225-012-0182-9

Wu SP, Liu YX, Yuan J, Wang Y, Hyde KD, Liu ZY (2014) *Phyllosticta* species from banana (*Musa* sp.) in Chongqing and Guizhou Provinces, China. Phytotaxa 188(3): 135–144. https://doi.org/10.11646/phytotaxa.188.3.2

Wulandari NF, Hyde KD, Duong LM, De Gruyter J, Meffert JP, Groenewald JZ, Crous PW (2009) *Phyllosticta citriasiana* sp. nov., the cause of citrus tan spot of *Citrus maxima* in Asia. Fungal Diversity 34: 23–39.

Wulandari NF, Bhat DJ, To-anun C (2013) A modern account of the genus *Phyllosticta*. Plant Pathology & Quarantine 3(2): 145–159. https://doi.org/10.5943/ppq/3/2/4

Zhang Z, Schwartz S, Wagner L, Miller W (2000) A greedy algorithm for aligning DNA sequences. Journal of Computational Biology 7(1–2): 203–214. https://doi.org/10.1089/10665270050081478

Zhang Y, Crous PW, Schoch CL, Hyde KD (2012) Pleosporales. Fungal Diversity 53(1): 1–221. https://doi.org/10.1007/s13225-011-0117-x

Zhang K, Zhang N, Cai L (2013) Typification and phylogenetic study of *Phyllosticta ampelicida* and *P. vaccinii*. Mycologia 105(4): 1030–1042. https://doi.org/10.3852/12-392

Zhang K, Shivas RG, Cai L (2015) Synopsis of *Phyllosticta* in China. Mycology 6(1): 50–75. https://doi.org/10.1080/21501203.2015.1027507

Zhou N, Chen Q, Carroll G, Zhang N, Shivas RG, Cai L (2015) Polyphasic characterization of four new plant pathogenic *Phyllosticta* species from China, Japan, and the United States. Fungal Biology 119(5): 433–446. https://doi.org/10.1016/j.funbio.2014.08.006

Supplementary material 1

The combined ITS, LSU, tef1, ACT and GAPDH sequences

Authors: Zhaoxue Zhang, Xiaoyong Liu, Xiuguo Zhang, Zhe Meng

Data type: Phylogenetic.

Explanation note: The combined ITS, LSU, tef1, ACT and GAPDH sequences.

Link: https://doi.org/10.3897/mycokeys.91.84803.suppl1

MycoKeys 91: 25–47 (2022)
doi: 10.3897/mycokeys.91.84970
https://mycokeys.pensoft.net

RESEARCH ARTICLE

A peer-reviewed open-access journal
MycoKeys
Launched to accelerate biodiversity research

Four new species of *Diaporthe* (Diaporthaceae, Diaporthales) from forest plants in China

Lingxue Cao[1,2,3], Dun Luo[4], Wu Lin[4], Qin Yang[1,2,3*], Xiaojun Deng[5*]

1 *Key Laboratory for Non-Wood Forest Cultivation and Conservation of the Ministry of Education, Central South University of Forestry and Technology, Changsha 410004, China* **2** *Key Laboratory of National Forestry and Grassland Administration for Control of Diseases and Pests of South Plantation, Central South University of Forestry and Technology, Changsha 410004, China* **3** *Hunan Provincial Key Laboratory for Control of Forest Diseases and Pests, Central South University of Forestry and Technology, Changsha 410004, China* **4** *Guangxi State-owned Bobai Forest Farm, Yulin, Guangxi 537600, China* **5** *Guangxi Zhuang Autonomous Region Forestry Research Institute, Nanning 530002, China*

Corresponding authors: Qin Yang (T20192466@csuft.edu.cn), Xiaojun Deng (dengxiaojun2008@sina.com)

Academic editor: Rungtiwa Phookamsak | Received 6 April 2022 | Accepted 13 June 2022 | Published 6 July 2022

Citation: Cao L, Luo D, Lin W, Yang Q, Deng X (2022) Four new species of *Diaporthe* (Diaporthaceae, Diaporthales) from forest plants in China. MycoKeys 91: 25–47. https://doi.org/10.3897/mycokeys.91.84970

Abstract

Species of *Diaporthe* inhabit a wide range of plant hosts as plant pathogens, endophytes and saprobes. During trips to collect forest pathogens in Beijing, Jiangxi, Shaanxi and Zhejiang Provinces in China, 16 isolates of *Diaporthe* were obtained from branch cankers and leaf spots. These isolates were studied by applying a polyphasic approach including morphological, cultural data, and phylogenetic analyses of the nuclear ribosomal internal transcribed spacer (ITS), calmodulin (*cal*), histone H3 (*his3*), partial translation elongation factor-1α (*tef-1a*) and β-tubulin (*tub2*) loci. Results revealed four new taxa, *D. celticola*, *D. meliae*, *D. quercicola*, *D. rhodomyrti* **spp. nov.** and two known species, *D. eres* and *D. multiguttulata*.

Keywords

Diaporthaceae, DNA phylogeny, four new taxa, systematics, taxonomy

* These authors contributed equally to this work.

Introduction

Diaporthe Nitschkes (syn. *Phomopsis*) is a large genus in the Diaporthaceae with plant pathogens, endophytes or saprobes (Muralli et al. 2006; Rossman et al. 2007; Santos and Phillips 2009; Santos et al. 2011; Udayanga et al. 2011, 2014a, b, 2015; Fan et al. 2015, 2018; Du et al. 2016; Dissanayake et al. 2017; Guarnaccia and Crous 2017, 2018; Guarnaccia et al. 2018; Yang et al. 2018, 2020, 2021a, b; Guo et al. 2020; Sun et al. 2021). Currently, more than 1100 epithets for *Diaporthe* and 950 for *Phomopsis* are listed in Index Fungorum (http://www.indexfungorum.org/; accessed 1 April 2022) with names often based on host association.

The family Diaporthaceae was established by von Höhnel (1917) and was accommodated in the order Diaporthales. Wehmeyer (1975) confined this family to include *Diaporthe* and *Mazzantia*. Later, Diaporthaceae was synonymised under Valsaceae (Barr 1978). However, analysis of LSU sequence data of diaporthalean taxa showed the distinct placement of Diaporthaceae in Diaporthales where it formed a well-supported clade (Castlebury et al. 2002). *Diaporthe*, the type genus of Diaporthaceae, is characterised by immersed ascomata and an erumpent pseudostroma with elongated perithecial necks (Gomes et al. 2013). Asci are unitunicate, clavate to cylindrical. Ascospores are fusoid, ellipsoid to cylindrical, hyaline, biseriate to uniseriate in the ascus, sometimes with appendages (Udayanga et al. 2011). The asexual morph is characterised by ostiolate conidiomata, with cylindrical phialides producing three types (alpha, beta, and gamma conidia) of hyaline, aseptate conidia (Udayanga et al. 2011; Gomes et al. 2013).

In China, the classification of *Diaporthe* has been progressing and the basis for the species identification is a combination of morphological, cultural and phylogenetical analyses (Huang et al. 2015; Gao et al. 2017; Guarnaccia and Crous 2017; Yang et al. 2017, 2018, 2020, 2021a, b; Manawasinghe et al. 2019; Jiang et al. 2021; Huang et al. 2021; Sun et al. 2021; Wang et al. 2021). The present study was conducted to identify *Diaporthe* species that cause dieback and leaf spot disease in Beijing, Jiangxi, Shaanxi and Zhejiang Provinces based on modern taxonomic concepts.

Materials and methods

Fungal isolation

From 2018 to 2020, sample collections have been ongoing in Beijing, Jiangxi, Shaanxi and Zhejiang Provinces, China (Table 1). Collected samples were taken to the laboratory for isolation and photographed, documented and then kept at 4 °C for further study.

A total of 16 isolates from host material were obtained by removing a mucoid conidia mass from conidiomata, spreading the suspension on the surface of 1.8% potato dextrose agar (PDA), and incubating at 25 °C for up to 24 h. Single germinating conidium was removed and plated onto fresh PDA plates. Specimens were deposited in the Museums of the Beijing Forestry University (BJFC) and Central South University

Table 1. Isolates and GenBank accession numbers of sequences used in this study.

Species	Isolate	GenBank accession numbers				
		ITS	*cal*	*his3*	*tef-1α*	*tub2*
Diaporthe acaciigena	CBS 129521*	KC343005	KC343247	KC343489	KC343731	KC343973
Diaporthe acericola	MFLUCC 17-0956*	KY964224	KY964137	NA	KY964180	KY964074
Diaporthe acerigena	CFCC 52554*	MH121489	MH121413	MH121449	MH121531	NA
Diaporthe acerigena	CFCC 52555	MH121490	MH121414	MH121450	MH121532	NA
Diaporthe acuta	PSCG 047*	MK626957	MK691125	MK726161	MK654802	MK691225
Diaporthe acutispora	LC6161*	KX986764	KX999274	KX999235	KX999155	KX999195
Diaporthe alangii	CFCC 52556*	MH121491	MH121415	MH121451	MH121533	MH121573
Diaporthe alangii	CFCC 52557	MH121492	MH121416	MH121452	MH121534	MH121574
Diaporthe albosinensis	CFCC 53066*	MK432659	MK442979	MK443004	MK578133	MK578059
Diaporthe albosinensis	CFCC 53067	MK432660	MK442980	MK443005	MK578134	MK578060
Diaporthe alleghaniensis	CBS 495.72*	KC343007	KC343249	KC343491	KC343733	KC343975
Diaporthe ambigua	CBS 114015*	KC343010	KC343252	KC343494	KC343736	KC343978
Diaporthe ampelina	STE-U 2660	AF230751	AY745026	NA	AY745056	JX275452
Diaporthe amygdali	CBS 126679*	MH864208	KC343264	KC343506	KC343748	KC343990
Diaporthe amygdali syn. *D. chongqingensis*	PSCG 435	MK626916	MK691209	MK726257	MK654866	MK691321
Diaporthe amygdali syn. *D. fusicola*	CGMCC 3.17087	KF576281	KF576233	NA	KF576256	KF576305
Diaporthe amygdali syn. *D. garethjonesii*	MFLUCC 12-0542a	KT459423	KT459470	NA	KT459457	KT459441
Diaporthe amygdali syn. *D. kadsurae*	CFCC 52586	MH121521	MH121439	MH121479	MH121563	MH121600
Diaporthe amygdali syn. *D. kadsurae*	CFCC 52587	MH121522	MH121440	MH121480	MH121564	MH121601
Diaporthe amygdali syn. *D. mediterranea*	SAUCC194.111	MT822639	MT855718	MT855606	MT855836	MT855951
Diaporthe amygdali syn. *D. ovoicicola*	CGMCC 3.17093	KF576265	KF576223	NA	KF576240	KF576289
Diaporthe amygdali syn. *D. sterilis*	CBS 136969	KJ160579	KJ160548	MF418350	KJ160611	KJ160528
Diaporthe amygdali syn. *D. ternstroemiae*	CGMCC 3.15183	KC153098	NA	NA	KC153089	NA
Diaporthe anacardii	CBS 720.97*	KC343024	KC343266	KC343508	KC343750	KC343992
Diaporthe angelicae	CBS 111592*	KC343027	KC343269	KC343511	KC343753	KC343995
Diaporthe apiculata	CFCC 53068	MK432651	MK442973	MK442998	MK578127	MK578054
Diaporthe apiculata	CFCC 53069	MK432652	MK442974	MK442999	MK578128	MK578055
Diaporthe aquatic	IFRDCC 3051*	JQ797437	NA	NA	NA	NA
Diaporthe arctii	DP0482*	KJ590736	KJ612133	KJ659218	KJ590776	KJ610891
Diaporthe arecae	CBS 161.64*	KC343032	KC343274	KC343516	KC343758	KC344000
Diaporthe arengae	CBS 114979*	KC343034	KC343276	KC343518	KC343760	KC344002
Diaporthe arezzoensis	MFLUCC 15-0127*	MT185503	NA	NA	NA	NA
Diaporthe aseana	MFLUCC 12-0299a*	KT459414	KT459464	NA	KT459448	KT459432
Diaporthe asheicola	CBS 136967*	KJ160562	KJ160542	NA	KJ160594	KJ160518
Diaporthe aspalathi	CBS 117169*	KC343036	KC343278	KC343520	KC343762	KC344004
Diaporthe australafricana	CBS 111886*	KC343038	KC343280	KC343522	KC343764	KC344006
Diaporthe australiana	CBS 146457*	MN708222	NA	NA	MN696522	MN696530
Diaporthe baccae	CBS 136972*	KJ160565	MG281695	MF418264	KJ160597	MF418509
Diaporthe batatas	CBS 122.21	KC343040	KC343282	KC343524	KC343766	KC344008
Diaporthe bauhiniae	CFCC 53071*	MK432648	MK442970	MK442995	MK578124	MK578051
Diaporthe bauhiniae	CFCC 53072	MK432649	MK442971	MK442996	MK578125	MK578052
Diaporthe beilharziae	BRIP 54792*	JX862529	NA	NA	JX862535	KF170921
Diaporthe benedicti	SBen914*	KM669929	KM669862	NA	KM669785	NA
Diaporthe betulae	CFCC 50469*	KT732950	KT732997	KT732999	KT733016	KT733020
Diaporthe betulae	CFCC 50470	KT732951	KT732998	KT733000	KT733017	KT733021
Diaporthe betulicola	CFCC 51128*	KX024653	KX024659	KX024661	KX024655	KX024657
Diaporthe betulicola	CFCC 51129	KX024654	KX024660	KX024662	KX024656	KX024658
Diaporthe betulina	CFCC 52560*	MH121495	MH121419	MH121455	MH121537	MH121577
Diaporthe betulina	CFCC 52561	MH121496	MH121420	MH121456	MH121538	MH121578
Diaporthe biconispora	ZJUD62*	KJ490597	NA	KJ490539	KJ490476	KJ490418
Diaporthe biguttulata	ZJUD47*	KJ490582	NA	KJ490524	KJ490461	KJ490403
Diaporthe bohemiae	CBS 143347*	MG281015	MG281710	MG281361	MG281536	MG281188
Diaporthe brasiliensis	CBS 133183*	KC343042	KC343284	KC343526	KC343768	KC344010
Diaporthe caatingaensis	URM7486*	KY085927	KY115597	KY115605	KY115603	KY115600
Diaporthe camelliae-sinensis	SAUCC194.92*	MT822620	MT855699	MT855588	MT855932	MT855817
Diaporthe canthi	CPC 19740*	JX069864	KC843174	NA	KC843120	KC843230
Diaporthe caryae	CFCC 52563*	MH121498	MH121422	MH121458	MH121540	MH121580
Diaporthe caryae	CFCC 52564	MH121499	MH121423	MH121459	MH121541	MH121581
Diaporthe cassines	CPC 21916*	KF777155	NA	NA	KF777244	NA

Species	Isolate	GenBank accession numbers				
		ITS	*cal*	*his3*	*tef-1α*	*tub2*
Diaporthe caulivora	CBS 127268*	MH864501	KC343287	KC343529	KC343771	KC344013
Diaporthe celticola	**CFCC 53074***	**MK573948**	**MK574587**	**MK574603**	**MK574623**	**MK574643**
Diaporthe celticola	**CFCC 53075**	**MK573949**	**MK574588**	**MK574604**	**MK574624**	**MK574644**
Diaporthe celticola	**CFCC 53076**	**MK573950**	**MK574589**	**MK574605**	**MK574625**	**MK574645**
Diaporthe cercidis	CFCC 52565*	MH121500	MH121424	MH121460	MH121542	MH121582
Diaporthe cercidis	CFCC 52566	MH121501	MH121425	MH121461	MH121543	MH121583
Diaporthe chamaeropis	CBS 454.81*	KC343048	KC343290	KC343532	KC343774	KC344016
Diaporthe charlesworthii	BRIP 54884m*	KJ197288	NA	NA	KJ197250	KJ197268
Diaporthe chensiensis	CFCC 52567*	MH121502	MH121426	MH121462	MH121544	MH121584
Diaporthe chensiensis	CFCC 52568	MH121503	MH121427	MH121463	MH121545	MH121585
Diaporthe chrysalidocarpi	SAUCC194.35*	MT822563	MT855646	MT855532	MT855760	MT855876
Diaporthe cichorii	MFLUCC 17-1023*	KY964220	KY964133	NA	KY964176	KY964104
Diaporthe cinnamomi	CFCC 52569*	MH121504	NA	MH121464	MH121546	MH121586
Diaporthe cinnamomi	CFCC 52570	MH121505	NA	MH121465	MH121547	MH121587
Diaporthe cissampeli	CPC 27302*	KX228273	NA	KX228366	NA	KX228384
Diaporthe citri	AR3405*	KC843311	KC843157	KJ420881	KC843071	KC843187
Diaporthe citri	CFCC 53079	MK573940	MK574579	MK574595	MK574615	MK574635
Diaporthe citriasiana	CGMCC 3.15224*	JQ954645	KC357491	KJ490515	JQ954663	KC357459
Diaporthe citrichinensis	CGMCC 3.15225*	JQ954648	KC357494	KJ420880	JQ954666	KJ490396
Diaporthe collariana	MFLU 17-2770*	MG806115	MG783042	NA	MG783040	MG783041
Diaporthe compactum	LC3083*	KP267854	NA	KP293508	KP267928	KP293434
Diaporthe conica	CFCC 52571*	MH121506	MH121428	MH121466	MH121548	MH121588
Diaporthe conica	CFCC 52572	MH121507	MH121429	MH121467	MH121549	MH121589
Diaporthe constrictospora	CGMCC 3.20096*	MT385947	MT424718	MW022487	MT424682	MT424702
Diaporthe convolvuli	CBS 124654	KC343054	KC343296	KC343538	KC343780	KC344022
Diaporthe coryli	CFCC 53083*	MK432661	MK442981	MK443006	MK578135	MK578061
Diaporthe coryli	CFCC 53084	MK432662	MK442982	MK443007	MK538176	MK578062
Diaporthe corylicola	CFCC 53986*	MW839880	MW836684	MW836717	MW815894	MW883977
Diaporthe corylicola	CFCC 53987	MW839867	MW836685	MW836718	MW815895	MW883978
Diaporthe crotalariae	CBS 162.33*	MH855395	JX197439	KC343540	GQ250307	KC344024
Diaporthe crousii	CAA 823*	MK792311	MK883835	MK871450	MK828081	MK837932
Diaporthe cucurbitae	DAOM 42078*	KM453210	NA	KM453212	KM453211	KP118848
Diaporthe cuppatea	CBS 117499	MH863021	KC343299	KC343541	KC343783	KC344025
Diaporthe cynaroidis	CBS 122676*	KC343058	KC343300	KC343542	KC343784	KC344026
Diaporthe cytosporella	FAU461	KC843307	KC843141	MF418283	KC843116	KC843221
Diaporthe diospyricola	CPC 21169*	KF777156	NA	NA	NA	NA
Diaporthe discoidispora	ZJUD89*	KJ490624	NA	KJ490566	KJ490503	KJ490445
Diaporthe dorycnii	MFLUCC 17-1015*	KY964215	NA	NA	KY964171	KY964099
Diaporthe drenthii	CBS 146453*	MN708229	NA	NA	MN696526	MN696537
Diaporthe durionigena	VTCC 930005*	MN453530	NA	NA	MT276157	MT276159
Diaporthe elaeagni-glabrae	LC4802*	KX986779	KX999281	KX999251	KX999171	KX999212
Diaporthe endophytica	CBS 133811*	KC343065	KC343307	KC343549	KC343791	KC344033
Diaporthe eres	AR5193*	KJ210529	KJ434999	KJ420850	KJ210550	KJ420799
Diaporthe eres	AR5211	KJ210538	KJ435043	KJ420875	KJ210559	KJ420828
Diaporthe eres	CBS 587.79	KC343153	KC343395	KC343637	KC343879	KC344121
Diaporthe eres	CFCC 52575	MH121510	NA	MH121470	MH121552	MH121592
Diaporthe eres	CFCC 52576	MH121511	MH121432	MH121471	MH121553	MH121593
Diaporthe eres	CFCC 52577	MH121512	MH121433	MH121472	MH121554	MH121594
Diaporthe eres	CFCC 52578	MH121513	MH121434	MH121473	MH121555	MH121595
Diaporthe eres	CFCC 52579	MH121514	NA	MH121474	MH121556	NA
Diaporthe eres	CFCC 52580	MH121515	NA	MH121475	MH121557	MH121596
Diaporthe eres	CFCC 52581	MH121516	NA	MH121476	MH121558	MH121597
Diaporthe eres	CGMCC 3.15181	KC153096	NA	NA	KC153087	KF576312
Diaporthe eres	CGMCC 3.17081	KF576282	NA	NA	KF576257	KF576306
Diaporthe eres	CGMCC 3.17089	KF576267	NA	NA	KF576242	KF576291
Diaporthe eres	DAOM 695742	KU552025	NA	NA	KU552023	KU574615
Diaporthe eres	MAFF 625034	JQ807469	KJ435023	KJ420868	JQ807418	KJ420819
Diaporthe eres	MFLU 17-0646	MG828895	MG829274	NA	MG829270	MG843877
Diaporthe eres	MFLUCC 16-0113	KU557563	KU557611	NA	KU557631	KU557587
Diaporthe eres	MFLUCC 17-0963	KY964190	KY964116	NA	KY964146	KY964073
Diaporthe eres syn. *D. alnea*	CBS 146.46	KC343008	KC343250	KC343492	KC343734	KC343976

Species	Isolate	GenBank accession numbers				
		ITS	*cal*	*his3*	*tef-1α*	*tub2*
Diaporthe eres syn. *D. camptothecicola*	CFCC 51632	KY203726	KY228877	KY228881	KY228887	KY228893
Diaporthe eres syn. *D. celastrina*	CBS 139.27	KC343047	KC343289	KC343531	KC343773	KC344015
Diaporthe eres syn. *D. celeris*	CBS 143349	MG281017	MG281712	MG281363	MG281538	MG281190
Diaporthe eres syn.*D. ellipicola*	CGMCC 3.17084	KF576270	NA	NA	KF576245	KF576294
Diaporthe eres syn. D. neilliae	CBS 144.27	KC343144	KC343386	KC343628	KC343870	KC344112
Diaporthe eres syn. *D. pulla*	CBS 338.89	KC343152	KC343394	KC343636	KC343878	KC344120
Diaporthe eres	**CSUFTCC101**	**ON076564**	**NA**	**ON081664**	**ON081656**	**NA**
Diaporthe eres	**CSUFTCC102**	**ON076565**	**NA**	**ON081665**	**ON081657**	**NA**
Diaporthe eres	**CSUFTCC103**	**ON076566**	**NA**	**ON081666**	**ON081658**	**NA**
Diaporthe eucalyptorum	CBS 132525*	MH305525	NA	NA	NA	NA
Diaporthe foeniculacea	CBS 111553*	KC343101	KC343343	KC343585	KC343827	KC344069
Diaporthe fraxini-angustifoliae	BRIP 54781*	JX862528	NA	NA	JX862534	KF170920
Diaporthe fraxinicola	CFCC 52582*	MH121517	MH121435	NA	MH121559	NA
Diaporthe fraxinicola	CFCC 52583	MH121518	MH121436	NA	MH121560	NA
Diaporthe fructicola	MAFF 246408*	LC342734	LC342738	LC342737	LC342735	LC342736
Diaporthe fulvicolor	PSCG 051*	MK626859	MK691132	MK726163	MK654806	MK691236
Diaporthe ganjae	CBS 180.91*	KC343112	KC343354	KC343596	KC343838	KC344080
Diaporthe ganzhouensis	CFCC 53087*	MK432665	MK442985	MK443010	MK578139	MK578065
Diaporthe ganzhouensis	CFCC 53088	MK432666	MK442986	MK443011	MK578140	MK578066
Diaporthe goulteri	BRIP 55657a*	KJ197290	NA	NA	KJ197252	KJ197270
Diaporthe grandiflori	SAUCC194.84*	MT822612	MT855691	MT855580	MT855809	MT855924
Diaporthe guangxiensis	JZB320087	MK335765	MK736720	NA	MK500161	MK523560
Diaporthe gulyae	BRIP 54025	JF431299	NA	NA	JN645803	KJ197271
Diaporthe guttulata	CGMCC 3.20100*	MT385950	MW022470	MW022491	MT424685	MT424705
Diaporthe helianthi	CBS 592.81*	KC343115	KC343357	KC343599	KC343841	KC344083
Diaporthe heliconiae	SAUCC194.77*	MT822605	MT855684	MT855573	MT855802	MT855917
Diaporthe heterophyllae	CPC 26215*	MG600222	MG600218	MG600220	MG600224	MG600226
Diaporthe heterostemmatis	SAUCC194.85*	MT822613	MT855692	MT855581	MT855810	MT855925
Diaporthe hickoriae	CBS 145.26*	KC343118	KC343360	KC343620	KC343844	KC344086
Diaporthe hispaniae	CBS 143351*	MG281123	MG281820	MG281471	MG281644	MG281296
Diaporthe hongkongensis	CBS 115448*	KC343119	KC343361	KC343603	KC343845	KC344087
Diaporthe hubeiensis	JZB320123*	MK335809	MK500235	NA	MK523570	MK500148
Diaporthe incomplete	LC6754*	KX986794	KX999289	KX999265	KX999186	KX999226
Diaporthe inconspicua	CBS 133813*	KC343123	KC343365	KC343607	KC343849	KC344091
Diaporthe infecunda	CBS 133812*	KC343126	KC343368	KC343610	KC343852	KC344094
Diaporthe irregularis	CGMCC 3.20092*	MT385951	MT424721	NA	MT424686	MT424706
Diaporthe isoberliniae	CPC 22549*	KJ869190	NA	NA	NA	KJ869245
Diaporthe juglandicola	CFCC 51134*	KU985101	KX024616	KX024622	KX024628	KX024634
Diaporthe kochmanii	BRIP 54033*	JF431295	NA	NA	JN645809	NA
Diaporthe kongii	BRIP 54031*	JF431301	NA	NA	JN645797	KJ197272
Diaporthe krabiensis	MFLUCC 17-2481*	MN047100	NA	NA	MN433215	MN431495
Diaporthe lenispora	CGMCC 3.20101*	MT385952	MW022472	MW022493	MT424687	MT424707
Diaporthe litchicola	BRIP 54900*	JX862533	NA	NA	JX862539	KF170925
Diaporthe litchi	SAUCC194.22*	MT822550	MT855635	MT855519	MT855747	MT855863
Diaporthe lithocarpi	CGMCC 3.15175*	KC135104	KF576235	NA	KC153095	KF576311
Diaporthe longicolla	FAU599	KJ590728	KJ612124	KJ659188	KJ590767	KJ610883
Diaporthe longispora	CBS 194.36*	MH855769	KC343377	KC343619	KC343861	KC344103
Diaporthe lusitanicae	CBS 123212*	MH863279	KC343378	KC343620	KC343862	KC344104
Diaporthe lutescens	SAUCC194.36*	MT822564	MT855647	MT855533	MT855761	MT855877
Diaporthe macadamiae	CBS 146455*	MN708230	NA	NA	MN696528	MN696539
Diaporthe macintoshii	BRIP 55064a*	KJ197289	NA	NA	KJ197251	KJ197269
Diaporthe malorum	CAA 734*	KY435638	KY435658	KY435648	KY435627	KY435668
Diaporthe marina	MFLU 17-2622*	MN047102	NA	NA	NA	NA
Diaporthe masirevicii	BRIP 54256*	KJ197276	NA	NA	KJ197238	KJ197256
Diaporthe mayteni	CBS 133185*	KC343139	KC343381	KC343623	KC343865	KC344107
Diaporthe maytenicola	CPC 21896*	KF777157	NA	NA	NA	KF777250
Diaporthe melastomatis	SAUCC194.55*	MT822583	MT855664	MT855551	MT855780	MT855896
Diaporthe melonis	CBS 435.87	KC343141	KC343383	KC343625	KC343867	KC344109
Diaporthe meliae	**CFCC 53089***	**MK432657**	**NA**	**ON081662**	**ON081654**	**MK578057**
Diaporthe meliae	**CFCC 53090**	**MK432658**	**NA**	**ON081663**	**ON081655**	**MK578058**
Diaporthe middletonii	BRIP 54884e*	KJ197286	NA	NA	KJ197248	KJ197266

Species	Isolate	GenBank accession numbers				
		ITS	*cal*	*his3*	*tef-1α*	*tub2*
Diaporthe minima	CGMCC 3.20097*	MT385953	MT424722	MW022496	MT424688	MT424708
Diaporthe minusculata	CGMCC 3.20098*	MT385957	MW022475	MW022499	MT424692	MT424712
Diaporthe miriciae	BRIP 54736j*	KJ197282	NA	NA	KJ197244	KJ197262
Diaporthe multigutullata	CFCC 53095	MK432645	MK442967	MK442992	MK578121	MK578048
Diaporthe multigutullata	CFCC 53096	MK432646	MK442968	MK442993	MK578122	MK578049
Diaporthe multigutullata	**CFCC 53098**	**MK573957**	**MK574592**	**MK574612**	**MK574632**	**MK574652**
Diaporthe multigutullata	**CFCC 53099**	**MK573958**	**MK574593**	**MK574613**	**MK574633**	**MK574653**
Diaporthe multigutullata	**CFCC 53100**	**MK573959**	**MK574594**	**MK574614**	**MK574634**	**MK574654**
Diaporthe musigena	CBS 129519*	KC343143	KC343385	KC343267	KC343869	KC344111
Diaporthe myracrodruonis	URM 7972	MK205289	MK205290	NA	MK213408	MK205291
Diaporthe neoarctii	CBS 109490*	KC343145	KC343387	KC343629	KC343871	KC344113
Diaporthe neoraonikayaporum	MFLUCC 14-1136*	KU712449	KU749356	NA	KU749369	KU743988
Diaporthe nothofagi	BRIP 54801*	JX862530	NA	NA	JX862536	KF170922
Diaporthe novem	CBS 127269	KC343155	KC343397	KC343639	KC343881	KC344123
Diaporthe ocoteae	CPC 26217*	KX228293	NA	NA	NA	KX228388
Diaporthe oraccinii	LC3166*	KP267863	NA	KP293517	KP267937	KP293443
Diaporthe ovalispora	ZJUD93*	KJ490628	NA	KJ490570	KJ490507	KJ490449
Diaporthe oxe	CBS 133186*	KC343164	KC343406	KC343648	KC343890	KC344132
Diaporthe padina	CFCC 52590*	MH121525	MH121443	MH121483	MH121567	MH121604
Diaporthe padina	CFCC 52591	MH121526	MH121444	MH121484	MH121568	MH121605
Diaporthe pandanicola	MFLUCC 17-0607*	MG646974	NA	NA	NA	MG646930
Diaporthe paranensis	CBS 133184*	KC343171	KC343413	KC343655	KC343897	KC344139
Diaporthe parapterocarpi	CPC 22729	KJ869138	NA	NA	NA	KJ869248
Diaporthe parvae	PSCG 035	MK626920	MK691169	MK726211	MK654859	MK691249
Diaporthe pascoei	BRIP 54847*	JX862538	NA	NA	JX862538	KF170924
Diaporthe passiflorae	CPC 19183*	JX069860	KY435644	KY435654	KY435623	KY435674
Diaporthe passifloricola	CPC 27480*	KX228292	NA	KX228367	NA	KX228387
Diaporthe penetriteum	LC3215	KP267879	NA	KP293532	KP267953	NA
Diaporthe perjuncta	CBS 109745*	KC343172	KC343414	KC343656	KC343898	KC344140
Diaporthe perseae	CBS 151.73	KC343173	KC343415	KC343657	KC343899	KC343141
Diaporthe pescicola	MFLUCC 16-0105*	KU557555	KU557603	NA	KU557623	KU557579
Diaporthe phaseolorum	AR4203*	KJ590738	KJ612135	KJ659220	KJ590739	KJ610893
Diaporthe phillipsii	CAA 817*	MK792305	MK883831	MK871445	MK828076	MN000351
Diaporthe podocarpi-macrophylli	LC6155*	KX986774	KX999278	KX999246	KX999167	KX999207
Diaporthe pometiae	SAUCC194.72*	MT822600	MT855679	MT855568	MT855797	MT855912
Diaporthe pseudoalnea	CFCC 54190*	MZ727037	MZ753468	MZ781302	MZ816343	MZ753487
Diaporthe pseudomangiferae	CBS 101339*	KC343181	KC343423	KC343665	KC343907	KC344149
Diaporthe pseudophoenicicola	CBS 176.77	KC343183	KC343425	KC343667	KC343909	KC344151
Diaporthe pseudotsugae	MFLU 15-3228*	KY964225	KY964138	NA	KY964181	KY964108
Diaporthe psoraleae	CPC 21634*	KF777158	NA	NA	KF777245	KF777251
Diaporthe psoraleae-pinnatae	CPC 21638*	KF777159	NA	NA	NA	KF777252
Diaporthe pterocarpi	MFLUCC 10-0575*	JQ619901	JX197453	NA	JX275418	NA
Diaporthe pterocarpicola	MFLUCC 10-0580a*	JQ619887	JX197433	NA	JX275403	JX275441
Diaporthe pungensis	SAUCC194.112*	MT822640	MT855719	MT855607	MT855837	MT855952
Diaporthe pyracanthae	CAA483	KY435635	KY435656	KY435645	KY435625	KY435666
Diaporthe quercicola	**CSUFTCC104***	**ON076567**	**ON081670**	**ON081667**	**ON081659**	**NA**
Diaporthe quercicola	**CSUFTCC105**	**ON076568**	**ON081671**	**ON081668**	**ON081660**	**NA**
Diaporthe quercicola	**CSUFTCC106**	**ON076569**	**ON081672**	**ON081669**	**ON081661**	**NA**
Diaporthe racemosae	CPC 26646*	MG600223	MG600219	MG600221	MG600225	MG600227
Diaporthe raonikayaporum	CBS 133182*	KC343188	KC343430	KC343672	KC343914	KC344156
Diaporthe ravennica	MFLUCC 16-0997	NA	NA	NA	MT394670	NA
Diaporthe rhodomyrti	**CFCC 53101***	**MK432643**	**MK442965**	**MK442990**	**MK578119**	**MK578046**
Diaporthe rhodomyrti	**CFCC 53102**	**MK432644**	**MK442966**	**MK442991**	**MK578120**	**MK578047**
Diaporthe rhusicola	CPC 18191*	JF951146	KC843124	NA	KC843100	KC843205
Diaporthe rosae	MFLUCC 17-2658*	MG828894	MG829273	NA	NA	MG843878
Diaporthe rosiphthora	COAD 2914	MT311197	MT313691	NA	MT313693	NA
Diaporthe rossmaniae	CAA 762*	MK792290	MK883822	MK871432	MK828063	MK837914
Diaporthe rostrata	CFCC 50062*	KP208847	KP208849	KP208851	KP208853	KP208855
Diaporthe rostrata	CFCC 50063	KP208848	KP208850	KP208852	KP208854	KP208856
Diaporthe rudis	AR3422	KC843331	KC843146	NA	KC843090	KC843177
Diaporthe saccarata	CBS 116311*	KC343190	KC343432	KC343674	KC343916	KC344158

Species	Isolate	GenBank accession numbers				
		ITS	*cal*	*his3*	*tef-1α*	*tub2*
Diaporthe sackstonii	BRIP 54669b*	KJ197287	NA	NA	KJ197249	KJ197267
Diaporthe salicicola	BRIP 54825*	JX862531	NA	NA	JX862537	KF170923
Diaporthe sambucusii	CFCC 51986*	KY852495	KY852499	KY852503	KY852507	KY852511
Diaporthe sambucusii	CFCC 51987	KY852496	KY852500	KY852504	KY852508	KY852512
Diaporthe schimae	CFCC 53103*	MK442640	MK442962	MK442987	MK578116	MK578043
Diaporthe schimae	CFCC 53104	MK442641	MK442963	MK442988	MK578117	MK578044
Diaporthe schini	CBS 133181*	KC343191	KC343433	KC343675	KC343917	KC344159
Diaporthe schisandrae	CFCC 51988*	KY852497	KY852501	KY852505	KY852509	KY852513
Diaporthe schisandrae	CFCC 51989	KY852498	KY852502	KY852506	KY852510	KY852514
Diaporthe schoeni	MFLU 15-1279*	KY964226	KY964139	NA	KY964182	KY964109
Diaporthe sclerotioides	CBS 296.67*	MH858974	KC343435	KC343677	KC343919	KC344161
Diaporthe searlei	CBS 146456*	MN708231	NA	NA	NA	MN696540
Diaporthe sennae	CFCC 51636*	KY203724	KY228875	NA	KY228885	KY228891
Diaporthe sennae	CFCC 51637	KY203725	KY228876	NA	KY228886	KY228892
Diaporthe sennicola	CFCC 51634*	KY203722	KY228873	KY228879	KY228883	KY228889
Diaporthe sennicola	CFCC 51635	KY203723	KY228874	KY228880	KY228884	KY228890
Diaporthe serafiniae	BRIP 55665a*	KJ197274	NA	NA	KJ197236	KJ197254
Diaporthe shaanxiensis	CFCC 53106*	MK432654	MK442976	MK443001	MK578130	NA
Diaporthe shaanxiensis	CFCC 53107	MK432655	MK432977	MK432002	MK578131	NA
Diaporthe siamensis	MFLUCC 10-0573a*	JQ619879	JX197423	NA	JX275393	JX275429
Diaporthe silvicola	CFCC 54191*	MZ727041	MZ753472	MZ753481	MZ816347	MZ753491
Diaporthe sojae	FAU635	KJ590719	KJ612116	KJ659208	KJ590762	KJ610875
Diaporthe spartinicola	CPC 24951*	KR611879	NA	KR857696	NA	KR857695
Diaporthe spinosa	PSCG 383*	MK626849	MK691129	MK726156	MK654811	MK691234
Diaporthe stictica	CBS 370.54	KC343212	KC343454	KC343696	KC343938	KC344180
Diaporthe subclavata	ZJUD95*	KJ490630	NA	KJ490572	KJ490509	KJ490451
Diaporthe subcylindrospora	KUMCC 17-0151	MG746629	NA	NA	MG746630	MG746631
Diaporthe subellipicola	KUMCC 17-0153*	MG746632	NA	NA	MG746633	MG746634
Diaporthe subordinaria	CBS 464.90	KC343214	KC343456	KC343698	KC343940	KC344182
Diaporthe taoicola	MFLUCC 16-0117*	KU557567	NA	NA	KU557635	KU557591
Diaporthe tectonae	MFLUCC 12-0777*	KU712430	KU749345	NA	KU749359	KU743977
Diaporthe tectonendophytica	MFLUCC 13-0471*	KU712439	KU749354	NA	KU749367	KU743986
Diaporthe tectonigena	LC6512	KX986782	KX999284	KX999254	KX999174	KX999214
Diaporthe terebinthifolii	CBS 133180*	KC343216	KC343458	KC343700	KC343942	KC344184
Diaporthe thunbergii	MFLUCC 10-0576a*	JQ619893	JX197440	NA	JX275409	JX275449
Diaporthe thunbergiicola	MFLUCC 12-0033*	KP715097	NA	NA	KP715098	NA
Diaporthe tibetensis	CFCC 51999*	MF279843	MF279888	MF279828	MF279858	MF279873
Diaporthe tibetensis	CFCC 52000	MF279844	MF279889	MF279829	MF279859	MF279874
Diaporthe torilicola	MFLUCC 17-1051*	KY964212	KY964127	NA	KY964168	KY964096
Diaporthe toxica	CBS 534.93*	KC343220	KC343462	KC343704	KC343946	KC344188
Diaporthe tulliensis	BRIP 62248a*	KR936130	NA	NA	KR936133	KR936132
Diaporthe ueckerae	FAU656*	KJ590726	KJ612122	KJ659215	KJ590747	KJ610881
Diaporthe ukurunduensis	CFCC 52592*	MH121527	MH121445	MH121485	MH121569	NA
Diaporthe ukurunduensis	CFCC 52593	MH121528	MH121446	MH121486	MH121570	NA
Diaporthe undulate	LC6624*	KX986798	NA	KX999269	KX999190	KX999230
Diaporthe unshiuensis	CFCC 52594	MH121529	MH121447	MH121487	MH121571	MH121606
Diaporthe unshiuensis	CFCC 52595	MH121530	MH121448	MH121488	MH121572	MH121607
Diaporthe vaccinii	CBS 160.32*	KC343228	KC343470	KC343712	KC343954	KC343196
Diaporthe vangueriae	CBS 137985*	KJ869137	NA	NA	NA	KJ869247
Diaporthe vawdreyi	BRIP 57887a*	KR936126	NA	NA	KR936129	KR936128
Diaporthe velutina	LC4421	KX986790	NA	KX999261	KX999182	KX999223
Diaporthe verniciicola	CFCC 53109*	MK573944	MK574583	MK574599	MK574619	MK574639
Diaporthe verniciicola	CFCC 53110	MK573945	MK574584	MK574600	MK574620	MK574640
Diaporthe viniferae	JZB320071	MK341551	MK500119	NA	MK500107	MK500112
Diaporthe virgiliae	CMW 40748	KP247556	NA	NA	NA	KP247575
Diaporthe xishuangbanica	LC6707*	KX986783	NA	KX999255	KX999175	KX999216
Diaporthe xunwuensis	CFCC 53085*	MK432663	MK442983	MK443008	MK578137	MK578063
Diaporthe xunwuensis	CFCC 53086	MK432664	MK442984	MK443009	MK578138	MK578064
Diaporthe yunnanensis	LC6168*	KX986796	KX999290	KX999267	KX999188	KX999228
Diaporthe zaobaisu	PSCG 031*	MK626922	NA	MK726207	MK654855	MK691245
Diaporthella corylina	CBS 121124*	KC343004	KC343246	KC343488	KC343730	KC343972

Strains in this study are marked in bold. NA: Not available. Ex-type/ex-epitype isolates are marked by *.

of Forestry and Technology (CSUFT). Axenic cultures were maintained in the China Forestry Culture Collection Centre (CFCC) and Central South University of Forestry and Technology Culture Collection (CSUFTCC).

Morphological and cultural characterization

Agar plugs (6 mm diam) were taken from the edge of actively growing cultures on PDA and transferred onto the centre of 9 cm diam Petri dishes containing 2% tap water agar supplemented with sterile pine needles (PNA) (Smith et al. 1996) and potato dextrose agar (PDA) and incubated at 25 °C under a 12 h near-ultraviolet light/12 h dark cycle to induce sporulation as described in recent studies (Gomes et al. 2013; Lombard et al. 2014). Colony characters and pigment production on PNA and PDA were noted in the 10-day culture. Colony features were rated according to the color charts of Rayner (1970). Cultures were examined periodically for the development of conidiomata. The microscopic examination was based on the morphological features of conidiomata obtained from the fungal growth mounted in clear lactic acid. At least 30 conidiomata and conidia were measured to calculate the mean size/length. Micro-morphological observations were done at ×1000 magnification using a Leica compound microscope (DM 2500) with interference contrast (DIC) optics. Descriptions, nomenclature, and illustrations of taxonomic novelties were deposited at MycoBank (www.MycoBank.org) (Crous et al. 2004).

DNA extraction, PCR amplification and sequencing

Genomic DNA was extracted from colonies grown on cellophane-covered PDA using a CTAB [cetyltrimethylammonium bromide] method (Doyle and Doyle 1990). For PCR amplifications of phylogenetic markers, five different primer pairs were used (Yang et al. 2018). The PCR conditions were: an initial denaturation step of 8 min at 95 °C followed by 35 cycles of 30 s at 95 °C, 30 s at 51 °C (ITS), 58 °C (*his3*) or 55 °C (*cal*, *tef-1a*, *tub2*), and 1 min at 72 °C, and a final elongation step of 5 min at 72 °C. PCR amplification products were assayed via electrophoresis in 2% agarose gels. DNA sequencing was performed using an ABI PRISM 3730XL DNA Analyzer with a BigDye Terminater Kit v.3.1 (Invitrogen, Waltham, MA, USA) at the Shanghai Invitrogen Biological Technology Company Limited (Beijing, China).

Phylogenetic analyses

The quality of our amplified nucleotide sequences was checked and combined by SeqMan v.7.1.0 and reference sequences (Table 1) were retrieved from the National Center for Biotechnology Information (NCBI), according to recent publications of the genus (Guo et al. 2020; Sun et al. 2021; Yang et al. 2021b). Sequences were aligned using MAFFT v. 6 (Katoh and Toh 2010) and manually corrected using Bioedit 7.0.9.0 (Hall 1999). Phylogenetic analyses were carried out with maximum likelihood analysis

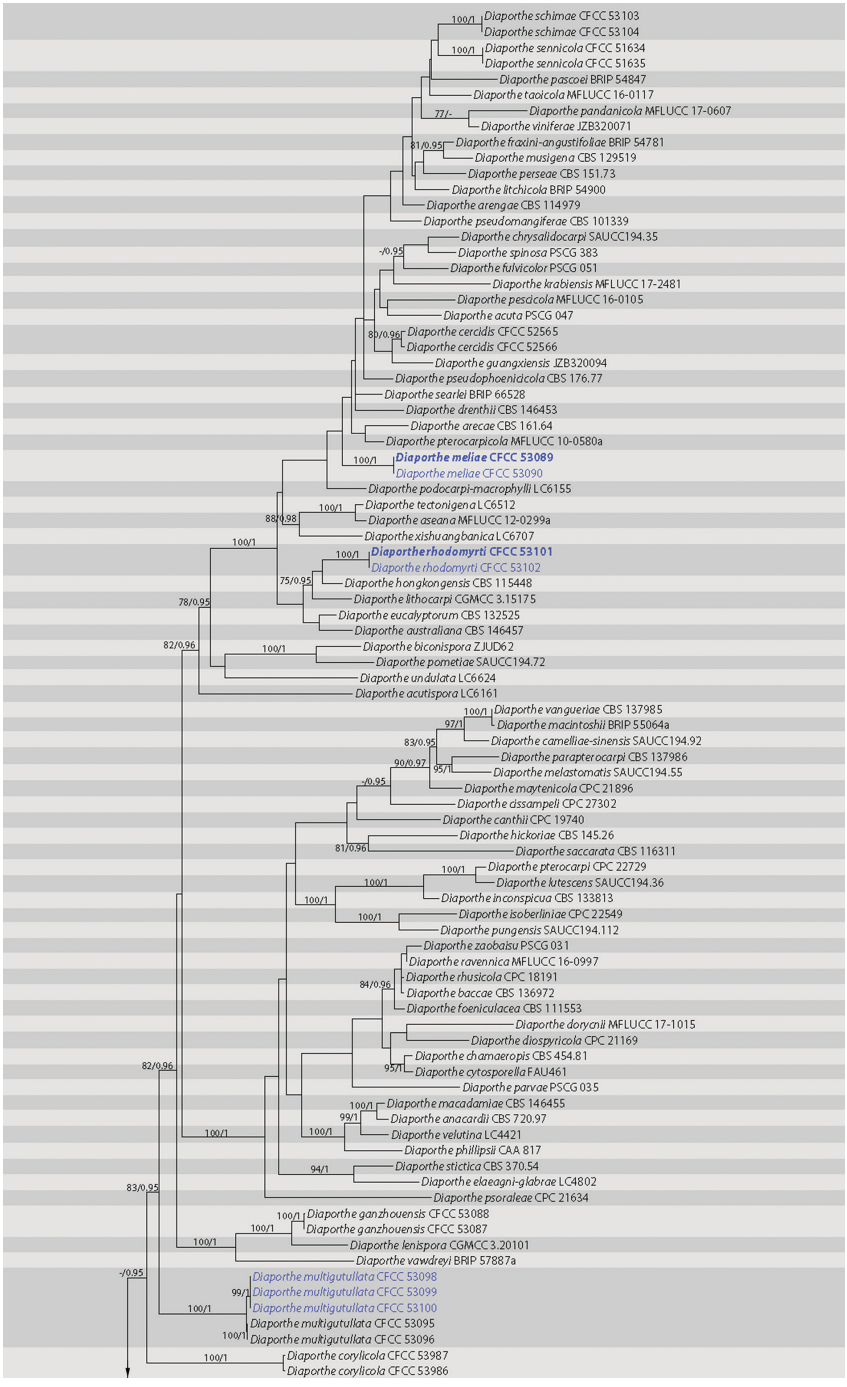

Figure 1. Phylogram of *Diaporthe* resulting from a maximum likelihood analysis based on combined ITS, *cal*, *his3*, *tef-1a* and *tub2*. The tree is rooted with *Diaporthella corylina*. Values above the branches indicate Maximum Likelihood bootstrap (left, ML BP ≥ 75%) and Bayesian probabilities (right, BI PP ≥ 0.95). Strains in current study are in blue and the ex-type cultures are in bold.

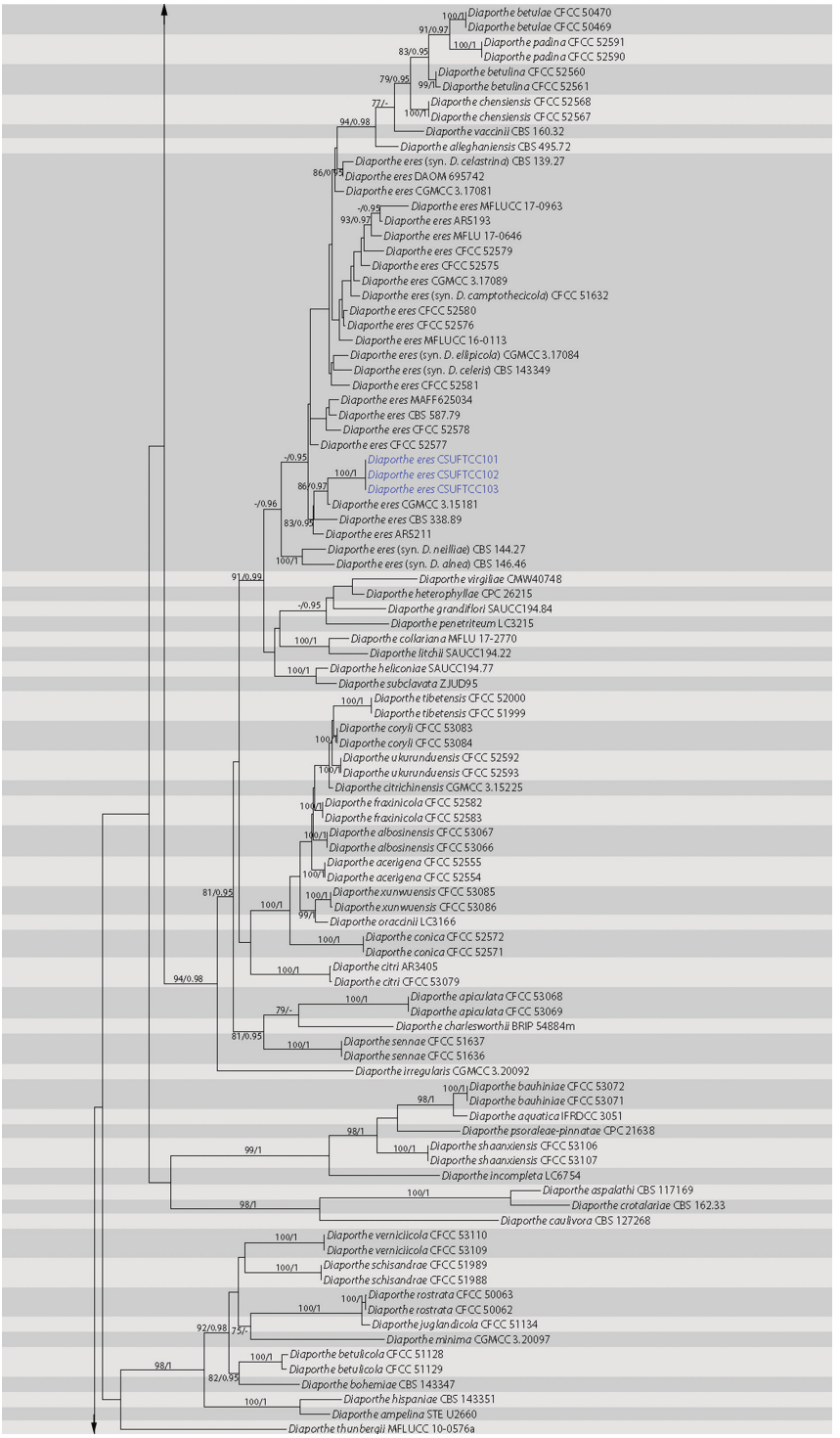

Figure 1. Continued.

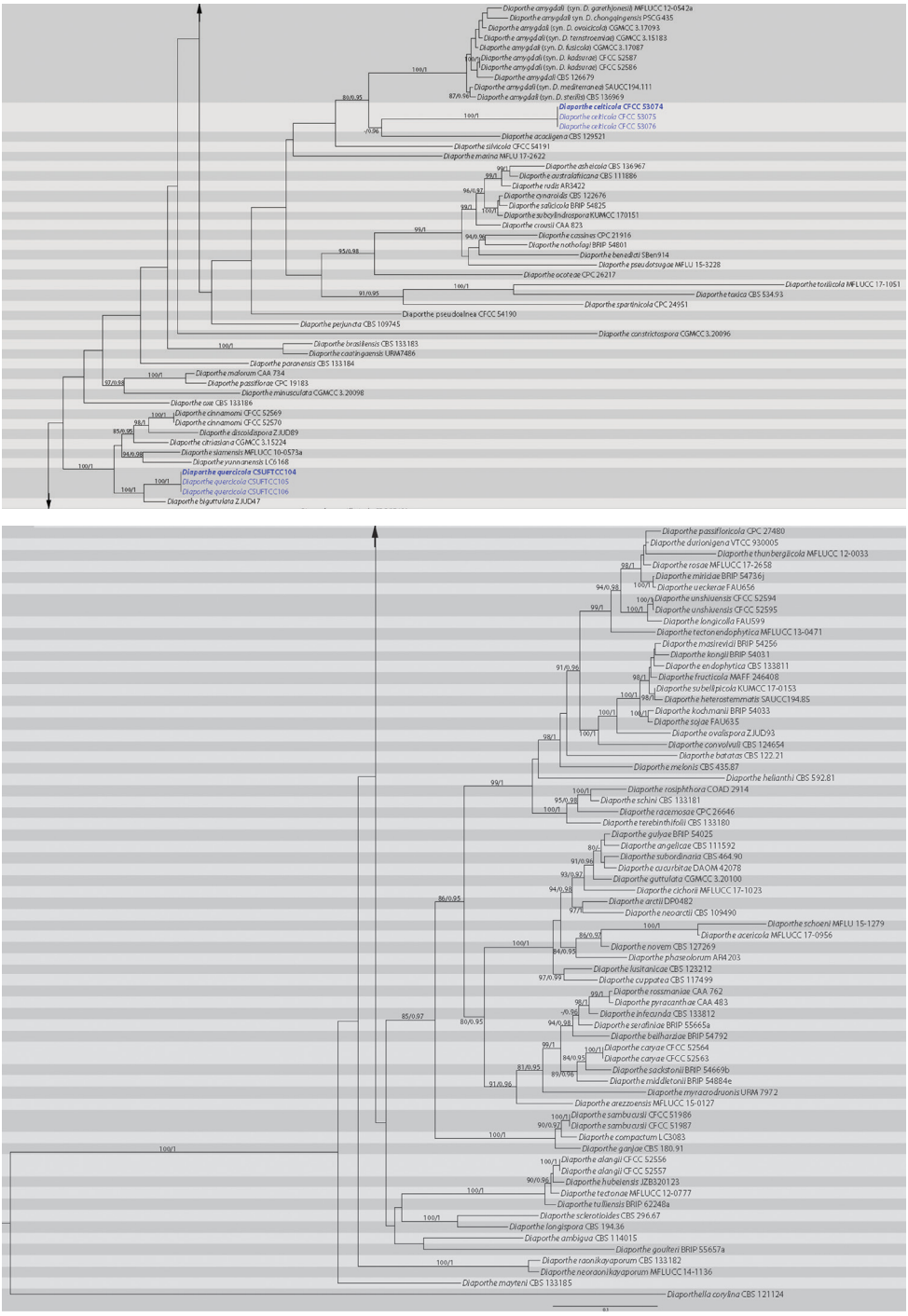

Figure 1. Continued.

(ML), which was performed at the CIPRES web portal (Miller et al. 2010), 1000 rapid bootstrap replicates were run with GTRGAMMA model of nucleotide evolution. Bayesian inference analysis (BI) was performed in MrBayes v. 3.2.0 (Ronquist and Huelsenbeck 2003). The best-fit nucleotide substitution models for each gene were selected using jModelTest v. 2.1.7 (Darriba et al. 2012) under the Akaike Information Criterion. The best nucleotide substitution model for ITS, *his3* and *tub2* was TrN+I+G, while HKY+I+G was selected for both *cal* and *tef-1a*. Phylogenetic trees were viewed in FigTree v1.4. The names of the isolates from the present study are marked in blue in the trees. Maximum likelihood bootstrap support values ≥ 75% (BT) are given at the nodes. Bayesian posterior probabilities ≥ 0.95 (PP) were thickened in the phylogenetic tree. Alignment and trees were deposited in TreeBASE (submission ID: S29621).

Results

Phylogenetic analyses

The sequence datasets for the ITS, *cal*, *his3*, *tef-1a* and *tub2*, were analysed in combination to infer the interspecific relationships within *Diaporthe*. The combined species phylogeny of the *Diaporthe* isolates consisted of 303 sequences, including the outgroup *Diaporthella corylina* (CBS 121124). A total of 2535 characters including gaps (512 for ITS, 524 for *cal*, 525 for *his3*, 463 for *tef-1a*, and 511 for *tub2*) were included in the phylogenetic analysis. Similar tree topologies were obtained by ML and BI methods, and the best scoring ML tree is shown in Fig. 1. The ML analysis yielded a tree with a likelihood value of ln: -76822.498401 and the following model parameters: alpha: 0.508079; Π(A): 0.214617, Π(C): 0.326518, Π(G): 0.235187 and Π(T): 0.223678. The phylogenetic tree inferred from the concatenated alignment resolved the sixteen *Diaporthe* isolates from branch cankers or leaf spots into six well-supported monophyletic clades that represent four novel species and two known species of *Diaporthe* (Fig. 1).

Taxonomy

Diaporthe celticola **C.M. Tian & Q. Yang, sp. nov.**
MycoBank No: 832920
Fig. 2

Diagnosis. Distinguished from the other *Diaporthe* species based on DNA sequence data and characterised by conidiomata with single necks erumpent through the host bark.

Etymology. Named after the host genus on which it was collected, *Celtis*.

Description. ***Conidiomata*** pycnidial, 535–605 × 210–225 μm diam, solitary and with single necks erumpent through host bark. ***Ectostromatic disc*** brown, one ostiole per disc, with yellowish cream conidial drops exuding from the ostioles. Tissue around the neck is cylindrical. ***Locule*** circular, undivided, 350–375 μm diam. ***Conidiophores***

reduced to conidiogenous cells. ***Conidiogenous cells*** unbranched, straight or sinuous, apical or base sometimes swelling, (8–)10.5–13(–14.5) × 1–1.5 µm (n = 30), L/W = 8.5–10.5. ***Alpha conidia*** hyaline, aseptate, ellipsoidal, biguttulate, (5–)6–7 × 3.5–4 µm (n = 30), L/W = 1.5–1.8. ***Beta conidia*** not observed.

Culture characters. Colony originally flat with white fluffy aerial mycelium, becoming light brown to olive-green mycelium with age, marginal area irregularly, with yellowish cream conidial drops exuding from the ostioles.

Specimens examined. China, Zhejiang Province: Hanzhou City, on branches of *Celtis vandervoetiana*, 12 May 2018, *Q. Yang* & *Y.M. Liang* (holotype BJFC-S1616; extype living culture: CFCC 53074; living cultures: CFCC 53075 and CFCC 53076).

Notes. Three strains representing *Diaporthe celticola* cluster in a well-supported clade (ML/BI = 100/1), and appear closely related to *D. acaciigena*. *Diaporthe celticola* can be distinguished based on ITS, *cal*, *his3*, *tef-1a*, and *tub2* loci from *D. acaciigena* (29/473 in ITS, 68/442 in *cal*, 53/460 in *his3*, 79/330 in *tef-1a*, and 49/415 in *tub2*). Morphologically, *D. celticola* is characterised by conidiomata with single necks erumpent through the host bark and can be distinguished from *D. acaciigena* by smaller alpha conidia

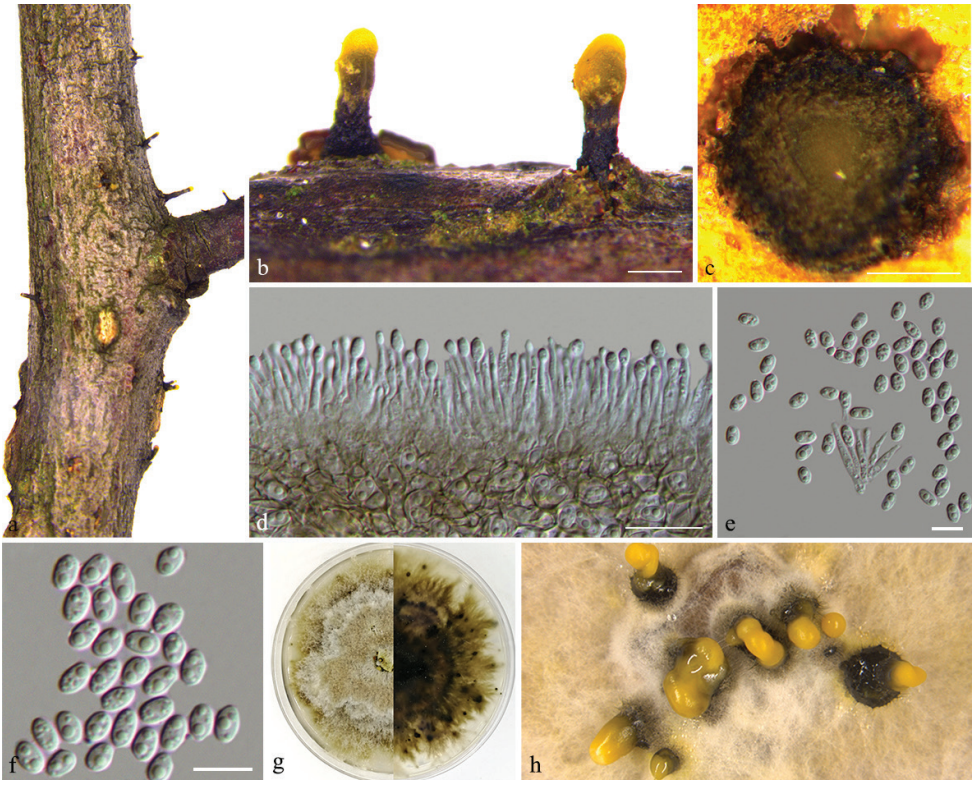

Figure 2. *Diaporthe celticola* (BJFC-S1616) **a, b** habit of conidiomata on twig **c** transverse section through conidiomata **d, e** conidiogenous cells with alpha conidia **f** alpha conidia **g, h** conidiomata formed on PDA. Scale bars: 200 µm (**b, c**); 10 µm (**d–f**).

(6–7 × 3.5–4 vs. 10–11 × 6–6.5 μm) (Crous et al. 2011). This is the first occasion that *Diaporthe* species have been discovered from infected branches on *Celtis vandervoetiana* and demonstrates it to be a new species based on phylogeny and morphology.

Diaporthe eres **Nitschke, Pyrenomyc. Germ. 2: 245, 1870.**

Description. See Udayanga et al. (2014b).

Specimens examined. China. Beijing: Pinggu District, on branches of *Populus* × *xiaohei*, 10 July 2020, *Q. Yang* (CSUFT101; living cultures: CSUFTCC101, CSUFTCC102, and CSUFTCC103).

Notes. *Diaporthe eres* is the type species of the genus and was originally described by Nitschke (1870), from *Ulmus* sp. in Germany, which has a widespread distribution and a broad host range as an endophyte or saprobe, or pathogen causing leaf spots, stem cankers and diseases of woody plants (Udayanga et al. 2014b). In the present study, three isolates (CSUFTCC101, CSUFTCC102, and CSUFTCC103) are embedded into the *D. eres* species based on DNA sequence data (Fig. 1). We therefore describe *D. eres* as a known species for this clade.

Diaporthe meliae **C.M. Tian & Q. Yang, sp. nov.**
MycoBank No: 829523
Fig. 3

Diagnosis. Distinguished from the phylogenetically closely-related species, *D. podocarpi-macrophylli*, in shorter alpha conidia.

Etymology. Named after the host genus on which it was collected, *Melia*.

Description. ***Conidiomata*** pycnidial, immersed in the host bark, scattered, erumpent through the bark surface, discoid, with a single locule. ***Ectostromatic disc*** dark brown, one ostiole per disc, (325–)330–375(–385) μm (n = 30) diam. ***Locule*** undivided, 420–640 × 385–515 μm (n = 30). ***Conidiophores*** reduced to conidiogenous cells. ***Conidiogenous cells*** (13.5–)15–26.5(–28) × 1.3–2.1(–2.3) μm (n = 30), L/W = 8.5–15.5, cylindrical, hyaline, branched, straight or slightly curved, tapering towards the apex. ***Alpha conidia*** hyaline, aseptate, fusiform, multi-guttulate, (6.7–)8–9.5(–10) × (2–)2.1–2.3 μm (n = 30), L/W = 3.4–4.5. ***Beta conidia*** not observed.

Culture characters. Colony originally flat with white felty aerial mycelium, becoming auburn furcate mycelium with age, with irregular margin, conidiomata absent.

Specimens examined. China, Shandong Province: Rizhao City, on branches of *Melia azedarach*, 20 April 2018, *N. Jiang* (holotype BJFC-S1668; ex-type living culture: CFCC 53089; living culture: CFCC 53090).

Notes. Two strains representing *Diaporthe meliae* cluster in a well-supported clade (ML/BI = 100/1), and appear closely related to *D. podocarpi-macrophylli*. *Diaporthe meliae* can be distinguished based on ITS, *his3*, *tef-1a*, and *tub2* loci from *D. podocarpi-macrophylli* (4/459 in ITS, 15/455 in *his3*, 25/349 in *tef-1a*, and 14/401 in *tub2*).

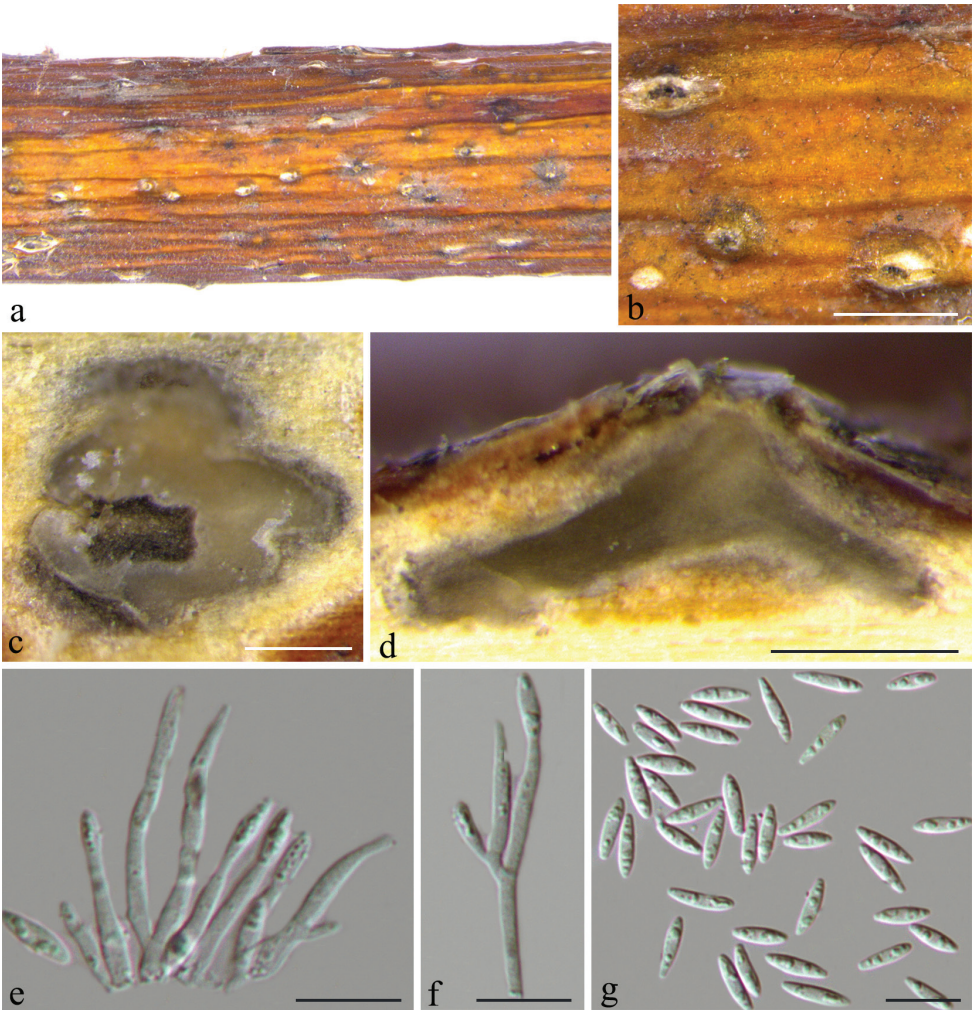

Figure 3. *Diaporthe meliae* (BJFC-S1668) **a, b** habit of conidiomata on twig **c** transverse section through conidiomata **d** longitudinal section through conidiomata **e, f** conidiogenous cells **g** alpha conidia. Scale bars: 1 mm(**b**); 200 μm (**c, d**); 10 μm (**e–g**).

Morphologically, *D. meliae* can be distinguished from *D. podocarpi-macrophylli* by its longer conidiogenous cells (15–26.5 vs. 6–18 μm) and alpha conidia (8–9.5 vs. 3.5–8.5 μm) (Gao et al. 2017).

Diaporthe multiguttulata **F. Huang, K.D. Hyde & Hong Y. Li, Fungal Biology 119(5): 343, 2015.**
Fig. 4

Description. See Yang et al. (2021a).

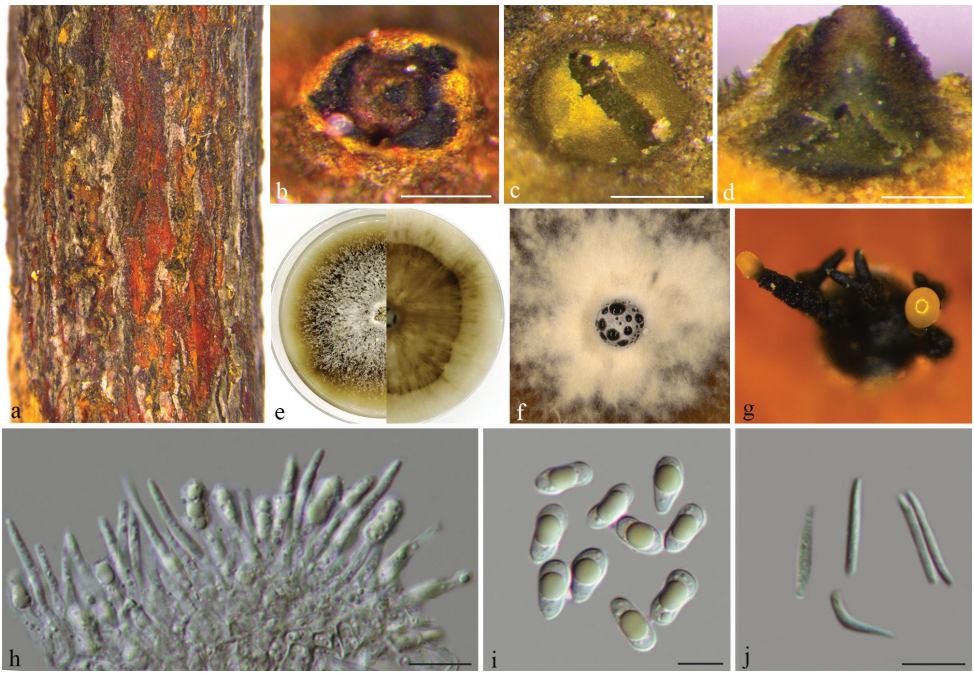

Figure 4. *Diaporthe multiguttulata* (BJFC-S1615) **a, b** habit of conidiomata on twig **c** transverse section through conidiomata **d** longitudinal section through conidiomata **e–g** conidiomata formed on PDA **h** conidiogenous cells **i** alpha conidia **g** beta conidia. Scale bars: 200 μm (**b–d**); 10 μm (**h–j**).

Specimens examined. China, Jiangxi Province: Ganzhou City, on branches of *Citrus maxima*, 11 May 2018, *Q. Yang, & Y.M. Liang* (BJFC-S1615; living cultures: CFCC 53098, CFCC 53099, and CFCC 53100).

Notes. *Diaporthe multiguttulata* is characterised by ellipsoidal alpha conidia with one large guttulate, and was originally described as an endophyte from healthy branch of *Citrus grandis* in Fujian Province, China (Huang et al. 2015). Yang et al. (2021a) identified three isolates from *Citrus maxima* as *D. multiguttulata* based on DNA sequence data and confirmed from the morphological characters. In the present study, isolates (CFCC 53098, CFCC 53099, and CFCC 53100) from an additional specimen were observed and supplemented with beta conidia (Fig. 4j).

Diaporthe quercicola **Q. Yang, sp. nov.**
MycoBank No: 843494
Fig. 5

Diagnosis. Distinguished from the phylogenetically closely-related species, *D. biguttulata*, by its filiform, eguttulate alpha conidia.

Etymology. Named after the host genus on which it was collected, *Quercus*.

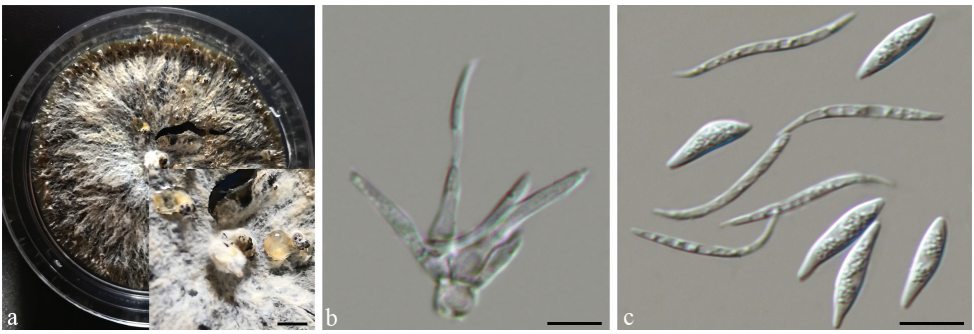

Figure 5. *Diaporthe quercicola* (CSUFTCC104) **a** conidiomata formed on PDA **b** conidiogenous cells **c** alpha and beta conidia. Scale bars: 200 μm (**a**); 10 μm (**b, c**).

Description. On PDA: ***Conidiomata*** pycnidial, 250–330 μm diam, globose, solitary or aggregated, deeply embedded in the medium, erumpent, single or clustered in groups of 3–5 pycnidia, coated with hyphae, cream to yellowish translucent conidial droplets exuded from the ostioles. ***Conidiophores*** reduced to conidiogenous cells. ***Conidiogenous cells*** hyaline, cylindrical, unbranched, straight, tapering towards the apex, (17–)20–26(–34.5) × 2.5–3.5 μm (n = 30), L/W = 6.5–9. ***Alpha conidia*** (6.5–)7–8.5(–9) × (1.5–)2–3 μm (n = 30), L/W = 3–4.5, aseptate, hyaline, fusiform, apex at both ends, eguttulate. ***Beta conidia*** hyaline, aseptate, filiform, straight or sinuous at one end, eguttulate, (21.5–)25.5–31(–33) × 1 μm (n = 30), L/W = 22.5–31.5.

Culture characters. Colony at first white, becoming dark brown with age. Aerial mycelium white, dense, fluffy, with yellowish conidial drops exuding from the ostioles after 20 days.

Specimens examined. China. Shaanxi Province: Xian City, on branches of *Quercus aliena*, 10 July 2020, *Q. Yang* (holotype CSUFTCC104; ex-type living culture: CSUFTCC104; living cultures: CSUFTCC105 and CSUFTCC106).

Notes. Three strains representing *Diaporthe quercicola* cluster in a well-supported clade (ML/BI = 100/1), and appear closely related to *D. biguttulata*. *Diaporthe quercicola* can be distinguished based on ITS, *his3*, and *tef-1a* loci from *D. biguttulata* (8/461 in ITS, 18/448 in *his3*, and 22/325 in *tef-1a*). Morphologically, *D. quercicola* can be distinguished from *D. biguttulata* by its fusiform, eguttulate alpha conidia and narrower beta conidia (1 vs. 0.9–1.6 μm) (Huang et al. 2015).

Diaporthe rhodomyrti **C.M. Tian & Q. Yang, sp. nov.**
MycoBank No: 829525
Fig. 6

Diagnosis. Distinguished from the phylogenetically closely-related species, *D. hongkongensis*, in narrower beta conidia.

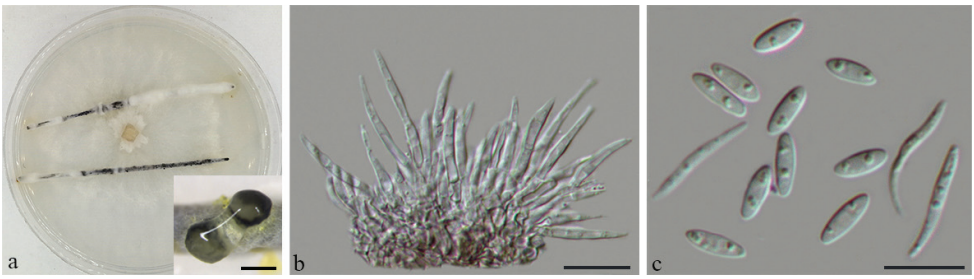

Figure 6. *Diaporthe rhodomyrti* (BJFC-S1660) **a** conidioma formed on PNA **b** conidiogenous cells **c** alpha and beta conidia. Scale bars: 500 μm (**a**); 10 μm (**b, c**).

Etymology. Named after the host genus on which it was collected, *Rhodomyrtus*.

Description. On PNA: ***Conidiomata*** pycnidial, 500–850 μm diam, globose or rostrate, black, erumpent in tissue, erumpent at maturity, often with translucent conidial drops exuding from ostioles. ***Conidiophores*** reduced to conidiogenous cells. ***Conidiogenous cells*** (14.5–)15.5–23(–25.5) × 1.5–2 μm (n = 30), L/W = 8.5–13, cylindrical, hyaline, unbranched, septate, straight, tapering towards the apex. ***Alpha conidia*** abundant in culture, hyaline, aseptate, ellipsoidal, biguttulate, 6–7(–8.5) × 2–2.5(–3) μm (n = 30), L/W = 2.8–3.3. ***Beta conidia*** hyaline, aseptate, filiform, straight to sinuous, eguttulate, (15–)16.5–21.5(–23) × 1–1.5 μm (n = 30), L/W = 15.5–16.5.

Culture characters. Colony entirely white at surface, reverse with pale brown pigmentation, white, fluffy aerial mycelium.

Specimens examined. China. Jiangxi Province: Ganzhou City, on leaves of *Rhodomyrtus tomentosa*, 10 May 2018, *Q. Yang* & *Y.M. Liang* (holotype BJFC-S1660; extype living culture: CFCC 53101; living culture: CFCC 53102).

Notes. This new species is introduced as molecular data, and shows it to be a distinct clade with high support (ML/BI = 100/1) and appears closely related to *Diaporthe hongkongensis*. *Diaporthe rhodomyrti* can be distinguished based on ITS, *cal*, *his3*, *tef-1a*, and *tub2* loci from *D. hongkongensis* (2/463 in ITS, 26/441 in *cal*, 11/434 in *his3*, 10/327 in *tef-1a*, and 2/420 in *tub2*). Morphologically, *D. rhodomyrti* can be distinguished from *D. hongkongensis* by its longer conidiogenous cells (15.5–23 vs. 5–12 μm) and narrower beta conidia (1–1.5 vs. 1.5–2 μm) (Gomes et al. 2013). This is the first time that *Diaporthe* species has been discovered from infected leaves on *Rhodomyrtus tomentosa* and demonstrate it as a new species based on phylogeny and morphology.

Discussion

In this study, investigations of forest pathogens in Beijing, Jiangxi, Shaanxi and Zhejiang Provinces was carried out. Identification of our collections was conducted, based on isolates from fruiting bodies using five combined loci (ITS, *cal*, *his3*, *tef-1a*, and *tub2*), as well as morphological characteristics. It includes *Diaporthe eres* and

D. multiguttulata, as well as four new species named *D. celticola*, *D. meliae*, *D. quercicola*, and *D. rhodomyrti*.

Diaporthe (Diaporthaceae, Sordariomycetes) are species-rich asexual taxa, which are common pathogens that cause a variety of diseases, including dieback, stem cankers, leaf spots, leaf and pod blights, fruit rots and seed decay (Uecker 1988; Rehner and Uecker 1994; Mostert et al. 2001; Thompson et al. 2001; Santos et al. 2011). Because many *Diaporthe* species have overlapping morphological traits, sequence data is essential to resolve this genus and introduce new species (Udayanga et al. 2014a). Combined gene sequence of ITS, *cal*, *his3*, *tef-1a*, and *tub2* is the optimal combination for species delimitation (Santos et al. 2017). However, removing the ITS locus has little effect on reconstructed phylogenies, identifying the *cal-his3-tef-1a-tub2* four loci tree as almost equivalent to the five loci phylogenetic tree.

Many confusions occur in species separation of *Diaporthe eres* complex with the lack of an ex-type culture or ex-epitype culture, although a broad species concept has historically been associated with *D. eres* (Udayanga et al. 2014b). Fan et al. (2018) demonstrated the effectiveness of three loci, including *cal*, *tef-1a* and *tub2*, for the identification of the *D. eres* complex in walnut trees. Similarly, Yang et al. (2018) also used three-locus sequences to identify *D. eres* species associated with different hosts in China, and Chaisiri et al. (2021) revealed the phylogenetic analysis from the combined dataset of *cal*, *his3*, *tef-1a* and *tub2* was highly effective, but the ITS region impeded species delimitation, which conforms with Yang et al. (2018).

Recently, several studies have been conducted associated with various hosts in China. For instance, the research conducted by Guo et al. (2020) revealed six novel *Diaporthe* species that infect pears and are responsible for pear shoot canker. Sun et al. (2021) showed high species diversity of *Diaporthe* in tropical rain forests, with description of eight new species. Wang et al. (2021) represented the first characterization of *Diaporthe* species associated with peach constriction canker in China, and contributed useful data for practicable disease management. Yang et al. (2021b) identified two new species from *Camellia oleifera*, which is an important edible oil woody plant in southern China. This study also characterises the taxonomic and morphological diversity of *Diaporthe* spp. associated with different hosts, which indicated there is a potential of *Diaporthe* species remains to be discovered in China.

Acknowledgements

This study is financed by National Natural Science Foundation of China (Project No.: 31670647) and the Research Foundation of Education Bureau of Hunan Province (Project No.: 19B608).

References

Barr ME (1978) The Diaporthales in North America with emphasis on *Gnomonia* and its segregates. Mycologia Memoir 7: 1–232.

Castlebury LA, Rossman AY, Jaklitsch WJ, Vasilyeva LN (2002) A preliminary overview of the Diaporthales based on large subunit nuclear ribosomal DNA sequences. Mycologia 94(6): 1017–1031. https://doi.org/10.1080/15572536.2003.11833157

Chaisiri C, Liu X, Lin Y, Fu Y, Zhu F, Luo C (2021) Phylogenetic and haplotype network analyses of *Diaporthe eres* species in China based on sequences of multiple loci. Biology 10(3): e179. https://doi.org/10.3390/biology10030179

Crous PW, Gams W, Stalpers JA, Robert V, Stegehuis G (2004) MycoBank: An online initiative to launch mycology into the 21st century. Studies in Mycology 50: 19–22.

Crous PW, Groenewald JZ, Shivas RG, Edwards J, Seifert KA, Alfenas AC, Alfenas RF, Burgess TI, Carnegie AJ, Hardy GESJ, Hiscock N, Hüberli D, Jung T, Louis-Seize G, Okada G, Pereira OL, Stukely MJC, Wang W, White GP, Young AJ, McTaggart AR, Pascoe IG, Porter IJ, Quaedvlieg W (2011) Fungal Planet description sheets: 69–91. Persoonia 26(1): 108–156. https://doi.org/10.3767/003158511X581723

Darriba D, Taboada GL, Doallo R, Posada D (2012) jModelTest 2: More models, new heuristics and parallel computing. Nature Methods 9(8): e772. https://doi.org/10.1038/nmeth.2109

Dissanayake AJ, Zhang W, Liu M, Hyde KD, Zhao WS, Li XH, Yan JY (2017) *Diaporthe* species associated with peach tree dieback in Hubei, China. Mycosphere 8(5): 533–549. https://doi.org/10.5943/mycosphere/8/5/2

Doyle JJ, Doyle JL (1990) Isolation of plant DNA from fresh tissue. Focus 12: 13–15. https://doi.org/10.2307/2419362

Du Z, Fan XL, Hyde KD, Yang Q, Liang YM, Tian CM (2016) Phylogeny and morphology reveal two new species of *Diaporthe* from *Betula* spp. in China. Phytotaxa 269(2): 90–102. https://doi.org/10.11646/phytotaxa.269.2.2

Fan XL, Hyde KD, Udayanga D, Wu XY, Tian CM (2015) *Diaporthe rostrata*, a novel ascomycete from *Juglans mandshurica* associated with walnut dieback. Mycological Progress 14(10): 1–8. https://doi.org/10.1007/s11557-015-1104-5

Fan XL, Yang Q, Bezerra JDP, Alvarez LV, Tian CM (2018) *Diaporthe* from walnut tree (*Juglans regia*) in China, with insight of *Diaporthe eres* complex. Mycological Progress 17(7): 1–13. https://doi.org/10.1007/s11557-018-1395-4

Gao YH, Liu F, Duan W, Crous PW, Cai L (2017) *Diaporthe* is paraphyletic. IMA Fungus 8(1): 153–187. https://doi.org/10.5598/imafungus.2017.08.01.11

Gomes RR, Glienke C, Videira SIR, Lombard L, Groenewald JZ, Crous PW (2013) *Diaporthe*: A genus of endophytic, saprobic and plant pathogenic fungi. Persoonia 31(1): 1–41. https://doi.org/10.3767/003158513X666844

Guarnaccia V, Crous PW (2017) Emerging citrus diseases in Europe caused by species of *Diaporthe*. IMA Fungus 8(2): 317–334. https://doi.org/10.5598/imafungus.2017.08.02.07

Guarnaccia V, Crous PW (2018) Species of *Diaporthe* on *Camellia* and *Citrus* in the Azores Islands. Phytopathologia Mediterranea 57: 307–319. https://doi.org/10.14601/Phytopathol_Mediterr-23254

Guarnaccia V, Groenewald JZ, Woodhall J, Armengol J, Cinelli T, Eichmeier A, Ezra D, Fontaine F, Gramaje D, Gutierrez-Aguirregabiria A, Kaliterna J, Kiss L, Larignon P, Luque J,

Mugnai L, Naor V, Raposo R, Sándor E, Váczy KZ, Crous PW (2018) *Diaporthe* diversity and pathogenicity revealed from a broad survey of grapevine diseases in Europe. Persoonia 40(1): 135–153. https://doi.org/10.3767/persoonia.2018.40.06

Guo YS, Crous PW, Bai Q, Fu M, Yang MM, Wang XH, Du YM, Hong N, Xu WX, Wang GP (2020) High diversity of *Diaporthe* species associated with pear shoot canker in China. Persoonia 45(1): 132–162. https://doi.org/10.3767/persoonia.2020.45.05

Hall T (1999) BioEdit: A user-friendly biological sequence alignment editor and analysis program for Windows 95/98/NT. Nucleic Acids Symposium Series 41: 95–98.

Huang F, Udayanga D, Wang X, Hou X, Mei X, Fu Y, Hyde KD, Li HY (2015) Endophytic *Diaporthe* associated with *Citrus*: A phylogenetic reassessment with seven new species from China. Fungal Biology 119(5): 331–347. https://doi.org/10.1016/j.funbio.2015.02.006

Huang ST, Xia JW, Zhang XG, Sun WX (2021) Morphological and phylogenetic analyses reveal three new species of *Diaporthe* from Yunnan, China. MycoKeys 78: 49–77. https://doi.org/10.3897/mycokeys.78.60878

Jiang N, Voglmayr H, Piao CG, Li Y (2021) Two new species of *Diaporthe* (Diaporthaceae, Diaporthales) associated with tree cankers in the Netherlands. MycoKeys 85: 31–56. https://doi.org/10.3897/mycokeys.85.73107

Katoh K, Toh H (2010) Parallelization of the MAFFT multiple sequence alignment program. Bioinformatics 26(15): 1899–1900. https://doi.org/10.1093/bioinformatics/btq224

Lombard L, Van Leeuwen GCM, Guarnaccia V, Polizzi G, Van Rijswick PC, Karin Rosendahl KC, Gabler J, Crous PW (2014) *Diaporthe* species associated with *Vaccinium*, with specific reference to Europe. Phytopathologia Mediterranea 53: 287–299. https://doi.org/10.14601/Phytopathol_Mediterr-14034

Manawasinghe IS, Dissanayake AJ, Li X, Liu M, Wanasinghe DN, Xu J, Zhao W, Zhang W, Zhou Y, Hyde KD, Brooks S, Yan J (2019) High genetic diversity and species complexity of *Diaporthe* associated with grapevine dieback in China. Frontiers in Microbiology 10: e1936. https://doi.org/10.3389/fmicb.2019.01936

Miller MA, Pfeiffer W, Schwartz T (2010) Creating the CIPRES Science Gateway for Inference of Large Phylogenetic Trees. Institute of Electrical and Electronics Engineers: New Orleans, LA, USA. https://doi.org/10.1109/GCE.2010.5676129

Mostert L, Crous PW, Kang JC, Phillips AJ (2001) Species of *Phomopsis* and a *Libertella* sp. occurring on grapevines with specific reference to South Africa: Morphological, cultural, molecular and pathological characterization. Mycologia 93(1): 146–167. https://doi.org/10.1080/00275514.2001.12061286

Muralli TS, Suryanarayanan TS, Geeta R (2006) Endophytic *Phomopsis* species: Host range and implications for diversity estimates. Canadian Journal of Microbiology 52(7): 673–680. https://doi.org/10.1139/w06-020

Nitschke T (1870) Pyrenomycetes Germanici. Breslau. Eduard Trewendt, Germany. 2: e245.

Rayner RW (1970) A mycological colour chart. Commonwealth Mycological Institute, Kew, UK.

Rehner SA, Uecker FA (1994) Nuclear ribosomal internal transcribed spacer phylogeny and host diversity in the coelomycete *Phomopsis*. Canadian Journal of Botany 72(11): 1666–1674. https://doi.org/10.1139/b94-204

Ronquist F, Huelsenbeck JP (2003) MrBayes 3: Bayesian phylogenetic inference under mixed models. Bioinformatics 19(12): 1572–1574. https://doi.org/10.1093/bioinformatics/btg180

Rossman AY, Farr DF, Castlebury LA (2007) A review of the phylogeny and biology of the Diaporthales. Mycoscience 48(3): 135–144. https://doi.org/10.1007/S10267-007-0347-7

Santos JM, Phillips AJL (2009) Resolving the complex of *Diaporthe* (*Phomopsis*) species occurring on *Foeniculum vulgare* in Portugal. Fungal Diversity 34: 111–125.

Santos JM, Vrandečić K, Ćosić J, Duvnjak T, Phillips AJL (2011) Resolving the *Diaporthe* species occurring on soybean in Croatia. Persoonia 27(1): 9–19. https://doi.org/10.3767/003158511X603719

Santos L, Alves A, Alves R (2017) Evaluating multi-locus phylogenies for species boundaries determination in the genus *Diaporthe*. PeerJ 5: e3120. https://doi.org/10.7717/peerj.3120

Smith H, Wingfeld MJ, Coutinho TA, Crous PW (1996) *Sphaeropsis sapinea* and *Botryosphaeria dothidea* endophytic in *Pinus* spp. and *Eucalyptus* spp. in South Africa. South African Journal of Botany 62(2): 86–88. https://doi.org/10.1016/S0254-6299(15)30596-2

Sun W, Huang S, Xia J, Zhang X, Li Z (2021) Morphological and molecular identification of *Diaporthe* species in south-western China, with description of eight new species. MycoKeys 77: 65–95. https://doi.org/10.3897/mycokeys.77.59852

Thompson SM, Tan YP, Young AJ, Neate SM, Aitken EAB, Shivas RG (2001) Stem cankers on sunflower (*Helianthus annuus*) in Australia reveal a complex of pathogenic *Diaporthe* (*Phomopsis*) species. Persoonia 27(1): 80–89. https://doi.org/10.3767/003158511X617110

Udayanga D, Liu X, McKenzie EH, Chukeatirote E, Bahkali AH, Hyde KD (2011) The genus *Phomopsis*: Biology, applications, species concepts and names of common phytopathogens. Fungal Diversity 50(1): 189–225. https://doi.org/10.1007/s13225-011-0126-9

Udayanga D, Castlebury LA, Rossman AY, Hyde KD (2014a) Species limits in *Diaporthe*: Molecular re-assessment of *D. citri*, *D. cytosporella*, *D. foeniculina* and *D. rudis*. Persoonia 32(1): 83–101. https://doi.org/10.3767/003158514X679984

Udayanga D, Castlebury LA, Rossman AY, Chukeatirote E, Hyde KD (2014b) Insights into the genus *Diaporthe*: Phylogenetic species delimitation in the *D. eres* species complex. Fungal Diversity 67(1): 203–229. https://doi.org/10.1007/s13225-014-0297-2

Udayanga D, Castlebury LA, Rossman AY, Chukeatirote E, Hyde KD (2015) The *Diaporthe sojae* species complex: Phylogenetic re-assessment of pathogens associated with soybean, cucurbits and other field crops. Fungal Biology 119(5): 383–407. https://doi.org/10.1016/j.funbio.2014.10.009

Uecker FA (1988) A world list of *Phomopsis* names with notes on nomenclature, morphology and biology. Mycological Memoirs 13: 1–231.

von Höhnel FXR (1917) System der Diaportheen. Borntraeger.

Wang X, Guo Y, Du Y, Yang Z, Huang X, Hong N, Xu WX, Wang GP (2021) Characterization of *Diaporthe* species associated with peach constriction canker, with two novel species from China. MycoKeys 80: 77–90. https://doi.org/10.3897/mycokeys.80.63816

Wehmeyer LE (1975) The pyrenomycetous fungi. Mycologia Memoir 6: 1–250.

Yang Q, Fan XL, Du Z, Tian CM (2017) *Diaporthe* species occurring on *Senna bicapsularis* in southern China, with descriptions of two new species. Phytotaxa 302(2): 145–155. https://doi.org/10.11646/phytotaxa.302.2.4

Yang Q, Fan XL, Guarnaccia V, Tian CM (2018) High diversity of *Diaporthe* species associated with dieback diseases in China, with twelve new species described. MycoKeys 39: 97–149. https://doi.org/10.3897/mycokeys.39.26914

Yang Q, Jiang N, Tian CM (2020) Three new *Diaporthe* species from Shaanxi Province, China. MycoKeys 67: 1–18. https://doi.org/10.3897/mycokeys.67.49483

Yang Q, Jiang N, Tian CM (2021a) New species and records of *Diaporthe* from Jiangxi Province, China. MycoKeys 77: 41–64. https://doi.org/10.3897/mycokeys.77.59999

Yang Q, Tang J, Zhou GY (2021b) Characterization of *Diaporthe* species on *Camellia oleifera* in Hunan Province, with descriptions of two new species. MycoKeys 84: 15–33. https://doi.org/10.3897/mycokeys.84.71701

MycoKeys 91: 49–66 (2022)
doi: 10.3897/mycokeys.91.86812
https://mycokeys.pensoft.net

RESEARCH ARTICLE

A peer-reviewed open-access journal
MycoKeys
Launched to accelerate biodiversity research

Phylogenetic, ecological and morphological characteristics reveal two new spider-associated genera in Clavicipitaceae

Wan-Hao Chen[1], Jian-Dong Liang[1], Xiu-Xiu Ren[1], Jie-Hong Zhao[1], Yan-Feng Han[2], Zong-Qi Liang[2]

1 *Center for Mycomedicine Research, Basic Medical School, Guizhou University of Traditional Chinese Medicine, Guiyang 550025, Guizhou, China* **2** *Institute of Fungus Resources, Department of Ecology, College of Life Sciences, Guizhou University, Guiyang 550025, Guizhou, China*

Corresponding author: Yan-Feng Han (swallow1128@126.com)

Academic editor: Xinlei Fan | Received 21 May 2022 | Accepted 20 June 2022 | Published 7 July 2022

Citation: Chen W-H, Liang J-D, Ren X-X, Zhao J-H, Han Y-F, Liang Z-Q (2022) Phylogenetic, ecological and morphological characteristics reveal two new spider-associated genera in Clavicipitaceae. MycoKeys 91: 49–66. https://doi.org/10.3897/mycokeys.91.86812

Abstract

Clavicipitaceous fungi are pathogenic to scale insects, white flies and other insect orders. However, a few species are spider-associated. Two new genera from China, *Neoaraneomyces* and *Pseudometarhizium*, are described based on phylogenetic, ecological and morphological characteristics. Two spider-associated species, *Neoaraneomyces araneicola*, *Pseudometarhizium araneogenum*, and an insect-associated species *Pseudometarhizium lepidopterorum* are included. The morphological characteristics of paecilomyces-like conidiogenous structures, present in many insect/spiders associated species make species-level identifications difficult. A phylogenetic analysis of the combined dataset (ITS, LSU, RPB2 and TEF), placed the two new genera in Clavicipitaceae. The new spider-associated species may be the result of convergent evolution to adapt to the ecological environment and may have undergone host jumping or altered their nutritional preferences.

Keywords

Clavicipitaceae, convergent evolution, morphology, nutritional preference, phylogeny

Introduction

Araneogenous or araneopathogenic fungi are spider-pathogenic fungi (Evans and Samson 1987) and found in diverse habitats, such as different kinds of monocot, dicot or coniferous plants including trees, grasses, bamboo, mosses, ferns, and lichens (Shrestha et al. 2019). The known araneogenous fungal genera include *Cordyceps* Fr., and the related anamorphic genera *Akanthomyces* Lebert, *Beauveria* Vuill., *Clathroconium* Samson & H.C. Evans, *Clonostachys* Corda, *Gibellula* Cavara, *Hevansia* Luangsa-ard, Hywel-Jones & Spatafora, *Hirsutella* Pat., *Hymenostilbe* Petch, *Nomuraea* Maubl. and *Purpureocillium* Luangsaard, Hywel-Jones, Houbraken & Samson (Chen et al. 2018). Shrestha et al. (2019) noted that araneogenous fungi are restricted to Cordycipitaceae and Ophiocordycipitaceae, with one exception in Bionectriaceae; there is no report to date of araneogenous fungi in the family Clavicipitaceae within Hypocreales.

Members of Clavicipitaceae are distributed worldwide and found in almost all terrestrial ecosystems. Currently, Clavicipitaceae contains 49 genera and over 500 species (Hyde et al. 2020; Mongkolsamrit et al. 2020; Gao et al. 2021). Among these genera, *Claviceps* Tul. and *Balansia* Speg. are pathogenic only to plants (Diehl 1950). *Pochonia* Bat. & O.M. Fonseca and *Rotiferophthora* G.L. Barron are pathogenic to a wide variety of invertebrates. Seven sexually reproductive genera, *Aschersonia* Mont. (*Hypocrella*), *Conoideocrella* D. Johnson, G.H. Sung, Hywel-Jones & Spatafora, *Orbiocrella* D. Johnson, G.H. Sung, Hywel-Jones & Spatafora, *Regiocrella* P. Chaverri & K.T. Hodge, *Samuelsia* P. Chaverri & K.T. Hodge and *Moelleriella* Bres. are pathogenic to scale insects and white flies (Hemiptera), while *Metarhizium* (*Metarcordyceps*) has a broad host association (Luangsa-ard et al. 2017).

During a survey of entomopathogenic fungi and their allies in southwestern China, infected insect and spider specimens were obtained, and some fungal strains were isolated and purified. The goal of this research is to identify those new strains by multigene phylogeny, morphological and ecological characteristics.

Materials and methods

Specimen collection and identification

Four infected insect and spider specimens (DY10171, DY10174, DY10180 and SD0536) were collected from Duyun City (26°21'24.71"N, 107°22'48.22"E) and Sandu County (25°57'22.21"N, 107°57'54.69"E), Guizhou Province, on 1 October and 1 May, 2019. Isolation of strains was conducted as described by Chen et al. (2019). Fungal colonies emerging from specimens were isolated and cultured at 25 °C for 14 days under 12 h light/12 h dark conditions following protocols described by Zou et al. (2010). The specimens and the isolated living strains were deposited in the Institute of Fungus Resources, Guizhou University (formally Herbarium of Guizhou Agricultural College; code, GZAC), Guiyang City, Guizhou, China.

Macroscopic and microscopic morphological characteristics of the fungi were examined, especially for the arrangement, shape and measurement of phialides and conidia, and also the growth rates were determined from cultures grown on potato dextrose agar (PDA) cultures incubated at 25 °C for 14 days. Hyphae and conidiogenous structures were mounted in lactophenol cotton blue or 20% lactic acid solution and observed with an optical microscope (OM, DM4 B, Leica, Germany).

DNA extraction, polymerase chain reaction amplification and nucleotide sequencing

DNA extraction was carried out by Fungal genomic DNA Extraction Kit (DP2033, BioTeke Corporation) in accordance with Liang et al. (2011). The extracted DNA was stored at –20 °C. The amplification of internal transcribed spacer (ITS) region, large subunit ribosomal RNA (LSU) gene, RNA polymerase II largest subunit 2 (RPB2) and translation elongation factor 1 alpha (TEF) by PCR was as described by White et al. (1990), Rakotonirainy et al. (1994), Castlebury et al. (2004) and van den Brink et al. (2012), respectively. Primer sequence information is shown in Suppl. material 1. PCR products were purified and sequenced at Sangon Biotech (Shanghai) Co. The resulting sequences were submitted to GenBank (Table 1).

Sequence alignment and phylogenetic analyses

Lasergene software (version 6.0, DNASTAR) was applied for the editing of DNA sequences in this study. The ITS, LSU, RPB2 and TEF sequences were downloaded from GenBank, based on Mongkolsamrit et al. (2018, 2020), Gao et al. (2021) and others selected on the basis of BLAST algorithm-based searches in GenBank (Table 1). A single gene data set was aligned and edited by MAFFT v7.037b (Katoh and Standley 2013) and MEGA v6.0 (Tamura et al. 2013). Combined sequences of ITS, LSU, RPB2 and TEF were performed by SequenceMatrix v.1.7.8 (Vaidya et al. 2011). The model was selected for Bayesian analysis by ModelFinder (Kalyaanamoorthy et al. 2017) in the software PhyloSuite v 1.2.2 (Zhang et al. 2020).

The combined genes were analyzed using Bayesian inference (BI) and maximum likelihood (ML) methods. For BI, a Markov chain Monte Carlo (MCMC) algorithm was used to generate phylogenetic trees with Bayesian probabilities using MrBayes v.3.2 (Ronquist et al. 2012) for the combined sequence datasets. The Bayesian analysis resulted in 20,001 trees after 10,000,000 generations. The first 4,000 trees, representing the burn-in phase of the analyses, were discarded, while the remaining 16,001 trees were used for calculating posterior probabilities in the majority rule consensus tree. After the analysis was finished, each run was examined using the program Tracer v1.5 (Drummond and Rambaut 2007) to determine burn-in and confirm that both runs had converged. ML analyses were constructed with IQ-TREE (Trifinopoulos et al. 2016) and the model was the default settings.

Table 1. List of strains and GenBank accession numbers of sequences used in this study.

Species	Strain No.	GenBank Accession No.			
		ITS	LSU	RPB2	TEF
Aciculosporium oplismeni	MAFF 246966	LC571760	LC571760	LC572054	LC572040
A. take	MAFF 241224	LC571753	LC571753	LC572048	LC572034
A. take	TNS-F-60465	LC571755	LC571756	LC572049	LC572035
Akanthomyces aculeatus	HUA 772	KC519371	-	-	KC519366
Aschersonia badia	BCC 8105	-	DQ518752	DQ522411	DQ522317
A. placenta	BCC 7869	-	EF469074	EF469104	EF469056
Atkinsonella hypoxylon	B4728	-	-	KP689514	KP689546
Balansia epichloe	A.E.G. 96-15a	-	-	EF468908	EF468743
B. henningsiana	GAM 16112	-	AY545727	DQ522413	AY489610
B. pilulaeformis	A.E.G. 94-2	-	AF543788	DQ522414	DQ522319
Bionectria ochroleuca	AFTOL-ID 187	-	DQ862027	DQ862013	DQ862029
B. vesiculosa	HMAS 183151	HM050304	HM050302	-	-
Calcarisporium arbuscula	CBS 221.73	AY271809	-	-	-
C. arbuscula	CBS 900.68	KT945003	KX442598	KX442597	KX442596
C. cordycipitiicola	CGMCC 3.17905	KT944999	KX442599	KX442594	KX442593
C. cordycipitiicola	CGMCC 3.17904	KT945001	KX442604	KX442607	KX442605
C. xylariicola	HMAS 276836	KX442603	KX442601	KX442606	KX442595
Calonectria ilicicola	CBS 190.50	GQ280605	GQ280727	KM232307	AY725726
Cephalosporium curtipes	CBS 154.61	AJ292404	AF339548	EF468947	EF468802
Claviceps fusiformis	ATCC 26019	JN049817	U17402	-	DQ522320
C. purpurea	GAM 12885	-	AF543789	DQ522417	AF543778
C. purpurea	S.A. cp11	-	EF469075	EF469105	EF469058
Clonostachys rosea	GJS90-227	-	AY489716	-	AY489611
Cocoonihabitus sinensis	HMAS254523	KY924870	KY924869	-	-
C. sinensis	HMAS254524	MF687395	MF687396	-	-
Collarina aurantiaca	FMR 11134	KJ807178	KJ807181	-	-
C. aurantiaca	FMR 11784	KJ807177	KJ807180	-	-
Conoideocrella luteorostrata	NHJ 11343	-	EF468850	-	EF468801
C. luteorostrata	NHJ 12516	-	EF468849	-	EF468800
C. tenuis	NHJ 6293	-	EU369044	EU369087	EU369029
Corallocytostroma ornithocopreoides	WAC 8705	-	-	LT216620	LT216546
Cordyceps brongniartii	BCC16585	JN049867	JF415967	JF415991	JF416009
C. militaris	OSC93623	JN049825	AY184966	-	DQ522332
Dactylonectria alcacerensis	CBS 129087	JF735333	KM231629	-	JF735819
*Dussiella tuberiformis**		-	-	JQ257020	JQ257027
Elaphocordyceps ophioglossoides	NBRC 106332	JN943322	JN941409	-	-
E. paradoxa	NBRC 106958	JN943324	JN941411	-	-
Ephelis japonica	CBS 236.64	MH858427	-	-	-
E. japonica	Eph.oryzae	AB038564	-	-	-
E. tripsaci	CBS 857.72	NR_153997	NG_059240	-	-
Epichloe elymi	C. Schardl 760	-	AY986924	-	AY986951
E. typhina	ATCC 56429	JN049832	U17396	DQ522440	AF543777
Flammocladiella aceris	CPC 24422	KR611883	KR611901	-	-
Fusarium circinatum	CBS 405.97	U61677	-	JX171623	KM231943
F. sublunatum	CBS 189.34	HQ897830	KM231680	-	-
Gelasinospora tetrasperma	AFTOL-ID 1287	-	DQ470980	DQ470932	DQ471103
Haptocillium sinense	CBS 567.95	AJ292417	AF339545	-	-
Helicocollum krabiensis	BCC 71374	-	KT222327	-	KT222342
H. surathaniensis	BCC 34463	-	KT222328	-	KT222336
H. surathaniensis	BCC 34464	-	KT222329	-	KT222337
Heteroepichloe bambusae	Ba-01	AB065426	-	-	-
H. bambusae	Bo-01	AB065428	-	-	-
H. sasae	E.sasae-H	AB065432	-	-	-

Species	Strain No.	GenBank Accession No.			
		ITS	LSU	RPB2	TEF
H. sasae	E.sasae-N	AB065431	-	-	-
Hydropisphaera erubescens	ATCC 36093	-	AF193230	AY545731	DQ518174
H. lutea	ATCC 208838	-	AF543791	DQ522446	AF543781
H. peziza	GJS92-101	-	AY489730	-	AY489625
H. rufa	DAOM JBT1003	JN942883	JN938865	-	-
Hypocrea americana	AFTO -ID 52	DQ491488	AY544649	-	DQ471043
Hypocrella discoidea	BCC 8237	JN049840	DQ384937	DQ452461	DQ384977
Hypomyces polyporinus	ATCC 76479	-	AF543793	-	AF543784
H. aurantius	GJS74-69	FJ442642	HM466684	FJ442744	FJ467643
Keithomyces sp.	CBS 126563	-	MT078856	-	MT078921
K. carneus	CBS 239.32	NR_131993	NG_057769	EF468938	EF468789
Lecanicillium attenuatum	CBS 402.78	AJ292434	AF339565	EF468935	EF468782
L. lecanii	CBS 101247	JN049836	KM283794	KM283859	DQ522359
L. psalliotae	CBS 367.86	-	KM283800	-	KM283823
Marquandomyces marquandii	CBS 182.27	NR_131994	EF468845	EF468942	EF468793
Marquandomyces sp.	CBS 127132	-	MT078857	MT078922	-
Metapochonia bulbillosa	CBS 145.70	-	AF339542	EF468943	EF468796
M. gonioides	CBS 891.72	AJ292409	AF339550	DQ522458	DQ522354
M. rubescens	CBS 464.88	-	AF339566	EF468944	EF468797
M. sulchlasporia	CBS 251.83	NR_154139	MH873311	-	KJ398790
Metarhiziopsis microspora	CEHS133a	EF464589	EF464571	-	-
M. microspora	INEHS133a	EF464583	EF464572	-	-
Metarhizium anisopliae	ARSEF 7487	-	-	DQ468370	DQ463996
M. anisopliae	CBS 130.71	MT078884	MT078853	MT078918	MT078845
M. flavoviride	CBS 125.65	MT078885	MT078854	MT078919	MT078846
M. flavoviride	CBS 700.74	-	MT078855	MT078920	MT078847
M. flavoviride	CBS 218.56	-	-	-	KJ398787
Moelleriella phyllogena	CUP 067785	-	EU392610	-	EU392674
M. phyllogena	CUP 067793	-	EU392608	-	EU392672
M. schizostachyi	BCC 14123	-	DQ518771	DQ522447	DQ522346
M. umbospora	CUP 067817	-	EU392628	-	EU392688
Mycophilomyces periconiae	CPC 27558	NR_154209	NG_059746	-	-
Myriogenospora atramentosa	A.E.G 96-32	-	AY489733	DQ522455	AY489628
Myrotheciomyces corymbiae	CPC 33206	NR_160351	NG_064542	-	-
Myrothecium inundatum	IMI158855	-	AY489731	-	AY489626
M. roridum	ATCC 16297	-	AY489708	-	AY489603
M. verrucaria	ATCC 9095	-	AY489713	-	AY489608
Nectria cinnabarina	CBS 125165	HM484548	HM484562	KM232402	HM484527
N. nigrescens	CBS 125148	HM484707	HM484720	KM232403	HM484672
Nectriopsis violacea	CBS 424.64	-	AY489719	-	-
Neoaraneomyces araneicola	DY101711	MW730520	MW730609	MW753026	MW753033
N. araneicola	DY101712	MW730522	MW730610	MW753027	MW753034
Neobarya parasitica	Marson s/n	KP899626	KP899626	-	-
Neonectria candida	CBS 151.29	JF735313	AY677333	-	JF735791
N. faginata	CBS 217.67	HQ840385	HQ840382	DQ789797	JF268746
N. neomacrospora	CBS 118984	HQ840388	HQ840379	DQ789810	JF268754
N. ramulariae	CBS 182.36	HM054157	HM042435	DQ789793	HM054092
Neurospora crassa	ICMP 6360	AY681193	AY681158	-	-
Niesslia exilis	CBS 560.74	-	AY489720	-	AY489614
Nigelia aurantiaca	BCC13019	-	GU979948	GU979971	GU979957
N. martiale	EFCC 6863	-	JF415974	-	JF416016
Ophiocordyceps heteropoda	EFCC 10125	JN049852	EF468812	EF468914	EF468752
O. sinensis	EFCC 7287	JN049854	EF468827	EF468924	EF468767
O. stylophor	OSC 111000	JN049828	DQ518766	DQ522433	DQ522337
Orbiocrella petchii	NHJ 6209	-	EU369039	EU369081	EU369023

Species	Strain No.	GenBank Accession No.			
		ITS	LSU	RPB2	TEF
O. petchii	NHJ 6240	-	EU369038	EU369082	EU369022
Papiliomyces liangshanensis	EFCC 1452	-	EF468815	-	EF468756
P. liangshanensis	EFCC 1523	-	EF468814	EF468918	EF468755
P. shibinensis	GZUH SB13050311	NR154178	-	-	KR153589
Parametarhizium changbaiense	CGMCC 19143	MN589741	MN589994	MT921829	MN908589
P. hingganense	CGMCC 19144	MN055703	MN061635	MT939494	MN065770
Parepichloe cinerea	Ne-01	AB065425	-	-	-
Peethambara spirostriata	CBS110115	-	AY489724	EF692516	AY489619
Periglandula ipomoeae	IasaF13	-	-	KP689517	KP689568
Pochonia boninensis	JCM 18597	AB709858	AB709831	AB758693	AB758463
P. globispora	CBS 203.86	DQ516079	-	-	-
Pseudometarhizium araneogenum	DY101741	MW730532	MW730618	MW753030	MW753037
P. araneogenum	DY101742	MW730534	MW730619	MW753031	MW753038
P. araneogenum	DY101801	MW730536	MW730623	MW753032	MW753039
P. araneogenum	DY101802	MW730545	MW730625	-	MW753040
P. lepidopterorum	SD05361	MW730543	MW730624	-	MW753041
P. lepidopterorum	SD05362	MW730611	MW730629	-	MW753042
Purpureocillium lavendulum	FMR 10376	-	FR775489	-	FR775516
P. lilacinus	CBS 284.36	-	-	EF468941	EF468792
Purpureomyces maesotensis	BCC 88441	MN781916	MN781877	MN781824	MN781734
P. maesotensis	BCC 85349	MN781928	MN781872	-	MN781729
P. maesotensis	BCC 89300	MN781917	MN781876	-	MN781733
Regiocrella camerunensis	ARSEF 7682	-	DQ118735	-	DQ118743
Romanoa terricola	WCM_17	KP794435	-	-	-
R. terricola	WCM_18	KP794436	-	-	-
Rosasphaeria moravica	LMM	JF440985	-	JF440986	JF440987
Rotiferophthora angustispora	CBS 101437	-	AF339535	DQ522460	AF543776
Roumegueriella rufula	CBS 346.85	-	DQ518776	DQ522461	DQ522355
R. rufula	GJS 91-164	-	EF469082	EF469116	EF469070
Samuelsia chalalensis	CUP 067856	-	EU392637	-	EU392691
S. mundiveteris	BCC 40021	-	GU552152	-	GU552145
S. rufobrunnea	CUP 067858	-	AY986918	-	AY986944
Sarocladium bacillisporum	CBS 425.67	NR_145039	MH870718	-	-
S. dejongiae	CBS 144929	NR_161153	NG_067854	-	-
S. implicatum	CBS 959.72	HG965023	MH878470	-	-
S. subulatum	CBS 217.35	MH855652	NG_070566	-	-
S. terricola	CBS 243.59	MH857853	MH869389	-	-
Shimizuomyces paradoxus	EFCC 6279	JN049847	EF469084	EF469117	EF469071
S. paradoxus	EFCC 6564	-	EF469083	EF469118	EF469072
Simplicillium lamellicola	CBS 116.25	AJ292393	MH866307	DQ522462	DQ522356
S. lanosoniveum	CBS 101267	AJ292395	-	DQ522463	DQ522357
S. lanosoniveum	CBS 704.86	AJ292396	AF339553	DQ522464	DQ522358
Sordaria fimicola	AFTOL-ID 216	DQ518178	-	-	DQ518175
Stachybotrys eucylindrospora	ATCC 18851	JN942887	JN938869	-	-
Sphaerostilbella aureonitens	GJS74-87	FJ442633	HM466683	FJ442763	-
S. berkeleyana	GJS82-274	-	U00756	-	AF543783
S. chlorohalonata	DAOM 235557	JN942888	JN938870	-	-
Stachybotrys microspora	CBS 186.79	-	-	DQ676580	DQ676604
Stephanonectria keithii	GJS92-133	-	AY489727	-	AY489622
Sungia yongmunensis	EFCC 2131	JN049856	EF468833	-	EF468770
S. yongmunensis	EFCC 2135	-	EF468834	-	EF468769
Tilachlidium brachiatum	CBS 506.67	KM231839	HQ232177	KM232415	KM231976
T. brachiatum	CBS 363.97	KM231838	KM231719	KM232414	KM231975
Tolypocladium inflatum	SCALT1007-002	KC963032	-	-	-
Trichoderma aggressivum	CBS100525	-	JN939837	JQ014130	-

Species	Strain No.	GenBank Accession No.			
		ITS	LSU	RPB2	TEF
T. arundinaceum	ATCC 90237	EU330927	-	EU338326	EU338291
T. viride	GJS89-127	-	AY489726	-	AY489621
Trichosphaerella ceratophora	CBS 130.82	KM231847	KM231727	KM232423	KM231983
Trichothecium indicum	CBS 123.78	-	NG_057651	-	-
T. roseum	DUCC 502	JN937590	JX458860	-	-
Tyrannicordyceps fratricida	TNS-F 19011	JQ349068	JQ257023	JQ257021	JQ257028
Ustilaginoidea dichromonae	MRL IB9228	-	-	JQ257018	JQ257025
U. virens	ATCC 16180	-	-	JQ257019	JQ257026
U. virens	MAFF 240421	-	JQ257011	JQ257017	JQ257026
Valetoniellopsis laxa	GJS96-174	-	AY015635	AY015638	-
Yosiokobayasia kusanagiensis	TNS-F18494	-	JF415972	-	JF416014

Note: * J.F. White, Scale on Arundinaria tecta, North Carolina, 2000.

Results

Phylogenetic analyses

Phylogenetic trees were generated in analysis 1 (to determine the family placement of the new strains) and analysis 2 (to determine the establishment of the new genera in Clavicipitaceae) (Figs 1 and 2, respectively). *Gelasinospora tetrasperma* Dowding (AFTOL-ID 1287), *Neurospora crassa* Shear & B.O. Dodge (ICMP 6360) and *Sordaria fimicola* (Roberge ex Desm.) Ces. & De Not. (AFTOL-ID 216) were used as the outgroups in analysis 1, whereas *Purpureocillium lilacinum* (Thom) Luangsa-ard, Houbraken, Hywel-Jones & Samson (CBS 284.36) and *P. lavendulum* Perdomo, Dania García, Gené, Cano & Guarro (FMR 10376) were used as the outgroups in analysis 2. The concatenated sequences of analysis 1 and 2 included 77 and 68 taxa, respectively, and consisted of 2,313 (ITS, 604; LSU, 570; RPB2, 576; and TEF, 563) and 2,470 (ITS, 583; LSU, 488; RPB2, 627; and TEF, 772) characters with gaps, respectively.

Analysis 1: The selected model for ML analysis was TIM2+F+I+G4. The final value of the highest scoring tree was –37,716.4419, which was obtained from an ML analysis of the dataset (ITS+LSU +RPB2+TEF). The parameters of the rate heterogeneity model used to analyze the dataset were estimated using the following frequencies: A = 0.2282, C = 0.2768, G = 0.2781, T = 0.2169; substitution rates AC = 1.4435, AG = 2.2494, AT = 1.4435, CG = 1.0000, CT = 5.4319 and GT = 1.0000, as well as the gamma distribution shape parameter α = 0.6711. The selected models for BI analysis were GTR+F+I+G4 (ITS, LSU and RPB2), and GTR+F+G4 (TEF). The phylogenetic trees (Fig. 1) constructed using ML and BI analyses were largely congruent and strongly supported in most branches. Each family was clustered into an independent clade. The new strains clustered into an independent clade (Clavicipitaceae) with close relationships to *Claviceps*, *Epichloe* (Fr.) Tul. & C. Tul., *Cephalosporium* Corda, *Metapochonia* Kepler, S.A. Rehner & Humber, *Hypocrella* Sacc. and *Shimizuomyces* Kobayasi.

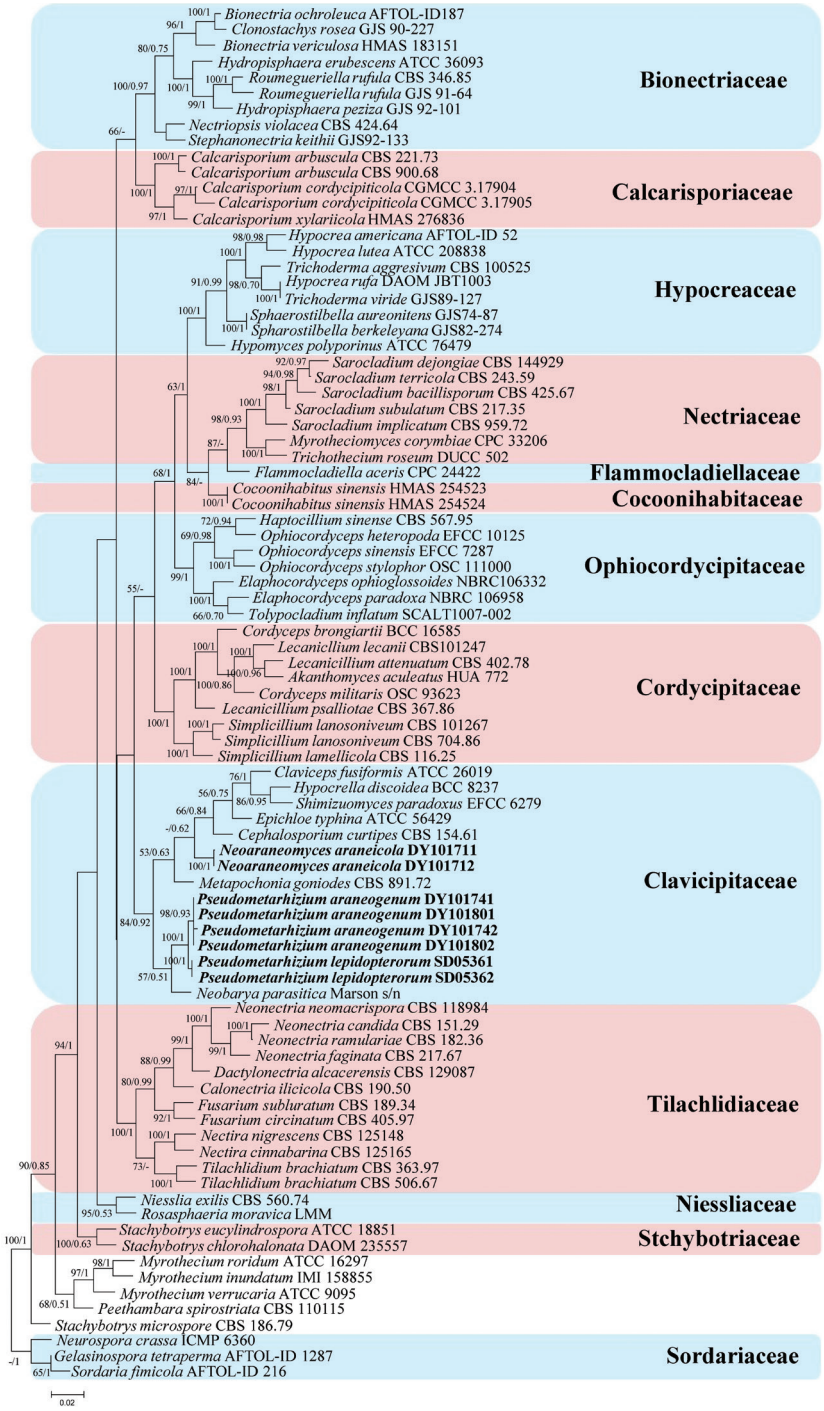

Figure 1. A maximum-likelihood phylogenetic tree of *Neoaraneomyces* and *Pseudometarhizium* in the order Hypocreales based on multigene dataset (ITS, LSU, RPB2 and TEF). Statistical support values (≥ 50%/0.5) are shown at the nodes for ML bootstrap support/BI posterior probabilities. The new taxa are in bold.

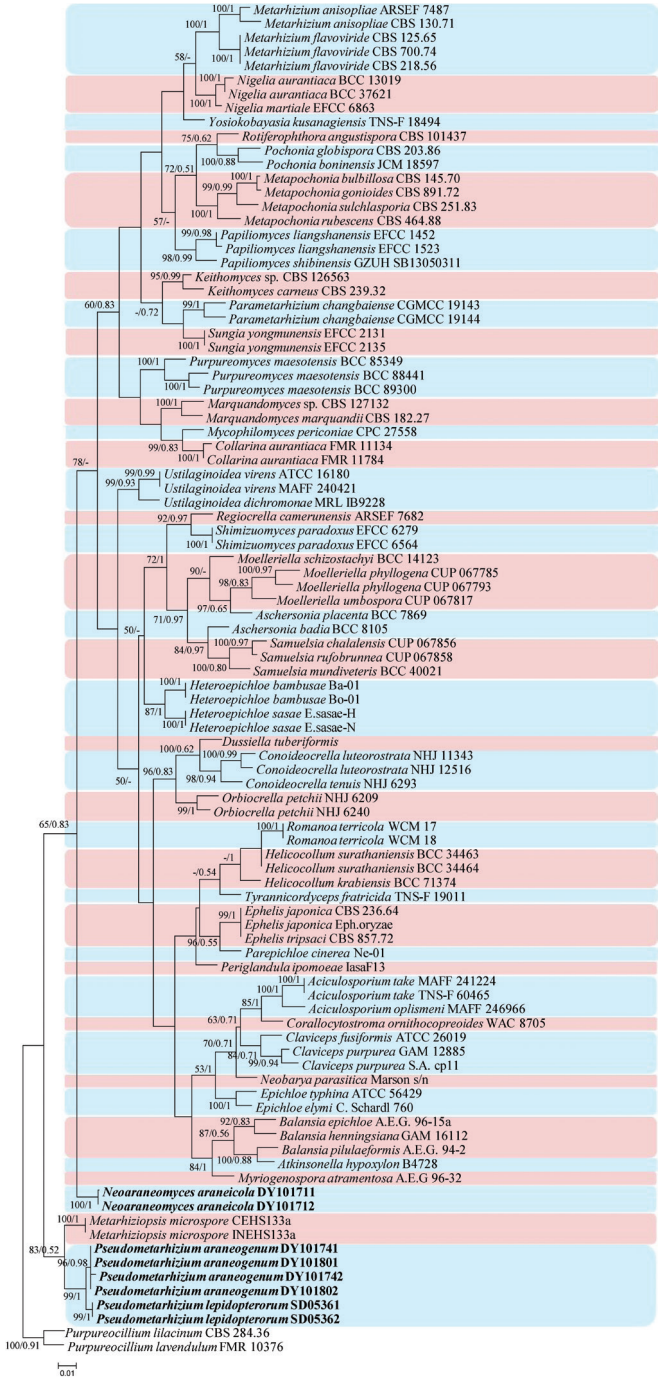

Figure 2. A maximum-likelihood phylogenetic tree of two new genera *Neoaraneomyces* and *Pseudometarhizium* and 39 genera in Clavicipitaceae, based on multigene dataset (ITS, LSU, RPB2 and TEF). Statistical support values (≥ 50%/0.5) are shown at the nodes for ML bootstrap support/BI posterior probabilities. The new taxa are in bold.

Analysis 2: The final value of the highest scoring tree was –29,543.7455, which was obtained from the ML analysis of the dataset (ITS+LSU+RPB2+TEF). The parameters of the GTR model used to analyze the dataset were estimated based on the following frequencies: A = 0.2303, C = 0.2800, G = 0.2801, T = 0.2096; substitution rates AC = 1.0000, AG = 3.0029, AT = 1.0000, CG = 1.0000, CT = 7.0264 and GT = 1.0000, as well as the gamma distribution shape parameter α = 0.3934. The selected models for BI analysis were GTR+F+I+G4 (ITS+LSU+TEF) and SYM+G4 (RPB2). The phylogenetic trees (Fig. 2) constructed using ML and BI analyses were largely congruent and strongly supported in most branched. Most genera clustered into independent clades. Strains DY101711 and DY101712 clustered into an independent clade while DY101741, DY101742, DY101801, DY101802, SD05361 and SD05362 clustered into two independent clades with close relationship with *Metarhiziopsis* D.W. Li, R.S. Cowles & C.R. Vossbrinck.

Taxonomy

Neoaraneomyces **W.H. Chen, Y.F. Han, J.D. Liang & Z.Q. Liang gen. nov.**
MycoBank No: 842644

Etymology. Referring to a new genus parasitic on spiders

Type species. *Neoaraneomyces araneicola* W.H. Chen, Y.F. Han, J.D. Liang & Z.Q. Liang.

Description. Colonies on PDA, white to grey, reverse yellowish. Conidiophores mononematous, usually arising from aerial hyphae, phialides solitary or in groups of two to three. Phialides emerging laterally from hyphae, forming a compact hymenium, abruptly narrowing into a neck. Conidia in chains, one-celled, hyaline, fusiform or ellipsoidal.

Host. Spider (Araneidae)

Habitat. Near roads and located on or under rocks.

Sexual morph. Unknown.

Notes. The genera *Akanthomyces*, *Beauveria*, *Clonostachys*, *Cordyceps*, *Engyodontium* de Hoog, *Gibellula*, *Hevansia*, *Hirsutella*, *Hymenostilbe*, *Lecanicillium* W. Gams & Zare, *Ophiocordyceps* Petch, *Purpureocillium*, and *Torrubiella* Boud. have been reported as spider-pathogenic fungi in Hypocreales (Shrestha et al. 2019). *Gibellula* is only found on spiders. *Neoaraneomyces* differs from *Gibellua* by its paecilomyces-like conidiogenous structures, phialides which were solitary or in groups of two to four, with fusiform to ellipsoidal conidia.

Neoaraneomyces araneicola **W.H. Chen, Y.F. Han, J.D. Liang & Z.Q. Liang, sp. nov.**
MycoBank No: 842645
Fig. 3

Type. Duyun City (26°21'27.96"N, 107°22'48.22"E), Qiannan Buyi and Miao Autonomous Prefecture, Guizhou, China. On a dead spider (Araneae), 1 October 2019, Wanhao Chen, GZAC DY10171 (holotype); ex-type living cultures, DY101711.

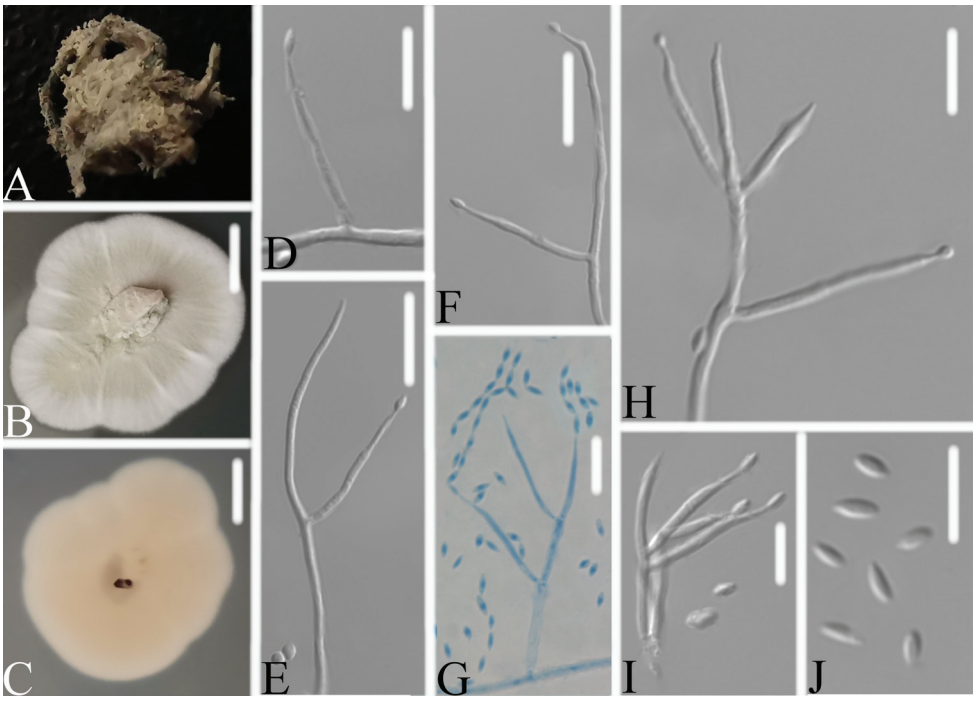

Figure 3. *Neoaraneomyces araneicola* **A** infected spider **B, C** PDA-containing culture plate showing **B** the front and **C** reverse sides of the colony **D–J** phialides, conidia in chains and conidia. Scale bars: 10 mm (**B, C**); 10 μm (**D–J**).

Description. Spider host completely covered by white mycelium. Conidiophores mononematous, arising from the lateral hyphae. Colonies on PDA, 3.0–3.2 cm diam. after 14 d at 25 °C, white to pale grey, powdery, consisting of a basal felt, reverse yellowish. Prostrate hyphae smooth, septate, hyaline, 1.4–2.2 μm diam. Erect conidiophores usually arising from aerial hyphae. Phialides single or in groups of two to three, 8.9–23.8 × 1.1–1.6 μm, with a cylindrical to ellipsoidal basal portion, tapering into a short distinct neck. Conidia in chains, hyaline, fusiform to ellipsoidal, one-celled, 2.9–4.4 × 1.3–2.0 μm. Sexual state not observed.

Host. Spider (Araneidae).

Habitat. Near the road, located on or under rocks.

Etymology. Referring to the ability to colonize spiders.

Additional strain examined. Duyun City (26°21'27.96"N, 107°22'48.22"E), Qiannan Buyi and Miao Autonomous Prefecture, Guizhou, China. On a dead spider (Araneae), 1 October 2019, Wanhao Chen, DY101712.

Pseudometarhizium **W.H. Chen, Y.F. Han, J.D. Liang & Z.Q. Liang gen. nov.**
MycoBank No: 842641

Etymology. Referring to *Metarhizium*-like colony.

Type species. *Pseudometarhizium araneogenum* W.H. Chen, Y.F. Han, J.D. Liang & Z.Q. Liang.

Description. Colonies on PDA, light green, reserve brown to light brown. Conidiophores synnematous or mononematous, erect, scattered. Phialides emerging laterally from synnemata or hyphae, forming a compact hymenium, abruptly narrowing into a helical neck. Conidia, one-celled, fusiform or ellipsoidal.

Host. Spider (Araneae).

Habitat. Near the road, located on or under rocks, or on the underside of leaves of broad-leaved plant species.

Sexual morph. Unknown.

Notes. The light green colonies of *Pseudometarhizium* are similar to those of *Metarhizium* species. However, *Pseudometarhizium* is easily distinguished by the combined datasets (ITS+LSU+RPB2+TEF), and had a close relationship with *Metarhiziopsis*. *Pseudometarhizium* can be easily distinguished from *Metarhiziopsis* by its paecilomyces-like structure and absence of sporodochia.

Pseudometarhizium araneogenum **W.H. Chen, Y.F. Han, J.D. Liang & Z.Q. Liang, sp. nov.**

MycoBank No: 842642

Fig. 4

Type. Duyun City (26°21'27.96"N, 107°22'48.22"E), Qiannan Buyi and Miao Autonomous Prefecture, Guizhou, China. On a dead spider (Araneae), 1 October 2019, Wanhao Chen, GZAC DY10180 (holotype), ex-type living cultures, DY101801.

Description. Spider host completely covered by white mycelium. Conidiophores mononematous, arise from the lateral hyphae. Colonies irregularly on PDA, 1.8–2.8 cm diam. after 14 d at 25 °C, white, consisting of a basal felt, floccose hyphal overgrowth, reverse yellowish to pale brown or green. Prostrate hyphae smooth, septate, hyaline, 1.0–1.2 μm diam. Erect conidiophores usually arising from aerial hyphae. Phialides solitary or in groups of two, 8.3–23.3 × 1.3–2.2 μm, with a cylindrical basal portion, tapering into a short distinct neck. Conidia in chains, hyaline, fusiform, one-celled, 3.4–5.8 × 1.4–1.8 μm. Sexual state not observed.

Host. Spider (Araneidae).

Habitat. Near the road, located on or under rocks.

Etymology. Referring to the ability to colonize spiders.

Additional specimen examined. Duyun City (26°21'27.96"N, 107°22'48.22"E) Qiannan Buyi and Miao Autonomous Prefecture, Guizhou, China. On a dead spider (Araneae), 1 October 2019, Wanhao Chen, GZAC DY10174, living cultures, DY101741, DY101742.

Remarks. *Pseudometarhizium araneogenum* distinguished from *P. lepidopterorum*, which has longer phialides (21.2–33.7 × 1.1–1.4 μm) and smaller conidia (3.1–4.3 × 1.3–1.5 μm).

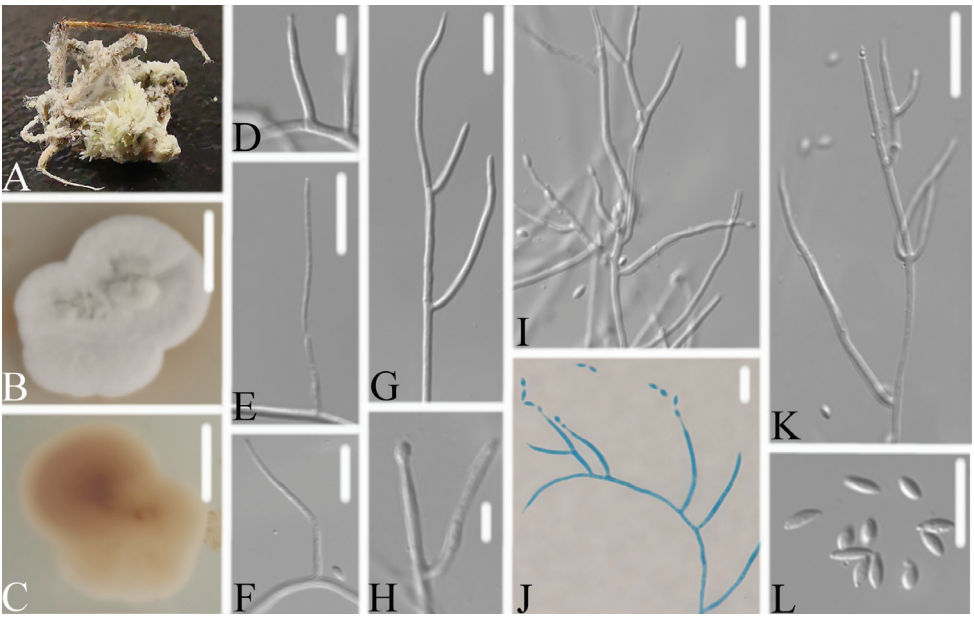

Figure 4. *Pseudometarhizium araneogenum* **A** infected spider **B, C** culture growing on PDA, **B** front and **C** the reverse sides of the colony **D–L** solitary phialides, or groups of two, conidia in short chains and individual. Scale bars: 10 mm (**B, C**); 10 μm (**D–L**).

Pseudometarhizium lepidopterorum **W.H. Chen, Y.F. Han, J.D. Liang & Z.Q. Liang, sp. nov.**

MycoBank No: 842643

Fig. 5

Type. Sandu County (25°57'22.21"N, 107°57'54.69"E), Qiannan Buyi and Miao Autonomous Prefecture, Guizhou, China. On a pupa (Lepidoptera), 1 May 2019, Wanhao Chen, GZAC SD0536 (holotype), ex-type living cultures, SD05361.

Description. Host pupa completely covered by white mycelium. Conidiophores arising from lateral hyphae of the synnemata. Colonies on PDA, 1.4–2.0 cm diam. after 14 d at 25 °C, white, consisting of a basal felt and cottony, floccose hyphal overgrowth, reverse yellowish to pale green. Prostrate hyphae smooth, septate, hyaline, 1.0–2.0 μm diam. Erect conidiophores usually arising from aerial hyphae. Phialides solitary or in groups of two to three, 21.2–33.7 × 1.1–1.4 μm, with a cylindrical basal portion, tapering into a short distinct neck. Conidia in chains, hyaline, fusiform, one-celled, 3.1–4.3 × 1.3–1.5 μm. Sexual state not observed.

Host. Pupa (Lepidoptera).

Habitat. On the underside of leaves of broad-leaved plant species.

Additional strain examined. Sandu County (25°57'22.21"N, 107°57'54.69"E) Qiannan Buyi and Miao Autonomous Prefecture, Guizhou, China. On a pupa (Lepidoptera), 1 May 2019, Wanhao Chen, SD05362.

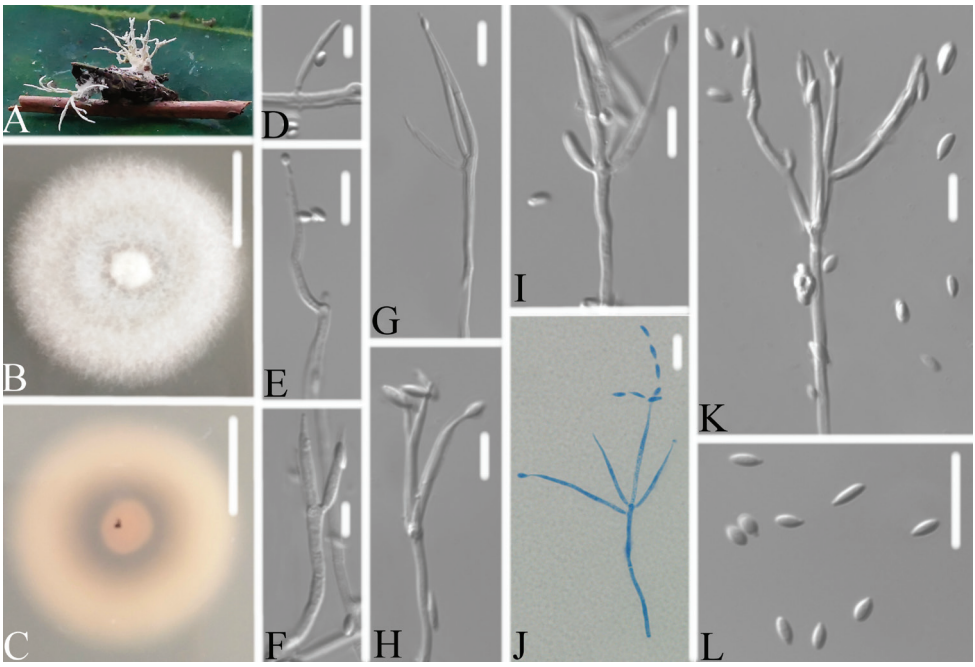

Figure 5. *Pseudometarhizium lepidopterorum* **A** infected pupa (Lepidoptera) **B, C** culture on PDA showing **B** front and **C** reverse sides of the colony **D–L** solitary phialides, or groups of two to three, and conidia in short chains and individual. Scale bars: 10 mm (**B, C**); 10 μm (**D–L**).

Etymology. Referring to its insect host, order Lepidoptera.

Remarks. *Pseudometarhizium lepidopterorum* distinguished from *P. araneogenum*, which has shorter phialides (8.3–23.3 × 1.3–2.2 μm) and longer conidia (3.4–5.8 × 1.4–1.8 μm).

Discussion

Paecilomyces-like conidiogenous structure is common throughout the Hypocreales (Luangsa-ard et al. 2004) and their presence in the new strains make it impossible to identify them using only morphological characteristics. To determine the family placement of the new strains, a phylogenetic tree was constructed with the combined dataset (ITS+LSU+RPB2+TEF) for 14 families of Hypocreales. The new strains clustered into the Clavicipitaceae clade, confirming that they belonged to this family.

Currently, Clavicipitaceae contains 49 genera (Hyde et al. 2020; Mongkolsamrit et al. 2020; Gao et al. 2021). A phylogenetic analysis was carried out based on the available sequences from 39 of these genera. The new strains clustered into independent clades, suggesting that they belong to new genera in the family Clavicipitaceae. Among the genera without available sequences, *Helminthascus* Tranzschel and *Sphaerocordyceps* Kobayasi are spider- and insect-associated teleomorph genera without an asexual state

(Hyde et al. 2020). The new strains were easily distinguished from *Helminthascus* and *Sphaerocordyceps* by their absence of a teleomorph state and pale green color in the natural state. Thus, the new strains are described as two new genera, based on phylogenetic analysis and morphological characteristics.

The evolutionary dynamics of fungi and their hosts are usually described either through coevolution or host shifts (Vega et al. 2009). In a common ecological niche, shifts to new hosts often occur in accordance with the fungal nutrient requirements. The common ancestor of Hypocreaceae and Clavicipitaceae corresponds to a departure from plant-based nutrition to a model that specializes in animals and fungi (Spatafora et al. 2007). Clavicipitaceous fungi, especially those of the genus *Metarhizium*, are pathogenic to scale insects, white flies and other insect orders. However, few spider-associated species have been reported. Based on comparison of their evolutional relationships with close relatives, we hypothesize that the new spider-associated genera might have undergone host jumps or transferred their nutritional preferences.

Both mononematous and synnematous conidiophores were reported in natural conditions in the present study. Synnematous entomopathogenic fungi (such as *Gibellula* spp.) are found on the abaxial leaf surfaces of shrubbery, forest floors and shallow soil layers (Hywel-Jones 1996). These entomopathogenic fungi do not spread by airflow diffusion but employ particular strategies, such as producing synnemata and sticky conidia, to accommodate various arthropod activities and facilitate conidial spread (Abbott 2002). In contrast, strains with mononematous conidiophores occur in more open portions of forests and favor dry conidial dispersal (Chen et al. 2020). *Pseudometarhizium lepidopterorum* was found on the undersides of leaves of broad-leaved plant species, whereas *Neoaraneomyces araneicola* and *P. araneogenum* were found near the road and were located on or under rocks. Thus, we speculate that the presence of synnemata may be the result of convergent evolution to adapt to the ecological environment.

Acknowledgements

This work was funded by National Natural Science Foundation of China (31860002), High-level Innovative Talents Training Object in Guizhou Province (Qiankehepingtairencai [2020]6005), Science and Technology Foundation of Guizhou Province (Qiankehejichu [2020]1Y060), Program of Innovative Scientific and technological Talent Team of Guizhou Province (2020-5010), Construction Program of Guizhou Engineering Research Center (Qian Fa Gai Gao Ji 2020-896), Guizhou Science and Technology Support Project (Qiankehezhicheng [2019]2776).

References

Abbott SP (2002) Insects and other arthropods as agents of vector-dispersal in fungi. http://www.thermapure.com/pdf/AbbottInsectdispersal-2.pdf

Castlebury LA, Rossman AY, Sung GH, Hyten AS, Spatafora JW (2004) Multigene phylogeny reveals new lineage for *Stachybotrys chartarum*, the indoor air fungus. Mycological Research 108(8): 864–872. https://doi.org/10.1017/S0953756204000607

Chen WH, Liu C, Han YF, Liang JD, Liang ZQ (2018) *Akanthomyces araneogenum*, a new Isaria-like araneogenous species. Phytotaxa 379(1): 66–72. https://doi.org/10.11646/phytotaxa.379.1.6

Chen WH, Liu C, Han YF, Liang JD, Tian WY, Liang ZQ (2019) Three novel insect-associated species of *Simplicillium* (Cordycipitaceae, Hypocreales) from Southwest China. MycoKeys 58: 83–102. https://doi.org/10.3897/mycokeys.58.37176

Chen WH, Han YF, Liang JD, Tian WY, Liang ZQ (2020) Morphological and phylogenetic characterisations reveal three new species of *Samsoniella* (Cordycipitaceae, Hypocreales) from Guizhou, China. MycoKeys 74: 1–15. https://doi.org/10.3897/mycokeys.74.56655

Diehl WW (1950) *Balansia* and the Balansiae in America. Agricultural monograph No. 4. U. S. D. A. Washington.

Drummond A, Rambaut A (2007) BEAST: Bayesian evolutionary analysis by sampling trees. BMC Evolutionary Biology 7(1): e214. https://doi.org/10.1186/1471-2148-7-214

Evans HC, Samson RA (1987) Fungal pathogens of spiders. The Mycologist 1(4): 152–159. https://doi.org/10.1016/S0269-915X(87)80107-6

Gao S, Meng W, Zhang L, Yue Q, Zheng X, Xu L (2021) *Parametarhizium* (Clavicipitaceae) gen. nov. with two new species as a potential biocontrol agent isolated from forest litters in Northeast China. Frontiers in Microbiology 12: e131. https://doi.org/10.3389/fmicb.2021.627744

Hyde KD, Norphanphoun C, Maharachchikumbura SSN, Bhat DJ, Jones EBG, Bundhun D, Chen YJ, Bao DF, Boonmee S, Calabon MS, Chaiwan N, Chethana KWT, Dai DQ, Dayarathne MC, Devadatha B, Dissanayake AJ, Dissanayake LS, Doilom M, Dong W, Fan XL, Goonasekara ID, Hongsanan S, Huang SK, Jayawardena RS, Jeewon R, Karunarathna A, Konta S, Kumar V, Lin CG, Liu JK, Liu NG, Luangsa-ard J, Lumyong S, Luo ZL, Marasinghe DS, McKenzie EHC, Niego AGT, Niranjan M, Perera RH, Phukhamsakda C, Rathnayaka AR, Samarakoon MC, Samarakoon SMBC, Sarma VV, Senanayake IC, Shang QJ, Stadler M, Tibpromma S, Wanasinghe DN, Wei DP, Wijayawardene NN, Xiao YP, Yang J, Zeng XY, Zhang SN, Xiang MM (2020) Refined families of Sordariomycetes. Mycosphere 11(1): 305–1059. https://doi.org/10.5943/mycosphere/11/1/7

Hywel-Jones N (1996) *Akanthomyces* on spiders in Thailand. Mycological Research 9(9): 1065–1070. https://doi.org/10.1016/S0953-7562(96)80214-0

Kalyaanamoorthy S, Minh BQ, Wong TK, Von Haeseler A, Jermiin LS (2017) ModelFinder: Fast model selection for accurate phylogenetic estimates. Nature Methods 14(6): 587–589. https://doi.org/10.1038/nmeth.4285

Katoh K, Standley DM (2013) MAFFT multiple sequence alignment software version 7: Improvements in performance and usability. Molecular Biology and Evolution 30(4): 772–780. https://doi.org/10.1093/molbev/mst010

Liang JD, Han YF, Zhang JW, Du W, Liang ZQ, Li ZZ (2011) Optimal culture conditions for keratinase production by a novel thermophilic *Myceliophthora thermophila* strain GZUIFR-

H49-1. Journal of Applied Microbiology 110(4): 871–880. https://doi.org/10.1111/j.1365-2672.2011.04949.x

Luangsa-ard JJ, Hywel-Jones NL, Samson RA (2004) The polyphyletic nature of *Paecilomyces* sensu lato based on 18S-generated rDNA phylogeny. Mycologia 96(4): 773–780. https://doi.org/10.1080/15572536.2005.11832925

Luangsa-ard JJ, Mongkolsamrit S, Thanakitpipattana D, Khonsanit A, Tasanathai K, Noisripoom W, Humber RA (2017) Clavicipitaceous entomopathogens: New species in *Metarhizium* and a new genus *Nigelia*. Mycological Progress 16(4): 369–391. https://doi.org/10.1007/s11557-017-1277-1

Mongkolsamrit S, Noisripoom W, Thanakitpipattana D, Wutikhun T, Spatafora JW, Luangsa-ard JJ (2018) Disentangling cryptic species with isaria-like morphs in Cordycipitaceae. Mycologia 110(1): 230–257. https://doi.org/10.1080/00275514.2018.1446651

Mongkolsamrit S, Noisripoom W, Tasanathai K, Khonsanit A, Thanakitpipattana D, Himaman W, Kobmoo N, Luangsa-ard JJ (2020) Molecular phylogeny and morphology reveal cryptic species in *Blackwellomyces* and *Cordyceps* (Cordycipitaceae) from Thailand. Mycological Progress 19(9): 957–983. https://doi.org/10.1007/s11557-020-01615-2

Rakotonirainy MS, Cariou ML, Brygoo Y, Riba G (1994) Phylogenetic relationships within the genus *Metarhizium* based on 28S rRNA sequences and isozyme comparison. Mycological Research 98(2): 225–230. https://doi.org/10.1016/S0953-7562(09)80190-1

Ronquist F, Teslenko M, van der Mark P, Ayres DL, Darling A, Höhna S, Larget B, Liu L, Suchard MA, Huelsenbeck JP (2012) MrBayes 3.2: Efficient Bayesian phylogenetic inference and model choice across a large model space. Systematic Biology 61(3): 539–542. https://doi.org/10.1093/sysbio/sys029

Shrestha B, Kubátová A, Tanaka E, Oh J, Yoon DH, Sung JM, Sung GH (2019) Spider-pathogenic fungi within Hypocreales (Ascomycota): Their current nomenclature, diversity, and distribution. Mycological Progress 18(8): 983–1003. https://doi.org/10.1007/s11557-019-01512-3

Spatafora JW, Sung GH, Sung JM, Hywel-Jones NL, White Jr JF (2007) Phylogenetic evidence for an animal pathogen origin of ergot and the grass endophytes. Molecular Ecology 16(8): 1701–1711. https://doi.org/10.1111/j.1365-294X.2007.03225.x

Tamura K, Stecher G, Peterson D, Filipski A, Kumar S (2013) MEGA6: Molecular evolutionary genetics analysis version 6.0. Molecular Biology and Evolution 30(12): 2725–2729. https://doi.org/10.1093/molbev/mst197

Trifinopoulos J, Nguyen LT, von Haeseler A, Minh BQ (2016) W-IQ-TREE: A fast online phylogenetic tool for maximum likelihood analysis. Nucleic Acids Research 44(W1): W232–W235. https://doi.org/10.1093/nar/gkw256

Vaidya G, Lohman DJ, Meier R (2011) SequenceMatrix: Concatenation software for the fast assembly of multi-gene datasets with character set and codon information. Cladistics 27(2): 171–180. https://doi.org/10.1111/j.1096-0031.2010.00329.x

van den Brink J, Samson RA, Hagen F, Boekhout T, de Vries RP (2012) Phylogeny of the industrial relevant, thermophilic genera *Myceliophthora* and *Corynascus*. Fungal Diversity 52(1): 197–207. https://doi.org/10.1007/s13225-011-0107-z

Vega FE, Goettel MS, Blackwell M, Chandler D, Jackson MA, Keller KM, Koike M, Maniania NK, Monzón A, Ownley BH, Pell JK, Rangel DEN, Roy HE (2009) Fungal entomopathogens: New insights on their ecology. Fungal Ecology 2(4): 149–159. https://doi.org/10.1016/j.funeco.2009.05.001

White TJ, Bruns T, Lee S, Taylor J (1990) Amplification and direct sequencing of fungal ribosomal RNA genes for phylogenetics. In: Innis MA, Gelfand DH, Sninsky JJ, White TJ (Eds) PCR protocols: a guide to methods and applications. Academic Press, New York, 315–322. https://doi.org/10.1016/B978-0-12-372180-8.50042-1

Zhang D, Gao F, Jakovlić I, Zou H, Zhang J, Li WX, Wang GT (2020) PhyloSuite: An integrated and scalable desktop platform for streamlined molecular sequence data management and evolutionary phylogenetics studies. Molecular Ecology Resources 20(1): 348–355. https://doi.org/10.1111/1755-0998.13096

Zou X, Liu AY, Liang ZQ, Han YF, Yang M (2010) *Hirsutella liboensis*, a new entomopathogenic species affecting Cossidae (Lepidoptera) in China. Mycotaxon 111(1): 39–44. https://doi.org/10.5248/111.39

Supplementary material 1

Table S1

Authors: Wan-Hao Chen, Jian-Dong Liang, Xiu-Xiu Ren, Jie-Hong Zhao, Yan-Feng Han, Zong-Qi Liang

Data type: COL.

Explanation note: Primers information for 5 DNA sequences.

Link: https://doi.org/10.3897/mycokeys.91.86812.suppl1

MycoKeys 91: 67–84 (2022)
doi: 10.3897/mycokeys.91.86693
https://mycokeys.pensoft.net

RESEARCH ARTICLE

A peer-reviewed open-access journal
MycoKeys
Launched to accelerate biodiversity research

Pseudocryphonectria elaeocarpicola gen. et sp. nov. (Cryphonectriaceae, Diaporthales) causing stem blight of *Elaeocarpus* spp. in China

Hua-Yi Huang[1], Huan-Hua Huang[1], Dan-Yang Zhao[1], Ti-Jiang Shan[2], Li-Li Hu[1]

1 *Guangdong Provincial Key Laboratory of Silviculture, Protection and Utilization, Guangdong Academy of Forestry, Guangzhou 510520, China* **2** *Guangdong Province Key Laboratory of Microbial Signals and Disease Control, College of Forestry and Landscape Architecture, South China Agricultural University, Guangzhou 510642, China*

Corresponding author: Li-Li Hu (hulili0113@sinogaf.cn)

Academic editor: S. Maharachchikumbura | Received 18 May 2022 | Accepted 15 June 2022 | Published 15 July 2022

Citation: Huang H-Y, Huang H-H, Zhao D-Y, Shan T-J, Hu L-L (2022) *Pseudocryphonectria elaeocarpicola* gen. et sp. nov. (Cryphonectriaceae, Diaporthales) causing stem blight of *Elaeocarpus* spp. in China. MycoKeys 91: 67–84. https://doi.org/10.3897/mycokeys.91.86693

Abstract

Cryphonectriaceae is a diaporthalean family containing important plant pathogens of which *Cryphonectria parasitica* is the most notorious one. An emerging stem blight disease on *Elaeocarpus apiculatus* (Elaeocarpaceae) and *E. hainanensis* was observed in Guangdong Province of China recently. Typical Cryphonectria blight-like symptoms including cankers on tree barks with obvious orange conidial tendrils were observed. Forty-eight isolates were obtained from diseased tissues and conidiomata formed on the hosts *E. apiculatus* and *E. hainanensis*. These isolates were further identified based on both morphology and molecular methods using the combined sequence data of the internal transcribed spacer (ITS) region, large subunit of the nrDNA (LSU), the translation elongation factor 1-alpha (*tef1*) and DNA-directed RNA polymerase II second largest subunit (*rpb2*) genes. As a result, the fungus represents an undescribed genus and species within the family Cryphonectriaceae. Hence, *Pseudocryphonectria elaeocarpicola* **gen. et sp. nov.** is proposed herein to represent these isolates from diseased barks of *E. apiculatus* and *E. hainanensis*. *Pseudocryphonectria* differs from the other genera of Cryphonectriaceae in having dimorphic conidia. Further inoculation results showed that *P. elaeocarpicola* is the causal agent of this emerging blight disease in China, which can quickly infect and kill the hosts *E. apiculatus* and *E. hainanensis*.

Keywords

Ascomycota, phylogeny, plant disease, taxonomy

Introduction

Diaporthales represents a species-rich fungal order usually inhabiting plant tissues as pathogens, endophytes and saprophytes (Rossman et al. 2007; Senanayake et al. 2017; Voglmayr et al. 2017; Fan et al. 2018; Jaklitsch and Voglmayr 2020; Jiang et al. 2021a). Cryphonectriaceae is a pathogenic family within Diaporthales including several serious plant pathogens (Gryzenhout et al. 2006; Chen et al. 2016). For example, *Cryphonectria parasitica* causes chestnut (*Castanea* spp.) blight disease worldwide (Rigling and Prospero 2017); *Chrysoporthe austroafricana*, *Ch. cubensis* and *Ch. deuterocubensis* result in eucalypt (*Eucalyptus* spp.) canker diseases in Africa, South America and Asia, respectively (Ferreira and Henfling 1976; Wingfield 1989; Old et al. 2003; Wang et al. 2020).

In a recent study, the family Cryphonectriaceae was re-evaluated based on morphological and molecular data of the ex-type strains, which accepted two subclades in the family with 21 genera and 55 species (Jiang et al. 2020). Subsequently, *Capillaureum* and *Parvosmorbus* were added to this family evidenced by both morphology and phylogeny (Ferreira et al. 2019; Wang et al. 2020). Currently, 23 genera were classified in Cryphonectriaceae based on morphological characters and combined sequence data of the internal transcribed spacer (ITS) region, large subunit of the nrDNA (LSU), and the translation elongation factor 1-alpha (*tef1*) and DNA-directed RNA polymerase II second largest subunit (*rpb2*) genes (Wijayawardene et al. 2018; Hyde et al. 2020; Jiang et al. 2020; Wang et al. 2020).

Cryphonectriaceae members are characterized by typical diaporthalean characters of perithecia with elongate beaks, often forming within stromatic tissues, deliquescent paraphyses, and asci that generally deliquesce, become detached from the perithecial wall when mature, and have a refractive apical annulus (Voglmayr et al. 2012; Senanayake et al. 2018; Jaklitsch and Voglmayr 2019; Jiang et al. 2019b; Fan et al. 2020; Udayanga et al. 2021). Species of Cryphonectriaceae except *Aurantiosacculus castaneae* are different from the other diaporthalean taxa by owning orange stromatic tissues at some stage during their life cycle, which turn purple in 3% KOH and yellow in lactic acid (Gryzenhout et al. 2006; Jiang et al. 2019a).

Trees and shrubs of *Elaeocarpus* (Elaeocarpaceae) are evergreen plants, of which several species are planted along streets and in parks. *E. apiculatus* and *E. hainanensis* are commonly used as garden trees in Guangdong Province, however, suffering a serious stem blight disease currently. The present study aims to identify the causal agent based on modern taxonomic approaches and to confirm its pathogenicity.

Materials and methods

Sample survey, fungal isolation and morphology

In the present study, we investigated stem blight disease of *Elaeocarpus apiculatus* and *E. hainanensis* in Guangdong Province of China during 2020 and 2022. The disease symptoms on the *Elaeocarpus* trees generally occur on host stems and branches, with cankered barks and orange conidial tendrils (Fig. 1). Most diseased trees died within five

months of infection during our investigations. Diseased barks with or without fruiting bodies were collected, packed in paper bags and transferred to the laboratory for isolation.

The diseased barks without orange fungal fruiting bodies were firstly surface-sterilized for 2 min in 75% ethanol, 4 min in 1.25% sodium hypochlorite, and 1 min in 75% ethanol, then rinsed for 2 min in distilled water and blotted on dry sterile filter paper. Then diseased tissues were cut into 0.5 cm × 0.5 cm pieces using a double-edge

Figure 1. Symptoms caused by *Pseudocryphonectria elaeocarpicola* on *Elaeocarpus* trees. **A, B** dead trees **C–E** cankered barks **F, G** orange conidial tendrils formed on the cankered barks.

blade, and transferred onto the surface of potato dextrose agar (PDA; 200 g potatoes, 20 g dextrose, 20 g agar per L), and incubated at 25 °C to obtain pure cultures. The diseased barks with fungal fruiting bodies were checked, and single conidial isolates were obtained from conidiomata by removing the mucoid conidial masses and spreading the suspension onto the surface of PDA. Agar plates were incubated at 25 °C to induce germination of the conidia. After inoculation for up to 48 h, single germinating conidium was then transferred to clean plates under a dissecting stereomicroscope with a sterile needle. The cultures were deposited in China Forestry Culture Collection Center (CFCC, http://cfcc.caf.ac.cn/), and the specimens in the herbarium of the Chinese Academy of Forestry (CAF, http://museum.caf.ac.cn/).

The morphological data of the new taxa in the present study were based on the conidiomata formed on the cankered barks, supplemented by cultural characters. The conidiomata were sectioned and photographed under a dissecting microscope (M205 C, Leica, Wetzlar, Germany). The conidiogenous cells and conidia were immersed in tap water, then the microscopic photographs were captured with an Axio Imager 2 microscope (Zeiss, Oberkochen, Germany) equipped with an Axiocam 506 color camera, using differential interference contrast (DIC) illumination. More than 50 conidia were randomly selected for measurement. Culture characters were recorded from PDA after 7 d incubation at 25 °C in the dark.

DNA extraction, PCR amplification and phylogenetic analyses

The fungal genomic DNA was extracted from mycelia grown on cellophane-covered PDA following the method in Doyle and Doyle (1990). DNA was checked by electrophoresis in 1% agarose gel, and the quality and quantity were measured using a NanoDrop 2000 (Thermo Scientific, Waltham, MA, USA). Four partial loci, ITS and LSU regions, *tef1* and *rpb2* genes were amplified by the following primer pairs: ITS1 and ITS4 for ITS (White et al. 1990), LR0R and LR5 for LSU (Vilgalys and Hester 1990), EF1-688F and EF2 for *tef1* (Carbone and Kohn 1999), and RPB2-5F and RPB2-7cR for *rpb2* (Liu et al. 1999). The polymerase chain reaction (PCR) conditions were as follows: an initial denaturation step of 5 min at 94 °C, followed by 35 cycles of 30 s at 94 °C, 50 s at 48 °C (ITS and LSU) or 54 °C (*tub2*) or 55 °C (*rpb2*), and 1 min at 72 °C, and a final elongation step of 10 min at 72 °C. PCR products were assayed via electrophoresis in 2% agarose gels. DNA sequencing was performed using an ABI PRISM 3730XL DNA Analyser with a BigDye Terminator Kit v.3.1 (Invitrogen, Waltham, MA, USA) at the Shanghai Invitrogen Biological Technology Company Limited (Beijing, China).

The sequences obtained in the present study were assembled using SeqMan v. 7.1.0, and reference sequences were retrieved from the National Center for Biotechnology Information (NCBI), based on recent publications (Chen et al. 2018; Jiang et al. 2019a, 2020; Wang et al. 2020). The sequences were aligned using MAFFT v. 6 and corrected manually using MEGA v. 7.0.21 (Katoh and Toh 2010).

The phylogenetic analyses of combined matrixes of the ITS-LSU loci and four loci (ITS-LSU-*tef1*-*rpb2*) were performed using Maximum Likelihood (ML) and Bayesian Inference (BI) methods. ML was implemented on the CIPRES Science Gateway portal

(https://www.phylo.org) using RAxML-HPC BlackBox 8.2.10 (Miller et al. 2010; Stamatakis 2014), employing a GTR-GAMMA substitution model with 1000 bootstrap replicates. Bayesian inference was performed using a Markov Chain Monte Carlo (MCMC) algorithm in MrBayes v. 3.0 (Ronquist and Huelsenbeck 2003). Two MCMC chains, starting from random trees for 1000000 generations and trees, were sampled every 100th generation, resulting in a total of 10000 trees. The first 25% of trees were discarded as burn-in of each analysis. Branches with significant Bayesian Posterior Probabilities (BPP > 0.9) were estimated in the remaining 7500 trees. Phylogenetic trees were viewed with FigTree v. 1.3.1 and processed by Adobe Illustrator CS5. The nucleotide sequence data of the new taxon were deposited in GenBank, and the GenBank accession numbers of all accessions included in the phylogenetic analyses are listed in Table 1.

Table 1. Isolates and GenBank accession numbers used in the phylogenetic analyses.

Species	Isolate	GenBank Accession Number			
		ITS	LSU	*tef1*	*rpb2*
Amphilogia gyrosa	CBS 112922*	AF452111	AY194107	MN271818	MN271782
Amphilogia gyrosa	CBS 112923	AF452112	AY194108	MN271819	MN271783
Aurantioporthe corni	CMW 10526	DQ120762	AF408343	NA	NA
Aurantioporthe corni	CBS 245.90	MN172403	MN172371	MN271822	MN271784
Aurantiosacculus acutatus	CBS 132181*	JQ685514	JQ685520	MN271823	NA
Aurantiosacculus eucalyptorum	CBS 130826*	JQ685515	JQ685521	MN271824	MN271785
Aurantiosacculus castaneae	CFCC 52456*	MH514025	MH514015	NA	MN271786
Aurapex penicillata	CBS 115740*	AY214311	AY194103	NA	NA
Aurapex penicillata	CBS 115742	AY214313	MN172372	NA	NA
Aurapex penicillata	CBS 115801	MN172404	MN172373	NA	MN271787
Aurifilum marmelostoma	CBS 124928*	FJ890495	MH874934	MN271827	MN271788
Aurifilum marmelostoma	CBS 124929	FJ882855	HQ171215	MN271828	MN271789
Capillaureum caryovora	CBL02*	MG192094	MG192104	NA	NA
Celoporthe dispersa	CBS 118782*	DQ267130	HQ730853	HQ730840	NA
Celoporthe eucalypti	CBS 127190*	HQ730837	HQ730863	HQ730850	MN271790
Celoporthe guangdongensis	CBS 128341*	HQ730830	HQ730856	HQ730843	NA
Celoporthe syzygii	CBS 127218*	HQ730831	HQ730857	HQ730844	NA
Celoporthe woodiana	CBS 118785*	DQ267131	MN172375	JQ824071	MN271791
Chrysomorbus lagerstroemiae	CBS 142594*	KY929338	KY929328	MN271830	NA
Chrysomorbus lagerstroemiae	CBS 142592	KY929330	KY929320	MN271831	NA
Chrysoporthe austroafricana	CBS 112916*	AF292041	AY194097	MN271832	NA
Chrysoporthe austroafricana	CBS 115843	AF273473	MN172377	MN271833	NA
Chrysoporthe cubensis	CBS 118654*	DQ368773	MN172378	MN271834	NA
Chrysoporthe cubensis	CBS 505.63	AY063476	MN172379	MN271835	MN271792
Chrysoporthe hodgesiana	CBS 115854*	AY692322	MN172380	MN271836	MN271793
Chrysoporthe hodgesiana	CBS 115744	AY956970	MN172381	MN271837	NA
Chrysoporthe inopina	CBS 118659*	DQ368777	MN172382	MN271838	NA
Chrysoporthe syzygiicola	CBS 124488*	FJ655005	MN172383	MN271839	NA
Chrysoporthe zambiensis	CBS 124503*	FJ655002	MN172384	MN271840	NA
Corticimorbus sinomyrti	CBS 140205*	KT167169	KT167179	MN271841	MN271794
Corticimorbus sinomyrti	CBS 140206	KT167170	KT167180	MN271842	MN271795
Cryphonectria citrina	CBS 109758*	MN172407	EU255074	MN271843	EU219342
Cryphonectria decipens	CBS 129351	EU442657	MN172385	MN271844	MN271796
Cryphonectria decipens	CBS 129353	EU442655	MN172386	MN271845	MN271797

Species	Isolate	GenBank Accession Number			
		ITS	LSU	*tef1*	*rpb2*
Cryphonectria japonica	CFCC 52148	MH514033	MH514023	MN271846	NA
Cryphonectria macrospora	CBS 109764	EU199182	AF408340	NA	EU220029
Cryphonectria neoparasitica	CFCC 52146*	MH514029	MH514019	MN271847	NA
Cryphonectria parasitica	ATCC 38755	MH843497	MH514021	NA	DQ862017
Cryphonectria parasitica	CFCC 52150	AY141856	EU199123	MN271848	NA
Cryphonectria quercus	CFCC 52138*	MG866024	NA	MN271849	NA
Cryphonectria quercicola	CFCC 52141*	MG866027	NA	MN271850	NA
Cryphonectria radicalis	CBS 112917	AF452113	AY194101	NA	NA
Cryptometrion aestuescens	CBS 124007*	GQ369457	MN172387	MN271851	MN271798
Cryptometrion aestuescens	CBS 124008	GQ369458	HQ171211	MN271852	MN271799
Diaporthe eres	LC3198	KP267873	KY011845	KP267947	NA
Diversimorbus metrosiderotis	CBS 132866*	JQ862871	JQ862828	MN271857	NA
Diversimorbus metrosiderotis	CBS 132865	JQ862870	JQ862827	MN271858	NA
Endothia chinensis	CFCC 52144*	MH514027	MH514017	MN271860	NA
Holocryphia eucalypti	CBS 115842*	MN172411	MN172391	MN271882	MN271804
Holocryphia capensis	CBS 132870*	JQ862854	JQ862811	MN271883	NA
Holocryphia gleniana	CBS 132871*	JQ862834	JQ862791	MN271884	NA
Holocryphia mzansi	CBS 132874*	JQ862841	JQ862798	MN271885	NA
Immersiporthe knoxdaviesiana	CBS 132862*	JQ862765	JQ862755	MN271886	MN271805
Immersiporthe knoxdaviesiana	CBS 132863	JQ862766	JQ862756	MN271887	MN271806
Latruncellus aurorae	CBS 125526*	GU726947	HQ730872	MN271888	NA
Latruncellus aurorae	CBS 124904	GU726946	HQ171213	MN271889	NA
Luteocirrhus shearii	CBS 130776*	KC197021	KC197019	MN271890	MN271807
Luteocirrhus shearii	CBS 130775	KC197024	KC197018	MN271891	MN271808
Microthia havanensis	CBS 115855	DQ368735	MN172393	NA	MN271811
Microthia havanensis	CBS 115841	DQ368736	MN172394	NA	NA
Microthia havanensis	CBS 115758	DQ368737	MN172395	NA	NA
Myrtonectria myrtacearum	CMW 46433*	MG585736	MG585750	NA	NA
Myrtonectria myrtacearum	CMW 46435	MG585737	MG585751	NA	NA
Parvosmorbus eucalypti	CSF2060	MN258787	MN258843	MN258829	NA
Parvosmorbus guangdongensis	CSF10437	MN258795	MN258851	MN258837	NA
Pseudocryphonectria elaeocarpicola	**CFCC 57515***	**ON489048**	**ON489050**	**ON456916**	**ON456918**
Pseudocryphonectria elaeocarpicola	**CFCC 57516**	**ON489049**	**ON489051**	**ON456917**	**ON456919**
Rostraureum tropicale	CBS 115725*	AY167435	MN172399	MN271895	MN271814
Rostraureum tropicale	CBS 115757	AY167438	MN172400	MN271896	MN271815
Ursicollum fallax	CBS 118663*	DQ368755	EF392860	MN271897	MN271816
Ursicollum fallax	CBS 118662	DQ368756	MN172401	MN271898	MN271817

Note: NA, not applicable. Ex-type strains are marked with *, and strains from the present study are in black bold.

Pathogenicity tests

Three isolates of the new species *Pseudocryphonectria elaeocarpicola* (ex-type strain: CFCC 57515, CFCC 57516 and CFCC 57517) were used for inoculations, and PDA plugs were used as the negative control. Three isolates were grown on PDA for four days at 25 °C before the tests. Inoculations were performed on 2-year-old seedlings of *Elaeocarpus apiculatus* and *E. hainanensis*, respectively. A total of 40 healthy seedlings were used for the pathogenicity tests. Five seedlings were inoculated with each isolate and the negative control. Inoculations were conducted following the method in Jiang et al. (2019a). The results were evaluated

after ten days by measuring the lengths of the lesions on the cambium. The re-isolations were made from the resultant lesions from all tested seedlings by cutting small pieces of discolored xylem and placing them onto the PDA plates. Re-isolates were identified based on the ITS sequences. Differences among isolates in lesion length were analyzed by one-way analysis of variance (ANOVA) followed by least significant difference (LSD) tests. Statistical analysis was carried out by R software (v. 3.4.3) and considered as significant at $p < 0.05$.

Results

Incidence and isolates

Surveys of *Elaeocarpus apiculatus* and *E. hainanensis* stem blight were conducted in Guangdong Province during 2020 and 2022. Disease incidence was evaluated based on the percentage of the two hosts showing symptoms of all the investigated plants. As shown in Table 2, the disease incidences are all above 85% in seven locations, which indicates this disease poses a serious threat to these two tree hosts.

A total of 42 isolates were obtained from the symptomatic tissues of *E. apiculatus* and *E. hainanensis*, and six isolates from the conidiomata formed on the cankered barks. They are identical based on the sequence data, hence isolates CFCC 57515 from *E. hainanensis* and CFCC 57516 from *E. apiculatus* were selected for phylogenetic analyses.

Table 2. Occurrence and incidence of *Elaeocarpus apiculatus* and *E. hainanensis* stem blight in different locations in Guangzhou City.

District	Location	Host	Diseased trees	Dead trees	Healthy Trees	Total	Disease incidence (%)
Tianhe	Longdong Street	*E. apiculatus*	9	10	0	19	100
Tianhe	Guangdong tree Park	*E. apiculatus*	14	9	2	25	92
Tianhe	Shuanglin Street	*E. apiculatus*	18	4	2	24	91.67
Tianhe	Guangdong Eco-Engineering Polytechnic	*E. apiculatus*	11	2	0	13	100
Tianhe	South China Botanical Garden	*E. apiculatus*	5	3	1	9	88.89
Liwan	Meihua Middle School	*E. hainanensis*	3	5	0	8	100
Yuexiu	Luhu Park	*E. apiculatus*	41	21	6	68	91.18

Phylogenetic analyses

The sequence dataset of the ITS-LSU gene matrix was analysed to infer the genus and species relationships within Cryphonectriaceae. The dataset consisted of 71 sequences including one outgroup taxon, *Diaporthe eres* (LC 3198). A total of 1580 characters including gaps were included in the phylogenetic analysis. The topologies resulting from ML and BI analyses of the concatenated dataset were congruent (Fig. 2). Isolates from the present study formed a distinct clade from the other genera of Cryphonectriaceae, which represents an undescribed genus.

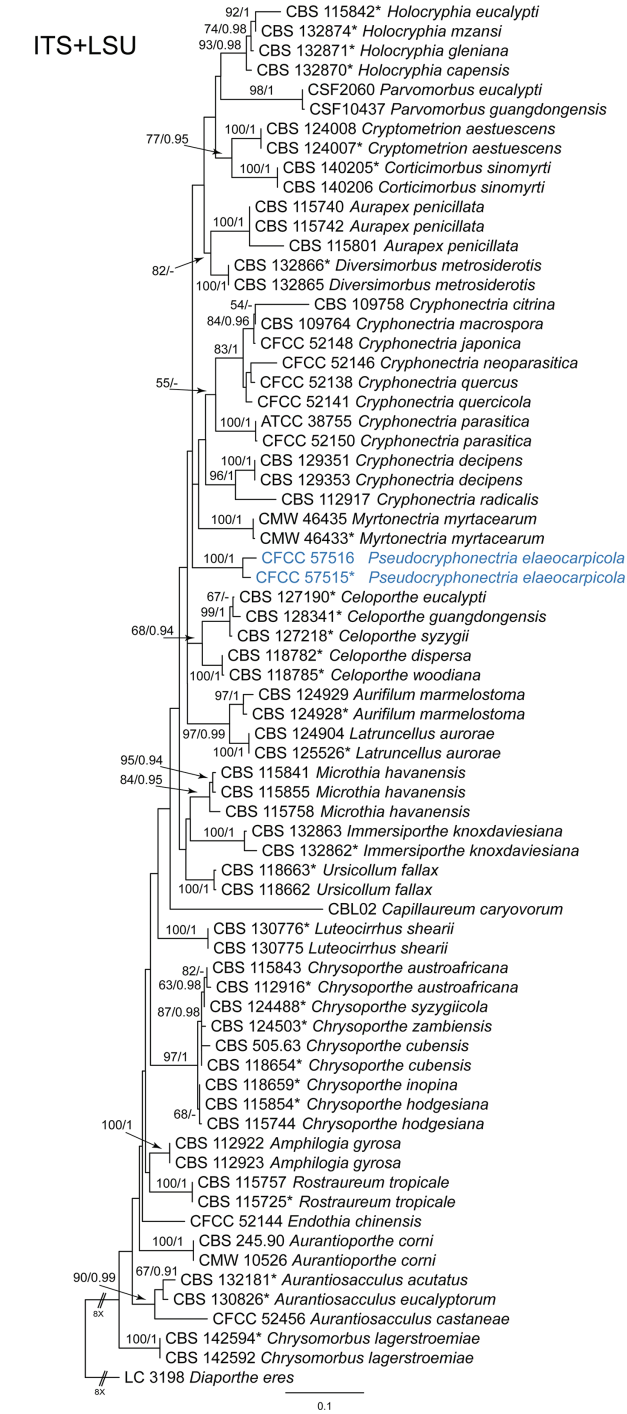

Figure 2. Phylogram of Cryphonectriaceae resulting from a maximum likelihood analysis based on combined ITS and LSU loci. Numbers above the branches indicate ML bootstrap values (left, ML-BS ≥ 50%) and Bayesian Posterior Probabilities (right, BPP ≥ 0.9). The tree is rooted with *Diaporthe eres* (LC 3198). Isolates from the present study are marked in blue, and ex-type strains are marked with *.

The combined four-loci sequence dataset (ITS, LSU, *tef1* and *rpb2*) was further analysed to compare with results of the phylogenetic analyses of the ITS-LSU gene matrix. The dataset consisted of 50 sequences including one outgroup taxon, *Diaporthe eres* (LC 3198). A total of 3226 characters including gaps (726 for ITS, 854 for LSU, 811 for *tef1* and 835 for *rpb2*) were included in the phylogenetic analysis. The topologies resulting from ML and BI analyses of the concatenated combined dataset were congruent (Fig. 3). Isolates from the present study formed a distinct clade which was congruent with that shown in Fig. 2.

Taxonomy

Pseudocryphonectria **Huayi Huang, gen. nov.**
MycoBank No: 844044

Etymology. Named derived from *pseudo-* and the genus name *Cryphonectria*.

Type species. *Pseudocryphonectria elaeocarpicola* Huayi Huang

Description. Sexual morph: Unknown. Asexual morph: *Conidiomata* pycnidial, aggregated or solitary, immersed under the host bark, subglobose to pulvinate, yellow to orange, multilocular, single ostiolate, forming long orange tendrils. *Conidiophores* cylindrical, aseptate, hyaline, sometimes reduced to conidiogenous cells. *Conidiogenous cells* lining inner cavity of conidiomata, phialidic, ampulliform, with attenuated or truncate apices, hyaline, smooth. *Conidia* dimorphic. *Microconidia* minute, aseptate, hyaline, smooth, cylindrical, straight. *Macroconidia* aseptate, hyaline, smooth, obclavate, straight or slightly curved.

Notes. *Pseudocryphonectria* has typical orange cryphonectriaceous stromata, which turns purple the 3% KOH and yellow in lactic acid. This genus is characterized by its dimorphic conidia from the same conidioma, which is different from the other genera of Cryphonectriaceae (Chen et al. 2013, 2016, 2018; Beier et al. 2015; Jiang et al. 2020).

Pseudocryphonectria elaeocarpicola **Huayi Huang, sp. nov.**
MycoBank No: 844045
Figs 4, 5

Etymology. Named after the host genus, *Elaeocarpus*.

Description. Sexual morph: Unknown. Asexual morph: *Conidiomata* pycnidial, aggregated or solitary, immersed under the host bark, subglobose to pulvinate, yellow to orange, 500–1200 μm wide, 150–450 μm high, multilocular, single ostiolate, forming long orange tendrils. ***Conidiophores*** cylindrical, aseptate, hyaline, sometimes reduced to conidiogenous cells. ***Conidiogenous cells*** lining inner cavity of conidiomata, phialidic, ampulliform, with attenuated or truncate apices, hyaline, smooth, 12.8–25.7 × 1.7–3.2 μm (n = 50). ***Conidia*** dimorphic. ***Microconidia*** minute, aseptate, hyaline, smooth, cylindrical, straight, (3.1–)3.3–4(–4.4) × (1.5–)1.6–2(–2.1) μm (n = 50), L/W = 1.6–2.7. ***Macroconidia*** aseptate, hyaline, smooth, obclavate, straight or slightly curved, (4.6–)5.1–6.1(–6.6) × (1.4–)1.6–2(–2.2) μm (n = 50), L/W = 2.5–3.9.

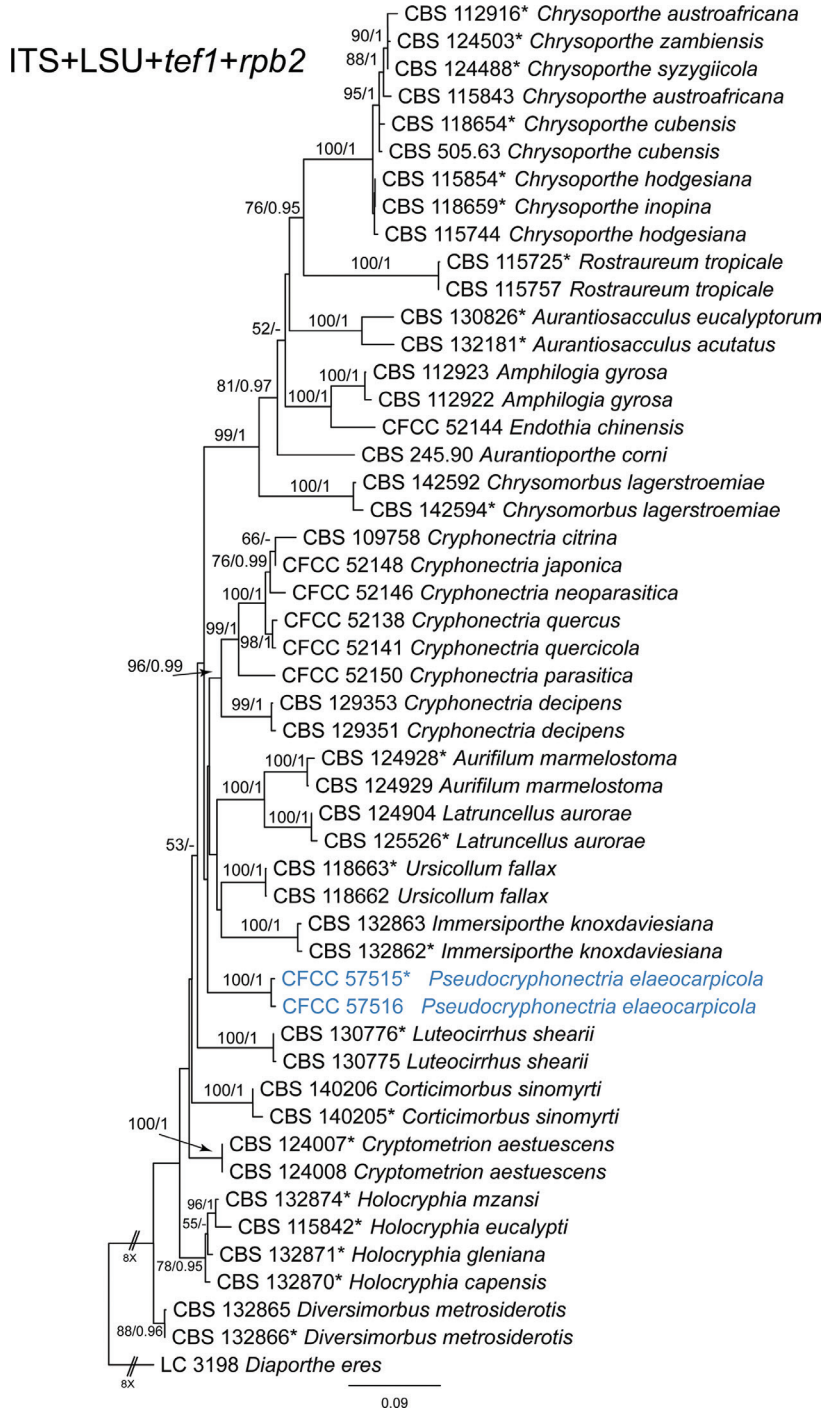

Figure 3. Phylogram of Cryphonectriaceae resulting from a maximum likelihood analysis based on combined ITS, LSU, *tef1* and *rpb2* loci. Numbers above the branches indicate ML bootstrap values (left, ML-BS ≥ 50%) and Bayesian Posterior Probabilities (right, BPP ≥ 0.9). The tree is rooted with *Diaporthe eres* (LC 3198). Isolates from the present study are marked in blue, and ex-type strains are marked with *.

Culture characters. ***Colonies*** on PDA flat, spreading, with aerial mycelium and entire margin, white to mouse grey, forming abundant orange conidiomata with orange conidial masses.

Specimens examined. China, Guangdong Province, Guangzhou City, Meihua middle school, 23°8'37.94"N, 113°14'18.12"E, 24 m asl, on stems and branches of *Elaeocarpus hainanensis*, 7 March 2022, Huayi Huang (CAF800051 holotype; ex-type

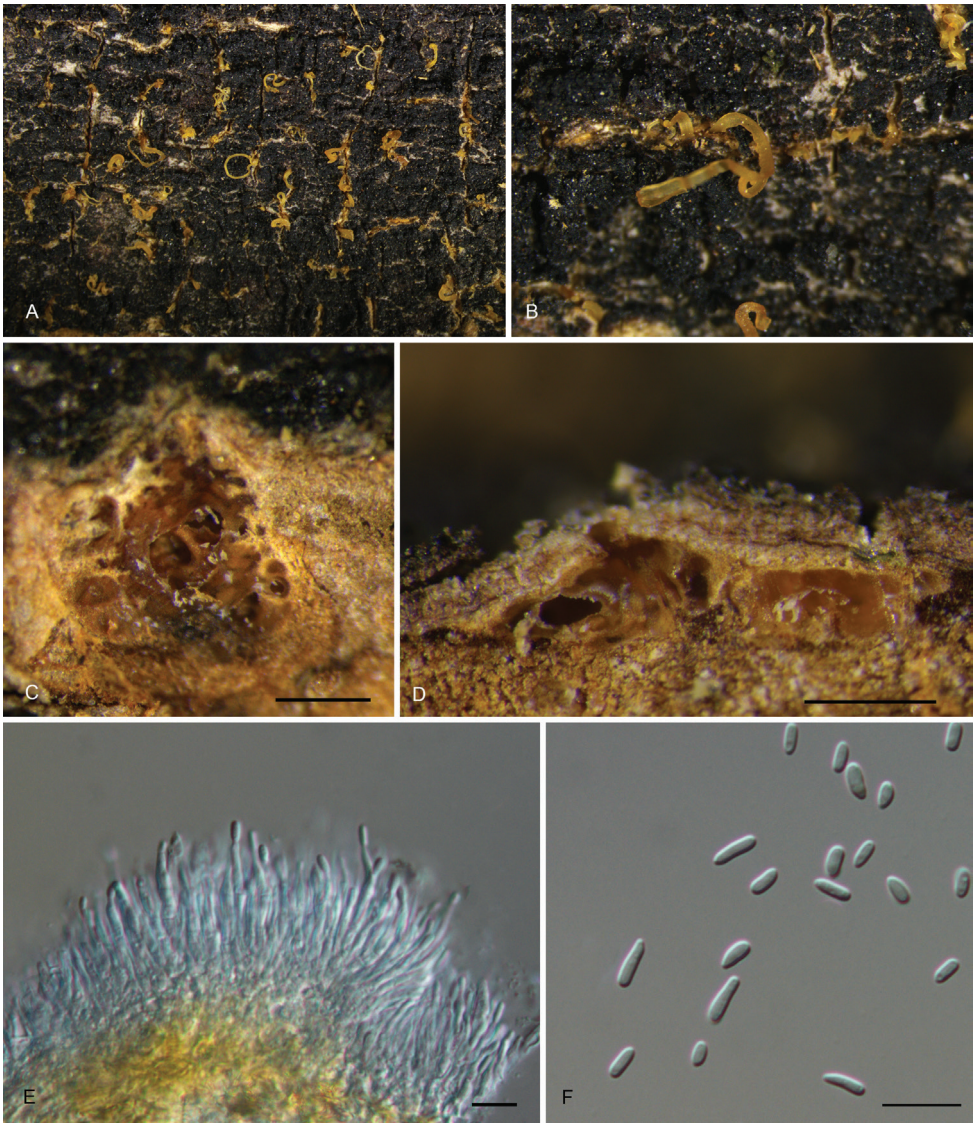

Figure 4. Morphology of *Pseudocryphonectria elaeocarpicola* from *Elaeocarpus hainanensis* **A, B** habit of conidiomata on the host stem **C** transverse section through the conidioma **D** longitudinal section through the conidioma **E** conidiogenous cells giving rise to conidia **F** macroconidia and microconidia. Scale bars: 300 μm (**C, D**); 10 μm (**E, F**).

living culture, CFCC 57515). Guangdong Province, Guangzhou City, Luhu Park, 23°9'11.15"N, 113°16'46.01"E, 92 m asl, on stems and branches of *E. apiculatus*, Huayi Huang, 15 March 2022 (CAF800055 paratype; ex-paratype living culture, CFCC 57516). Guangdong Province, Guangzhou City, Longdong straight street, 23°11'41.02"N, 113°22'8.33"E, 46 m asl, on stems and branches of *E. apiculatus*, Huayi Huang, 1 April 2022 (DY03, culture, CFCC 57517). Guangdong Province, Guangzhou City, South China botanical garden, 23°11'3.5"N, 113°21'41.53"E, 39 m asl, on stems and branches of *E. apiculatus*, Huayi Huang, 11 April 2022 (DY24, culture, DY24-2). Guangdong Province, Guangzhou City, Linke 1st street, 23°11'35.81"N, 113°22'46.69"E, 74 m asl, on stems and branches of *E. apiculatus*, Huayi Huang, 15 April 2022 (DY32; culture, DY32-1). Guangdong Province, Guangzhou City, Nonglin middle street, 23°11'23.84"N, 113°22'43.08"E, 46 m asl, on stems and branches of *E. apiculatus*, Huayi Huang, 15 April 2022 (DY42, culture, DY42-1).

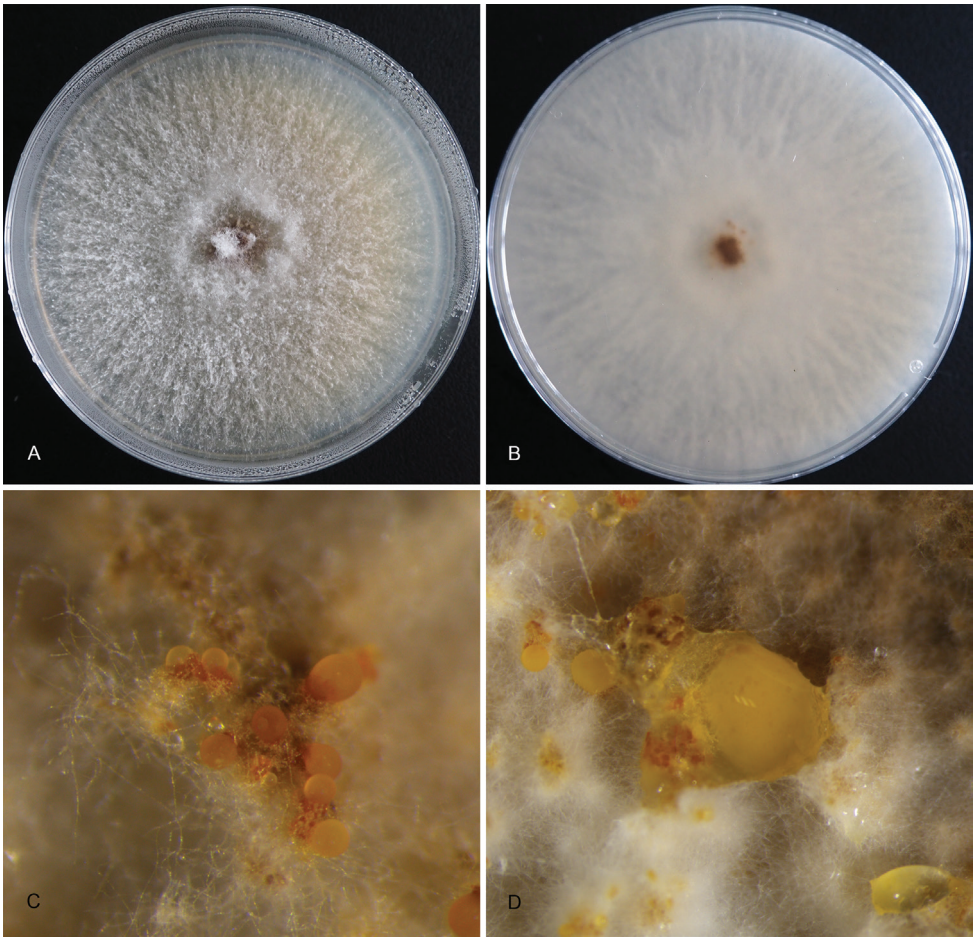

Figure 5. Morphology of *Pseudocryphonectria elaeocarpicola* from PDA **A, B** colonies **C, D** orange conidiomata.

Notes. *Pseudocryphonectria elaeocarpicola* is the sole species within the new genus, which causes serious stem blight of *Elaeocarpus* trees. Another notorious pathogen in Cryphonectriaceae, *Cryphonectria parasitica*, causes serious chestnut worldwide. Morphologically, *P. elaeocarpicola* is similar to *C. parasitica* in the appearance of conidiomata with orange conidial tendrils formed on the host bark. However, *P. elaeocarpicola* can be distinguished from *C. parasitica* by its obvious dimorphic conidia (Jiang et al. 2019a). Phylogenetically, isolates of *P. elaeocarpicola* clustered into a distinct clade in the phylograms of Cryphonectriaceae (Figs 2, 3).

Pathogenicity tests

Ten days after inoculation on young seedlings of *Elaeocarpus apiculatus* and *E. hainanensis*, isolates CFCC 57515, CFCC 57516 and CFCC 57517 all caused death of the host, and formed orange conidiomata on the barks, and the negative control only produced minor lesions (Fig. 6). Statistical analyses of data showed no significant difference among three tested isolates on two hosts of *E. apiculatus* and *E. hainanensis*, however, significantly different from the negative control (Fig. 7). Isolates were obtained from lesions produced on tested seedlings, and were identical to *Pseudocryphonectria elaeocarpicola* based on the sequence data and morphology of conidiomata formed on the barks. Hence, *P. elaeocarpicola* can quickly infect *E. apiculatus* and *E. hainanensis*, and kill the hosts.

Discussion

In the present study, the causal agent of stem blight on *Elaeocarpus apiculatus* and *E. hainanensis* was identified using both morphological and phylogenetical approaches, which revealed a new genus and species, namely *Pseudocryphonectria elaeocarpicola*. Further pathogenicity test conducted on the two original hosts *E. apiculatus* and *E. hainanensis* confirmed the high virulence of the fungal pathogen. In ten days, the fungus can infect the host and kill both *E. apiculatus* and *E. hainanensis*. As shown in Table 2, the pathogen kills more than a half of the diseased adult trees during our investigations, which is similar to its relative fungus *Cryphonectria parasitica* in pathogenicity (Rigling and Prospero 2017). Luckily, we timely discovered the fungus and report it herein, and the disease control studies have been in progress.

In the fungal order Diaporthales, many species were reported as forest pathogens causing leaf spots, cankers, fruit rot or blight diseases (Visentin et al. 2012; Pasche et al. 2016; Shuttleworth and Guest 2017; Jiang et al. 2021b; Pan et al. 2021; Lin et al. 2022), moreover, cryphonectriaceous members are known to be serious pathogens (Chen et al. 2013, 2016; Beier et al. 2015; Ferreira et al. 2019; Wang et al. 2020). This family is easily recognized based on the disease symptoms and their obvious orange conidioma formed on the cankered barks, together with their hyaline and small conidia (Gryzenhout et al. 2006). However, within this family, genera are similar in

Figure 6. Results of pathogenicity tests on *Elaeocarpus apiculatus* and *E. hainanensis* using isolates CFCC 57515, CFCC 57516 and CFCC 57517. Row 1: appearance of the hosts after incubation in 10 days; row 2: conidiomata formed on the barks.

morphology which are usually distinguished by the molecular data (Jiang et al. 2020; Wang et al. 2020). Most genera in this family are known to own only one or two species; this may be caused by most samples on important trees like Fagaceae, Melastomataceae, and Myrtaceae and limited samples from the other hosts (Jiang et al. 2020; Wang et al. 2020). In the present study, *Elaeocarpus* (Elaeocarpaceae) usually being overlooked hosts, were found to be new hosts of Cryphonectriaceae pathogens.

There is still room for further exploration, such as the infection opportunity, sources of the primary infection and the alternative hosts of the pathogen. More importantly, the effective control methods to protect *Elaeocarpus* hosts are urgent to be studied due to the quick infection and high virulence.

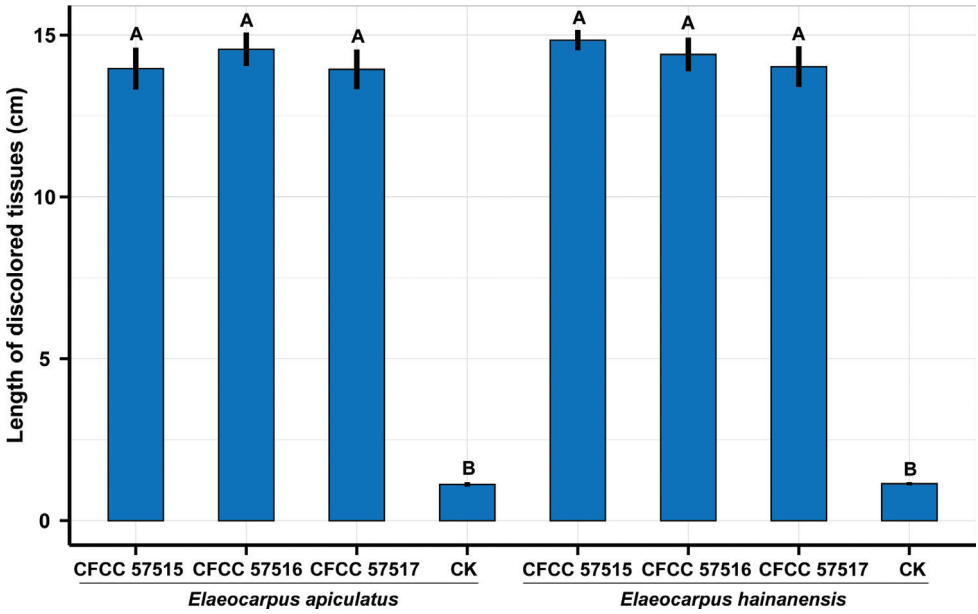

Figure 7. Histogram of lesion lengths resulting from inoculation on *Elaeocarpus apiculatus* and *E. hainanensis* using isolates CFCC 57515, CFCC 57516 and CFCC 57517. Different letters above the error bars indicate treatments that were significantly different (p = 0.05).

Acknowledgements

This research was funded by Forestry Science and Technology Innovation Project of Guangdong (2020KJCX004) and the Guangdong Basic and Applied Basic Research Foundation (2019A1515011814). We thank Dr. Ning Jiang for his assistance with this paper.

References

Beier GL, Hokanson SC, Bates ST, Blanchette RA (2015) *Aurantioporthe corni* gen. et comb. nov., an endophyte and pathogen of *Cornus alternifolia*. Mycologia 107(1): 66–79. https://doi.org/10.3852/14-004

Carbone I, Kohn LM (1999) A method for designing primer sets for speciation studies in filamentous ascomycetes. Mycologia 3(3): 553–556. https://doi.org/10.1080/00275514.1999.12061051

Chen SF, Wingfield MJ, Roux J (2013) *Diversimorbus metrosiderotis* gen. et sp. nov. and three new species of *Holocryphia* (Cryphonectriaceae) associated with cankers on native *Metrosideros angustifolia* trees in South Africa. Fungal Biology 117(5): 289–310. https://doi.org/10.1016/j.funbio.2013.02.005

Chen SF, Wingfield MJ, Li GQ, Liu FF (2016) *Corticimorbus sinomyrti* gen. et sp. nov. (Cryphonectriaceae) pathogenic to native *Rhodomyrtus tomentosa* (*Myrtaceae*) in South China. Plant Pathology 65(8): 1254–1266. https://doi.org/10.1111/ppa.12507

Chen SF, Liu QL, Li GQ, Wingfield MJ, Roux J (2018) A new genus of Cryphonectriaceae isolated from *Lagerstroemia speciosa* in southern China. Plant Pathology 67(1): 107–123. https://doi.org/10.1111/ppa.12723

Doyle JJ, Doyle JL (1990) Isolation of plant DNA from fresh tissue. Focus 12: 13–15. https://doi.org/10.2307/2419362

Fan XL, Bezerra JDP, Tian CM, Crous PW (2018) Families and genera of diaporthalean fungi associated with canker and dieback of tree hosts. Persoonia 40(1): 119–134. https://doi.org/10.3767/persoonia.2018.40.05

Fan XL, Bezerra JDP, Tian CM, Crous PW (2020) *Cytospora* (Diaporthales) in China. Persoonia 45(1): 1–45. https://doi.org/10.3767/persoonia.2020.45.01

Ferreira FA, Henfling JDM (1976) O cancro do eucalipto causadopor *Diaporthe cubensis* Bruner. Fitopatologia Brasileira 1: 129–169.

Ferreira MA, de Oliveira MES, Silva GA, Mathioni SM, Mafia RG (2019) *Capillaureum caryovora* gen. sp. nov. (Cryphonectriaceae) pathogenic to pequi (*Caryocar brasiliense*) in Brazil. Mycological Progress 18(3): 385–403. https://doi.org/10.1007/s11557-018-01461-3

Gryzenhout M, Myburg H, Wingfield BD, Wingfield MJ (2006) Cryphonectriaceae (Diaporthales), a new family including *Cryphonectria*, *Chrysoporthe*, *Endothia* and allied genera. Mycologia 98(2): 239–249. https://doi.org/10.1080/15572536.2006.11832696

Hyde KD, Norphanphoun C, Maharachchikumbura SSN, et al. (2020) Refined families of Sordariomycetes. Mycosphere 11(1): 305–1059. https://doi.org/10.5943/mycosphere/11/1/7

Jaklitsch WM, Voglmayr H (2019) European species of *Dendrostoma* (Diaporthales). MycoKeys 59: 1–26. https://doi.org/10.3897/mycokeys.59.37966

Jaklitsch WM, Voglmayr H (2020) The genus *Melanconis* (Diaporthales). MycoKeys 63: 69–117. https://doi.org/10.3897/mycokeys.63.49054

Jiang N, Fan XL, Tian CM (2019a) Identification and pathogenicity of Cryphonectriaceae species associated with chestnut canker in China. Plant Pathology 68(6): 1132–1145. https://doi.org/10.1111/ppa.13033

Jiang N, Fan XL, Crous PW, Tian CM (2019b) Species of *Dendrostoma* (Erythrogloeaceae, Diaporthales) associated with chestnut and oak canker diseases in China. MycoKeys 48: 67–96. https://doi.org/10.3897/mycokeys.48.31715

Jiang N, Fan XL, Tian CM, Crous PW (2020) Reevaluating Cryphonectriaceae and allied families in Diaporthales. Mycologia 112(2): 267–292. https://doi.org/10.1080/00275514.2019.1698925

Jiang N, Voglmayr H, Bian DR, Piao CG, Wang SK, Li Y (2021a) Morphology and phylogeny of *Gnomoniopsis* (Gnomoniaceae, Diaporthales) from Fagaceae leaves in China. Journal of Fungi 7(10): e792. https://doi.org/10.3390/jof7100792

Jiang N, Voglmayr H, Piao CG, Li Y (2021b) Two new species of *Diaporthe* (Diaporthaceae, Diaporthales) associated with tree cankers in the Netherlands. MycoKeys 85: 31–56. https://doi.org/10.3897/mycokeys.85.73107

Katoh K, Toh H (2010) Parallelization of the MAFFT multiple sequence alignment program. Bioinformatics 26(15): 1899–1900. https://doi.org/10.1093/bioinformatics/btq224

Lin L, Pan M, Tian CM, Fan XL (2022) Fungal richness of *Cytospora* species associated with willow canker disease in China. Journal of Fungi 8(4): 377. https://doi.org/10.3390/jof8040377

Liu YJ, Whelen S, Hall BD (1999) Phylogenetic relationships among ascomycetes: Evidence from an RNA polymerse II subunit. Molecular Biology and Evolution 16(12): 1799–1808. https://doi.org/10.1093/oxfordjournals.molbev.a026092

Miller MA, Pfeiffer W, Schwartz T (2010) Creating the CIPRES Science Gateway for Inference of Large Phylogenetic Trees; Institute of Electrical and Electronics Engineers: New Orleans, LA, USA, 1–7. https://doi.org/10.1109/GCE.2010.5676129

Old KM, Wingfield MJ, Yuan ZQ (2003) A manual of diseases of eucalypts in South-East Asia. Centre for International Forestry Research, Jakarta, Indonesia, 1–106.

Pan M, Zhu HY, Liang LY, Tian CM, Fan XL (2021) Studies of canker and dieback of oak tree in China, with two *Cytospora* species described. Plant Pathology 70(9): 2005–2015. https://doi.org/10.1111/ppa.13435

Pasche S, Calmin G, Auderset G, Crovadore J, Pelleteret P, Mauch-Mani B, Barja F, Paul B, Jermini M, Lefort F (2016) *Gnomoniopsis smithogilvyi* causes chestnut canker symptoms in *Castanea sativa* shoots in Switzerland. Fungal Genetics and Biology 87: 9–21. https://doi.org/10.1016/j.fgb.2016.01.002

Rigling D, Prospero S (2017) *Cryphonectria parasitica*, the causal agent of chestnut blight: Invasion history, population biology and disease control. Molecular Plant Pathology 19(1): 7–20. https://doi.org/10.1111/mpp.12542

Ronquist F, Huelsenbeck JP (2003) MrBayes 3: Bayesian phylogenetic inference under mixed models. Bioinformatics 19(12): 1572–1574. https://doi.org/10.1093/bioinformatics/btg180

Rossman AY, Farr DF, Castlebury LA (2007) A review of the phylogeny and biology of the Diaporthales. Mycoscience 48(3): 135–144. https://doi.org/10.1007/S10267-007-0347-7

Senanayake IC, Crous PW, Groenewald JZ, Maharachchikumbura SSN, Jeewon R, Phillips AJL, Bhat DJ, Perera RH, Li QR, Li WJ, Tangthirasunun N, Norphanphoun C, Karunarathna SC, Camporesi E, Manawasighe IS, Al-Sadi AM, Hyde KD (2017) Families of Diaporthales based on morphological and phylogenetic evidence. Studies in Mycology 86(1): 217–296. https://doi.org/10.1016/j.simyco.2017.07.003

Senanayake IC, Jeewon R, Chomnunti P, Wanasinghe DN, Norphanphoun C, Karunarathna A, Pem D, Perera RH, Camporesi E, McKenzie EHC, Hyde KD, Karunarathna SC (2018) Taxonomic circumscription of Diaporthales based on multigene phylogeny and morphology. Fungal Diversity 93(1): 241–443. https://doi.org/10.1007/s13225-018-0410-z

Shuttleworth LA, Guest DI (2017) The infection process of chestnut rot, an important disease caused by *Gnomoniopsis smithogilvyi* (Gnomoniaceae, Diaporthales) in Oceania and Europe. Australasian Plant Pathology 46(5): 397–405. https://doi.org/10.1007/s13313-017-0502-3

Stamatakis A (2014) RAxML version 8: A tool for phylogenetic analysis and post-analysis of large phylogenies. Bioinformatics 30(9): 1312–1313. https://doi.org/10.1093/bioinformatics/btu033

Udayanga D, Miriyagalla SD, Manamgoda DS, Lewers KS, Gardiennet A, Castlebury LA (2021) Molecular reassessment of diaporthalean fungi associated with strawberry, including the leaf blight fungus, *Paraphomopsis obscurans* gen. et comb. nov. (*Melanconiellaceae*). IMA Fungus 12(1): 1–21. https://doi.org/10.1186/s43008-021-00069-9

Vilgalys R, Hester M (1990) Rapid genetic identification and mapping of enzymatically amplified ribosomal DNA from several *Cryptococcus* species. Journal of Bacteriology 172(8): 4238–4246. https://doi.org/10.1128/jb.172.8.4238-4246.1990

Visentin I, Gentile S, Valentino D, Gonthier P, Tamietti G, Cardinale F (2012) *Gnomoniopsis castanea* sp. nov.(Gnomoniaceae, Diaporthales) as the causal agent of nut rot in sweet chestnut. Journal of Plant Pathology 94: 411–419.

Voglmayr H, Rossman AY, Castlebury LA, Jaklitsch WM (2012) Multigene phylogeny and taxonomy of the genus *Melanconiella* (Diaporthales). Fungal Diversity 57(1): 1–44. https://doi.org/10.1007/s13225-012-0175-8

Voglmayr H, Castlebury LA, Jaklitsch WM (2017) *Juglanconis* gen. nov. on Juglandaceae, and the new family Juglanconidaceae (Diaporthales). Persoonia 38(1): 136–155. https://doi.org/10.3767/003158517X694768

Wang W, Li GQ, Liu QL, Chen SF (2020) Cryphonectriaceae on *Myrtales* in China: Phylogeny, host range, and pathogenicity. Persoonia 45(1): 101–131. https://doi.org/10.3767/persoonia.2020.45.04

White TJ, Bruns T, Lee S, Taylor J (1990) Amplification and direct sequencing of fungal ribosomal RNA genes for phylogenetics. PCR Protocols: A Guide to Methods and Applications 18: 315–322. https://doi.org/10.1016/B978-0-12-372180-8.50042-1

Wijayawardene NN, Hyde KD, Lumbsch HT, Liu JK, Maharachchikumbura SSN, Ekanayaka AH, Tian Q, Phookamsak R (2018) Outline of Ascomycota: 2017. Fungal Diversity 88(1): 167–263. https://doi.org/10.1007/s13225-018-0394-8

Wingfield MJ (1989) First record of *Cryphonectria* canker of *Eucalyptus* in South Africa. Phytophylactica 21: 311–313.

MycoKeys 91: 85–96 (2022)
doi: 10.3897/mycokeys.91.86257
https://mycokeys.pensoft.net

RESEARCH ARTICLE

A peer-reviewed open-access journal
MycoKeys
Launched to accelerate biodiversity research

Morphological characteristics and phylogenetic evidence reveal two new species of *Acremonium* (Hypocreales, Sordariomycetes)

Xin Li[1], Zhi-Yuan Zhang[1], Yu-Lian Ren[1], Wan-Hao Chen[2], Jian-Dong Liang[2], Ji-Mei Pan[1], Jian-Zhong Huang[3], Zong-Qi Liang[1], Yan-Feng Han[1]

1 *Institute of Fungus Resources, Department of Ecology, College of Life Sciences, Guizhou University, Guiyang 550025, Guizhou, China* **2** *Basic Medical School, Guizhou University of Traditional Chinese Medicine, Guiyang 550025, Guizhou, China* **3** *Engineering Research Center of Industrial Microbiology, Ministry of Education, Fujian Normal University, Fuzhou 350108, Fujian, China*

Corresponding author: Yan-Feng Han (swallow1128@126.com)

Academic editor: Andrew Miller | Received 7 May 2022 | Accepted 4 July 2022 | Published 15 July 2022

Citation: Li X, Zhang Z-Y, Ren Y-L, Chen W-H, Liang J-D, Pan J-M, Huang J-Z, Liang Z-Q, Han Y-F (2022) Morphological characteristics and phylogenetic evidence reveal two new species of *Acremonium* (Hypocreales, Sordariomycetes). MycoKeys 91: 85–96. https://doi.org/10.3897/mycokeys.91.86257

Abstract

Using chicken feathers as bait, *Acremonium globosisporum* **sp. nov.** and *Acremonium curvum* **sp. nov.** were collected from the soil of Yuncheng East Garden Wildlife Zoo and Zhengzhou Zoo in China. They were identified by combining the morphological characteristics and the two-locus DNA sequence (LSU and ITS) analyses. In the phylogenetic tree, both new species clustered into separate subclades, respectively. They were different from their allied species in their morphology. The description, illustrations, and phylogenetic tree of the two new species were provided.

Keywords

Acremonium, filamentous fungi, phylogeny, taxonomy

Introduction

The genus *Acremonium* Link, established in 1929, with *A. alternatum* Link as the type species, is one of the largest and most complex genera of asexually typified. The morphological characteristics consist of hyphae septate, mostly tapered and lateral phialides, produced singly or in small groups, and unicellular conidia produced in mucoid

heads or unconnected chains (Summerbell et al. 2011). Nowadays, *Acremonium* has 217 records in the Index Fungorum (http://www.indexfungorum.org/Names/Names.asp, retrieval on 30 Jun. 2022). The traditionally circumscribed *Acremonium* is polyphyletic, which explains why many *Acremonium* species were transferred to other genera and families (Yang et al. 2019). Thus, there are still many unidentified, suspect or misidentified taxa that require taxonomic investigation.

Due to the poor differentiation of asexual forms of the genus *Acremonium*, it is difficult to identify species only by morphological differences. To address this issue, there are many unidentified and suspicious species that require further phylogenetic analysis. To date, many isolates of *Acremonium* spp. lack the gene loci such as SSU, *TEF 1-a* and *RPB2* (Table 1), therefore, phylogenetic analyses of this genus are generally performed based on the single locus sequences, especially LSU (Hyde et al. 2020).

In the present study, two new species of *Acremonium* were identified in a survey of keratinolytic fungi from China, which were enriched by the baiting technique. We provided a description, illustrations, and phylogenetic tree for the two new species.

Materials and methods

Fungal isolation and morphology

Soil samples were collected from Yuncheng East Garden Wildlife Zoo (35°6'26"N, 111°4'24"E) (three isolates), Yuncheng City, Shanxi Province and Zhengzhou Zoo (34°47'20"N, 113°40'41"E) (one isolate), Zhengzhou City, Henan Province, China by Yu-Lian Ren on July 2021. We collected 3–10 cm below the soil surface, placed the samples in sterile Ziploc plastic bags (Kaixin Biotechnology, Guizhou, China), and transported them to the laboratory (Zhang et al. 2019a, b). Then, they were treated and isolated according to the baiting method (using chicken feathers as bait: a method specifically designed for isolating keratinophilic microbes) of Zhang et al. (2020a, b; 2021). We washed the chicken feathers, sterilized them in an autoclave for 30 minutes at 121 °C, and dried them in an oven at 50 °C. The sterile and dried chicken feathers were mixed with soil samples and then wet with sterile distilled water and cultured at darkroom temperature for 1 month (Li et al. 2022).

Then, the 2 g samples were weighed in a conical flask with glass beads containing 20 mL sterile water and mixed evenly by eddy shock for 10 min. Next, 1 mL samples were mixed evenly in 9 mL sterile water in a sterile environment and diluted to 10^{-3}. Then, 1 mL 10^{-3} samples were put into a sterile petri dish, and SDA medium containing 50 mg/L penicillin and 50 mg/L streptomycin was added and mixed. The target strains were isolated. The purified strains were transferred to PDA, OA, and MEA plates for dark culture at 25 °C for 7 days. Microscopic features were examined by making direct wet mounts with 25% lactic acid on PDA, with a light microscope.

The cultures were placed to slowly dry at 50 °C to produce the dried holotype. The dried holotype was deposited in the Mycological Herbarium of the Institute of Microbiology, Chinese Academy of Sciences, Beijing, China (**HMAS**), while ex-type

Table 1. Strains included in the present study.

Species	Strains	LSU	ITS	SSU	*TEF 1-α*	*RPB2*
Acremonium alcalophilum	CBS 114.92[T]	JX158443	DQ825967	JX158486	JX158399	JX158465
Acremonium alternatum	CBS 407.66[T]	HQ231988	HE798150			
Acremonium alternatum	CBS 831.97	HQ231989				
Acremonium arthrinii	MFLU 18-1225[T]	MN036334		MN036335	MN038169	
Acremonium behniae	CBS 146824[T]	MW175400	MW175360			
Acremonium biseptum	CBS 750.69[T]	HQ231998				
Acremonium blochii	CBS 993.69	HQ232002	HE608636			
Acremonium borodinense	CBS 101148[T]	HQ232003	HE608635			
Acremonium brachypenium	CBS 866.73[T]	HQ232004	AB540570			
Acremonium camptosporum	CBS 756.69[T]	HQ232008		HQ232186		
Acremonium cavaraeanum	CBS 101149[T]	HF680202	HF680220			
Acremonium cavaraeanum	CBS 111656	HF680203	HF680221			
Acremonium cavaraeanum	CBS 758.69	HQ232012	HF680222			
Acremonium cerealis	CBS 207.65	HQ232013				
Acremonium cerealis	CBS 215.69	HQ232014				
Acremonium chiangraiense	MFLUCC 14-0397[T]	MN648329	MN648324			
Acremonium chrysogenum	CBS 144.62[T]	HQ232017		HQ232187		
Acremonium chrysogenum	CBS 401.65	MH870276	MH858636			
Acremonium citrinum	CBS 384.96[T]	HF680217	HF680236			
Acremonium dimorphosporum	CBS 139050[T]	LN810506	LN810515			
Acremonium exiguum	CBS 587.73[T]	HQ232035				
Acremonium exuviarum	UAMH 9995[T]	HQ232036	AY882946			
Acremonium felinum	CBS 147.81[T]	AB540488	AB540562			
Acremonium flavum	CBS 596.70[T]	HQ232037		HQ232191		
Acremonium flavum	CBS 316.72	MH872204	MH860487			
Acremonium fuci	CBS 112868[T]		AY632653			
Acremonium fuci	CBS 113889		AY632652			
Acremonium fusidioides	CBS 109069	HF680204	HF680223			
Acremonium fusidioides	CBS 991.69	HF680211	HF680230			
Acremonium fusidioides	CBS 840.68[T]	HQ232039	FN706542			
Acremonium hansfordii	CBS 390.73	HQ232043	AB540578			
Acremonium hennebertii	CBS 768.69[T]	HQ232044	HF680238			
Acremonium inflatum	CBS 212.69[T]	HQ232050				
Acremonium mali	ACCC 39305[T]	MF993114	MF987658			
Acremonium moniliforme	CBS 139051[T]	LN810507	LN810516			
Acremonium moniliforme	FMR 10363	LN810508	LN810517			
Acremonium parvum	CBS 381.70A	HQ231986	HF680219			
Acremonium persicinum	CBS 310.59[T]	HQ232077				
Acremonium persicinum	CBS 101694	HQ232085				
Acremonium pinkertoniae	CBS 157.70[T]	HQ232089		HQ232202		
Acremonium polychroma	CBS 181.27[T]	HQ232091	AB540567			
Acremonium potronii	CBS 189.70	HQ232094				
Acremonium pseudozeylanicum	CBS 560.73[T]	HQ232101				
Acremonium pteridii	CBS 782.69[T]	HQ232102				
Acremonium pteridii	CBS 784.69	HQ232103				
Acremonium sclerotigenum	CBS 124.42[T]	HQ232126	FN706552	HQ232209		
Acremonium sclerotigenum	A101	KC987215	KC987139	KC987177	KC998961	
Acremonium sclerotigenum	A130	KC987242	KC987166	KC987204	KC998988	
Acremonium sp.	E102	KC987248	KC987172	KC987210	KC998994	KC999030
Acremonium spinosum	CBS 136.33[T]	HQ232137	HE608637	HQ232210		
Acremonium stroudii	CBS 138820[T]		KM225291			
Acremonium tumulicola	CBS 127532[T]	AB540478	AB540552			
Acremonium variecolor	CBS 130360[T]	HE608651	HE608647			
Acremonium variecolor	CBS 130361	HE608652	HE608648			
Acremonium verruculosum	CBS 989.69[T]	HQ232150				
Acrophialophora hechuanensis	GZUIFR-H08-1[T]	MK926789	DQ185070	EU053286		
Brunneomyces brunnescens	CBS 559.73[T]	HQ231966	LN810520	HQ232184	LN810534	
Brunneomyces hominis	UTHSC 06-415[T]	LN810509	KP131517		LN810535	
Bryocentria brongniartii	M139	EU940105		EU940052		

Species	Strains	LSU	ITS	SSU	*TEF 1-α*	*RPB2*
Bryocentria brongniartii	M190	EU940125		EU940052		
Bryocentria metzgeriae	M140	EU940106				
Bulbithecium hyalosporum	CBS 318.91^{T}	AF096187	HE608634			
Cephalosporium purpurascens	CBS 149.62^{T}	HQ232071				
Cosmospora lavitskiae	CBS 530.68^{T}	HQ231997				
Emericellopsis alkalina	CBS 127350^{T}	KC987247	KC987171	KC987209	KC998993	KC999029
Emericellopsis terricola	CBS 120.40^{T}	U57082	U57676	U44112		
Gliomastix roseogrisea	CBS 134.56^{T}	HQ232121				
Hapsidospora irregularis	ATCC 22087^{T}	AF096192		AF096177		
Kiflimonium curvulum	CBS 430.66^{T}	HQ232026	HE608638	HQ232188		
Lanatonectria flavolanata	CBS 230.31	HQ232157				
Leucosphaerina arxii	CBS 737.84^{T}	HE608662	HE608640			
Nigrosabulum globosum	ATCC 22102^{T}	AF096195				
Paracremonium contagium	CBS 110348^{T}	HQ232118	KM231831		KM231966	
Parasarocladium breve	CBS 150.62^{T}	HQ232005				
Parasarocladium radiatum	CBS 142.62^{T}	HQ232104		HQ232205		
Pestalotiopsis hawaiiensis	CBS 114491^{T}	KM116239	KM199339		KM199514	
Pestalotiopsis spathulata	CBS 356.86^{T}	KM116236	KM199338		KM199513	
Phialemonium atrogriseum	CBS 604.67^{T}	HQ231981	HE610367	FJ176825		
Pseudoacremonium sacchari	CBS 137990^{T}	KJ869201	KJ869144			
Sarcopodium vanillae	CBS 100582	HQ232174	KM231780		KM231911	
Sarocladium bacillisporum	CBS 425.67^{T}	HQ231992	HE608639	HQ232179		
Sarocladium bactrocephalum	CBS 749.69^{T}	HQ231994	HG965006	HQ232180		
Sarocladium strictum	CBS 346.70^{T}	HQ232141	AY214439	HQ232211		
Sarocladium terricola	CBS 243.59^{T}	HQ232046		HQ232196		
Selinia pulchra	AR 2812	GQ505992	HM484859		HM484841	
Trichothecium crotocinigenum	CBS 129.64^{T}	HQ232018	AJ621773			
Trichothecium indicum	CBS 123.78^{T}	AF096194		AF096179		
Trichothecium roseum	DAOM 208997	U69891		U69892		
Trichothecium sympodiale	ATCC 36477	U69889		U69890		
Acremonium curvum	CGMCC 3.20954 = GZUIFR 22.035^{T}	ON041050	ON041034	ON876754	ON494579	ON494583
Acremonium globosisporum	CGMCC 3.20955 = GZUIFR 22.036^{T}	ON041051	ON041035	ON876755	ON494580	ON494584
Acremonium globosisporum	GZUIFR 22.037	ON041052	ON041036	ON876756	ON494581	ON494585
Acremonium globosisporum	GZUIFR 22.038	ON041053	ON041037	ON876757	ON494582	ON494586

Notes: "T" stands for Ex-type strains.

living culture was stored in PDA test tubes which were deposited in the China General Microbiological Culture Collection Center (**CGMCC**), and the Institute of Fungus Resources, Guizhou University, Guiyang City, Guizhou, China (**GZUIFR**).

DNA extraction, PCR amplification, and sequencing

We used a 5% chelex-100 solution for total genomic DNA extraction. ITS1/ITS4 (White et al. 1990), LROR/LR7 (Vilgalys and Hester 1990), EF1-983F/ EF1-2218R (Rehner and Buckley 2005), fRPB2-5f/ fRPB2-7cR (Liu et al. 1999), and NS1 and NS4 (White et al. 1990) primers were used for amplification of the internal transcribed spacers (ITS), the 28S nrRNA locus (LSU), translation elongation factor 1-alpha gene region (TEF 1-α), RNA polymerase II second largest subunit gene (RPB2), and small subunit rDNA (SSU), respectively. Purification and sequencing were performed by Quintarabio (Wuhan, China). The new sequences were submitted to GenBank (Table 1).

Phylogenetic analyses

The ITS and LSU sequences of *Acremonium* were downloaded from GenBank (Table 1). Two strains of *Pestalotiopsis spathulata* (CBS 356.86) and *P. hawaiiensis* (CBS 114491) were chosen as the outgroup taxa. The TBtools were used for name simplification and renaming (Chen et al. 2020). Sequences were aligned by MAFFT v7.037 (Katoh and Standley 2013). Multi-locus was concatenated by PhyloSuite v1.16 (Zhang et al. 2020a).

Bayesian inference (BI) and maximum likelihood (ML) methods were used in the analysis. For BI analysis was conducted with MrBayes v3.2 (Ronquist et al. 2012) and Markov chain Monte Carlo (MCMC) simulations; ML analysis was performed using IQ-TREE v1.6.11 (Nguyen et al. 2015), as outlined in Li et al (2022). All analyses were performed in PhyloSuite V1.16 (Zhang et al. 2020b).

Results

Phylogeny

Based on a BLAST search (https://blast.ncbi.nlm.nih.gov/Blast.cgi) using the LSU sequences, our isolates were identified as belonging to the genus *Acremonium*. To further determine the phylogenetic position of these strains, we performed a multi-locus phylogenetic analysis. The dataset was composed of LSU (1–430 bp) and ITS (431–1005 bp) gene, comprising a total of 1005 characters (including gaps). The best-fit partition model for ML analysis and BI analysis is shown in Table 2. The results showed that the CGMCC 3.20955, GZUIFR 22.037, and GZUIFR 22.038 are still grouped in the *Pinkertoniae*-clade (Fig.1). The CGMCC 3.20954 is still grouped in the *Chrysogenum*-clade (Fig.1).

Table 2. The best-fit substitution models are used in multi-locus phylogenetic construction.

	LSU	ITS
ML analysis	TN+F+R5	GTR+F+R4
BI analysis	GTR+F+I+G4	GTR+F+I+G4

Taxonomy

Acremonium globosisporum **Xin Li, Y.F. Han & Z.Q. Liang, sp. nov.**
MycoBank No: 843765
Fig. 2

Type. Yuncheng East Garden Wildlife Zoo, Yuncheng City, Shanxi Province, China N35°6'26", E111°4'24", isolated from green belt soil, July 2021, Yu-Lian Ren (dried holotype culture HMAS 351939, ex-holotype culture CGMCC 3.20955 = GZUIFR 22.036). ITS sequences, GenBank ON041035; LSU sequences, GenBank ON041051; SSU sequences, GenBank ON876755; *TEF 1-a* sequences, GenBank ON494580; *RPB2* sequences, GenBank ON494584.

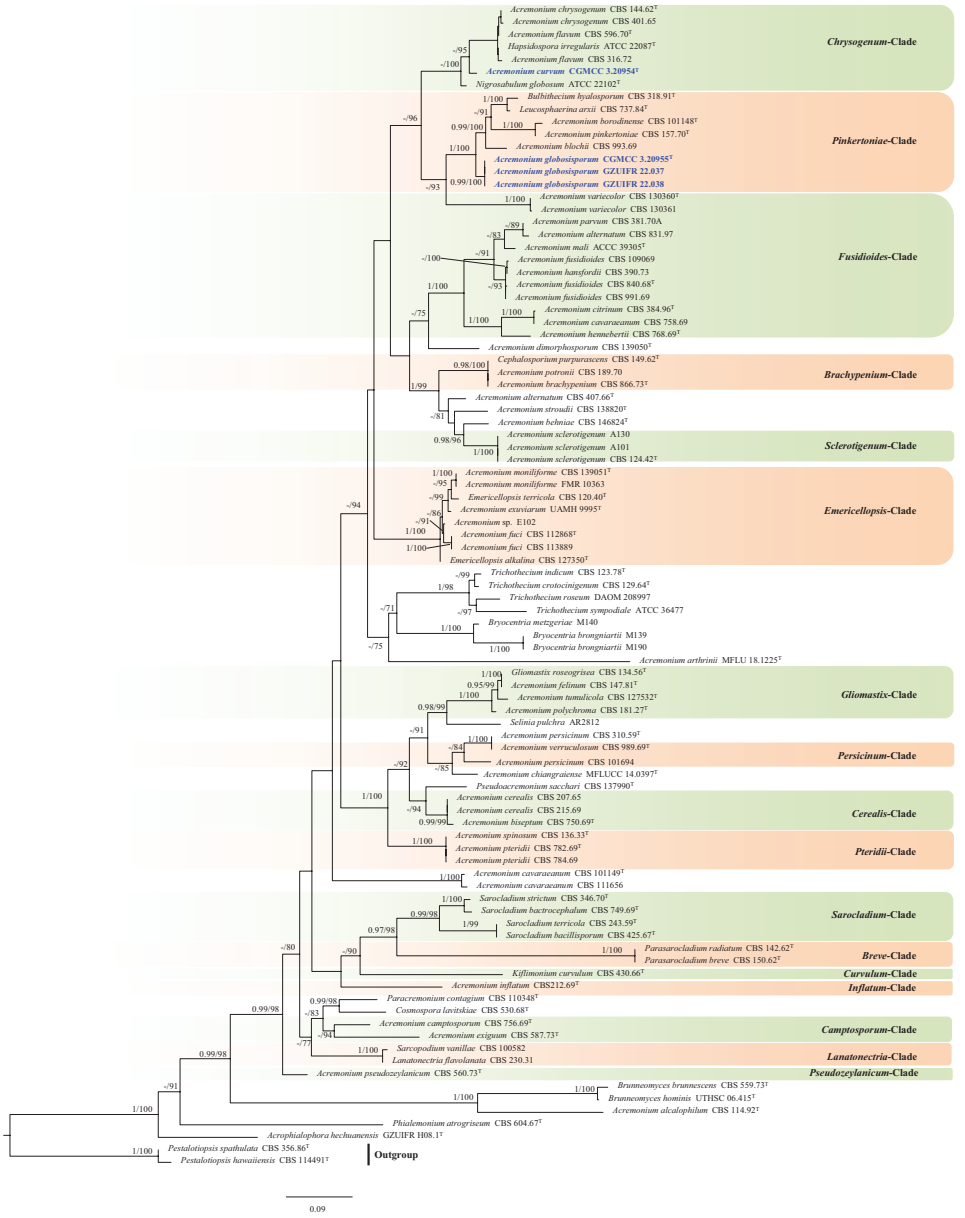

Figure 1. Phylogenetic tree of the genus *Acremonium* constructed from LSU and ITS. Bayesian posterior probability (≥ 0.95) and ML bootstrap values (≥ 70%) are indicated along branches (BPP/ML).

Description. *Colonies* on PDA and OA at 25 °C attaining 11–13 mm and 9–11 mm diam respectively after 7 d, white, flat or raised, velvety to slightly cottony. On MEA at 25 °C, reaching 8–10 mm after 7 d, white to yellowish white, raised, slimy. *Hyphae* hyaline, septate, sometimes winding and inflate, 1.5–11.0 µm wide. *Sporulation* abundant. *Phialides* are mostly borne singly, hyaline, erect to slightly curved, sometimes

forming a collarette, 9.0–22.0 µm long, tapering from 1.5–3.5 µm near the base to 0.5–1.5 µm. *Conidia* cohering in long chains, with minutely truncate ends, up to 27.5 µm long, globose or subglobose, 2.5–4.5 × 2.5–4.5 µm ($\bar{x} \pm$ SD = 3.4 ± 0.77 × 3.6 ± 0.52, n = 50) diam. *Chlamydospores* and teleomorph stage were not observed.

Etymology. *globosisporum*. A reference to the global conidia.

Additional specimens examined. Yuncheng East Garden Wildlife Zoo, Yuncheng City, Shanxi Province, China N35°6'26", E111°4'24", isolated from green belt soil, July 2021, Yu-Lian Ren, GZUIFR 22.037, ITS, LSU, SSU, *TEF 1-a*, *RPB2* sequences GenBank ON041036, ON041052, ON876756, ON494581, ON494585; GZUIFR 22.038, ITS, LSU, SSU, *TEF 1-a*, *RPB2* sequences GenBank ON041037, ON041053, ON876757, ON494582, ON494586.

Known distribution. Yuncheng City, Shanxi Province, China.

Notes. The phylogeny results showed that the CGMCC 3.20955, GZUIFR 22.037 and GZUIFR 22.038 still nested in the *Pinkertoniae*-clade. The morphological characteristics of *Acremonium globosisporum* were similar to other species of the *Pinkertoniae*-clade in that phialides were erect on the hyphae; sporulation was abundant, and conidia were subglobose (Ito et al. 2000). However, *Acremonium globosisporum* hyphae were sometimes winding and inflated, with conidia cohering in long chains, unlike other species.

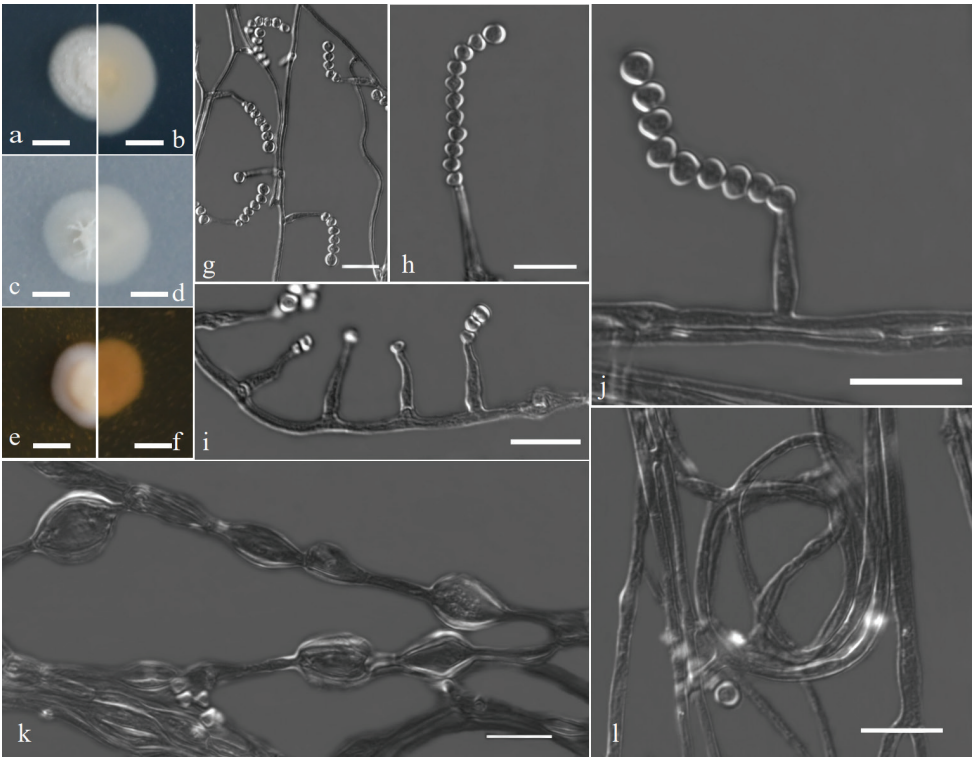

Figure 2. Morphology of *Acremonium globosisporum* sp. nov. **a–f** colony on PDA, OA and MEA after 7 d at 25 °C (upper surface and lower surface) **g–j** conidia are borne on the phialides **k–l** winding hyphae and inflate hyphae. Scale bars: 4 mm (**a–f**); 10 µm (**g–l**).

Acremonium curvum **Xin Li, Y.F. Han & Z.Q. Liang, sp. nov.**
MycoBank No: 843766
Fig. 3

Type. Zhengzhou Zoo, Zhengzhou City, Henan Province, China N34°47'20", E113°40'41", isolated from green belt soil, July 2021, Yu-Lian Ren (dried holotype culture HMAS 351938, ex-holotype culture CGMCC 3.20954 = GZUIFR 22.035). ITS sequences, GenBank ON041034, LSU sequences, GenBank ON041050; SSU sequences, GenBank ON876754; *TEF 1-a* sequences, GenBank ON494579; *RPB2* sequences, GenBank ON494583.

Description. *Colonies* on PDA and OA at 25 °C attaining 11–14 mm and 7–9 mm diam respectively after 7 d, white, flat, radially folded or rugose. On MEA at 25 °C, reaching 6–8 mm after 7 d, white to yellowish-white, slimy. *Hyphae* hyaline, septate, sometimes winding, 1.5–2.5 µm wide. *Sporulation* abundant. *Phialides* are mostly borne singly, curved, slightly inflated at the base, tapered at the tip, up to 38.0 µm long. tapering from 1.5–3.5 µm near the base to 0.5–1.5 µm. *Conidia* cohering together on the top of phialides, one-celled, solitary, or several fascicled, ovoid or subglobose, 3.0–7.0 × 2.5–3.5 µm ($\bar{x} \pm SD = 4.1 \pm 1.18 \times 3.2 \pm 0.77$, n = 50) diam. *Chlamydospores* and teleomorph stage were not observed.

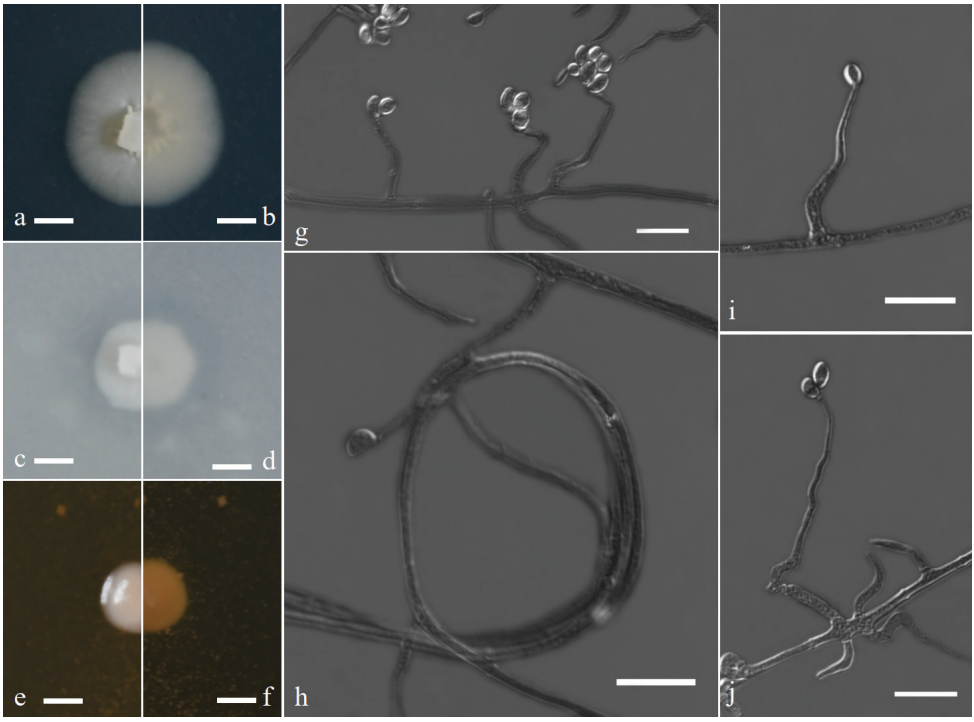

Figure 3. Morphology of Acremonium curvum sp. nov. **a–f** colony on PDA, OA and MEA after 7 d at 25 °C (upper surface and lower surface) **g, l, j** conidia are borne on the phialides **h** Winding hyphae. Scale bars: 4 mm (**a–f**); 10 µm (**g–j**).

Etymology. *curvum*. Referring to the curved Phialides.

Known distribution. Henan Province, China.

Notes. Based on the multi-locus analysis we found that *Acremonium curvum* had close phylogenetic affinities to other taxa of the *Chrysogenum*-clade. Morphologically, *A. curvum* was similar to other taxa of the *Chrysogenum*-clade in having simple or rarely branched conidiophores, slightly inflated at the base and tapered at tip phialides, and ovoid to subglobose conidia (Yang et al. 2019). Conidia of *Hapsidospora irregularis* and *A. curvum* had several fascicled at the tips of the conidiophores (Malloch and Cain 1970). However, *A. curvum* was differentiated by having mostly curved phialides and the conidia were several fascicled at the tips of the phialides.

Discussion

In the present study, four strains of *Acremonium* fungi were isolated from soil in the Shanxi and Henan Province, China. Two-locus (LSU and ITS) phylogenetic analyses in combination with morphological characteristics were used for identification. As a result, two new species of *A. curvum* (one isolate) and *A. globosisporum* (three isolates) were proposed.

With the development of biotechnology, a growing number of studies have combined morphological and phylogenetic features to distinguish between species. This provides the basis for more precise species naming. Generally, the fungal ITS marker includes considerably more sequence variability, and consequently provides high interspecific resolution, and also some degree of intraspecific variability (Nilsson et al. 2008). Therefore, ITS has been widely used in studies of fungal inter- and intraspecific relationships (Dai et al. 2020; Szczepańska et al. 2021). There are numerous ITS sequences stored in public databases, which are incomparable to other molecular markers (Zhang et al. 2022). In addition, according to Vu et al. (2019), combining ITS and LSU can improve the accuracy of fungal species discrimination with high generality. They think that fungi commonly present in clinical, environmental, or economically relevant communities can often be identified to species level by their ITS and LSU barcodes (Vu et al. 2019).

Although, Yang et al. (2019) used a multi-locus phylogenetic analysis in introducing the new species *Acremonium arthrinii*, lacking loci such as SSU, *TEF 1-a* and *RPB2* (Table 1) in the isolates of *Acremonium* spp. were relatively serious, so it is not difficult to find that the strains with SSU and *TEF 1-a* in this analysis were not yet 50% or even 30% of the total number of strains. Therefore, although we sequenced these above loci in the new isolates, they were not included in the phylogenetic analysis. In the future, the phylogeny relationships of *Acremonium* members will undoubtedly vary and become clearer with the increase of the number and type of molecular used.

In recent years, *Acremonium* spp. has been reported to cause immunocompetent and immunocompromised individual diseases, such as brain abscess (Anis et al. 2021), fungal keratitis (Liu et al. 2021), fungal osteomyelitis (Jalan et al. 2021), and fungal maxillary sinusitis (Durbec et al. 2011). In the present study, all strains were isolated by

a method specifically designed for the isolation of keratinophilic microbes. Therefore, more studies are necessary to confirm whether *A. curvum* and *A. globosisporum* are opportunistic infectious pathogens that infect the skin and cause skin infection, as well as their potential application in the degradation of keratin-rich matrices.

Acknowledgements

This work was financially supported by the National Natural Science Foundation of China (no. 32060011, 32160007, 31860002), "Hundred" Talent Projects of Guizhou Province (Qian Ke He [2020] 6005), and the Key Areas of Research and Development Program of Guangdong Province (no. 2018B020205003), and Construction Program of Biology First-class Discipline in Guizhou (GNYL [2017] 009). We appreciate MDPI for the English-language editing of the whole manuscript.

References

Anis A, Sameeullah F, Bhatti JM (2021) A rare case of brain abscesses caused by *Acremonium* species. Cureus 13(4): e14396. https://doi.org/10.7759/cureus.14396

Chen CJ, Chen H, Zhang Y, Thomas HR, Frank MH, He YH, Xia R (2020) TBtools: An integrative toolkit developed for interactive analyses of big biological data. Molecular Plant 13(8): 1194–1202. https://doi.org/10.1016/j.molp.2020.06.009

Dai YD, Wu CK, Yuan F, Wang YB, Huang LD, Chen ZH, Zeng WB, Wang Y, Yang ZL, Zeng PS, Lemetti P, Mo XX, Yu H (2020) Evolutionary biogeography on *Ophiocordyceps sinensis*: An indicator of molecular phylogeny to geochronological and ecological exchanges. Geoscience Frontiers 11(3): 807–820. https://doi.org/10.1016/j.gsf.2019.09.001

Durbec M, Bienvenu AL, Picot S, Dubreuil C, Cosmidis A, Tringali S (2011) Maxillary sinus fungal infection by *Acremonium*. European Annals of Otorhinolaryngology, Head and Neck Diseases 128(1): 41–43. https://doi.org/10.1016/j.anorl.2010.10.004

Hyde KD, Dong Y, Phookamsak R, Jeewon R, Bhat DJ, Jones EBG, Liu NG, Abeywickrama PD, Mapook A, Wei D, Perera RH, Manawasinghe IS, Pem D, Bundhun D, Karunarathna A, Ekanayaka AH, Bao DF, Li JF, Samarakoon MC, Chaiwan N, Lin CG, Phutthacharoen K, Zhang SN, Senanayake IC, Goonasekara ID, Thambugala KM, Phukhamsakda C, Tennakoon DS, Jiang HB, Yang J, Zeng M, Huanraluek N, Liu JK, Wijesinghe SN, Tian Q, Tibpromma S, Brahmanage RS, Boonmee S, Huang SK, Thiyagaraja V, Lu YZ, Jayawardena RS, Dong W, Yang EF, Singh SK, Singh SM, Rana S, Lad SS, Anand G, Devadatha B, Niranjan M, Sarma VV, Liimatainen K, Aguirre-Hudson B, Niskanen T, Overall A, Alvarenga RLM, Gibertoni TB, Pfliegler WP, Horváth E, Imre A, Alves AL, Bahkali AH, Doilom M, Elgorban AM, Maharachchikumbura SSN, Rajeshkumar KC, Haelewaters D, Mortimer PE, Zhao Q, Lumyong S, Xu JC, Sheng J (2020) Fungal diversity notes 1151–1276: Taxonomic and phylogenetic contributions on genera and species of fungal taxa. Fungal Diversity 100(1): 5–277. https://doi.org/10.1007/s13225-020-00439-5

Ito T, Okane I, Nakagiri A, Gams W (2000) Two species of *Acremonium* section *Acremonium*: *A. borodinense* sp. nov. and *A. cavaraeanum* rediscovered. Mycological Research 104(1): 77–80. https://doi.org/10.1017/S0953756299008977

Jalan D, Saini MK, Elhence P, Elhence A, Jain P (2021) Calcaneal osteomyelitis caused by *Acremonium* sp. in an immunocompetent adult – A case report. The Foot 47: e101781. https://doi.org/10.1016/j.foot.2021.101781

Katoh K, Standley DM (2013) MAFFT multiple sequence alignment software version 7: Improvements in performance and usability. Molecular Biology and Evolution 30(4): 772–780. https://doi.org/10.1093/molbev/mst010

Li X, Zhang ZY, Chen WH, Liang JD, Huang JZ, Han YF, Liang ZQ (2022) A new species of *Arthrographis* (Eremomycetaceae, Dothideomycetes), from the soil in Guizhou, China. Phytotaxa 538(3): 175–181. https://doi.org/10.11646/phytotaxa.538.3.1

Liu YJ, Whelen S, Hall BD (1999) Phylogenetic relationships among Ascomycetes: Evidence from an RNA polymerse II subunit. Molecular Biology and Evolution 16(12): 1799–1808. https://doi.org/10.1093/oxfordjournals.molbev.a026092

Liu J, Freiberg FJ, Yeung SN, Iovieno A (2021) Late-onset recurrent *Acremonium* fungal keratitis after therapeutic penetrating keratoplasty. Canadian Journal of Ophthalmology 56(4): e135–e137. https://doi.org/10.1016/j.jcjo.2021.02.006

Malloch D, Cain RF (1970) Five new genera in the new family Pseudeurotiaceae. Canadian Journal of Botany 48(10): 1815–1825. https://doi.org/10.1139/b70-267

Nguyen LT, Schmidt HA, von Haeseler A, Minh BQ (2015) IQ-TREE: A fast and effective stochastic algorithm for estimating maximum-likelihood phylogenies. Molecular Biology and Evolution 32(1): 268–274. https://doi.org/10.1093/molbev/msu300

Nilsson RH, Kristiansson E, Ryberg M, Hallenberg N, Larsson KH (2008) Intraspecific ITS variability in the kingdom fungi as ex-pressed in the international sequence databases and its implications for molecular species identification. Evolutionary Bioinformatics Online 4: 193–201. https://doi.org/10.4137/EBO.S653

Rehner SA, Buckley E (2005) A *Beauveria* phylogeny inferred from nuclear ITS and EF1-α sequences: Evidence for cryptic diversification and links to *Cordyceps teleomorphs*. Mycologia 97(1): 84–98. https://doi.org/10.3852/mycologia.97.1.84

Ronquist F, Teslenko M, van der Mark P, Ayres DL, Darling A, Höhna S, Larget B, Liu L, Suchard MA, Huelsenbeck JP (2012) MrBayes 3.2: Efficient Bayesian phylogenetic inference and model choice across a large model space. Systematic Biology 61(3): 539–542. https://doi.org/10.1093/sysbio/sys029

Summerbell RC, Gueidan C, Schroers HJ, de Hoog GS, Starink M, Arocha Rosete Y, Guarro J, Scott JA (2011) *Acremonium* phylogenetic overview and revision of *Gliomastix*, *Sarocladium*, and *Trichothecium*. Studies in Mycology 68(1): 139–162. https://doi.org/10.3114/sim.2011.68.06

Szczepańska K, Guzow-Krzemińska B, Urbaniak J (2021) Infraspecific variation of some brown *Parmeliae* (in Poland) – a comparison of ITS rDNA and non-molecular characters. MycoKeys 85: 127–160. https://doi.org/10.3897/mycokeys.85.70552

Vilgalys R, Hester M (1990) Rapid genetic identification and mapping of enzymatically amplified ribosomal DNA from several *Cryptococcus* species. Journal of Bacteriology 172(8): 4238–4246. https://doi.org/10.1128/jb.172.8.4238-4246.1990

Vu D, Groenewald M, de Vries M, Gehrmann T, Stielow B, Eberhardt U, Al-Hatmi A, Groenewald JZ, Cardinali G, Houbraken J, Boekhout T, Crous PW, Robert V, Verkley GJM (2019) Large-scale generation and analysis of filamentous fungal DNA barcodes boosts coverage for kingdom fungi and reveals thresholds for fungal species and higher taxon delimitation. Studies in Mycology 92(1): 135–154. https://doi.org/10.1016/j.simyco.2018.05.001

White TJ, Bruns T, Lee S, Taylor J (1990) Amplification and direct sequencing of fungal ribosomal RNA genes for phylogenetics. In: Innis MA, Gelfand DH, Sninsky JJ, White TJ (Eds) PCR protocols: a guide to methods and applications, Academic Press, San Diego, California, 315–322. https://doi.org/10.1016/B978-0-12-372180-8.50042-1

Yang CL, Xu XL, Jeewon R, Boonmee S, Liu YG, Hyde KD (2019) *Acremonium arthrinii* sp. nov., a mycopathogenic fungus on *Arthrinium yunnanum*. Phytotaxa 420(4): 283–299. https://doi.org/10.11646/phytotaxa.420.4.4

Zhang ZY, Chen WH, Zou X, Han YF, Huang JZ, Liang ZQ, Deshmukh SK (2019a) Phylogeny and taxonomy of two new *Plectosphaerella* (Plectosphaerellaceae, Glomerellales) species from China. MycoKeys 57: 47–60. https://doi.org/10.3897/mycokeys.57.36628

Zhang ZY, Han YF, Chen WH, Liang ZQ (2019b) *Gongronella sichuanensis* (Cunninghamellaceae, Mucorales), a new species isolated from soil in China. Phytotaxa 416(2): 167–174. https://doi.org/10.11646/phytotaxa.416.2.4

Zhang ZY, Dong CB, Chen WH, Mou QR, Lu XX, Han YF, Huang JZ, Liang ZQ (2020a) The enigmatic Thelebolaceae (Thelebolales, Leotiomycetes): One new genus *Solomyces* and five new species. Frontiers in Microbiology 11: e572596. https://doi.org/10.3389/fmicb.2020.572596

Zhang ZY, Zhao YX, Shen X, Chen WH, Han YF, Huang JZ, Liang ZQ (2020b) Molecular phylogeny and morphology of *Cunninghamella guizhouensis* sp. nov. (Cunninghamellaceae, Mucorales), from soil in Guizhou, China. Phytotaxa 455(1): 31–39. https://doi.org/10.11646/phytotaxa.455.1.4

Zhang ZY, Shao QY, Li X, Chen WH, Liang JD, Han YF, Huang JZ, Liang ZQ (2021) Culturable fungi from urban soils in China I: Description of 10 new taxa. Microbiology Spectrum 9(2): e00867–e21. https://doi.org/10.1128/Spectrum.00867-21

Zhang Z, Chen W, Liang Z, Zhang L, Han Y, Huang J, Liang Z (2022) Revealing the non-overlapping characteristics between original centers and genetic diversity of *Purpureocillium lilacinum*. Fungal Ecology [accepted].

MycoKeys 91: 97–111 (2022)
doi: 10.3897/mycokeys.91.84730
https://mycokeys.pensoft.net

RESEARCH ARTICLE

A peer-reviewed open-access journal
MycoKeys
Launched to accelerate biodiversity research

Two new species of *Craterellus* (Cantharellales, Hydnaceae) with veined hymenophore from north-eastern China

Gui-Ping Zhao[1], Jia-Jun Hu[1], Yong-Lan Tuo[1], Yu Li[1], Bo Zhang[1]

1 *Engineering Research Center of Edible and Medicinal Fungi, Ministry of Education, Jilin Agricultural University, Changchun, Jilin 130118, China*

Corresponding authors: Bo Zhang (zhangbofungi@126.com), Yu Li (yuli966@126.com)

Academic editor: Bao-Kai Cui | Received 1 April 2022 | Accepted 7 June 2022 | Published 19 July 2022

Citation: Zhao G-P, Hu J-J, Tuo Y-L, Li Y, Zhang B (2022) Two new species of *Craterellus* (Cantharellales, Hydnaceae) with veined hymenophore from north-eastern China. MycoKeys 91: 97–111. https://doi.org/10.3897/mycokeys.91.84730

Abstract

In this contribution to the genus *Craterellus* in northern China, two new species are introduced: *Craterellus connatus* and *C. striatus*. These species and *C. atrobrunneolus*, initially described in south-western China, are highly similar and closely related. The species delimitation is molecularly supported by multigene phylogenetic analysis of the nr LSU and *tef*-1α region. *Craterellus connatus* is characterised by its medium-sized basidiomata, greyish-brown and smooth pileus with an off-white margin, the hymenophore with a strongly anastomosing vein, turning khaki upon drying, connate stipe, broad ellipsoid to ellipsoid basidiospores (6.1–7.8 × 4.8–5.9 μm), slender basidia with (2)4–6 sterigmata and the absence of clamp connection. *Craterellus striatus* is characterised by its small-sized basidiomata, fibrillose, greyish-brown to yellowish-brown, fully perforated pileus with a brown fringe, the hymenophore with a forking vein, the stipe inflated at the base, broad ellipsoid to ellipsoid basidiospores (6.8–8.0 × 5.1–6.0 μm), 2–6 spored basidia, encrusted hyphae and the absence of clamp connection. Detailed macroscopic and microscopic descriptions, accompanied by illustrations and a taxonomic discussion, are presented. A key to the Chinese *Craterellus* species is also provided.

Keywords

Chinese species, molecular phylogeny, morphology

Introduction

Craterellus Pers., typified with *C. cornucopioides* (L.) Pers. (Persoon 1825), belongs to *Hydnaceae* of *Cantharellales* (Hibbett et al. 2014). It is well represented in northern temperate zones and occurs in the tropics (Dahlman et al. 2000). Species in this genus are characterised by funnel-shaped fruiting bodies, hollow stipes, usually dark grey to black or yellow pileus (Corner 1966). *Craterellus* is an important genus of wild edible mushrooms and is renowned for its high economic, medicinal and ecological values (Pilz 2003). Approximately 162 records of *Craterellus* (including infraspecific taxa) have been found in Index Fungorum (http://www.indexfungorum.org). However, most of these species have been transferred to other genera, based on a phylogenetic analysis of the large nuclear subunit (nr LSU) and the internal transcribed spacer region (ITS), including *Cantharellus* Adans. ex Fr., *Gomphus* Pers. and *Polyozellus* Murrill etc. (Dahlman et al. 2000; Contu et al. 2009; Olariaga et al. 2009; Wilson et al. 2012; Montoya et al. 2021). Nearly 100 names have been considered legitimate in MycoBank (https://www.mycobank.org/) to date.

In China, species diversity, taxonomy and phylogeny of macrofungi have been investigated in recent years, many new species having been discovered (Zhong et al. 2018; Cui et al. 2019; Sun et al. 2020; Zhang et al. 2020a; Cao et al. 2021a, b; Liu et al. 2021, 2022a, b; Ji et al. 2022; Sun et al. 2022). *Craterellus* is one of the important fungal genera of macrofungi, 14 species of *Craterellus* having been recorded in China: *C. albidus* Chun Y. Deng, M. Zhang & J. Zhang, *C. atratus* (Corner) Yomyart, Watling, Phosri, Piap. & Sihan., *C. atrobrunneolus* T. Cao & H.S. Yuan, *C. aureus* Berk. & M.A. Curtis, *C. badiogriseus* T. Cao & H.S. Yuan, *C. cornucopioides*, *C. croceialbus* T. Cao & H.S. Yuan, *C. lutescens* (Fr.) Fr., *C. luteus* T.H. Li & X.R. Zhong, *C. macrosporus* T. Cao & H.S. Yuan, *C. odoratus* (Schwein.) Fr., *C. sinuosus* (Fr.) Fr., *C. squamatus* T. Cao & H.S. Yuan, *C. tubaeformis* (Fr.) Quél (Bi 1994; Mao 1998; Dai et al. 2010; Gu et al. 2012; Li et al. 2015; Zhong et al. 2018; Zhang et al. 2020a; Cao et al. 2021a, b). Nevertheless, due to their less attractive appearance, which can be confused with the environment, it is challenging to find *Craterellus* species in the field, causing them to be overlooked and thus remain undescribed. In addition, some species of *Craterellus*, especially those with the non-perforated pileus, are easily confused with other morphologically similar taxa, for example,, some species of *Clitocybe* (Fr.) Staude, *Gomphus* or *Polyozellus*, making it never easily distinguished from others in fieldwork.

During a recent survey of macrofungi in northern China, we discovered some exciting and novel species of *Craterellus*. In this contribution, the subsequent morphological and molecular analyses of the transcription elongation factor 1-alpha (*tef*-1α) and nr LSU sequences represented two new species, *C. connatus* G. P. Zhao, J. J. Hu, B. Zhang & Y. Li and *C. striatus* G. P. Zhao, J. J. Hu, B. Zhang & Y. Li which are described and illustrated herein. A key of *Craterellus* in China is provided as well.

Materials and methods

Vouchers and morphological analyses

This paper is principally based on materials collected by the senior author and collaborators over the past four years in northern China and specimens have been deposited at the Mycological Herbarium of Jilin Agricultural University (**HMJAU**).

Photographs and descriptions of macroscopic morphological characteristics were made from fresh materials in the field. The colours correspond to the "Flora of British fungi: colour identification chart" (Royal Botanic Garden 1969). Collections were dried in an oven at 45 °C and rehydrated with 95% alcohol. All microscopic observations and measurements were made in ammoniacal Congo red with a 5% aqueous potassium hydroxide (KOH) solution to improve tissue dissociation and matrix dissolution. Melzer's Reagent was also used in the study. Measurements of basidiospores cite length and length/width ratio (Q) in this format: (minimum–) mean minus standard deviation–mean value–mean plus standard deviation (–maximum measured), Q_m = average Q of all basidiospores measured ± sample standard deviation; spore measurements are based on 20 spores. Microscopic features were examined with the aid of the ZEISS Axio Lab A1.

DNA extraction, amplification and sequencing

Genomic DNA was extracted from dried or fresh material stored in desiccant silica gel. The extraction method followed the nuclear Plant Genomic DNA Kit (Kangwei Century Biotechnology Company Limited, Beijing, China). The amplified segments were the nr LSU and the *tef*-1α regions. The nr LSU region was amplified using LR0R and LR5 (Vilgalys and Hester 1990). The *tef*-1α region was amplified using tefF and tefR (Morehouse et al. 2003). Polymerase chain reaction (PCR) amplifications were performed in a total volume of 25 μl containing 1 μl template DNA, 1 μl of each primer, 10.5 μl distilled water and 12.5 μl PCR mix (2× Es Taq MasterMix, CWBIO, China). PCR amplification conditions followed Vilgalys and Hester (1990) for the nr LSU region and Morehouse et al. (2003) for the *tef*-1α region. The PCR products were subjected to electrophoresis on 1% agarose gel. Sequencing was performed by Sangon Biotech (Shanghai, China) using the same primer pairs used for the PCR.

Phylogenetic analyses

This study is based on around 25 specimens, including two outgroups (*Hydnum ellipsosporum* Ostrow & Beenken and *Cantharellus cibarius* Fr.) (Bijeesh et al. 2018; Zhong et al. 2018; Zhang et al. 2020a; Cao et al. 2021b). Sequences of the nr LSU and *tef*-1α regions were newly produced in this study and downloaded from GenBank (http://www.ncbi.nlm.nih.gov/). Detailed sample information is provided in Table 1.

Table 1. Information on the specimens that were used in the phylogenetic analyses. Sequences that were newly generated in this study are indicated in black bold. T: Type.

Taxon	Voucher number	Country	GenBank accession number		References
			nr LSU	*tef*-1α	
Craterellus albidus	HGASMF013581 (T)	China	MT921161	–	Zhang et al. (2020a)
C. albidus	HGASMF0110046	China	MT921162		Zhang et al. (2020a)
C. albostrigosus	CAL1624 (T)	India	MG593194	–	Bijeesh et al. (2018)
C. atratoides	TH9232 (T)	Guyana	NG042660	–	Wilson et al. (2012)
C. atratoides	MCA1313	Guyana	JQ915119	–	Wilson et al. (2012)
C. atratus	MCA1070	Guyana	JQ915118	–	Wilson et al. (2012)
C. atratus	TH9203	Guyana	JQ915133	–	Wilson et al. (2012)
C. atrobrunneolus	Yuan13878 (T)	China	MN894058	–	Cao et al. (2021b)
C. badiogriseus	Yuan 14776 (T)	China	MW979532	MW999432	Cao et al. (2021a)
C. badiogriseus	Yuan 14779	China	MW979533	MW999433	Cao et al. (2021a)
C. caeruleofuscus	MH17001	USA	MT237468	–	Genbank
C. cinereofimbriatus	TH9075 (T)	Guyana	JQ915131	–	Wilson et al. (2012)
C. cinereofimbriatus	TH8999	Guyana	JQ915130	–	Wilson et al. (2012)
C. cinereofimbriatus	TH9264	Guyana	JQ915138	–	Wilson et al. (2012)
C. connatus	**HMJAU 61462 (T)**	**China**	**OM509448**	**ON125915**	**This study**
C. connatus	**HMJAU 61462**	**China**	**–**	**ON125916**	**This study**
C. cornucopioides	HbO53302	Norway	AF105301	–	Dahlman et al. (2000)
C. cornucopioides	UPSF11801	USA	AF105299	–	Dahlman et al. (2000)
C. excelsus	MCA3107	Guyana	JQ915121	–	Wilson et al. (2012)
C. excelsus	TH7515	Guyana	JQ915127	–	Wilson et al. (2012)
C. fallax	AFTOL286	USA	AY700188	–	Genbank
C. ignicolor	UPSF11794	USA	AF105314	–	Dahlman et al. (2000)
C. indicus	PUN3884 (T)	India	HM113529	–	Kumari et al. (2012)
C. indicus	MSR7	India	HQ450770		Kumari et al. (2012)
C. indicus	MSR8	India	HQ450771		Kumari et al. (2012)
C. inusitatus	CAL 1625 (T)	India	MG593195	–	Bijeesh et al. (2018)
C. lutescens	UPSF11789	Sweden	AF105302	–	Dahlman et al. (2000)
C. lutescens	UPSF11790	Sweden	AF105303	–	Dahlman et al. (2000)
C. lutescens	UPSF11791	Spain	AF105304	–	Dahlman et al. (2000)
C. luteus	GDGM46432	China	MG727898	–	Zhong et al. (2018)
C. luteus	GDGM48105 (T)	China	MG701171	–	Zhong et al. (2018)
C. luteus	GDGM49495	China	MG806926	–	Zhong et al. (2018)
C. striatus	**HMJAU 61463 (T)**	**China**	**OM509446**	**ON125913**	**This study**
C. striatus	**HMJAU 61463**	**China**	**OM509447**	**ON125914**	**This study**
C. odoratus	UPSF11794	USA	AF105306	–	Dahlman et al. (2000)
C. olivaceoluteus	TH9205 (T)	Guyana	JQ915135	–	Wilson et al. (2012)
C. olivaceoluteus	MCA3186	Guyana	JQ915124	–	Wilson et al. (2012)
C. parvogriseus	CAL1533 (T)	India	MF421098	–	Das et al. (2017)
C. parvogriseus	CAL1534	India	NG059049	–	Das et al. (2017)
C. pleurotoides	TH9220 (T)	Guyana	JQ915136	–	Wilson et al. (2012)
C. pleurotoides	MCA3124	Guyana	JQ915123	–	Wilson et al. (2012)
C. strigosus	MAC1750	Guyana	JQ915120	–	Wilson et al. (2012)
C. strigosus	TH9204 (T)	Guyana	JQ915134	–	Wilson et al. (2012)
C. tubaeformis	UPSF11793	Sweden	AF105307	–	Dahlman et al. (2000)
C. tubaeformis	BB 07.293	Slovakia	KF294640	GQ914989	Buyck and Hofstetter (2011)
Cantharellus cibarius	BIO 10986 (T)	Sweden	KR677539	KX828823	Olariaga et al. (2017)
Hydnum ellipsosoporxum	FD3281	Switzerland	KX086217	–	Genbank

Sequences were assembled and edited using the software package Sequencher 5.4.6 (Gene Codes Corp., USA). Alignment of sequence data was performed with MUSCLE in MEGA 7.0.21 (Kumar et al. 2016). For Bayesian Inference (BI) analyses, the most suitable substitution model for each gene partition was calculated with ModelFinder (Kalyaanamoorthy et al. 2017) in PhyloSuite 1.2.2. (Zhang et al. 2020b). BI analyses were performed using MrBayes in PhyloSuite 1.2.2 (Zhang et al. 2020b), implementing the Markov Chain Monte Carlo (MCMC) technique. Four simultaneous Markov chains were run from random trees, keeping one tree every 200th generation until the average standard deviation of split frequencies was below 0.01. The Maximum Likelihood analysis was performed using RAxML-HPC2 on XSEDE 8.2.12 (Stamatakis 2014) in the CIPRES Science Gateway portal (https://www.phylo.org/portal2/tools.action) with the GTRGAMMA model and searching for the most likely tree with 1000 heuristic replicates. The bootstrap support (BS) of ≥ 50% in the ML tree and BPP of ≥ 0.75 indicated statistical significance. The phylogenetic trees were visualised using FigTree 1.4.23 (Andrew 2016).

Results

Phylogeny

Seven new DNA sequences (3 nr LSU, 4 *tef*-1α) were produced for this study. After removing introns and low-homology regions, the final combined alignment of these two genes totalled 2,027 characters (nr LSU: 1,024 characters; *tef*-1α: 1,003 characters). The best models for the BI analysis of the concatenated dataset were SYM+I+G4 for nr LSU and SYM+G4 for tef-1α. The most likely tree inferred by ML analysis of the combined dataset exhibited a quite similarly supported topology as the Bayesian majority-rule consensus tree with an average standard deviation of split frequencies = 0.005143. The most likely tree, based on 1000 searches, is depicted in Fig. 1 with associated bootstrap values. Maximum Likelihood Bootstrap (MLBS) and Bayesian Posterior Probability (BPP) were established along the branches. Phylogenetic analyses show (Fig. 1) that our two new species, *C. connatus* and *C. striatus* were clustered together with *C. atrobrunneolus* in a monophyletic clade (MLBS = 99%, BPP = 1.00). *C. connatus* (MLBS = 88%, BPP = 0.93) formed sister relationships (MLBS = 88%, BPP = 0.87) with *C. striatus* (MLBS = 60%, BPP = 0.77).

Taxonomy

Craterellus connatus **G.P. Zhao, J.J. Hu, B. Zhang & Y. Li, sp. nov.**
MycoBank No: 842527
Figs 2, 3

Holotype. China. Jilin Province, Jilin City, Jiaohe County, Lafashan National Forest Part, Red Leaves Canyon, alt. 802.5 m, 43.75°N, 127.10°E, 5 September 2018, Bo Zhang HMJAU 61462, GenBank Acc. nos.: nr LSU = OM509448, *tef*-1α = ON125915, ON125916).

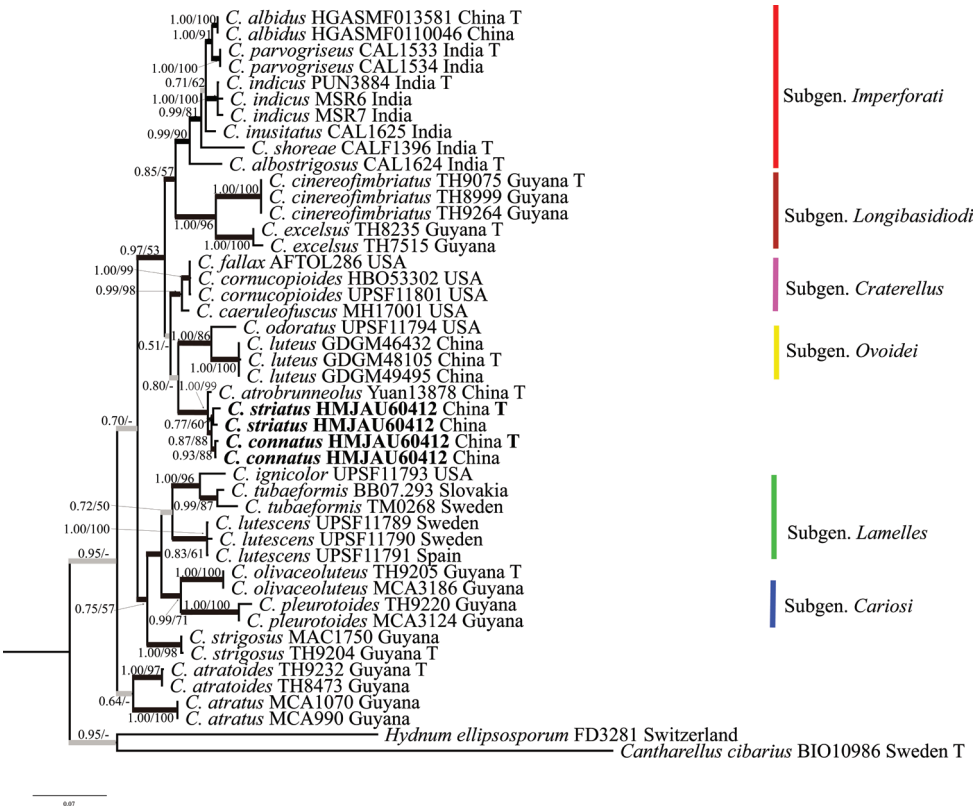

Figure 1. BI best tree inferred from the nr LSU and *tef*-1α region analysis for 25 specimens. Branches that received both bootstrap support (MLBS) ≥ 50% and Bayesian posterior probabilities (PP) ≥ 0.75 are in bold; branches supported by either MLBS or BPP are in grey. Both values (MLBS/BPP) are reported along the branches. Taxon names shown in bold indicate the specimens examined in this study.

Etymology. *Connatus*: referring to several stipes grown together from the base upwards.

Diagnosis. Differs from other *Craterellus* species by its greyish-brown and smooth pileus with an off-white margin, hymenophore with a strongly anastomosing vein and the colouration turning khaki upon drying.

Description. ***Pileus*** 18–30 mm in diam., infundibuliform, deeply depressed at the centre, perforated continuously to the base of the stipe; margin inrolled when young, then expand upwards, becoming upturned finally, broadly wavy; surface greyish-brown in the centre, the marginal edge dirty white, smooth. ***Hymenophore*** consists of longitudinal, anastomosing veined, off-white, turning khaki when drying and decurrent. ***Stipe*** 25–30 × 3 mm, equal to subcylindrical, hollow, central, smooth, greyish-brown. ***Text*** fleshy, greyish-brown. ***Odour*** light. ***Taste*** unknown. ***Spore print*** not obtained.

Basidiospores 6.1–6.9–7.8(8.1) × 4.8–5.3–5.9 μm, Q = (1.16)1.20–1.32–1.45(1.56), Q_m = 1.32 ± 0.09, broad ellipsoid to ellipsoid, smooth, thin-walled, pale

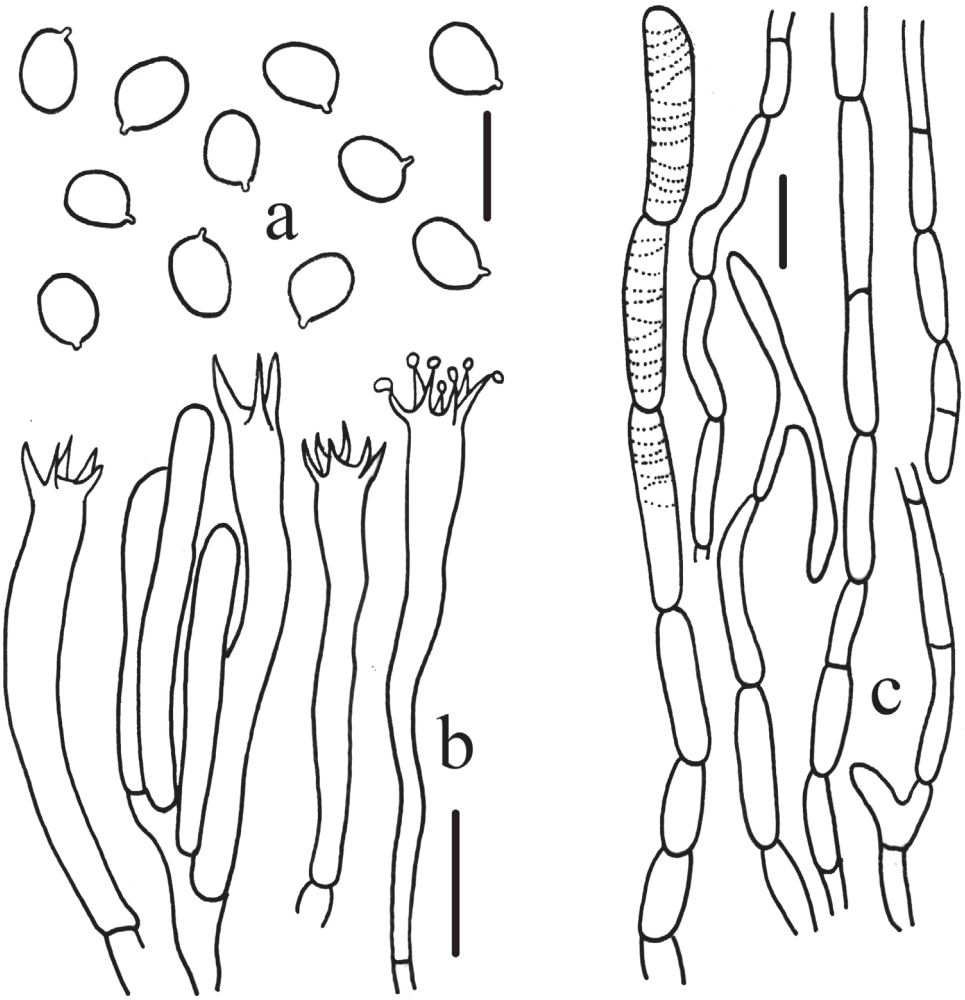

Figure 2. *Craterellus connatus* (HMJAU 60411, holotype) **A** fresh basidiocarps **B** connate stipes **C** margin of pileus **D** hymenophore. Scale bars: 1 cm (**A, B**)

yellow in 5% aqueous KOH, inamyloid. ***Basidia*** (40)50–72.5(75) × (6)7.5–8(10) μm, clavate, sterigmata (2)4-6. ***Cystidia*** absent. ***Hymenium*** in transverse section 125–175 μm thick, yellowish-brown in 5% aqueous KOH. ***Pileipellis*** scarcely differentiated from the trama, a cutis of vastly inflated hyphae, yellowish-brown in 5% aqueous KOH; individual hyphae (22)27–63(64) × 6–15 μm, thin-walled, branched occasionally, secondary septation absent, hyaline in 5% aqueous KOH. ***Pileus trama*** up to 500 μm thick, subparallel, yellowish-brown in 5% aqueous KOH; individual hyphae (29)33–60(125) × (4)5–12(13) μm, cylindrical, thin-walled, branching frequently, secondary septation absent. ***Subhymenium*** up to 10 μm thick. ***Stipitipellis*** composed of a tightly packed mass of subparallel, narrow, cylindrical hyphae, yellowish-brown in 5% aqueous KOH; individual hyphae (33)37–79(102) × 4–13(16) μm, thin-walled,

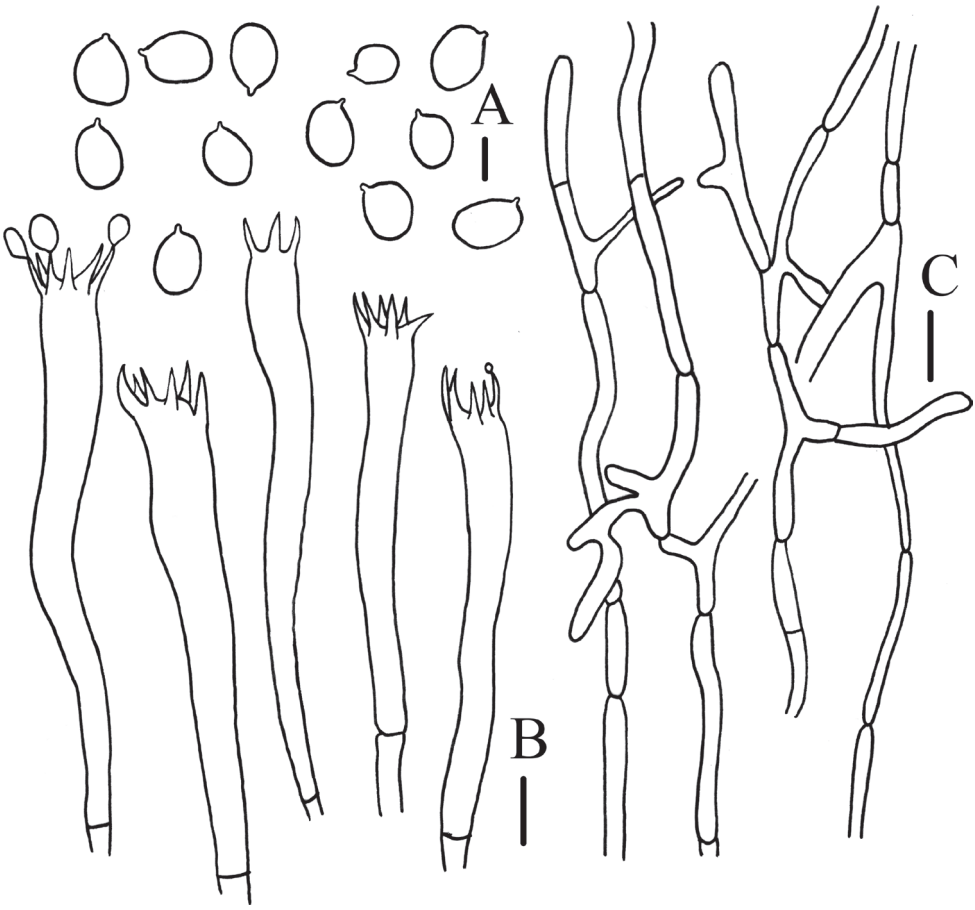

Figure 3. Microscopic characteristics of *Craterellus connatus* (HMJAU 60411) **A** basidiospores **B** basidia **C** pileipellis. Scale bars: 5 μm (**A**); 10 μm (**B**); 20 μm (**C**).

hyaline to pale yellow in 5% aqueous KOH, branched frequently, secondary septation absent. ***Clamp connections*** absent.

Habitat. Scattered or gregarious in small clusters on the ground in coniferous and angiosperm mixed forests.

Craterellus striatus **G.P. Zhao, J.J. Hu, B. Zhang & Y. Li, sp. nov.**
MycoBank No: 842531
Figs 4, 5

Holotype. China. Jilin Province, Baishan City, Fusong County, Quanyang Town, alt. 780.4 m, 42.23°N, 121.30°E, 22 August 2021, G. P. Zhao, J. J. Hu, and Bo Zhang (HMJAU 61463, GenBank Acc. nos.: nr LSU = OM509446, OM509447, *tef*-1α = ON125913, ON125914).

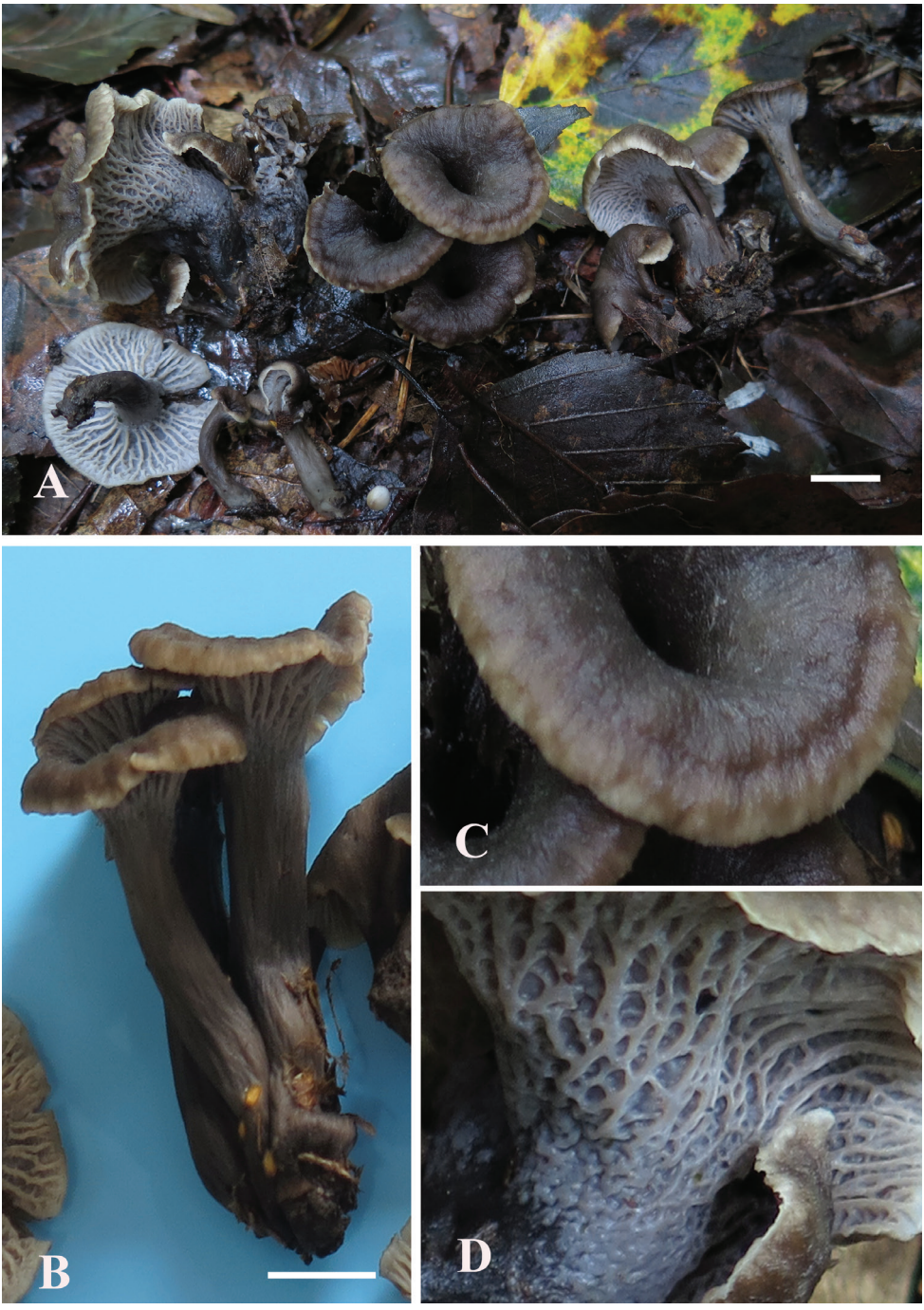

Figure 4. *Craterellus striatus* (HMJAU 60412, holotype) **A** Fresh basidiocarps **B** Stipe **C** Pileus **D** Hymenophore. Scale bars: 1 cm (**A, B**)

Etymology. *Striatus*: referring to the fringe of pileus.

Diagnosis. Differs from other *Craterellus* species by the fibrillose, greyish-brown to yellowish-brown, fully perforated pileus with a brown fringe, the hymenophore with a forking vein, not anastomosing and non-discolouring upon drying.

Description. ***Fruiting body*** 12–45 mm high. ***Pileus*** 3–21 mm in diam., 1–10 mm tall, plane-convex firstly, soon infundibuliform and usually perforated continuous to the base of the stipe; margin inrolled when young, then expanding outwards, old becoming incurved, broadly wavy; surface blackish-brown, cream near the margin at first, gradually lighter to the centre with age, yellowish-brown finally, turning pale greyish-brown when drying, covered with brown fringe and fibrillose scales. ***Hymenophore*** decurrent, consisting of longitudinal ridges (<1 mm) with prominent forking, cross vein and off-white. ***Stipe*** 11–35 × 1–6 mm, cylindrical, inflated at the base, up to

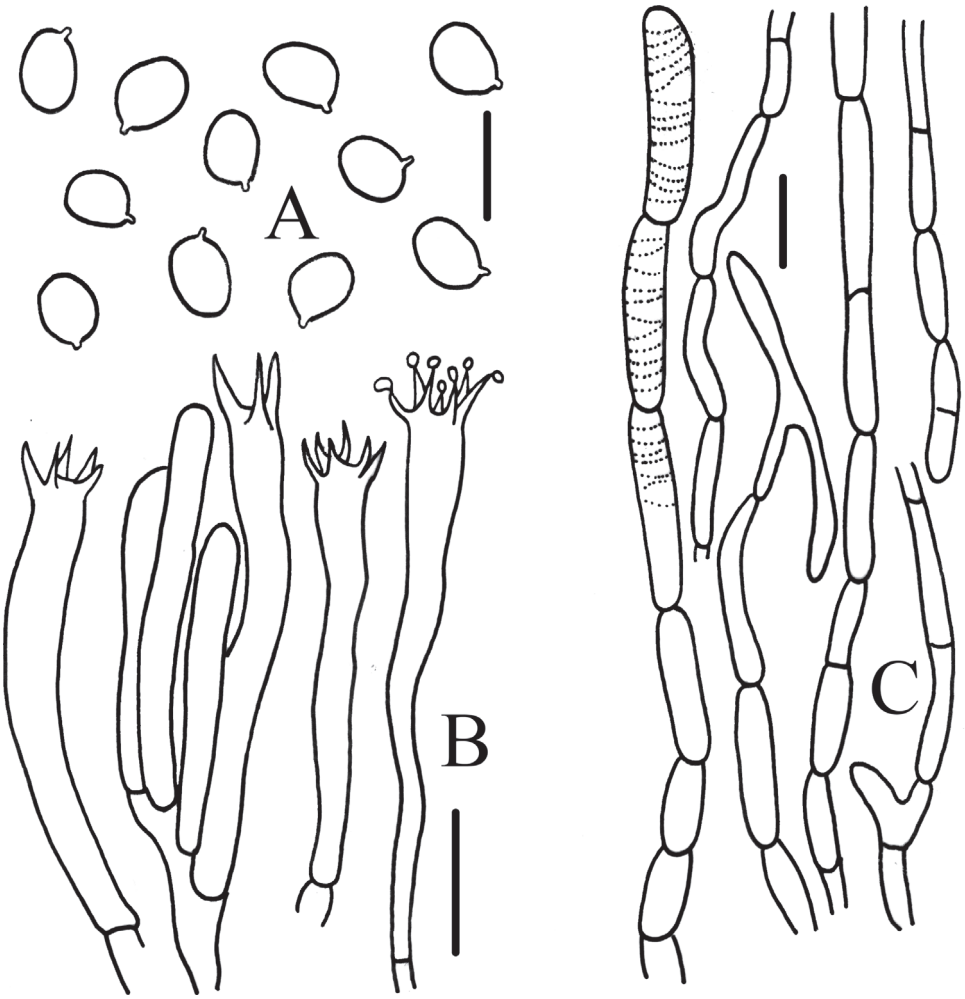

Figure 5. Microscopic characteristics of *Craterellus striatus* (HMJAU 60412) **A** spores **B** basidiobasidia **C** pileipellis. Scale bars: 10 μm (**A**); 20 μm (**B**); 40 μm (**C**).

10 mm in diam., hollow, central, smooth, blackish-brown. ***Text*** leathery, dirty white. ***Odour*** light. ***Taste*** unknown. ***Spore print*** not obtained.

Basidiospores (6.5)6.8–7.4–8.0(8.8) × (5.0)5.1–5.5–6.0 μm, Q = (1.18)1.22–1.36–1.53(1.73), Q_m = 1.36 ± 0.12, broad ellipsoid to ellipsoid, smooth, thin-walled, hyaline to pale yellow in 5% aqueous KOH, inamyloid. ***Basidia*** (34)40–67(68) × 6–9 μm, slender, sterigmata 2–6. ***Cystidia*** absent. ***Hymenium*** in transverse section 45 μm thick, yellowish-brown in 5% aqueous KOH. ***Pileipellis*** scarcely differentiated from trama, a cutis of largely cylindrical hyphae, yellowish-brown in 5% aqueous KOH; individual hyphae (30)40–70(73) × (4)5–14(15) μm, thin-walled, encrusted, branched frequently, secondary septation absent, hyaline in 5% aqueous KOH. ***Pileus trama*** up to 500 μm thick, subparallel, yellowish-brown in 5% aqueous KOH; individual hyphae (29)33–60(125) × (4)5–12(13) μm, cylindrical, thin-walled, encrusted, branching frequently, secondary septation absent. ***Subhymenium*** up to 10 μm thick. ***Stipitipellis*** composed of a tightly-packed mass of subparallel, narrow, cylindrical hyphae, yellowish-brown in 5% aqueous KOH; individual hyphae (33)37–79(102) × 4–13(16) μm, thin-walled, hyaline to pale yellow in 5% aqueous KOH, branched frequently, secondary septation absent. ***Clamp connections*** absent.

Habitat. Scattered to gregarious on the ground in a coniferous and angiosperm mixed forest.

Key to reported species of *Craterellus* in China

1	Clamp connections present	**2**
–	Clamp connections absent	**4**
2	Stipe golden yellow to orangish-yellow	**3**
–	Stipe grey	***C. atratus***
3	Pileus perforate to the base of the stipe	***C. tubaeformis***
–	Pileus not perforate	***C. lutescens***
4	Basidiomata not brown, absolutely light colour	**5**
–	Basidiomata greyish-brown to blackish-brown	**7**
5	Pileus white	***C. albidus***
–	Pileus yellow	**6**
6	Pileus very small, usually < 10 mm in diam	***C. aureus***
–	Pileus large, usually > 90 mm in diam	***C. luteus***
7	Basidiospores 10–15 μm long, average length > 11 μm	**10**
–	Basidiospores 6–12 μm long, average length < 11 μm	**8**
8	Hymenophore smooth to slightly folded	**9**
–	Hymenophore with well-developed veins or gill-folds	***C. striatus***
9	Basidia long, up to 106 μm long	***C. badiogriseus***
–	Basidia short	**13**
10	Basidia with 2 sterigmata	**11**
–	Basidia with 2–4 sterigmata	**12**
11	Basidiospores broad, up to 11.5 μm wide	***C. macrosporus***
–	Basidiospores 2–4 μm wide	***C. cornucopioides***

12	Pileus surface smooth	***C. croceialbus***
–	Pileus surface often with darker brown raised scales	***C. squamatus***
13	Margin dirty white	***C. connatus***
–	Margin not dirty white	***C. atrobrunneolus***

Discussion

In our study, two new species formed a sister relationship with *Craterellus atrobrunneolus.* These three species show close morphological and phylogenetic similarities with each other. All species share the brown pileus, grey hymenophore, hollow stipe, narrow basidia and absence of clamps. *Craterellus atrobrunneolus* was initially described in south-western China. It is characterised by a dark brown to brownish-grey colouration, convex to plano-convex pileus with shallow depression, but not perforated centre, smooth to slightly folded hymenophore, absence of clamp connections in all tissues, narrow basidia with 2–6 sterigmata and broad ellipsoid to subglobose basidiospores (Cao et al. 2021b). *Craterellus connatus* is recognised in the field by the medium-sized, nearly fleshy basidiomata with the greyish-brown, fully perforated pileus, an off-white margin, strongly anastomosed, veined hymenophore and hollow stipe. Microscopically, it possesses broad ellipsoid to ellipsoid basidiospores (Q_m = 1.32 ± 0.09), slender basidia with (2)4–6 sterigmata and an absence of clamp connections. *Craterellus striatus* is characterised by its small-sized basidiomata, blackish-brown pileus that turns yellowish-brown upon drying and is covered with brown fringe and spinous scales and off-white hymenophore consisting of longitudinal ridges (<1 mm) with prominent forking. It has a hollow and brown stipe and broad ellipsoid to ellipsoid basidiospores, 2–6 spored basidia, encrusted hyphae and the absence of the clamp connection.

Craterellus atrobrunneolus differs by its dark brown to almost black throughout, convex but not perforated pileus, while *C. connatus* possesses greyish-brown pileus with an off-white margin and *C. striatus* possesses yellowish-brown, perforated pileus with brown fringe. Microscopically, *C. atrobrunneolus* possesses broad ellipsoid to subglobose basidiospores, while *C. connatus* and *C. striatus* possess broad ellipsoid to ellipsoid basidiospores. In addition, *C. atrobrunneolus* have 2–6 spored basidia, while *C. connatus* have mostly 4–6 spored basidia. *Craterellus striatus* have encrusted hyphae, while *C. atrobrunneolus* did not. Although the two new species have similar microscopic characteristics (spores and basidia), they are separated by their colouration of dried pileus and hymenophore and the configuration of hymenophore. *Craterellus striatus* is smaller (both pileus and stipe) than *C. connatus*. Further, *C. striatus* has a hymenophore composed of the forked longitudinal ridge and non-discolouring upon drying, whereas *C. connatus* has an anastomosing veined hymenophore, which turns khaki upon drying. Morphology and phylogenetic analyses indicated that the two new species in this study are not conspecific.

However, *Craterellus atrobrunneolus* was not included in any subgenus in Cao et al. (2021a). According to our study, *C. atrobrunneolus*, *C. conatus* and *C. striatus* have

formed an isolated branch. Further research is needed to obtain a more precise infrageneric classification. Additionally, this study suggests that China, especially northeastern China, has considerable fungal diversity and possibly many endemic species.

Acknowledgements

This study is funded by the National Natural Science Foundation of China (No. 31970020), the Scientific and Technological Tackling Plan for the Key Fields of Xinjiang Production and Construction Corps (No. 2021AB004), the National Key R & D of the Ministry of Science and Technology (2019YFD1001905-33), Research on the creation of excellent edible mushroom resources and high quality & efficient ecological cultivation technology in Jiangxi Province (20212BBF61002) and the National Key R & D of Ministry of Science and Technology (2018YFE0107800).

References

Andrew R (2016) Fig tree: tree figure drawing tool version 1.4.3. Institute of evolutionary biology, United Kingdom, University of Edinburgh. http://tree.bio.ed.ac.uk/software/figtree/

Bi ZS (1994) Macrongus flora of Guangdong province. Guangdong Science and Technology Press, Guangzhou, 311–313.

Bijeesh C, Kumar AM, Vrinda KB, Pradeep CK (2018) Two new species of *Craterellus* (*Cantharellaceae*) from tropical India. Phytotaxa 346(2): 157–168. https://doi.org/10.11646/phytotaxa.346.2.3

Buyck B, Hofstetter V (2011) The contribution of tef-1 sequences to species delimitation in the *Cantharellus cibarius* complex in the southeastern USA. Fungal Diversity 49(1): 35–46. https://doi.org/10.1007/s13225-011-0095-z

Cao T, Hu YP, Yu JR, Wei TZ, Yuan HS (2021a) A phylogenetic overview of the *Hydnaceae* (*Cantharellales*, *Basidiomycota*) with new taxa from China. Studies in Mycology 99(1): e100121. https://doi.org/10.1016/j.simyco.2021.100121

Cao T, Yu JR, Hu YP, Yuan HS (2021b) *Craterellus atrobrunneolus* sp. nov. from southwestern China. Mycotaxon 136(1): 59–71. https://doi.org/10.5248/136.59

Contu M, Vizzini A, Carbone M, Setti L (2009) Identity and neotypification of *Craterellus cinereus* and description of *Cantharellus atrofuscus* sp. nov. Mycotaxon 110(1): 139–149. https://doi.org/10.5248/110.139

Corner EJH (1966) A monograph of Canthareiloid fungi. Oxford University Press, London, 84–98.

Cui BK, Li HJ, Ji X, Zhou JL, Song J, Si J, Yang ZL, Dai YC (2019) Species diversity, taxonomy and phylogeny of *Polyporaceae* (*Basidiomycota*) in China. Fungal Diversity 97(1): 137–392. https://doi.org/10.1007/s13225-019-00427-4

Dahlman M, Danell E, Spatafora JW (2000) Molecular systematics of *Craterellus*: Cladistic analysis of nuclear LSU rDNA sequence data. Mycological Research 104(4): 388–394. https://doi.org/10.1017/S0953756299001380

Dai YC, Zhou LW, Yang ZL, Wen HA, Bau T, Li TH (2010) A revised checklist of edible fungi in China. Junwu Xuebao 29(1): 1–21.

Das K, Ghosh A, Chakraborty D, Li J, Qiu L, Baghela A, Halama M, Hembrom M, Mehmood T, Parihar A, Pencakowski B, Bielecka M, Reczyńska K, Sasiela D, Singh U, Song Y, Świerkosz K, Szczęśniak K, Uniyal P, Zhang JB, Buyck B (2017) Fungal biodiversity profiles 31–40. Cryptogamie. Mycologie 38(3): 353–406. https://doi.org/10.7872/crym/v38.iss3.2017.353

Gu XW, Wu RB, He BW, Ying GH, Liu DY (2012) Edible macrofungi resources in the mountain area of southern Zhejiang. Journal of Zhejiang Agricultural Sciences 11: 1515–1519.

Hibbett DS, Bauer R, Binder M, Giachini AJ, Hosaka K, Justo A, Larsson E, Larsson KH, Lawrey JD, Miettinen O, Nagy LG, Nilsson RH, Weiss M, Thorn RG (2014) 14 Agaricomycetes. Systematics and Evolution, 373–429. https://doi.org/10.1007/978-3-642-55318-9_14

Ji X, Zhou JL, Song CG, Xu TM, Wu DM, Cui BK (2022) Taxonomy, phylogeny and divergence times of *Polyporus* (*Basidiomycota*) and related genera. Mycosphere 13(1): 1–52. https://doi.org/10.5943/mycosphere/13/1/1

Kalyaanamoorthy S, Minh BQ, Wong TK, Von Haeseler A, Jermiin LS (2017) ModelFinder: Fast model selection for accurate phylogenetic estimates. Nature Methods 14(6): 587–589. https://doi.org/10.1038/nmeth.4285

Kumar S, Stecher G, Tamura K (2016) MEGA7: Molecular evolutionary genetics analysis version 7.0 for bigger datasets. Molecular Biology and Evolution 33(7): 1870–1874. https://doi.org/10.1093/molbev/msw054

Kumari D, Upadhyay RC, Reddy MS (2012) *Craterellus indicus* sp. nov., a new species associated with *Cedrus deodara* from the western Himalayas, India. Mycological Progress 11(3): 769–774. https://doi.org/10.1007/s11557-011-0788-4

Li Y, Li H, Yang ZL, Bau T, Dai YC (2015) Atlas of Chinese macrofungal resources. Central Chinese Farmer Press, Zhengzhou, 692–693.

Liu S, Han ML, Xu TM, Wang Y, Wu DM, Cui BK (2021) Taxonomy and phylogeny of the *Fomitopsis pinicola* complex with descriptions of six new species from east Asia. Frontiers in Microbiology 12: e644979. https://doi.org/10.3389/fmicb.2021.644979

Liu S, Sun YF, Wang Y, Xu TM, Song CG, Chen YY, Cui BK (2022a) Taxonomy and molecular phylogeny of *Trametopsis* (*Polyporales*, *Basidiomycota*) with descriptions of two new species. MycoKeys 90: 31–51. https://doi.org/10.3897/mycokeys.90.84717

Liu S, Xu TM, Song CG, Zhao CL, Wu DM, Cui BK (2022b) Species diversity, molecular phylogeny and ecological habits of *Cyanosporus* (*Polyporales*, *Basidiomycota*) with an emphasis on Chinese collections. MycoKeys 86: 19–46. https://doi.org/10.3897/mycokeys.86.78305

Mao XL (1998) Economic fungi of China. Science Press, Beijing, 821–826.

Montoya L, Herrera M, Bandala V, Ramos-Fernández A (2021) Two new species and a new record of yellow *Cantharellus* from tropical *Quercus* forests in eastern Mexico with the proposal of a new name for the replacement of *Craterellus confluens*. MycoKeys 80: 91–114. https://doi.org/10.3897/mycokeys.80.61443

Morehouse EA, James TY, Ganley AR, Vilgalys R, Berger L, Murphy PJ, Longcore JE (2003) Multilocus sequence typing suggests the chytrid pathogen of amphibians is a recently emerged clone. Molecular Ecology 12(2): 395–403. https://doi.org/10.1046/j.1365-294X.2003.01732.x

Olariaga I, Salcedo I, Parra L (2009) Proposal to conserve the name *Craterellus cinereus* (Pers.: Fr.) Donk with a conserved type against *Craterellus cinereus* Pers. (*Basidiomycota*). Taxon 58(1): 294–295. https://doi.org/10.1002/tax.581031

Olariaga I, Moreno G, Manjón JL, Salcedo I, Hofstetter V, Rodríguez D, Buyck B (2017) *Cantharellus* (*Cantharellales*, *Basidiomycota*) revisited in Europe through a multigene phylogeny. Fungal Diversity 83(1): 263–292. https://doi.org/10.1007/s13225-016-0376-7

Persoon CH (1825) Mycologia europaea (Vol. 2). Ioannis Iacobi Palmii, Erlangae 4.

Pilz D (2003) Ecology and management of commercially harvested chanterelle mushrooms (Vol. 576). Pacific Northwest Research Station, Portland, 1–83. https://doi.org/10.2737/PNW-GTR-576

Royal Botanic Garden E (1969) Flora of British fungi: colour identification chart. HM Stationery Office, Edinburgh.

Stamatakis A (2014) RAxML version 8: A tool for phylogenetic analysis and post-analysis of large phylogenies. Bioinformatics 30(9): 1312–1313. https://doi.org/10.1093/bioinformatics/btu033

Sun YF, Costa-Rezende DH, Xing JH, Zhou JL, Zhang B, Gibertoni TB, Gates G, Glen M, Dai YC, Cui BK (2020) Multi-gene phylogeny and taxonomy of *Amauroderma* s. lat. (*Ganodermataceae*). Persoonia 44(1): 206–239. https://doi.org/10.3767/persoonia.2020.44.08

Sun YF, Xing JH, He XL, Wu DM, Song CG, Liu S, Vlasák J, Gates G, Gibertoni TB, Cui BK (2022) Species diversity, systematic revision and molecular phylogeny of *Ganodermataceae* (*Polyporales*, *Basidiomycota*) with an emphasis on Chinese collections. Studies in Mycology 101: 287–415. https://doi.org/10.3114/sim.2022.101.05

Vilgalys R, Hester M (1990) Rapid genetic identification and mapping of enzymatically amplified ribosomal DNA from several Cryptococcus species. Journal of Bacteriology 172(8): 4238–4246. https://doi.org/10.1128/jb.172.8.4238-4246.1990

Wilson AW, Aime MC, Dierks J, Mueller GM, Henkel TW (2012) *Cantharellaceae* of Guyana I: New species, combinations and distribution records of *Craterellus* and a synopsis of known taxa. Mycologia 104(6): 1466–1477. https://doi.org/10.3852/11-412

Zhang J, Wu D, Deng CY, Zhang M, Dauner L, Wijayawardene NN (2020a) A new species of *Craterellus* (*Cantharellales*, *Hydnaceae*) from Guizhou Province, China. Phytotaxa 472(3): 259–268. https://doi.org/10.11646/phytotaxa.472.3.4

Zhang D, Gao F, Jakovlić I, Zou H, Zhang J, Li WX, Wang GT (2020b) PhyloSuite: An integrated and scalable desktop platform for streamlined molecular sequence data management and evolutionary phylogenetics studies. Molecular Ecology Resources 20(1): 348–355. https://doi.org/10.1111/1755-0998.13096

Zhong XR, Li TH, Jiang ZD, Deng WQ, Huang H (2018) A new yellow species of *Craterellus* (*Cantharellales*, *Hydnaceae*) from China. Phytotaxa 360(1): 35–44. https://doi.org/10.11646/phytotaxa.360.1.3

MycoKeys 91: 113–149 (2022)
doi: 10.3897/mycokeys.91.83091
https://mycokeys.pensoft.net

RESEARCH ARTICLE

A peer-reviewed open-access journal
MycoKeys
Launched to accelerate biodiversity research

Comprehensive treatise of *Hevansia* and three new genera *Jenniferia*, *Parahevansia* and *Polystromomyces* on spiders in Cordycipitaceae from Thailand

Suchada Mongkolsamrit[1], Wasana Noisripoom[1], Kanoksri Tasanathai[1], Noppol Kobmoo[1], Donnaya Thanakitpipattana[1], Artit Khonsanit[1], Booppa Petcharad[2], Baramee Sakolrak[3], Winanda Himaman[3]

1 *Plant Microbe Interaction Research Team, National Center for Genetic Engineering and Biotechnology (BIOTEC), 113 Thailand Science Park, Phahonyothin Road, Khlong Nueng, Khlong Luang, Pathum Thani, 12120, Thailand* **2** *Department of Biotechnology, Faculty of Science and Technology, Thammasat University, Pathum Thani, 12120, Thailand* **3** *Forest Entomology and Microbiology Research Group, Forest and Plant Conservation Research Office, 61 Department of National Parks, Wildlife and Plant Conservation, Phahonyothin Road, Chatuchak, Bangkok, 10900, Thailand*

Corresponding author: Suchada Mongkolsamrit (suchada@biotec.or.th)

Academic editor: Marc Stadler | Received 4 March 2022 | Accepted 2 July 2022 | Published 26 July 2022

Citation: Mongkolsamrit S, Noisripoom W, Tasanathai K, Kobmoo N, Thanakitpipattana D, Khonsanit A, Petcharad B, Sakolrak B, Himaman W (2022) Comprehensive treatise of *Hevansia* and three new genera *Jenniferia*, *Parahevansia* and *Polystromomyces* on spiders in Cordycipitaceae from Thailand. MycoKeys 91: 113–149. https://doi.org/10.3897/mycokeys.91.83091

Abstract

Collections of pathogenic fungi found on spiders from Thailand were selected for a detailed taxonomic study. Morphological comparison and phylogenetic analyses of the combined ITS, LSU, *tef1*, *rpb1* and *rpb2* sequence data indicated that these specimens formed new independent lineages within the Cordycipitaceae, containing two new genera occurring on spiders, i.e. *Jenniferia* **gen. nov.** and *Polystromomyces* **gen. nov.** Two new species in *Jenniferia*, *J. griseocinerea* **sp. nov.** and *J. thomisidarum* **sp. nov.**, are described. Two strains, NHJ 03510 and BCC 2191, initially named as *Akanthomyces cinereus* (*Hevansia cinerea*), were shown to be part of *Jenniferia*. By including sequences of putative *Hevansia* species from GenBank, we also revealed *Parahevansia* as a new genus with the ex-type strain NHJ 666.01 of *Pa. koratensis*, accommodating specimens previously named as *Akanthomyces koratensis* (*Hevansia koratensis*). One species

of *Polystromomyces*, *Po. araneae* **sp. nov.**, is described. We established an asexual-sexual morph connection for *Hevansia novoguineensis* (Cordycipitaceae) with ex-type CBS 610.80 and proposed a new species, *H. minuta* **sp. nov.** Based on characteristics of the sexual morph, *Hevansia* and *Polystromomyces* share phenotypic traits by producing stipitate ascoma with fertile terminal heads; however, they differ in the shape and colour of the stipes. Meanwhile, *Jenniferia* produces non-stipitate ascoma with aggregated superficial perithecia forming a cushion. A new morphology of ascospores in *Jenniferia* is described, illustrated and compared with other species in Cordycipitaceae.

Keywords
Cordycipitaceae, *Hevansia*, *Jenniferia*, *Parahevansia*, *Polystromomyces*, spider pathogenic fungi

Introduction

Members of Cordycipitaceae (Hypocreales, Ascomycota) are parasitic on spiders (Araneae) and several orders of insects from larva to adult states (Sung et al. 2007; Shrestha et al. 2016). Several species of this family are recognised for their economic importance, such as *Cordyceps militaris* (L.) Fr., a famous traditional Chinese medicine, edible mushroom and source of bioactive compounds (Wu et al. 2021) and others that are being used or developed as biopesticides against different insect pests (Wang et al. 2019; Sun et al. 2020). Seventeen genera are established in this family from combined molecular phylogenetic and morphological evidence (Zare and Gams 2016; Kepler et al. 2017; Mongkolsamrit et al. 2018, 2020b; Thanakitpipattana et al. 2020; Wang et al. 2020; Zhang et al. 2020). Recently, the genera *Pseudogibellula* Samson & H.C. Evans and *Pleurodesmospora* Samson, W. Gams & H.C. Evans were clarified, based on molecular phylogenetic analyses and confirmed to be members of Cordycipitaceae (Chen et al. 2021b; Mongkolsamrit et al. 2021), suggesting that the taxonomic diversity of this family is still under-explored.

Arthropod pathogenic fungi in Cordycipitaceae have a distinctive fleshy texture and pallid (white to yellow) to brightly coloured stipitate stromata with loosely embedded or superficial perithecia. Species with these features include *Cordyceps militaris* (L.) Fr., *Blackwellomyces pseudomilitaris* (Hywel-Jones & Sivichai) Spatafora & Luangsa-ard, *Flavocillium bifurcatum* H. Yu, Y.B. Wang, Y. Wang, Q. Fan & Zhu L. Yang and *Samsoniella inthanonensis* Mongkols., Noisrip., Thanakitp., Spatafora & Luangsa-ard (Sung et al. 2007; Kepler et al. 2017; Mongkolsamrit et al. 2018; Wang et al. 2020). Nonetheless, some Cordycipitaceae species are characterised by possessing non-stipitate ascomata, such as *Akanthomyces thailandicus* Mongkols., Spatafora & Luangsa-ard and *Gibellula cebrennini* Tasan., Kuephadungphan & Luangsa-ard (Mongkolsamrit et al. 2018; Kuephadungphan et al. 2020), which are parasitic on the spiders, *Hyperdermium pulvinatum* J.F. White, R.F. Sullivan, Bills & Hywel-Jones and *H. caulium* (Berk. & M.A. Curtis) P. Chaverri & K.T. Hodge occurring on scale insects (Sullivan et al. 2000; Chaverri et al. 2008).

Hevansia and *Gibellula* were separated from other genera, based on monophyletic clades in the Cordycipitaceae (Kepler et al. 2017). *Hevansia* was erected with *H. novoguineensis* (synonym: *Akanthomyces novoguineensis* Samson & B.L. Brady) as the type species infecting spiders collected from Papua New Guinea (Samson and Brady 1982). *Hevansia* and *Gibellula* species are specialised parasites on spiders that inhabit the undersides of leaves. However, the asexual morph of *Hevansia* differs from *Gibellula* in the production of phialides in monolayer with mono- or polyphialidic conidiogenous cells, whereas species in *Gibellula* produce the primary synnemata bearing predominantly aspergillus-like conidiophores or occasionally growing penicillate or granulomanus-like conidiophores (Samson and Brady 1982; Samson and Evans 1992; Kuephadungphan et al. 2020, 2022).

At present, most of the species in *Hevansia* have been described, based on asexual morphs that were reported from China, Papua New Guinea, Sri Lanka, Taiwan and Thailand (Samson and Evans 1974; Samson and Brady 1982; Hywel-Jones 1996; Hsieh et al. 1997; Huang et al. 2000). *Hevansia nelumboides*, the only species from Japan, has been accepted and described, based on sexual characters producing short stipes with fertile terminal heads, immersed perithecia and ascospores disarticulating into part-spores (Kobayasi and Shimizu 1977; Kepler et al. 2017). The sexual morph of *Gibellula* is well-known for forming a torrubiella-like state and ascospores that disarticulate into part-spores. Species in *Gibellula* have been reported from several countries including China, Ecuador, Ghana, Taiwan and Thailand (Samson and Evans 1992; Hsieh et al. 1997; Kuephadungphan et al. 2020; Chen et al. 2021a).

From surveys of arthropod pathogenic fungi in Thailand's national parks, collections of pathogens on spiders were found on the underside of leaves from forest plants. Based on the macroscopic features of the sexual morph, some specimens possess non-stipitate ascomata with aggregated superficial perithecia forming a cushion. In contrast, some specimens have stipes with fertile heads at the terminal part arising from the spiders' abdominal region which closely match with *H. nelumboides*. Asexually reproductive species that produce several synnemata on spiders were also included in this study. The goal of these investigations is to elucidate the phylogenetic and taxonomic placement of these collections of parasitic fungi on spiders through multilocus molecular phylogenetic analyses and the observation of diagnostic macro- and micro-morphological characteristics. Additionally, this work has allowed us to refine the diagnostic characters of the species classification of *Hevansia*.

Materials and methods

Specimen collection and isolation

The fungal specimens were collected in forests during the rainy season from 2009 to 2020. The specimens of fungi occurring on spiders found on the underside of living leaves of forest plants were collected carefully to preserve host and fungal structures,

then were put in plastic boxes and carried to the laboratory for isolation. The materials were examined under a stereomicroscope (Olympus SZ61). The protocol for isolation from sexual and asexual morphs followed previous studies (Luangsa-ard et al. 2018; Mongkolsamrit et al. 2018). The cultures were grown on potato dextrose agar (PDA; freshly diced potatoes 200 g, dextrose 20 g, agar 15 g, in 1 litre distilled water) and deposited at the BIOTEC Culture Collection (BCC), Thailand. The specimens were dried in an electric food dryer (50–55 °C) overnight and stored in plastic boxes before storage at the BIOTEC Bangkok Herbarium (BBH), National Biobank of Thailand. The identification of the spider hosts was conducted after cultures of fungal pathogens were acquired. The spider hosts were identified, based on morphological characteristics, such as eyes, cephalic regions and legs (Deeleman-Reinhold 2001).

Morphological observation

Important macroscopic and microscopic features of the fungal specimens were observed using a stereomicroscope (Olympus CX31) and a compound microscope (Olympus SZ61). The fungal materials, including perithecia, asci, ascospores, phialides and conidia, were mounted on microscope slides and stained in lactophenol cotton blue solution for observation. The characteristics of these materials (shape and size) were determined and measured according to Mongkolsamrit et al. (2018, 2020b). Cultures were grown on oatmeal agar (OA, Difco, oatmeal 60 g, agar 12.5 g, in 1 litre distilled water) and PDA agar plates at 25 °C under light/dark condition (L:D = 14:10) for 21 days, depending on the sporulation in culture. The colours of the specimens and colonies grown on OA and PDA were described and codified following the Royal Horticultural Society (RHS 2015).

DNA extraction, amplification and sequencing

Genomic DNA was extracted from the mycelia of 10–14 days old cultures on PDA using a modified cetyltrimethyl ammonium bromide (CTAB) method as previously described in Mongkolsamrit et al. (2009). Nuclear loci were sequenced, including the nuc rDNA region encompassing the internal transcribed spacers (ITS), ITS1 and ITS2, the partial gene regions of the nuc 28S rDNA (Large Subunit Ribosomal DNA: LSU), the translation elongation factor-1α gene (*tef1*), the largest (*rpb1*) and second largest (*rpb2*) subunits of RNA polymerase II. Polymerase chain reaction (PCR) primers used to amplify these markers were ITS5 and ITS4 for ITS (White et al. 1990), LROR and LR5 for LSU (Vilgalys and Hester 1990; Rehner and Samuels 1994), 983F and 2218R for *tef1* (Rehner and Buckley 2005), CRPB1 and RPB1Cr for *rpb1* (Castlebury et al. 2004), RPB2-5F2 and RPB2-7Cr for *rpb2* (Liu et al. 1999; O'Donnell et al. 2007). The thermocycler conditions for PCR amplifications used in this study followed the method described in Sung et al. (2007). The purified PCR products were sequenced with PCR amplification primers for Sanger dideoxy sequencing. The sequences obtained in this study were deposited in GenBank (Table 1).

Table 1. List of taxa included in the phylogenetic analyses and their GenBank accession numbers.

Species	Code	Host/ Substratum	GenBank accession numbers					References
			ITS	LSU	*tef1*	*rpb1*	*rpb2*	
Akanthomyces aculeatus	HUA 772	Lepidoptera; Sphingidae	KC519371	KC519370	KC519366	—	—	Sanjuan et al. (2014)
A. aculeatus	HUA 186145^{T}	—	—	MF416520	MF416465	—	—	Kepler et al. (2017)
A. kanyawimiae	TBRC 7244^{T}	Araneae; spider	MF140752	MF140716	MF140836	—	—	Mongkolsamrit et al. (2018)
A. lecanii	CBS 101247	Homoptera	—	AF339555	DQ522359	DQ522407	—	Sung et al. (2001); Spatafora et al. (2007)
A. sulphureus	TBRC 7248^{T}	Araneae; spider	MF140758	MF140722	MF140843	MF140787	MF140812	Mongkolsamrit et al. (2018)
A. thailandicus	TBRC 7245^{T}	Araneae; spider	MF140754	—	MF140839	—	MF140809	Mongkolsamrit et al. (2018)
A. waltergamsii	TBRC 7252^{T}	Araneae; spider	MF140748	MF140714	MF140834	MF140782	MF140806	Mongkolsamrit et al. (2018)
Ascopolyporus polychrous	P.C. 546	Plant	—	DQ118737	DQ118745	DQ127236	—	Chaverri et al. (2005)
A. villosus	ARSEF 6355	Plant	AY886544	—	DQ118750	DQ127241	—	Bischoff et al. (2005); Chaverri et al. (2005)
Beauveria bassiana	ARSEF 1564^{T}	Lepidoptera	HQ880761	—	HQ880974	HQ880833	HQ880905	Rehner et al. (2011)
B. bassiana	ARSEF 7518	Hymenoptera	HQ880762	—	HQ880975	HQ880834	HQ880906	Rehner et al. (2011)
Blackwellomyces aurantiacus	BCC 85060^{T}	Lepidoptera	MT000692	MT003028	MK411598	MK411600	MT017819	Mongkolsamrit et al. (2020b)
B. aurantiacus	BCC 85061	Lepidoptera	MT000693	MT003029	MK411599	MK411601	MT017820	Mongkolsamrit et al. (2020b)
B. pseudomilitaris	BCC 1919^{T}	Lepidoptera	—	MF416534	MF416478	—	MF416440	Kepler et al. (2017)
B. pseudomilitaris	BCC 2091	Lepidoptera	—	MF416535	MF416479	—	MF416441	Kepler et al. (2017)
Cordyceps araneae	BCC 85066^{T}	Arachnid; Araneae	MT000703	MT003038	MT017851	MT017811	MT017829	Mongkolsamrit et al. (2020b)
C. inthanonensis	BCC 55812^{T}	Lepidoptera	MT000706	MT003041	—	MT017815	MT017832	Mongkolsamrit et al. (2020b)
C. inthanonensis	BCC 56302	Lepidoptera	MT000705	MT003040	MT017853	MT017814	MT017831	Mongkolsamrit et al. (2020b)
C. kuiburiensis	BCC 90322^{T}	Araneidae	MN099707	MK968816	MK988032	MK988030	—	Crous et al. (2019)
C. militaris	OSC 93623	Lepidoptera	JN049825	AY184966	DQ522332	DQ522377	—	Sung and Spatafora (2004); Spatafora et al. (2007); Kepler et al. (2012)
C. militaris	YFCC 6587	Lepidoptera	—	MN576818	MN576988	MN576878	MN576932	Wang et al. (2020)
C. nidus	HUA 186125^{T}	Araneidae	—	KC610752	KC610722	—	KC610711	Chiriví´ et al. (2017)
C. piperis	CBS 116719	Hemiptera	—	AY466442	DQ118749	DQ127240	EU369083	Chaverri et al. (2005); Bischoff et al. (2004); Johnson et al. (2009); Kepler et al. (2017)
Engyodontium aranearum	CBS 309.85	Arachnida	—	AF339526	DQ522341	DQ522387	DQ522439	Sung et al. (2001); Kepler et al. (2017)
Flavocillium bifurcatum	YFCC 6101^{T}	Lepidoptera; Noctuidae	—	MN576781	MN576951	MN576841	MN576897	Wang et al. (2020)
Gamszarea humicola	CGMCC3 19303^{T}	Soil	MK329092	MK328997	MK336027	—	MK335979	Zhang et al. (2020)
G. humicola	LC 12462	Soil	MK329093	MK328998	MK336028	—	MK335980	Zhang et al. (2020)

Species	Code	Host/ Substratum	GenBank accession numbers					References
			ITS	LSU	*tef1*	*rpb1*	*rpb2*	
Gibellula cebrennini	BCC 39705	Arachnida; *Cebrenninus* cf. *magnus*	MH532874	MH394673	MH521895	MH521822	MH521859	Kuephadungphan et al. (2020)
G. cebrennini	BCC 53605[T]	Arachnida; *Cebrenninus* cf. *magnus*	MT477069	MT477062	MT503328	MT503321	MT503336	Kuephadungphan et al. (2020)
G. clavulifera var. *alba*	ARSEF 1915	Arachnida	JN049837	DQ518777	DQ522360	—	DQ522467	Chaverri et al. (2005); Spatafora et al. (2007); Crous et al. (2019)
G. gamsii	BCC 25798	Arachnida; Araneida	MH152532	MH152542	EU369018	EU369056	EU369076	Kuephadungphan et al. (2019)
G. gamsii	BCC 27968[T]	Arachnida; Araneida	MH152529	MH152539	MH152560	MH152547	—	Kuephadungphan et al. (2019)
G. scorpioides	BCC 43298	Arachnida, *Portia* sp.	MT477074	MH394677	MH521900	MH521816	MH521858	Kuephadungphan et al. (2020)
G. scorpioides	BCC 47976[T]	Arachnida, *Portia* sp.	MT477078	MT477066	MT503335	MT503325	MT503339	Kuephadungphan et al. (2020)
Hevansia arachnophila	NHJ 2633	Arachnida	MH532900	GQ249978	MH521917	MH521843	MH521884	Ridkaew et al. Unpublished data (2009); Kuephadungphan Unpublished data (2018)
H. arachnophila	NHJ 2465	Arachnida	MH532899	—	MH521916	**ON470205**	**ON470207**	Kuephadungphan Unpublished data (2018); this study
H. minuta	BCC 47519[T]	Araneae, *Meotipa* sp.	**MZ684087**	**MZ684002**	**MZ707811**	**MZ707826**	**MZ707833**	**This study**
H. minuta	BCC 47520	Araneae, *Meotipa* sp.	**MZ684088**	**MZ684003**	**MZ707812**	**MZ707827**	**MZ707834**	**This study**
H. nelumboides	TNS 16306	Araneidae	—	—	MF416475	—	MF416438	Kepler et al. (2017)
H. novoguineensis	BCC 2190	Arachnida	—	MF416531	MF416474	—	—	Kepler et al. (2017)
H. novoguineensis	BCC 42675	Araneae	**MZ684089**	**MZ684004**	**MZ707814**	—	**MZ707835**	**This study**
H. novoguineensis	BCC 49323	Araneae	**MZ684090**	**MZ684005**	**MZ707813**	—	**MZ707836**	**This study**
H. novoguineensis	CBS 610.80[T]	Arachnida	MH532831	MH394646	MH521885	—	MH521844	Mongkolsamrit et al. (2020b)
H. cf. *novoguineensis*	BCC 2093	Arachnida	—	MF416530	MF416473	—	MF416437	Kepler et al. (2017)
H. cf. *novoguineensis*	NHJ 4314	Arachnida	—	—	EU369012	EU369051	EU369071	Johnson et al. (2009)
H. cf. *websteri*	BCC 23860	Arachnida	GQ250009	GQ249979	GQ250030	—	—	Kuephadungphan et al. (2019)
H. cf. *websteri*	BCC 36541	Arachnida	MH532868	MH394669	MH521889	MH521811	MH521849	Kuephadungphan Unpublished data (2018)
Hyperdermium pulvinatum	P.C. 602	Hemiptera	—	DQ118738	DQ118746	DQ127237	—	Chaverri et al. (2005)
Jenniferia cinerea	BCC 2191	Arachnida, *Amyciaea* sp.	GQ250000	GQ249971	GQ250029	—	—	Kuephadungphan et al. (2019)
J. cinerea	NHJ 03510[T]	Araneae, *Amyciaea* sp.	GQ249999	GQ249970	EU369009	EU369048	EU369070	Johnson et al. (2009); Ridkaew et al. Unpublished data (2009)
J. griseocinerea	BCC 42062[T]	Araneae, *Diaea* sp.	**MZ684091**	**MZ684006**	**MZ707815**	**MZ707828**	**MZ707837**	**This study**
J. griseocinerea	BCC 42063	Araneae, *Diaea* sp.	**MZ684092**	**MZ684007**	**MZ707816**	**MZ707829**	**MZ707838**	**This study**
J. griseocinerea	BCC 54893	Araneae, *Diaea* cf. *dorsata*	**MZ684093**	**MZ684008**	**MZ707817**	—	**MZ707839**	**This study**

Species	Code	Host/ Substratum	GenBank accession numbers					References
			ITS	LSU	*tef1*	*rpb1*	*rpb2*	
J. griseocinerea	BCC 57821	Araneae, *Diaea* cf. *dorsata*	**MZ684094**	**MZ684009**	**MZ707818**	—	**MZ707840**	**This study**
J. thomisidarum	BCC 48932	Araneae, *Diaea* cf. *dorsata*	**MZ684095**	**MZ684012**	**MZ707819**	—	**MZ707841**	**This study**
J. thomisidarum	BCC 49257	Araneae, *Diaea* cf. *dorsata*	**MZ684096**	**MZ684013**	**MZ707820**	—	—	**This study**
J. thomisidarum	BCC 54482	Araneae, *Diaea* cf. *dorsata*	**MZ684097**	**MZ684014**	**MZ707821**	—	—	**This study**
J. thomisidarum	BCC 66224	Araneae, *Diaea* cf. *dorsata*	**MZ684098**	**MZ684015**	**MZ707822**	—	**MZ707842**	**This study**
J. thomisidarum	BCC 37881[T]	Araneae, *Diaea* cf. *dorsata*	**MZ684099**	**MZ684010**	**MZ707823**	**MZ707830**	**MZ707843**	**This study**
J. thomisidarum	BCC 37882	Araneae, *Diaea* cf. *dorsata*	**MZ684100**	**MZ684011**	**MZ707824**	**MZ707831**	**MZ707844**	**This study**
Lecanicillium antillanum	CBS 350.85[T]	Agaric	—	AF339536	DQ522350	DQ522396	DQ522450	Sung et al. (2001); Chaverri et al. (2005); Spatafora et al. (2007)
L. aranearum	CBS 726.73a	Arachnid, Araneae	—	AF339537	EF468781	EF468887	EF468934	Sung et al. (2001); Sung et al. (2007)
Liangia sinensis	YFCC 3103[T]	*Beauveria yunnanensis*	—	MN576782	MN576952	MN576842	MN576898	Wang et al. (2020)
L. sinensis	YFCC 3104	*Beauveria yunnanensis*	—	MN576783	MN576953	MN576843	MN576899	Wang et al. (2020)
Neotorrubiella chinghridicola	BCC 39684	Orthopterida	—	MK632096	MK632072	MK632148	MK632071	Thanakitpipattana et al. (2020)
N. chinghridicola	BCC 80733[T]	Orthopterida	—	MK632097	—	MK632176	MK632149	Thanakitpipattana et al. (2020)
Parahevansia koratensis	NHJ 666.01	Arachnida	GQ250010	GQ249981	GQ250031	—	—	Ridkaew et al. Unpublished data (2009)
Pa. koratensis	NHJ 2662	Lepidoptera	GQ250008	GQ249982	GQ250032	**ON470206**	**ON470208**	Ridkaew et al. Unpublished data (2009); this study
Pleurodesmospora lepidopterorum	DY 10501[T]	Lepidoptera	MW826576	—	MW834317	MW834315	MW834316	Chen et al. (2021b)
P. lepidopterorum	DY 10502	Lepidoptera	MW826577	—	MW834319	—	MW834318	Chen et al. (2021b)
Polystromomyces araneae	BCC 93301[T]	Arachnida	**MZ684101**	**MZ684016**	**MZ707825**	**MZ707832**	**MZ707845**	This study
Pseudogibellula formicarum	BCC 84257	*Ophiocordyceps flavida*	MT508782	MT512653	MT533480	MT533473	—	Mongkolsamrit et al. (2021)
P. formicarum	CBS 433.73	*Pahothyreus tarsatus*	MH860731	MH872442	MT533481	MT533475	—	Vu et al. (2019); Mongkolsamrit et al. (2021);
Samsoniella aurantia	TBRC 7271[T]	Lepidoptera	MF140764	MF140728	MF140846	MF140791	MF140818	Mongkolsamrit et al. (2018)
S. aurantia	TBRC 7272	Lepidoptera	MF140763	MF140727	MF140845	—	MF140817	Mongkolsamrit et al. (2018)
Simplicillium lanosoniveum	CBS 704.86	*Hemileia vastatrix*	—	AF339553	DQ522358	DQ522406	DQ522464	Sung et al. (2001); Spatafora et al. (2007)
S. lanosoniveum	CBS 101267	*Hemileia vastatrix*	—	AF339554	DQ522357	DQ522405	DQ522463	Sung et al. (2001); Spatafora et al. (2007)

The accession numbers marked in bold font refer to sequences new in this study or have been generated by our group in Thailand. [T]ex-type species.

Sequence alignment and phylogenetic analyses

The DNA sequences generated in this study were examined for ambiguous bases and corrected using BioEdit v. 7.2.5 (Hall 1999), then submitted to GenBank. Sequences of ITS, LSU, *tef1*, *rpb1* and *rpb2*, of closely-related taxa for the analyses were taken from previous studies as shown in Table 1. The phylogenetic analyses for combined and single-locus alignments were performed using RAxML-HPC2 on XSEDE v. 8.2.12 (Stamatakis 2014) in CIPRES Science Gateway portal, with GTRGAMMA+I model and 1000 bootstrap iterations. Bayesian Inference (BI) of the phylogenetic relationship was performed in MrBayes v. 3.2.7a (Ronquist et al. 2012), with best-fit models selected using MrModeltest v. 2.2 (Nylander 2004). The best model was GTR + G + I. Markov Chain Monte Carlo (MCMC) simulations were run for 2,000,000 generations, sampling every 1000 and discarding the first 10% as burn-in. The remaining 20,001 trees were used to calculate the posterior probability values. RAxML and BI output were imported into TreeView v. 1.6.6 to visualise the phylogenetic tree (Page 1996).

Results

Molecular phylogeny

We generated 65 new sequences (15 ITS, 15 LSU, 15 *tef1*, 7 *rpb1* and 13 *rpb2*) from living cultures (Table 1). *Gamszarea humicola* Z.F. Zhang & L. Cai (3.19303 and LC 12462) was used as an outgroup. The combined dataset from 77 specimens, with multi-locus sequences totalling an alignment length of 4231 characters with gaps (ITS 656, LSU 841, *tef1* 921, *rpb1* 764 and *rpb2* 1049) was analysed. The maximum-likelihood phylogenetic analyses resulted in a multi-locus tree with maximum likelihood bootstrap values (MLB) shown in Fig. 1 and in single-locus trees (Suppl. material 1: Figs S1–S5). The nodes were also evaluated with Bayesian posterior probabilities (BPP). Bold lines in the tree represent 100% of MLB and 1.00 of BPP.

The phylogenetic analyses supported *Hevansia* as a monophyletic clade with maximum support (MLB = 86 / BPP = 1.00), including ex-type *H. novoguineensis* (CBS 610.80) from Papua New Guinea as the type species. The strain BCC 42675, isolated from a sexual morph from Thailand, clustered with *H. novoguineensis* (CBS 610.80) with high support (MLB = 93 / BPP = 1.00), revealing a sexual morph connection to this species. Two strains from Thailand (BCC 2093, NHJ 4314) formed a sister clade to the clade containing the ex-type strain of *H. novoguineensis* with maximum support for the separating node (MLB = 98 / BPP = 1.00). This separation was observed with the phylogenetic signal from only LSU, *tef1*, while the other markers either did not have sufficient sample coverage for comparison (ITS, *rpb1*: Suppl. material 1: Figs S1 and S4) or did not recover this separation (*rpb2*: Suppl. material 1: Fig. S5). These two specimens were thus named as *H.* cf. *novoguineensis* herein. Two unknown *Hevansia*

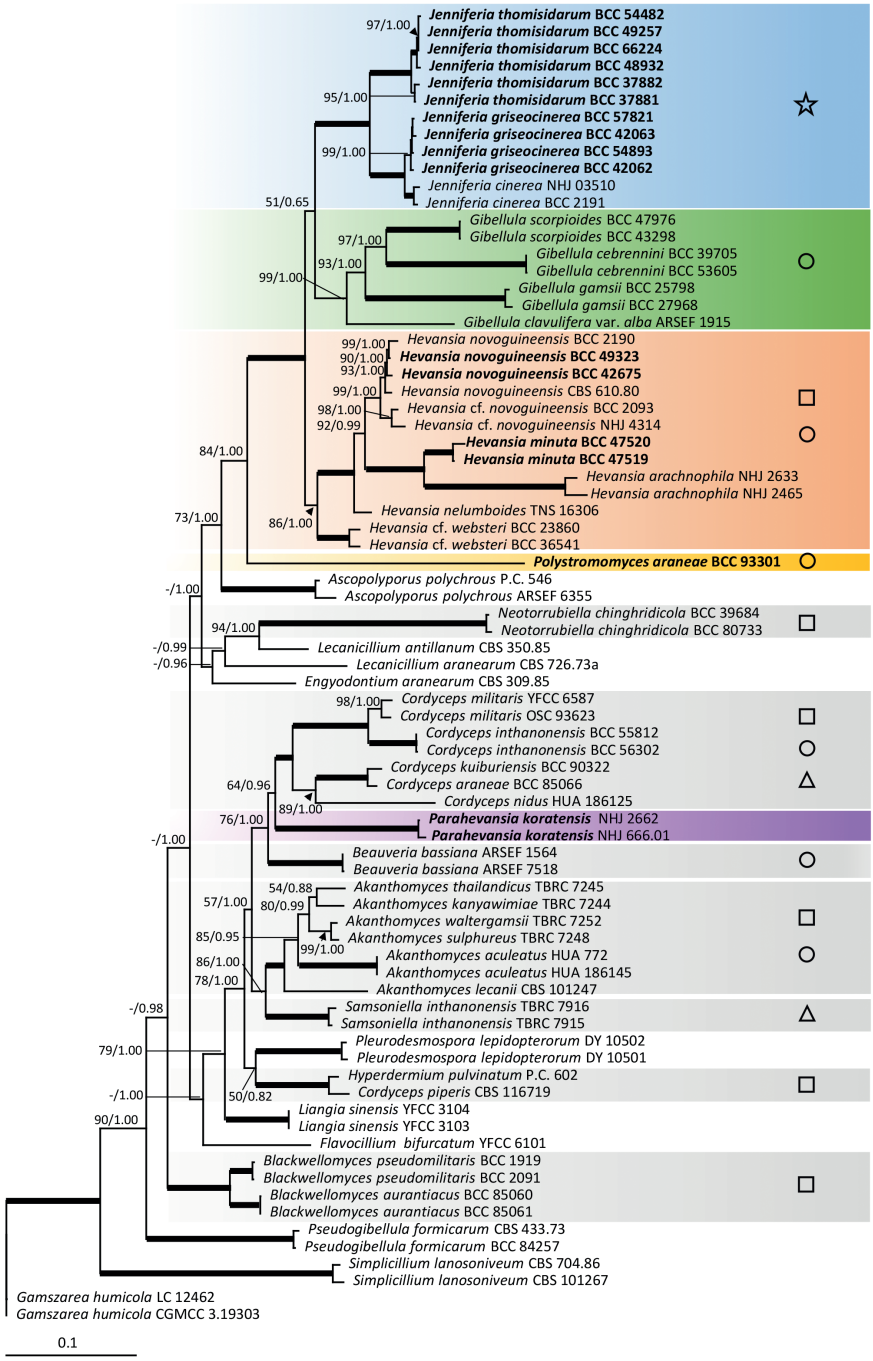

Figure 1. RAxML tree of *Hevansia*, *Jenniferia*, *Parahevasia*, *Polystromomyces* and related genera in the Cordycipitaceae from a combined ITS, LSU, *tef1*, *rpb1* and *rpb2* dataset. Numbers at the major nodes represent Maximum Likelihood Bootstrap (MLB) and Bayesian Posterior Probabilities (BPP). Bold lines in the tree represent 100% of MLB and 1.00 of BPP. Symbols on the right-hand side correspond to the types of ascospore morphologies found in each genus that are observed in natural specimens of Cordycipitaceae described in Fig. 2.

strains from both an asexual state (BCC 47520) and a sexual state (BCC 47519) were found as a well-supported clade (MLB = 100 / BPP = 1.00) within *Hevansia*, but separated from *H. novoguineensis*, which was also recovered by all single-locus phylogenies. These two *Hevansia* strains were thus proposed as a new species, *Hevansia minuta*. Furthermore, two strains of *H. arachnophila* (NHJ 2465, NHJ 2633) and two strains of *H.* cf. *websteri* (BCC 23860, BCC 36541) were included in our phylogenetic analyses and shown to belong to *Hevansia*. Additionally, a strain formerly named as *Hevansia koratensis* (NHJ 666.01 (BCC 1485)) and a strain previously recognised as *H. websteri* (NHJ 2662 (BCC 2113)) formed together an independent clade with strong support (MLB = 100/ BPP = 1.00), out of the *Hevansia* clade and in the proximity of *Cordyceps* species. Hence, this clade does not belong to *Hevansia* and is proposed as a new genus named *Parahevansia* (Fig. 1).

The combined-genes phylogenetic tree revealed one important terminal monophyletic clade close to *Gibellula* with total support (MLB = 100 / BPP = 1.00), Fig. 1. This clade is proposed as a new genus named *Jenniferia*. The genus *Jenniferia* formed a monophyletic clade separated from *Hevansia* and *Gibellula* for all the markers used in this study (Suppl. material 1: Figs S1–S5). *Jenniferia* contains two novel species, *Jenniferia griseocinerea* and *J. thomisidarum* and includes *J. cinerea*, which is proposed as a new combination of *H. cinerea* to this genus. *Jenniferia griseocinerea* is distinguished from *J. cinerea*, based on the separated monophyletic clades in the multi-locus phylogeny (Fig. 1). The separation between the two species was recovered in most of the single-locus phylogenies (*tef1*, *rpb1* and *rpb2*, but not ITS nor LSU: Suppl. material 1: Figs S1–S5).

The combined-genes analysis also revealed a deep taxon from a unique specimen (BCC 93301), branched as sister to the three genera occurring on spider egg sac (*Gibellula*, *Hevansia* and *Jenniferia*), which was thus proposed as a new genus *Polystromomyces*. The branching of this specimen had high support (MLB = 84 / BPP = 1.00) and was found consistently amongst different markers (Suppl. material 1: Figs S1–S5). This taxon was never within the three main genera occurring on spiders (*Gibellula*, *Hevansia* and *Jenniferia*), supporting the status of a different genus. *Polystromomyces* contains a new species, *Po. araneae*.

Overview of types of ascospores in Cordycipitaceae

Different types of ascospore morphologies were observed in natural specimens of Cordycipitaceae as shown in Fig. 2. Three types observed previously include: (a) filiform, multiseptate, whole ascospores, (b) filamentous, multiseptate ascospores disarticulating into part-spores and (c) bola-shaped, whole ascospores, non-disarticulating, characterised by a thread-like structure connected to fusiform, terminal, multi-septate parts at both ends, resembling a skipping rope. We observed a new type of ascospore morphology in *Jenniferia* as shown in Fig. 2(d), in which septate part-spores are alternately connected with thread-like structures along the whole ascospore. The ascospore morphologies shown in Fig. 2a, b and d were observed on spider-pathogenic fungi in this study.

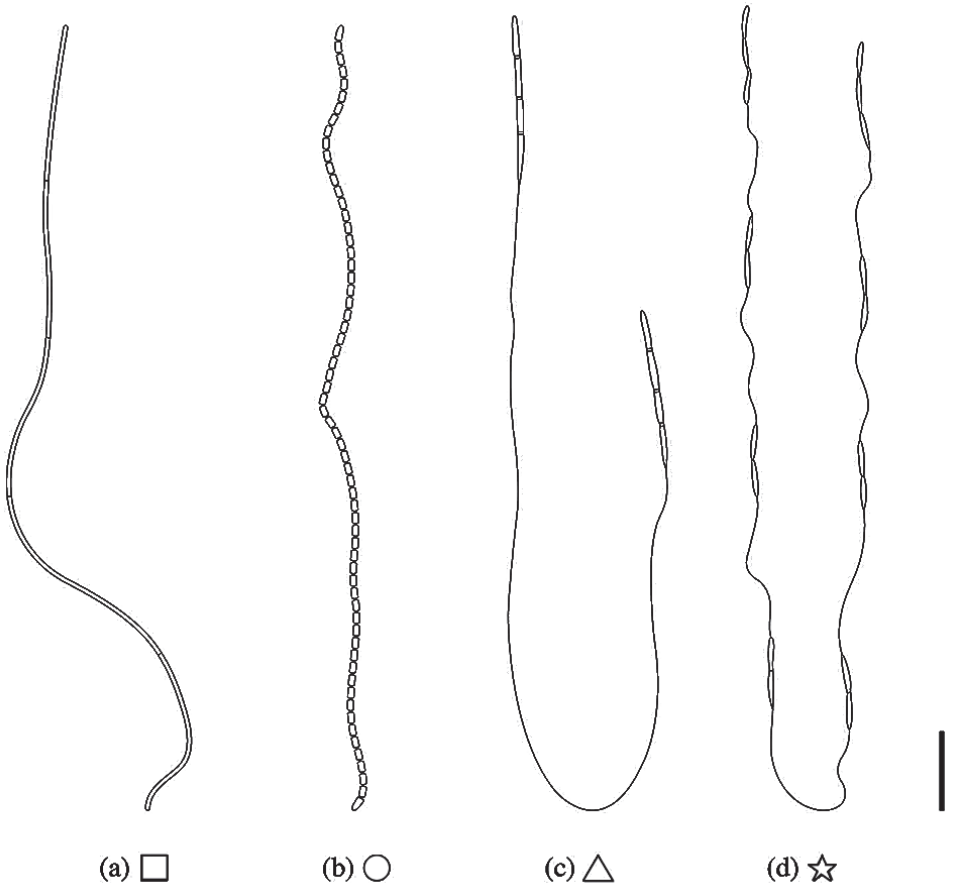

Figure 2. The types of ascospores morphologies observed in natural specimens of Cordycipitaceae: **a** filiform, multiseptate, whole ascospores (square) **b** filamentous, multiseptate ascospores disarticulating into part-spores (circle) **c** bola-shaped, whole ascospores (triangle) and **d** whole ascospores with septate part-spores alternately connected with thread-like structures (star). Scale bars: 10 μm (**a, b**); 20 μm (**c, d**).

Taxonomy

Hevansia **Luangsa-ard, Hywel-Jones & Spatafora, in Kepler, Luangsa-ard, Hywel-Jones, Quandt, Sung, Rehner, Aime, Henkel, Sanjuan, Zare, Chen, Li, Rossman, Spatafora, Shrestha, IMA Fungus 8: 348 (2017). Emend. S. Mongkolsamrit, W. Noisripoom & K. Tasanathai**

≡ *Akanthomyces novoguineensis* Samson & B.L. Brady, Trans. Br. mycol. Soc. 79: 571 (1982).

Type species. *Hevansia novoguineensis* (Samson & B.L. Brady) Luangsa-ard, Hywel-Jones & Spatafora, IMA Fungus 8: 349 (2017).

Emended generic description (modified from Kepler et al. 2017). *Circumscription*: The sexual morph characteristics in genus are emended, based on three species *H. minuta*, *H. nelumboides* and *H. novoguineensis* producing sexual morph as members of *Hevansia* lineage in Fig. 1. Sexual morph: *Stromata* arising from dorsal abdomen, stipe 1–10 mm, fertile part at the terminal of stipe, ca. 1–3 × 1–2 mm, white to cream. *Perithecia* immersed, narrowly ovoid. *Asci* cylindrical with thickened caps, 8-spored, ascospores hyaline, filiform, whole or disarticulating into part-spores. Asexual morph: *Synnemata* erect, simple or branched, solitary to numerous, cylindrical to clavate, mycelium covering host, white, cream to ash-grey or brownish-white. *Phialides* in a monolayer, sparsely scattered or crowded, on mycelium or on a basal cell, smooth-walled, cylindrical, globose, obovoid, with distinct necks. *Conidia* one-celled, smooth-walled, hyaline, occasionally in a short chain, clavate, cylindrical, fusiform to narrowly obclavate. Colony on PDA white, reverse cream, orange to pale red. Some species produce pale red pigment diffusing in the medium.

Notes. Two specimens of *H. arachnophila* (NHJ 2465, NHJ 2633) were described by Hywel-Jones (1996). While the type strain of *H. websteri* (NHJ 2661) and living cultures are unavailable, available sequences of *H. arachnophila* and two strains of *H. websteri* (BCC 23860, BCC 36541) were retrieved from the GenBank nucleotide database and used in this study. The phylogenetic tree revealed that *H. arachnophila* and *H. websteri* (BCC 23860, BCC 36541) belong to the genus *Hevansia* (Fig. 1). The two strains of *H. websteri* (BCC 23860, BCC 36541) were not designated as type, nor as neotype. These strains (BCC 23860, BCC 36541) were thus named as *Hevansia* cf. *websteri*. *Hevansia longispora* and *H. ovalongata* were not included in the phylogenetic study because multi-locus sequence data are unavailable. To better resolve the genus *Hevansia*, *H. longispora*, *H. ovalongata* and *H. websteri* should be recollected from the locality and designated as neotypes and studied for their phylogenetic affinity to other *Hevansia* species in the future. However, *H. longispora*, *H. ovalongata* and *H. websteri* were accepted in *Hevansia* following complete and well-illustrated descriptions by Hywel-Jones (1996), Hsieh et al. (1997) and Huang et al. (2000).

Hevansia novoguineensis (Samson & B.L. Brady) Luangsa-ard, Hywel-Jones & Spatafora

Fig. 3

Remark. The description below is based on natural specimens collected in Thailand.

Description. Spider hosts covered by light yellow to pale yellow (158A–B) mycelium. Sexual morph: *Stromata* stipitate, solitary or multiple. *Stipes* cylindrical, arising from the dorsal region of the host, white to pale yellow, 3–5 mm long, 0.5–1 mm broad. *Fertile heads* produce at the terminal of stipes, disc-shaped, upper surface slightly convex, 1–3 × 1–2 mm. *Perithecia* completely immersed, narrowly ovoid, 500–750 × 200–300 µm, ostioles strong orange yellow (163B). *Asci* cylindrical, 8-spored, 350–450 µm

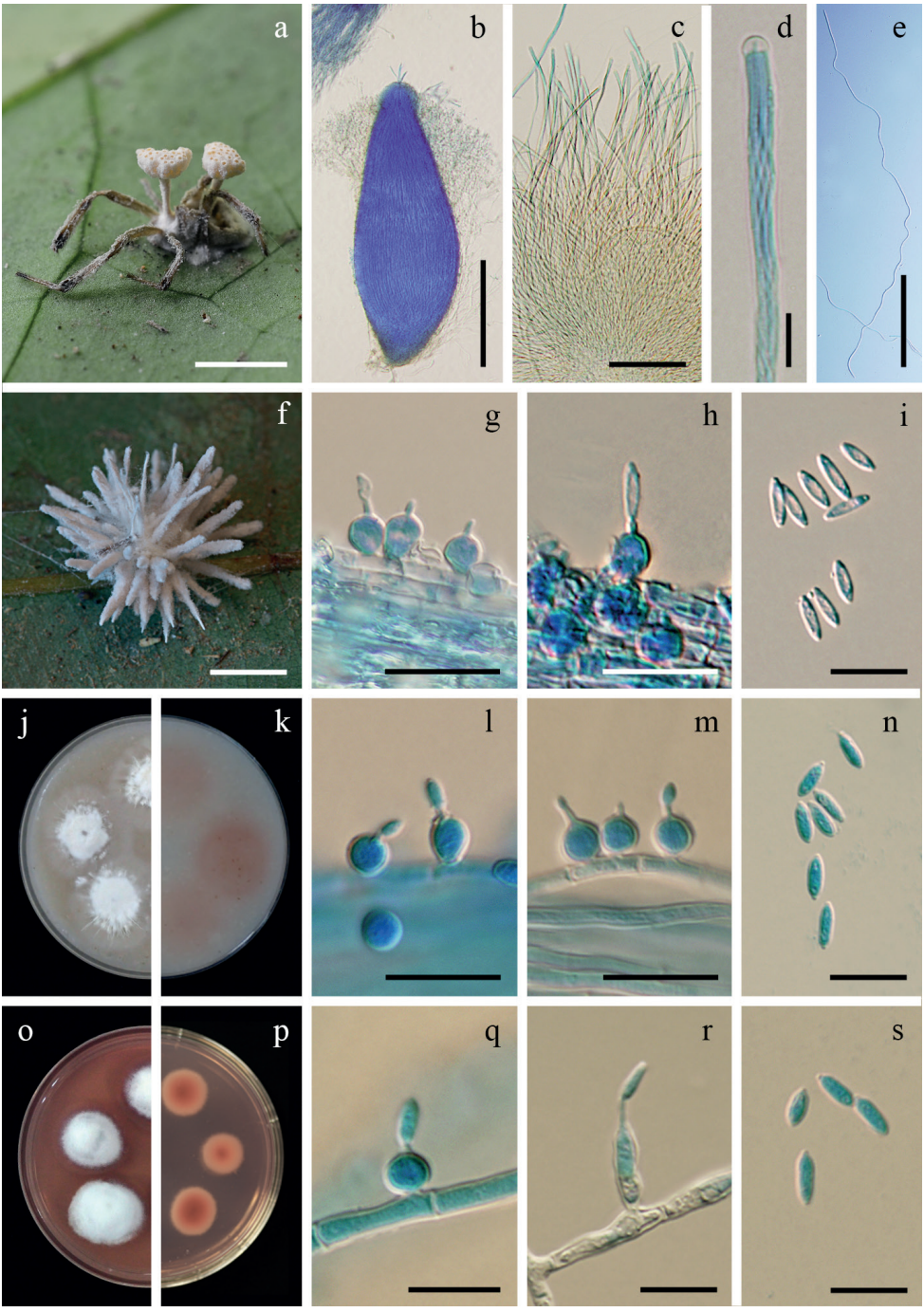

Figure 3. *Hevansia novoguineensis* **a** fungus on a spider (BBH 32171) **b** perithecium **c** asci **d** ascus tip **e** filiform, whole ascospore **f** fungus on a spider (BBH 31299) **g–i** phialides with conidia on synnema **j, k** colonies on OA at 21 days (**j** obverse, **k** reverse) **l–n** phialides with conidia on OA **o, p** colonies on PDA at 21 days with purplish-red pigment diffusing in agar medium (**o** obverse, **p** reverse) **q–s** phialides with conidia on PDA. Scale bars: 5 mm (**a, f**); 200 µm (**b**); 100 µm (**c, e**); 10 µm (**d, g–i, l–n, q, r, s**).

long, 5–7 µm broad, with cap 3–5 µm thick. *Ascospores* hyaline, filiform, whole ascospores, 400–460 × 1–1.5 µm. Asexual morph: *Synnemata* multiple, cylindrical, occasionally acuminate apex, white, up to 8 mm long, 50–200 µm broad. *Conidiogenous cells* phialidic, scattered along with the synnemata. *Phialides* solitary, globose to subglobose, arising from the mycelium, (4)5–5.5(6) × (4)5–5.5(6) µm, with distinct necks, 0.5–1.5 × 0.5–1 µm. *Conidia* hyaline, fusoid or fusiform-elliptical, (2)6–8(10) × 1–2(2.5) µm.

Culture characteristics. Colonies on OA attaining a diam. of 18–20 mm in 21 days, cottony with high mycelium density in the middle of colonies, mycelium with low density around the margin of colonies, flattened, white, reverse deep pink (180D). Sparse synnemata with conidiogenous cells producing conidia observed after 30 days, white, on the edge of a colonies. *Phialides* solitary, globose to subglobose, (4)5.5–6.5(7) × 3.5–5(5.5) µm, distinct necks, 1–3 × 0.5–1 µm. *Conidia* hyaline, fusoid, fusiform-elliptical, (2)6–10(13) × 1–3 µm.

Colonies on PDA attaining a diam. of 7–9(10) mm in 21 days, cottony with high mycelium density, white, moderate purplish-red to dark purplish-pink (186B–C) pigment diffusing in the medium, reverse moderate red (180 A–B). Sporulation observed after 30 days with absence of synnemata. *Phialides* arising from aerial hyphae, solitary, mostly globose to subglobose, occasionally cylindrical, (4)5.5–11.5(15) × 2–3.5(5) µm, distinct necks, 0.5–2 × 0.5–1 µm. *Conidia* hyaline, fusoid, fusiform-elliptical, cylindrical, (2)6–9.5(11) × 1–3 µm.

Host. Spiders (Araneae, Theridiidae).

Habitat. Specimens were found on the underside of dicot leaves of forest plants.

Materials examined. Thailand, Nakhon Ratchasima Province, Khao Yai National Park, 14°26'20.72"N, 101°22'20.02"E, on spider (Web builder, Araneae) attached to the underside of a dicot leaf of forest plants, 10 June 2010, K. Tasanathai, P. Srikitikulchai, S. Mongkolsamrit, R. Ridkaew, MY6026.01 (BBH 32171, BCC 42675) isolated from ascospores; idem, 6 April 2010, K. Tasanathai, S. Mongkolsamrit, T. Chohmee, A. Khonsanit, R. Ridkaew, MY6988.01 (BBH 31299, BCC 49323) isolated from conidia; Kamphaeng Phet, Khlong Lan National Park, 16°7'46.84"N, 99°16'53.11"E, on spider (Web builder, Araneae, Theridiidae) attached to the underside of a dicot leaf of forest plants, 6 November 2007, K. Tasanathai, S. Mongkolsamrit, P. Srikitikulchai, B. Thongnuch, R. Ridkaew, A. Khonsanit, W. Chaygate, MY2770 (BBH 22744, BCC 28581), MY2771 (BBH 22745, BCC 28582), MY2775 (BBH 22747, BBC 28585).

Notes. *Hevansia novoguineensis* is morphologically similar to *H. nelumboides*, both species producing fertile heads at the terminal end of stipes. The perithecia are completely immersed. However, *H. novoguineensis* differs from *H. nelumboides* in producing whole ascospores. *Hevansia nelumboides* produces multiseptated ascospores disarticulating into part-spores (Kobayasi and Shimizu 1977; Shimizu 1994). Based on natural specimens, the conidia from Thai specimens are shorter than those reported for specimens from Papua New Guinea (2–10 × 1–2.5 µm vs. 10.5–17.5 × 1.5–3 µm) (Samson and Brady 1982). In addition, there are other species producing the fertile heads at the terminal end of stipes infecting ants (Hymenoptera), for example,

Ophiocordyceps binata (H.C. Evans & Samson) J.P.M. Araújo, H.C. Evans & D.P. Hughes, *O. pseudolloydii* (H.C. Evans & Samson) G.H. Sung, J.M. Sung, Hywel-Jones & Spatafora and *O. lloydii* (H.S. Fawc.) G.H. Sung, J.M. Sung, Hywel-Jones & Spatafora (Araújo et al. 2020). *Ophiocordyceps binata* is most similar to *H. novoguineensis* by producing disc-shaped fertile heads, while fertile heads in *O. pseudolloydii* and *O. lloydii* are subglobose.

Currently accepted species of *Hevansia*

***Hevansia arachnophila* (Petch) Luangsa-ard, Hywel-Jones & Spatafora, IMA Fungus 8: 348 (2017).**

≡ *Trichosterigma arachnophilum* Petch [as 'arachnophila'], Trans. Br. mycol. Soc. 8: 215 (1923).
≡ *Hirsutella arachnophila* (Petch) Petch, Trans. Br. mycol. Soc. 9: 93 (1923).
≡ *Akanthomyces arachnophilus* (Petch) Samson & H.C. Evans, Acta bot. neerl. 23: 33 (1974).

***Hevansia longispora* (B. Huang, S.B. Wang, M.Z. Fan & Z.Z. Li) Luangsa-ard, Hywel-Jones & Spatafora, IMA Fungus 8: 349 (2017).**

≡ *Akanthomyces longisporus* B. Huang, S.B. Wang, M.Z. Fan & Z.Z. Li, Mycosystema 19: 172 (2000).

***Hevansia nelumboides* (Kobayasi & Shimizu) Luangsa-ard, Hywel-Jones & Spatafora, IMA Fungus 8: 349 (2017).**

≡ *Cordyceps nelumboides* Kobayasi & Shimizu, Kew Bull. 31: 557 (1977).

***Hevansia ovalongata* (L.S. Hsieh, Tzean & W.J. Wu) Luangsa-ard, Hywel-Jones & Spatafora, IMA Fungus 8: 349 (2017).**

≡ *Akanthomyces ovalongatus* L.S. Hsieh, Tzean & W.J. Wu, Mycologia 89: 321 (1997).

***Hevansia websteri* (Hywel-Jones) Luangsa-ard, Hywel-Jones & Spatafora, IMA Fungus 8: 349 (2017).**

≡ *Akanthomyces websteri* Hywel-Jones, Mycol. Res. 100: 1068 (1996).

Hevansia minuta **Tasanathai, Noisripoom & Mongkolsamrit, sp. nov.**
MycoBank No: 843088
Fig. 4

Typification. Thailand, Chumphon Province, Heo Lom Waterfall, 9°43'45.04"N, 98°40'52.71"E, on spider (Web builder, Araneae, Theridiidae, *Meotipa* sp.) attached to the underside of a dicot leaf of forest plants, 30 May 2011, K. Tasanathai, P. Srikitikulchai, A. Khonsanit, K. Sansatchanon, D. Thanakitpipattana, MY6537.01 (BBH 30490, holotype), ex-type culture BCC 47519 isolated from ascospores.

Etymology. Refers to the small stroma of this species.

Description. Spider host covered by white mycelium. Sexual morph: *Stromata* stipitate, arising from the dorsal region of the host, solitary, cylindrical to enlarging apically, white to cream, 10 mm long, 1 mm broad. *Fertile head* oval, ca. 2–2.5 mm long, ca. 1.5 mm broad. *Perithecia* completely immersed, narrowly ovoid, 400–500 × 100–170 µm. *Asci* cylindrical, 8-spored, 325–450 × 3–5 µm, with cap 2–5 µm thick. *Ascospores* hyaline, filiform, whole ascospores, 320–450 × 0.5–1.5 µm. Asexual morph: *Conidiogenous cells* phialidic scattered along with the stipe. *Phialides* solitary, globose to ovoid, arising from the mycelium, 5–7 × 5–6 µm, distinct necks, 1–2 × 0.5–1 µm. *Conidia* hyaline, fusiform, 2–7 × 2–3 µm.

Culture characteristics. Colonies on OA attaining a diam. of 15–18(20) mm in 21 days, cottony with high mycelium density, white. *Conidia* and reproductive structures not observed.

Colonies on PDA attaining a diam. of 8–9(10) mm in 21 days, cottony with high mycelium density, white, reverse pale yellow (161C–D). *Conidia* and reproductive structures not observed.

Host. Spiders (Araneae, Theridiidae, *Meotipa* sp.).

Habitat. Specimens were found on the underside of dicot leaves of forest plants.

Additional materials examined. Thailand, Chumphon Province, Heo Lom Waterfall, 9°43'45.04"N, 98°40'52.71"E, on spider (Web builder, Araneae, Theridiidae, *Meotipa* sp.) attached to the underside of a dicot leaf of forest plants, 30 May 2011, K. Tasanathai, P. Srikitikulchai, A. Khonsanit, K. Sansatchanon, D. Thanakitpipattana, MY06537.02 (BBH 30490, paratype), ex-paratype culture BCC 47520 isolated from conidia.

Notes. *Hevansia minuta* differs significantly from *H. novoguineensis* and *H. nelumboides* in the shape of the fertile heads, which is oval in *H. minuta* and disc-shaped, slightly convex on the upper surface in *H. novoguineensis* and *H. nelumboides*. Additionally, *H. minuta* differs from *H. novoguineensis* in the size of the perithecia. In *H. minuta*, perithecia are smaller than those reported for *H. novoguineensis* (400–500 × 100–170 µm vs. 500–750 × 200–300 µm) (Table 2). Synnema in *H. minuta* was not observed in the natural specimen, while the other species in *Hevansia* produce synnemata (Table 3). *Hevansia minuta* does not produce pigment in culture. Meanwhile, *H. novoguineensis* produces a purplish-red pigment diffusing in PDA plates.

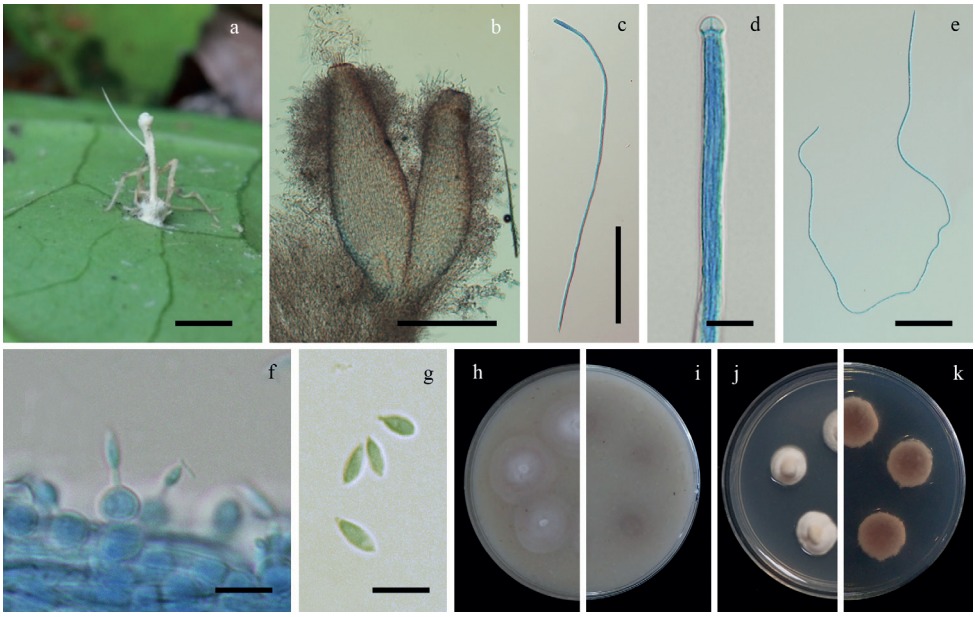

Figure 4. *Hevansia minuta* **a** fungus on a spider (BBH 30490) **b** perithecia **c** ascus **d** ascus tip **e** filiform, whole ascospore **f, g** phialides with conidia **h, i** colonies on OA at 21 days (**h** obverse, **i** reverse) **j, k** colonies on PDA at 21 days (**j** obverse, **k** reverse). Scale bars: 5 mm (**a**), 100 µm (**b**), 50 µm (**c**), 10 µm (**d, f, g**), 20 µm (**e**).

Key to the species of *Hevansia*

Based on sexual state characters

1 Ascospores filamentous, disarticulating into part-spores, immersed perithecia, solitary or multiple stipes.....***H. nelumboides***
– Ascospores filiform, whole ascospores, immersed perithecia, solitary or multiple stipes.....**2**
2 Ascospores 320–450 × 0.5–1.5 µm, solitary stipe.....***H. minuta***
– Ascospores 400–460 × 1–1.5 µm, solitary or multiple stipes.....
.....***H. novoguineensis***

Based on asexual state characters

1 Phialides mostly arising from the mycelium, globose to subglobose **2**
– Phialide arising on basal cells, obovoid, ellipsoid, cylindrical.....**3**
2 Conidia cymbiform, 3.5–6 × 1–1.5 µm ..... ***H. arachnophila***
– Conidia fusiform, 2–7 × 2–3 µm .....***H. minuta***
– Conidia cylindrical, fusoid, fusiform-elliptical, (from Thailand, 2–10 × 1–2.5 µm); occasionally curved, (Papua New Guinea, 10.5–17.5 × 1.5–3 µm.....***H. novoguineensis***

– Conidia oblong, obovate or broadly ellipsoidal 6–10.3 × 2.4–4.4 µm ..... ***H. ovalongata***
3 Conidia cylindrical to fusiform 8.8–14.8 × 2–3 µm ..... ***H. longispora***
– Conidia cylindrical, 4–7 × 1–1.5 µm ..... ***H. websteri***

Table 2. Morphological comparisons of sexual morphs in *Hevansia*, *Jenniferia* and *Polystromomyces*.

Species	Host	Stromata	Fertile part	Perithecia	Asci	Ascospores	References
Hevansia minuta	Spider (Theridiidae, *Meotipa* sp.)	Stipitate, solitary, white to cream, 10 mm long, 1 mm broad	Oval, ca. 2–2.5 mm long, ca. 1.5 mm broad	Immersed, narrowly ovoid, 400–500 × 100–170 µm	Cylindrical, 325–450 × 3–5 µm	Filiform, whole ascospores, 320–450 × 0.5–1.5 µm	This study
H. nelumboides	Spider	Stipitate, white, 4 mm long, 0.4 mm broad	Disc-shaped, 2 × 0.8 mm	Immersed, fusoid-ellipsoidal, 535–545 × 180–190 µm	400–450 × 5–6 µm	Part-spores, ca. 5 × 1 µm	Kobayasi and Shimizu (1977)
H. novoguineensis	Spider (Theridiidae)	Stipitate, solitary, or multiple, cylindrical, white to pale yellow, 3–5 mm long, 0.5–1 mm broad	Disc-shaped, upper surface slightly convex, 1–3 × 1–2 mm	Immersed, narrowly ovoid, 500–750 × 200–300 µm	Cylindrical, 350–450 × 5–7 µm	Filiform, whole ascospores, 400–460 × 1–1.5 µm	This study
Jenniferia griseocinerea	Spider (Thomisidae, *Diaea* cf. *dorsata*, *Diaea* sp.)	Non-stipitate	Perithecia aggregated in clusters forming a cushion	Superficial, ovoid, 650–850 × 250–320 µm	Cylindrical, 375–460 × 5–6 µm	Whole ascospores with septate part-spores alternately connected with thread-like structures, up to 400 µm long, each cell narrowly fusiform, 10–15 × 1–2 µm, filiform regions, 35–45 × 0.2–0.8 µm	This study
J. thomisidarum	Spider (Thomisidae, *Diaea* cf. *dorsata*)	Non-stipitate	Perithecia aggregated in clusters forming a cushion	Superficial, obpyriform, 850–1100 × 300–400 µm	Cylindrical, 520–700 × 4–6 µm	Whole ascospores with septate part-spores alternately connected with thread-like structures, up to 680 µm long, each cell narrowly fusiform, 10–20 × 1–2 µm, filiform regions, 30–50 × 0.2–0.8 µm	This study
Polystromomyces araneae	Spider egg sac	Stipitate, multiple, moderate yellow, 8–12 mm long, 1–3 mm broad	Disc-shaped, upper surface slightly convex, 3–4 × 2–3.5 mm	Immersed, narrowly ovoid, 1000–1400 × 200–350 µm	Cylindrical, 400–1000 µm long, 3.5–6 µm	Part-spores, cylindrical, 2–6 × 1–3 µm	This study

Jenniferia Mongkolsamrit, Noisripoom & Tasanathai, gen. nov.

MycoBank No: 843089

Type species. *Jenniferia thomisidarum* Mongkolsamrit, Noisripoom & Tasanathai.

Etymology. In honour of Dr. Jennifer Luangsa-ard, for her support and guidance in arthropod pathogenic fungi research.

Description. Spider hosts covered with pale yellow to dark greyish-yellow mycelium. Sexual morph: *Stromata* non-stipitate. *Perithecia* growing in subiculum, superficial, aggregated in clusters forming a cushion. *Asci* cylindrical with thickened caps. *Ascospores* hyaline, septate part-spores alternately connected with thread-like structures along the whole ascospore (Fig. 2d). Asexual morph: *Synnemata* arising from all parts of host, numerous, cylindrical to clavate. *Conidiogenous cells* phialidic, producing along

the synnemata or upper part of the synnemata. *Phialides* flask-shaped with distinct necks. *Conidia* hyaline, fusiform or cylindrical.

Notes. *Jenniferia* is strongly supported as a monophyletic clade by having unique morphological characteristics of perithecia and ascospores. In sexual morph specimens, this genus produces aggregated superficial perithecia forming a cushion with septate part-spores alternately connected with thread-like structures along the whole ascospore (Fig. 2d), which are not seen in any allied genera of the family.

***Jenniferia cinerea* (Hywel-Jones) Mongkolsamrit & Noisripoom, comb. nov.**
MycoBank No: 843090
Fig. 5

≡ *Akanthomyces cinereus* Hywel-Jones, Mycol. Res. 100: 1068 (1996).
≡ *Hevansia cinerea* (Hywel-Jones) Luangsa-ard, Hywel-Jones & Spatafora, IMA Fungus 8: 349 (2017).

Description and illustration. See Hywel-Jones (1996).

Host. Spiders (Araneae, Thomisidae, *Amyciaea* sp.).

Habitat. Specimens were found on the underside of dicot leaves and bamboo leaves of forest plants.

Figure 5. *Jenniferia cinerea* **a, b** fungus on a spider (BBH 2649, NHJ 03510, BCC 6839) **c, d** fungus on a spider (BBH 4896, NHJ 05984, BCC 2191). Scale bars: 5 mm (**b, d**).

Table 3. Morphological comparisons of asexual morphs in *Hevansia*, *Jenniferia* and *Parahevansia*.

Species	Host	Synnemata	Phialides	Conidia	References
Hevansia arachnophila	Spider	Simple, solitary (rarely two or three together), cylindrical, cream, up to 6 mm long, 45–100 µm broad	Globose, 3–4.5 µm broad, with distinct necks, 1–2 × 0.5 µm	Cymbiform, 3.5–6 × 1–1.5 µm	Hywel-Jones (1996)
H. longispora	Spider	Multiple, clavate, brown, 250–700 µm long	Ellipsoid to cylindrical, 7–15 × 2–4 µm	Cylindrical to fusiform, 8.8–14.8 × 2–3 µm	Huang et al. (2000)
H. minuta	Spider (Theridiidae, *Meotipa* sp.)	Non-synnemata	Globose to ovoid, 5–7 × 5–6 µm with distinct necks, 1–2 × 0.5 µm	Fusiform, 2–7 × 2–3 µm	This study
H. nelumboides	Spider	NA	Elongate	Ovoid, 5 × 3 µm	Kobayasi and Shimizu (1977)
H. novoguineensis	Spider (Theridiidae)	Multiple, cylindrical, occasionally acuminate apex, white, up to 8 mm long, 50–200 µm broad	Globose to subglobose, 4–6 × 4–6 µm, with distinct necks, 0.5–1.5 × 0.5–1 µm	Fusoid or fusiform-elliptical, 2–10 × 1–2.5 µm	This study
H. novoguineensis	Spider	Multiple, slender, acuminate apex, white to pale yellow, 3.5 mm long, 50–150 µm broad	Globose to ovoid, 5–6.5 × 4–6 µm broad, with distinct necks, 2–3 × 0.8–1.5 µm	Cylindrical, curved or slightly fusiform, 10.5–17.5 × 1.5–3 µm	Samson and Brady (1982)
H. ovalongata	Spider	Multiple, simple, or branch, white to greyish-orange, 2.2–9 mm long, 112–520 µm broad	Globose to subglobose, cylindrical, or ellipsoid, 6–8.7×4–6.4µm,withdistinct necks, 1.4–3.2 × 0.8–1.8 µm	Ellipsoid, obovate to oblong, 6–10.3 × 2.4–4.4 µm	Hsieh et al. (1997)
H. websteri	Spider	Simple, cylindrical, cream-white, up to 12 mm long, 50–70 µm broad	Ellipsoid, 4.5–8.5 × 2–3.5 µm, with distinct necks, 1.5–3 × 0.5 µm	Cylindrical, 4–7 × 1–1.5 µm	Hywel-Jones (1996)
Jenniferia cinerea	Spider (Thomisidae, *Amyciaea* sp.)	Multiple, clavate, grey, up to 3 mm long, 60–70 µm broad	Cylindrical, 3.5–6.5 × 1.5–2 µm, with distinct necks, 2–2.5 × 0.5 µm	Clavate, 3.5–5.5 × 1–1.5 µm	Hywel-Jones (1996)
J. griseocinerea	Spider (Thomisidae, *Diaea* cf. *dorsata, Diaea* sp.)	Two types of synnemata, long synnemata, cylindrical with blunt end, grey to pale brown, 2.5–5 mm long, 100–150 µm broad, middle of long synnemata, 50–80 µm broad; short synnemata, cylindrical, pale grey to dark grey, up to 450 µm long, 20–50 µm broad	Flask-shaped, 5–10 × 3–5 µm, with distinct necks, 2–3.5 × 0.5–1 µm	Fusiform, 3–6 × 1–2 µm	This study
J. thomisidarum	Spider (Thomisidae, *Diaea* cf. *dorsata*)	Multiple, cylindrical to clavate, greyish-brown, up to 800 µm long, 30–100 µm broad	Cylindrical, 7–16 × 2–5 µm, with distinct necks, 1–5 × 1–1.5 µm	Fusiform, cylindrical, 3–12 × 1–3 µm	This study
Parahevansia koratensis	Spider (Salticidae)	Multiple, simple, brown at the sterile base, becoming grey white, up to 6 mm long, 50 µm broad	Obovoid to ellipsoid, 4–5.5 × 3–3.5 µm, with distinct necks, 2.5–3 × 0.5–1 µm	Clavate, 4.5–5.5 × 1–1.5 µm	Hywel-Jones (1996)

NA, information not provided in the original description.

Material examined. Thailand, Ranong Province, Khlong Nakha Wildlife Sanctuary, 9°27'34.52"N, 98°30'16.15"E, on spider (Araneae), 21 April 1994, Hywel-Jones NL, Nasit R, Plomhan R, Sivichai S, Thienhirun S, NHJ 3531 holotype, holotype damaged and no culture living, Neotype designated here: THAILAND, Ranong Province, Khlong Nakha Wildlife Sanctuary, 9°27'34.52"N, 98°30'16.15"E, on spider (Non-web builder, Araneae, Thomisidae, *Amyciaea* sp.), 21 April 1994, Hywel-Jones NL, Nasit R, Plomhan R, Sivichai S, Thienhirun S, NHJ 03510 (BBH 2649, holotype), ex-type culture BCC 6839.

Notes. Based on the asexual morph of species in *Jenniferia*, they share similar characteristics in producing grey mycelium covering the spider host and multiple cylindrical synnemata from all parts of the host. The phylogenetic analysis supported *J. cinerea* as a sibling species to *J. griseocinerea*, but they have differences in producing synnemata. *Jenniferia cinerea* produces long synnemata, while *J. griseocinerea* produces short and long synnemata (Fig. 6). *Jenniferia cinerea* was not found as a sexual morph, whereas both *J. griseocinerea* and *J. thomisidarum* were found with sexual and asexual morphs (Tables 2 and 3). The shape of conidia in *J. cinerea* is clavate, but conidia in *J. griseocinerea* are fusiform and in *J. thomisidarum* are fusiform to cylindrical (Table 3). The spider hosts of *J. cinerea* from both specimens presented herein are identified as *Amyciaea* sp. belonging to the family Thomisidae.

***Jenniferia griseocinerea* Tasanathai, Noisripoom & Mongkolsamrit, sp. nov.**
MycoBank No: 843091
Fig. 6

Typification. Thailand, Nakhon Ratchasima Province, Khao Yai National Park, 14°26'20.72"N, 101°22'20.02"E, on spider (Non-web builder, Araneae, Thomisidae, *Diaea* sp.) attached to the underside of a dicot leaf of forest plants, 31 May 2010, K. Tasanathai, P. Srikitikulchai, S. Mongkolsamrit, T. Chohmee, A. Khonsanit, R. Somnuk, K. Sansatchanon, MY6006.01 (BBH 29656, holotype), ex-type culture BCC 42062 isolated from ascospores.

Etymology. Named after the colour of the fresh specimens, from the Latin '*griseo*', referring to dark grey and '*cinerea*' meaning ash grey.

Description. Spider hosts covered by yellowish-grey mycelium (156C). Sexual morph: *Stromata* non-stipitate. *Perithecia* growing in subiculum, aggregated in clusters, superficial, ovoid, 650–850 × 250–320 µm, ostiole pale brown. *Asci* cylindrical, 8-spored, 375–460 µm long, 5–6 µm broad, with cap 2–6 µm thick. *Ascospores* hyaline, whole ascospores with septate part-spores alternately connected with thread-like structures, four-terminal cells on each end with six alternating pairs of cells and filaments, sixteen cells per ascospore, up to 400 µm long, each cell narrowly fusiform, 10–15 × 1–2 µm, filiform regions, 35–45 × 0.2–0.8 µm. Asexual morph: Two types of synnemata were produced from all parts of the hosts. Several long synnemata, grey becoming pale brown at terminal ends, cylindrical with blunt end, 2.5–5 mm long, 100–150 µm broad, middle of long synnemata, 50–80 µm broad. *Conidiogenous cells* producing along long synnemata. Short synnemata, pale grey to dark grey, cylindrical, up to 450 µm long, 20–50 µm broad. *Conidiogenous cells* producing at the upper part of synnemata. *Phialides* flask-shaped at the base, 5–10 × 3–5 µm, tapering into distinct necks, 2–3.5 × 0.5–1 µm. *Conidia* hyaline, fusiform, 3–6 × 1–2 µm.

Culture characteristics. Colonies on OA attaining a diam. of 18–20 mm in 21 days, cottony with high mycelium density, white, reverse pale yellow (165D). *Conidia* and reproductive structures not observed.

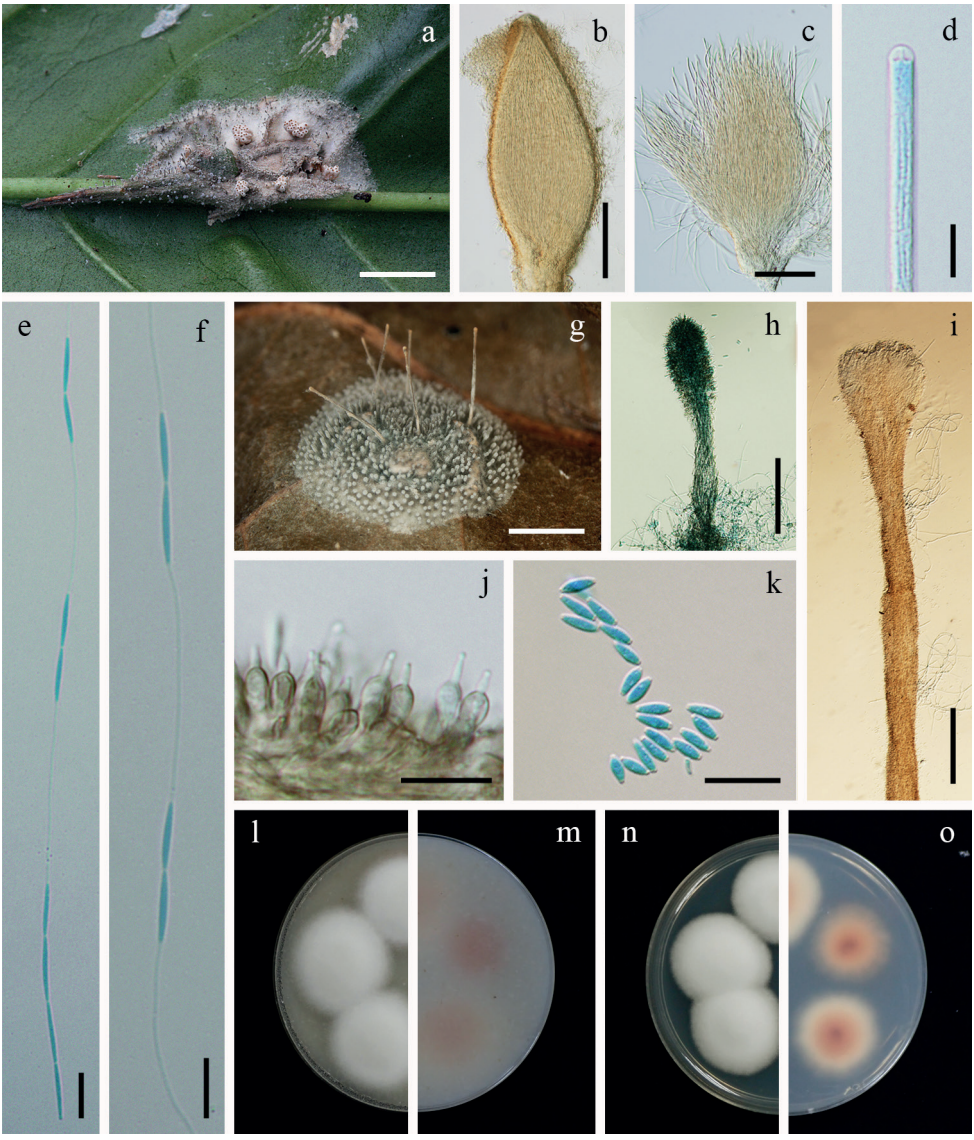

Figure 6. *Jenniferia griseocinerea* **a** fungus on a spider (BBH 29656) **b** perithecium **c** asci **d** ascus tip **e, f** whole ascospores with septate part-spores alternately connected with thread-like structures **g** fungus on a spider (BBH 33219) **h** short synnema **i** long synnema **j** phialides **k** conidia **l, m** colonies on OA at 21 days (**l** obverse, **m** reverse) **n, o** colonies on PDA at 21 days (**n** obverse, **o** reverse). Scale bars: 2 mm (**a, g**); 200 μm (**b**); 100 μm (**c, h, i**); 10 μm (**d, e, f, j, k**).

Colonies on PDA attaining a diam. of (16)17–20 mm in 21 days, cottony with high mycelium density, white, reverse pale yellow (165D). *Conidia* and reproductive structures not observed.

Host. Spiders (Araneae, Thomisidae, *Diaea* cf. *dorsata*, *Diaea* sp.).

Habitat. Specimens were found on the underside of dicot leaves of forest plants.

Additional materials examined. Thailand, Nakhon Ratchasima Province, Khao Yai National Park, 14°26'20.72"N, 101°22'20.02"E, on spider (Non-web builder, Araneae, Thomisidae, *Diaea* sp.) attached to the underside of a dicot leaf of forest plants, 31 May 2010, K. Tasanathai, P. Srikitikulchai, S. Mongkolsamrit, T. Chohmee, A. Khonsanit, R. Somnuk, K. Sansatchanon, MY6006.02 (BBH 29656, paratype) ex-paratype culture BCC 42063 isolated from conidia; idem, on spider (Non-web builder, Araneae, Thomisidae, *Diaea* cf. *dorsata*) attached to the underside of a dicot leaf of forest plants, 8 November 2012, S. Mongkolsamrit, A. Khonsanit, W. Noisripoom, P. Srikitikulchai, R. Somnuk, MY8241 (BBH 33219) culture BCC 57821 isolated from conidia; idem, 9 August 2012, K. Tasanathai, S. Mongkolsamrit, A. Khonsanit, W. Noisripoom, K. Sansatchanon, MY7627 (BBH 36128) culture BCC 54893 isolated from conidia.

Notes. Based on the multi-gene phylogenetic analyses presented in Fig. 1, *Jenniferia griseocinerea* is closely related to *J. cinerea*. It shares similarity with *J. cinerea* in the production of several cylindrical synnemata arising from all parts of the spider host. However, *J. griseocinerea* differs from *J. cinerea* in producing long and short synnemata, while *J. cinerea* produces only long synnemata. The shape of phialides in *J. griseocinerea* from the specimens differs from *J. cinerea* and *J. thomisidarum*. Phialides in *J. griseocinerea* are flask-shaped, while phialides in *J. cinerea* and *J. thomisidarum* are cylindrical. Conidia in *J. griseocinerea* and *J. thomisidarum* are fusiform, occasionally cylindrical in *J. thomisidarum.* The conidia in *J. griseocinerea* are shorter than those reported for *J. thomisidarum* (3–6 × 1–2 µm vs. 3–12 × 1–3 µm) (Table 3).

***Jenniferia thomisidarum* Mongkolsamrit, Noisripoom & Tasanathai, sp. nov.**
MycoBank No: 843092
Fig. 7

Typification. Thailand, Nakhon Ratchasima Province, Khao Yai National Park, 14°26'20.72"N, 101°22'20.02"E, on spider (Non-web builder, Araneae, Thomisidae, *Diaea* cf. *dorsata*) attached to the underside of a dicot leaf of forest plants, 23 July 2009, K. Tasanathai, P. Srikitikulchai, S. Mongkolsamrit, R. Ridkaew, MY5032.01 (BBH 29502, holotype), ex-type culture BCC 37881 isolated from ascospores.

Etymology. Named after the host belonging to the family Thomisidae (Araneae).

Description. Spider hosts covered by dense greyish-brown mycelium (199C–D). Sexual morph: *Stromata* non-stipitate. *Perithecia* growing in subiculum, aggregated in clusters, superficial, obpyriform, 850–1100 × 300–400 µm, ostiole pale brown. *Asci* cylindrical, 8-spored, 520–700 µm long, 4–6 µm broad, with cap 2–6 µm thick. *Ascospores* hyaline, whole ascospores with septate part-spores alternately connected with thread-like structures, three-terminal cells on each end with six alternating pairs of cells and filament, eighteen cells per ascospore, up to 680 µm long, each

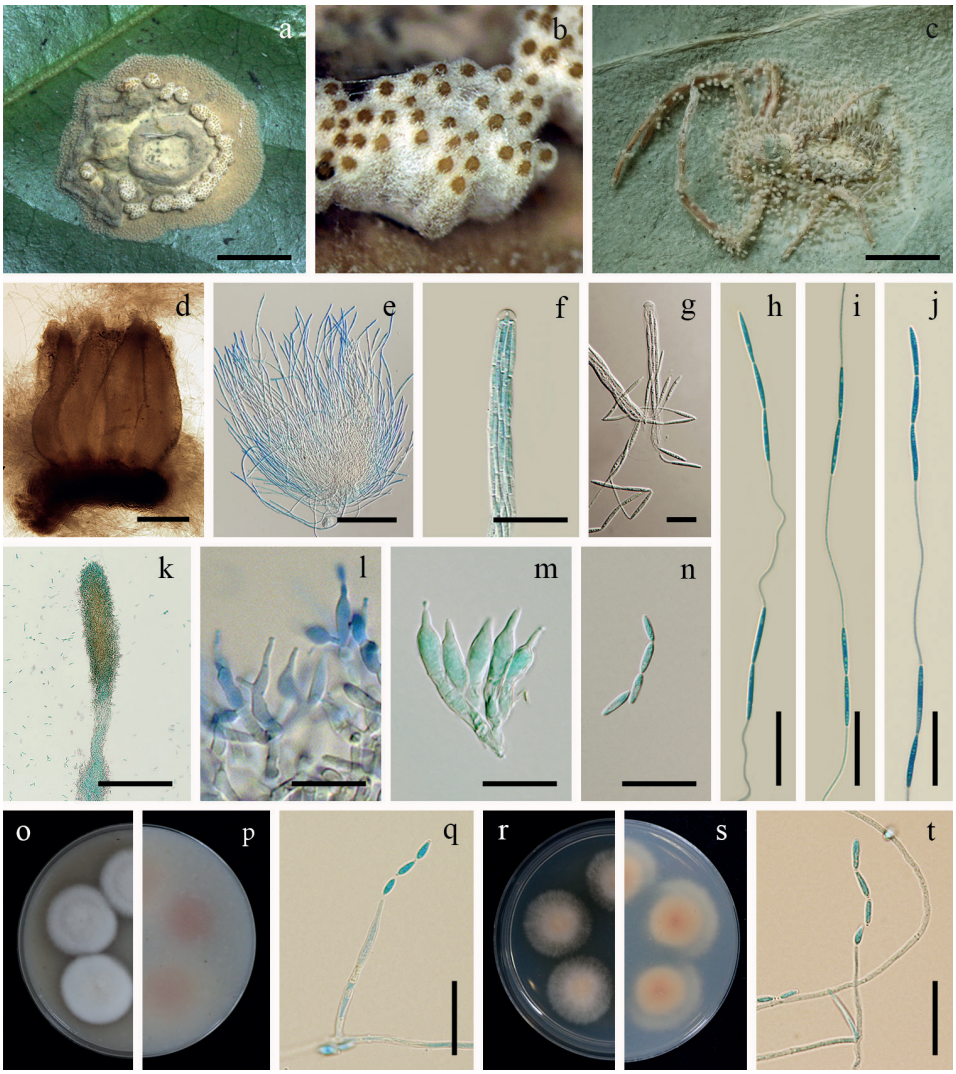

Figure 7. *Jenniferia thomisidarum* **a** fungus on a spider (BBH 29502) **b** perithecia **c** fungus on a spider (BBH 30660) **d** perithecia **e** asci **f, g** ascus tip **h–j** whole ascospores with septate part-spores alternately connected with thread-like structures **k** synnema with conidiogenous cells **l, m** phialides **n** conidia **o**, **p** colonies on OA at 21 days (**o** obverse, **p** reverse) **q** phialide with conidia on OA **r, s** colonies on PDA at 21 days (**r** obverse, **s** reverse) **t** phialide with conidia on PDA. Scale bars: 2 mm (**a, c**); 300 µm (**d**); 200 µm (**e**); 100 µm (**k**); 10 µm (**f, g, l, m, n**); 20 µm (**h, i, j, q, t**).

cell narrowly fusiform, 10–20 × 1–2 µm, filiform regions, 30–50 × 0.2–0.8 µm. Asexual morph: *Synnemata* arising from the mycelial mat, numerous, greyish-brown, cylindrical to clavate, erect up to 800 µm long, 30–100 µm broad. *Conidiogenous cells* producing at the upper part of synnemata, mostly monophialidic or some polyphialidic. *Phialides* cylindrical, (7)10–15(16) × 2–4(5) µm, tapering into a

distinct neck, (1)1.5–3.5(5) × 1–1.5 µm. *Conidia* hyaline, fusiform, cylindrical, (3)8.5–10.5(12) × 1–3 µm.

Culture characteristics. Colonies on OA attaining a diam. of (12)14–15 mm in 21 days, cottony with high mycelium density, white, reverse pale orange (165D), poor sporulation. *Phialides* arising from aerial hyphae, solitary, awl-shaped, lecanicillium-like, 20–40 × 1–2 µm. *Conidia* in chains, hyaline, fusiform, cylindrical, smooth, (3)7.5–10.5(12) × (1.5)2–2.5(3) µm.

Colonies on PDA attaining a diam. of 8–10 mm in 21 days, cottony with high mycelium density in the middle of colonies, mycelium with low density around the margin of colonies, pale orange, reverse moderate orange (167D), poor sporulation. *Phialides* arising from aerial hyphae, solitary, awl-shaped, lecanicillium-like, 10–35 × 1–2 µm. *Conidia* in the chains, hyaline, fusiform, cylindrical, smooth, (3)6.5–9.5(10) × (1.5)2–2.5(3) µm.

Host. Spiders (Araneae, Thomisidae, *Diaea* cf. *dorsata*).

Habitat. Specimens were found on the underside of dicot leaves of forest plants.

Additional materials examined. Thailand, Nakhon Ratchasima Province, Khao Yai National Park, 14°26'20.72"N, 101°22'20.02"E, on spider (Non-web builder, Araneae, Thomisidae, *Diaea* cf. *dorsata*) attached to the underside of a dicot leaf of forest plants, 23 July 2009, K. Tasanathai, P. Srikitikulchai, S. Mongkolsamrit, R. Ridkaew, MY5032.02 (BBH 29502, paratype), ex-paratype culture BCC 37882 isolated from conidia; idem, 7 August 2011, K. Tasanathai, P. Srikitikulchai, S. Mongkolsamrit, A. Khonsanit, W. Noisripoom, K. Sansatchanon, MY6813 (BBH 30660, culture BCC 48932); idem, 3 August 2011, K. Tasanathai, P. Srikitikulchai, S. Mongkolsamrit, A. Khonsanit, W. Noisripoom, K. Sansatchanon, MY6866 (BBH30690), culture BCC 49257; idem, 9 August 2012, K. Tasanathai, S. Mongkolsamrit, A. Khonsanit, W. Noisripoom, MY7598 (BBH 32822), culture BCC 54482; MY7599 (BBH 32823), culture BCC 54483; MY7600 (BBH 32824), culture BCC 32824; idem, 26 June 2012, K. Tasanathai, P. Srikitikulchai, S. Mongkolsamrit, A. Khonsanit, W. Noisripoom, K. Sansatchanon, R. Somnuk, MY8636 (BBH35789), culture BCC 64182; idem, 7 August 2013, P. Srikitikulchai, S. Mongkolsamrit, A. Khonsanit, W. Noisripoom, MY8878 (BBH 336396), culture BCC 66224.

Notes. In sexual morph specimens found in nature, *Jenniferia thomisidarum* resembles *J. griseocinerea* by the formation of non-stipitate ascomata. The perithecia of both species are superficial and aggregate in clusters, challenging the identification of the species rank. The ascospores are of the same type by septate part-spores alternately connected with thread-like structures along the whole ascospore (Fig. 2d). Ascospores in *J. thomisidarum* are longer than those reported for *J. griseocinerea* (Table 2). *Jenniferia thomisidarum* differs from *J. griseocinerea* in the size and shape of the perithecia and asci. In *J. thomisidarum*, perithecia and asci are larger and longer than those reported for *J. griseocinerea* (850–1100 × 300–400 µm vs. 650–850 × 250–320 µm; 520–700 × 4–6 µm vs. 375–460 × 5–6 µm). The perithecia in *J. thomisidarum* are obpyriform, while perithecia in *J. griseocinerea* are ovoid.

Key to the species of *Jenniferia*

Based on sexual state characters

1 Ascospores septate part-spores alternately connected with thread-like structures along the whole ascospore, non-stipitate ascomata, superficial perithecia up to 400 µm long.....***J. griseocinerea***
– Ascospores septate part-spores alternately connected with thread-like structures along the whole ascospore, non-stipitate ascomata, superficial perithecia to 680 µm long.....***J. thomisidarum***

Based on asexual state characters

1 Synnemata, multiple, two types of synnemata, long synnemata cylindrical with a blunt end, short synnemata.....***J. griseocinerea***
– Synnemata, multiple, one type of synnemata.....**2**
2 Conidia 3.5–5.5 × 1–1.5 µm, clavate.....***J. cinerea***
– Conidia, 3–12 × 1–3 µm, fusiform, cylindrical.....***J. thomisidarum***

Parahevansia **Mongkolsamrit & Noisripoom, gen. nov.**
MycoBank No: 844040

Type species. *Parahevansia koratensis* (Hywel-Jones) Mongkolsamrit & Noisripoom, comb. nov., Mycol. Res. 100: 1067 (1996).

Etymology. Morphologically resembling the genus *Hevansia*, but being phylogenetically distinct.

Description. Asexual morph: *Synnemata* arising from all parts of host, numerous, simple, brown at the sterile base becoming grey white with fertile part. *Conidiogenous cells* phialidic producing upper part of the synnemata. *Phialides* in a monolayer, single on basal lateral cells of synnemata, crowded, obovoid to ellipsoid with distinct necks. *Conidia* in chain, hyaline, smooth-walled, clavate.

Notes. *Parahevansia koratensis*, the type species of this genus, was originally described as species of *Akanthomyces* (Hywel-Jones, 1996) and later transferred to *Hevansia* (Kepler et al. 2017). Our multi-gene phylogenetic analyses supported *Parahevansia* as a monophyletic clade with strong support (MLB = 100 / BPP = 1.00, Fig. 1). Therefore, we introduced *Parahevansia* as a new genus that accommodates a single species, *Pa. koratensis*.

Parahevansia koratensis **(Hywel-Jones) Mongkolsamrit & Noisripoom, comb. nov.,**
MycoBank No: 844041

≡ *Akanthomyces koratensis* Hywel-Jones, Mycol. Res. 100: 1068 (1996).

≡ *Hevansia koratensis* (Hywel-Jones) Luangsa-ard, Hywel-Jones & Spatafora, IMA Fungus 8: 349 (2017).

Typification. Thailand, Nakhon Ratchasima Province, Khao Yai National Park, 14°26'20.72"N, 101°22'20.02"E, on spider (Araneae, Salticidae), 12 December 1991, N.L. Hywel-Jones, NHJ 666.01 holotype.

Description and illustration. See Hywel-Jones (1996).

Host. Spider (Araneae, Salticidae).

Habitat. Specimens were found on the underside of dicot leaves of forest plants.

Notes. Both *Parahevansia koratensis* and *H. novoguineensis* occur on spiders and both produce white mycelium with reddish pigment diffusing in agar media (Hywel-Jones 1996). However, the sporulation of *H. novoguineensis* is produced on media, while no sporulation on media in *Pa. koratensis* was observed. Based on the phylogenetic tree (Fig. 1), NHJ 2662 clustered with the ex-type strain NHJ 666.01 of *Pa. koratensis*. The insect host of the strain NHJ 2662 was recorded as a Lepidoptera larva. This result shows that *Pa. koratensis* is parasitic on spiders and Lepidoptera larva.

Polystromomyces **Mongkolsamrit, Noisripoom, Sakolrak & Himaman, gen. nov.**
MycoBank No: 843093

Type species. *Polystromomyces araneae* Mongkolsamrit, Noisripoom, Sakolrak & Himaman.

Etymology. From Latin "poly" (many), referring to many stromata of the fungus on the host.

Description. Sexual morph: *Stromata* stipitate, multiple, pale yellow mycelium covering the host. Stipes arising from spider egg sac, cylindrical at the base, slightly enlarged midway to the terminal end of the stipe below the fertile head. *Fertile heads* produce at the terminal stipes, disc-shaped, upper surface slightly convex. *Perithecia* completely immersed, ovoid. *Asci* cylindrical. *Ascospores* hyaline, filiform, disarticulating into part-spores. Colony on PDA and OA, white, producing microcycle conidiation.

Notes. *Polystromomyces* contains a new species, *Po. araneae*. It shares similarity with species in *Hevansia* in producing multiple stipes with fertile heads at the apex. This specimen is found on a spider egg sac (Araneae) attached to the underside of a dicot leaf. There is no record of the asexual morph on the specimen.

Polystromomyces araneae **Mongkolsamrit, Noisripoom, Sakolrak & Himaman, sp. nov.**
MycoBank No: 843094
Fig. 8

Typification. Thailand, Tak Province, Umphang Wildlife Sanctuary, 15°55'36.33"N, 98°45'12.15"E, on spider egg sac (Araneidae *sensu lato*) attached to the underside of a

dicot leaf, 6 December 2020, B. Sakolrak, MY12684 (BBH 49054, holotype), ex-type culture BCC 93301 isolated from ascospores.

Etymology. From Latin, "aranea" refers to a spider host.

Description. Hosts covered by dense pale yellow mycelium (162D). Sexual morph: *Stromata* stipitate, arising from the host, multiple, cylindrical at the base, slightly enlarged midway to the terminal stipe below the fertile head, moderate yellow (162A–B), 8–12 mm long, 1–3 mm broad. *Fertile head* disc-shaped, upper surface slightly convex, 3–4 × 2–3.5 mm. *Perithecia* completely immersed, narrowly ovoid, 1000–1400 × 200–350 µm, ostiole pale brownish-orange (165B). *Asci* cylindrical,

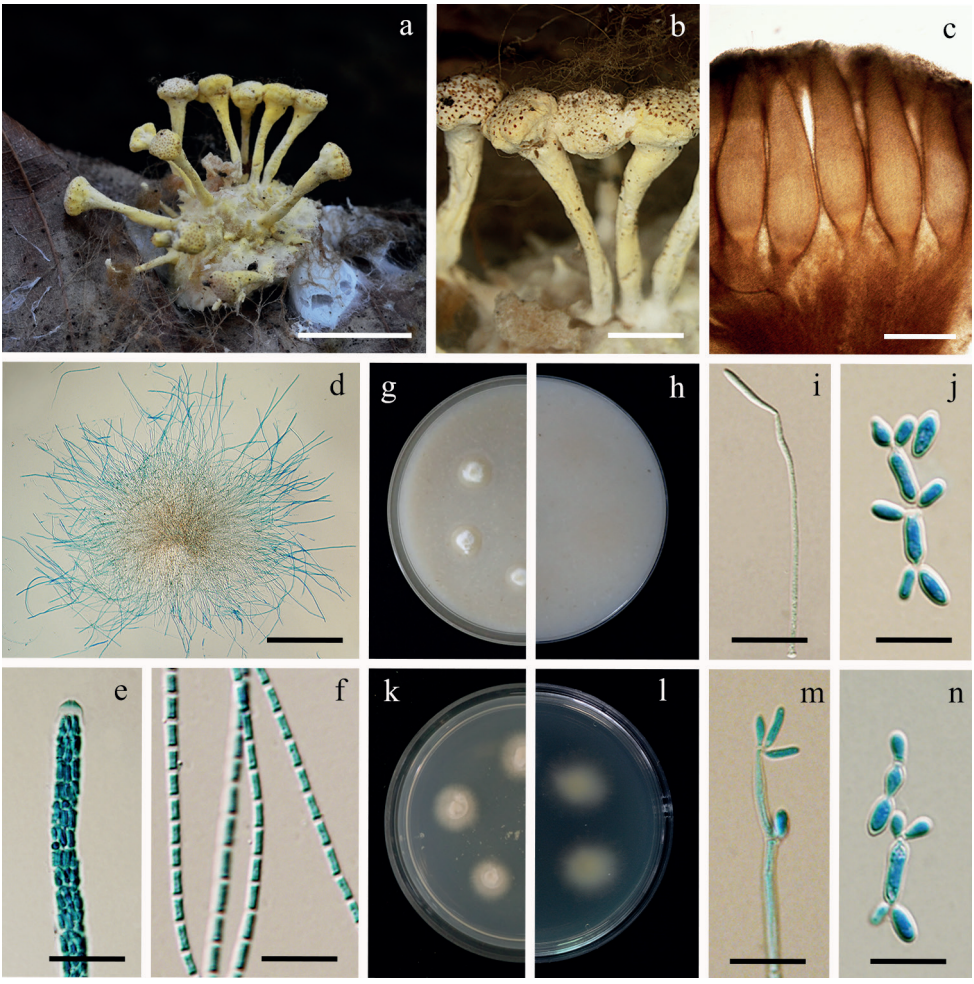

Figure 8. *Polystromomyces araneae* **a** fungus on a spider egg sac (BBH 49054) **b** fertile heads **c** perithecia **d** asci **e** ascus tip **f** part-spores **g, h** colonies on OA at 21 days (**g** obverse, **h** reverse) **i** conidium formation from a hypha on OA **j** microcycle conidiation on OA **k, l** colonies on PDA at 21 days (**k** obverse, **l** reverse) **m** conidia formation from a hypha on PDA **n** microcycle conidiation on PDA. Scale bars: 10 mm (**a**); 3 mm (**b**); 200 µm (**c, d**); 10 µm (**e, f, i, j, m, n**).

8-spored, 400–1000 µm long, 3.5–6 µm broad, with cap 2–5 µm thick. *Ascospores* hyaline, dissociating into 128 part-spores, cylindrical, 2–6 × 1–3 µm.

Culture characteristics. Colonies on OA attaining a diam. of 8–10 mm in 21 d, mycelium sparse, white, reverse pale yellow (161C). *Conidia* forming on vegetative hyphae or by microcyclic conidiation, hyaline, clavate to cylindrical, 2–10 × 1–5 µm.

Colonies on PDA attaining a diam. of 8–10 mm in 20 d, mycelium sparse, white, reverse pale yellow (161C). *Conidia* forming on vegetative hyphae or by microcyclic conidiation, hyaline, clavate to cylindrical, 2–12 × 1–5 µm.

Host. Spider egg sac.

Habitat. Specimen was found on the underside of a dicot leaf of a forest plant.

Notes. Based on natural specimens, *Po. araneae* closely resembles *H. nelumboides* and *H. novoguineensis* by producing fertile heads at the end of the stipes. The perithecia of these species are completely immersed. The ascospores of *Po. araneae* and *H. nelumboides* are filamentous, multiseptate ascospores disarticulating into part-spores, whereas *H. novoguineensis* produces filiform, whole ascospores. However, *Po. araneae* differs from *H. nelumboides* in the size of the perithecia. In *Po. araneae*, perithecia are larger than those reported for *H. nelumboides* (1000–1400 × 200–350 µm vs. 535–545 × 180–190 µm) (Table 2). *Polystromomyces araneae* produces microcycle conidiation from conidia on culture, while the microcyclic sporulation is often seen in discharged ascospores in *Metarhizium phuwiangense* Luangsa-ard, Mongkols., Himaman, Thanakitp. & Samson and *Purpureomyces khaoyaiensis* (Hywel-Jones) Luangsa-ard, Samson & Thanakitp (Mongkolsamrit et al. 2020a).

Discussion

In this study, we conducted comparative morphological studies and phylogenetic analyses of spider parasitic fungi belonging to *Hevansia*, *Jenniferia*, *Parahevansia* and *Polystromomyces.* Kepler et al. (2017) established *Hevansia* with two species, i.e. *H. nelumboides* and *H. novoguineensis*, based on a split inferred from molecular data. Our molecular analyses revealed the sexual-asexual link between the Thai material (BCC 42675) and the ex-type culture of *H. novoguineensis* (CBS 610.80) and a novel species, *H. minuta* (Fig. 1). The sexual morph morphological characters in *Hevansia* (observed in *H. novoguineensis*, *H. minuta* and *H. nelumboides*) include stipes with terminal fertile heads arising from the dorsal region of their spider hosts (Figs 3a and 4a, this study; Fig. 3J in Kepler et al. 2017). *Hevansia* cf. *novoguineensis* (BCC 2093 and NHJ 4314) formed a subclade genetically close to *H. novoguineensis*, but the herbarium materials of these strains were not available for comparison. Considering that *H.* cf. *novoguineensis* formed a sister clade to *H. novoguineensis* (Fig. 1), but this relation was not consistently found between the markers, we propose that *H. novoguineensis* is a species complex and that *H.* cf. *novoguineensis* could potentially be considered as a different species if more molecular markers could unambiguously demonstrate its separation from the clade containing the ex-type strain.

In this study, the genus *Polystromomyces* is established with a single species (*Po. araneae*); it formed the basal lineage to *Hevansia*, *Jenniferia* and *Gibellula* and shared the same ecological habitat (on the underside of dicot leaves of forest plants). *Polystromomyces araneae* shares morphological similarity to *Hevansia* by producing multiple stromata with fertile heads at the terminal part of stipes. Notably, *Po. araneae* can be distinguished from *Hevansia* by the shape of stipes. The stipes in *Polystromomyces* are cylindrical at the base and slightly enlarged midway to the terminal below the disc-shaped fertile heads. In contrast, the stipes of *Hevansia* are connected in a cylindrical arrangement with the fertile heads, resembling lotus seed pods on stems.

The novel genus *Jenniferia* was proposed to accommodate *Jenniferia cinerea*, *J. griseocinerea* and *J. thomisidarum*. Based on the natural specimens, the sexual morph of species within *Jenniferia* produce non-stipitate ascomata. The lack of stipe is a shared trait amongst pathogenic fungi species on spiders in Cordycipitaceae, such as *Gibellula* spp., *Akanthomyces thailandicus* and *A. sulphureus*, forming a torrubiella-like sexual morph (Mongkolsamrit et al. 2018; Kuephadungphan et al. 2020). However, species in *Jenniferia* described here can be easily distinguished from species in *Gibellula* spp., *A. thailandicus* and *A. sulphureus* by the superficial and aggregated perithecia in clusters forming a cushion (a distinctive character of *Jenniferia*), causing species in this genus to be easily recognisable in the field.

We reviewed valid species according to a current classification through molecular data combined with the observation of ascospore micro-morphology. Many studies revealed that cordycipitaceous fungi produced three types of ascospore morphology shown through the illustration and description in Figs 1 and 2(a–c). The filiform whole ascospores type (Fig. 2a) with the shape of thread is observed in *Akanthomyces sulphureus*, *Blackwellomyces* spp., *Cordyceps kuiburiensis*, *Hyperdermium* (e.g. *H. bertonii*, *H. pulvinatum*) and *Neotorrubiella chinghridicola* (Mongkolsamrit et al. 2018, 2020b; Crous et al. 2019; Sullivan et al. 2000; Thanakitpipattana et al. 2020). The presence of multiseptate ascospores disarticulating into part-spores (Fig. 2b) can be seen in several genera, such as *Akanthomyces* (e.g. *A. thailandicus*, *A. pyralidarum* and *A. noctuidarum*), *Beauveria* (e.g. *B. asiatica*, *B. gryllotalpidicola*), *Cordyceps* (e.g. *C. militaris*, *C. inthanonensis* and *C. nidus*) and also includes species in *Gibellula* (Mains 1958; Chiriví et al. 2017; Mongkolsamrit et al. 2018, 2020b; Aini et al. 2020; Kuephadungphan et al. 2020). The bola-ascospores morphology was noted in the description of *Cordyceps bifusispora* O.E. Erikss. and *Cordyceps ninchukispora* (C.H. Su & H.H. Wang) G.H. Sung, J.M. Sung, Hywel-Jones & Spatafora (Fig. 2c) by Eriksson (1982) and Su and Wang (1986), respectively. Many *Cordyceps* species producing bola-ascospores were reported from Thailand and China (Tasanathai et al. 2016; Mongkolsamrit et al. 2018, 2020b; Wang et al. 2020). *Samsoniella*, a recent established genus also produces bola-ascospores (Mongkolsamrit et al. 2018; Wang et al. 2020). Examination of our specimens of *Jenniferia* revealed that its ascospores possess a unique shape not seen before in Cordycipitaceae. In this study, we are introducing another ascospore morphology (Fig. 2d), which is an autapomorphic character within *Jenniferia* that can be used to identify at the genus level.

There are two types of phialides in species of *Hevansia.* Some species produce globose to subglobose phialides with a distinct neck along the synnemata (e. g. *H. arachnophila*, *H. minuta*, *H. novoguineensis* and *H. ovalongata*), whereas other species produce phialides on the basal cells along the synnemata (e.g. *H. longispora* and *H. websteri*). These characters can be informative for recognising species of *Hevansia*. All species in *Jenniferia* produce the asexual morph and only two species are occasionally found producing sexual and asexual morphs on the same specimens, i.e. *J. griseocinerea* and *J. thomisidarum*. The *Jenniferia* asexual morph in nature differs from species in *Hevansia* in possessing pale grey to ash grey synnemata scattered over the body and legs of its host. Notably, *J. griseocinerea* significantly differs by producing two types of synnemata (Fig. 6g–i). In contrast, the anamorph of *Hevansia* (e.g. *H. novoguineensis*) produces white synnemata arising from the host (Fig. 3f).

Spider hosts associated with the *Jenniferia* species were identified as *Diaea* cf. *dorsata* for all specimens of *J. griseocinerea* and *J. thomisidarum*, except one specimen of *J. griseocinerea* that was identified as *Diaea* sp. Meanwhile, *Amyciaea* sp. is found as the host of *J. cinerea*. *Jenniferia* is, thus, up to now exclusively associated with the spider genera *Diaea* and *Amyciaea* in the family Thomisidae. A review by Shrestha et al. (2019) reported pathogenic fungi on spiders found in Thomisidae and includes *Gibellula* spp. on *Tmarus* spp. (Costa 2014), *Torrubiella albolanata* on a thomisid spider (Petch 1944) and *T. neofusiformis* on a thomisid spider (Kobayasi and Shimizu 1982). Recently, an additional species occurring on Thomisidae was found, including *Gibellula cebrennini* associated with *Cebrenninus* cf. *magnus* (Kuephadungphan et al. 2020).

Hevansia species are specialised parasites on spiders. *Parahevansia*, proposed as a new genus that accommodates *Pa. koratensis* (≡ *Akanthomyces koratensis*), is parasitic on a salticid spider (Salticidae) and Lepidoptera larva (Hywel-Jones 1996; Shrestha et al 2019, in this study). *Polystromomyces araneae* occurs on the spider egg sac (Araneidae *sensu lato*) attached to the underside of a dicot leaf. *Cordyceps araneae* Mongkols., Tasan., Noisrip., Himaman & Luangsa-ard has also been reported on spider egg sac inhabiting the leaf litter (Mongkolsamrit et al. 2020b). Although *Po. araneae* is most similar to *H. nelumboides* and *H. novoguineensis* by producing stipes with fertile heads at the terminal, the two latter species are found on adult spiders.

Acknowledgements

This research was supported by the Platform Technology Management Section, National Center for Genetic Engineering and Biotechnology (BIOTEC), Grant No. P19-50231. We thank Nalun Chaichanyut for photos of the specimens. We are indebted to the Department of National Parks, Wildlife and Plant Conservation for their cooperation and support of our research project. We would like to thank Dr. Philip James Shaw for the thoughtful editing of the manuscript and the three anonymous reviewers and editors whose suggestions and comments helped improve the manuscript.

References

Aini AN, Mongkolsamrit S, Wijanarka W, Thanakitpipattana D, Luangsa-ard JJ, Budiharjo A (2020) Diversity of *Akanthomyces* on moths (Lepidoptera) in Thailand. MycoKeys 71: 1–22. https://doi.org/10.3897/mycokeys.71.55126

Araújo JPM, Evans HC, Fernandes IO, Ishler MJ, Hughes DP (2020) Zombie-ant fungi cross continents: II. Myrmecophilous hymenostilboid species and a novel zombie lineage. Mycologia 112(6): 1138–1170. https://doi.org/10.1080/00275514.2020.1822093

Bischoff JF, White Jr JF (2004) *Torrubiella piperis* sp. nov. (Clavicipitaceae, Hypocreales), a new teleomorph of the *Lecanicillium* complex. Studies in Mycology 50: 89–94.

Bischoff JF, Chaverri P, White Jr JF (2005) Clarification of the host substrate of *Ascopolyporus* and description of *Ascopolyporus philodendrus* sp. nov. Mycologia 97(3): 710–717. https://doi.org/10.1080/15572536.2006.11832800

Castlebury LA, Rossman AY, Sung GH, Hyten AS, Spatafora JW (2004) Multigene phylogeny reveals new lineage for *Stachybotrys chartarum*, the indoor air fungus. Mycological Research 108(8): 864–872. https://doi.org/10.1017/S0953756204000607

Chaverri P, Bischoff J, Evans H, Hodge K (2005) *Regiocrella*, a new entomopathogenic genus with a pycnidial anamorph and its phylogenetic placement in the Clavicipitaceae. Mycologia 97(6): 1225–1237. https://doi.org/10.1080/15572536.2006.11832732

Chaverri P, Liu M, Hodge KT (2008) A monograph of the entomopathogenic genera *Hypocrella*, *Moelleriella*, and *Samuelsia* gen. nov. (Ascomycota, Hypocreales, Clavicipitaceae), and their aschersonia-like anamorphs in the Neotropics. Studies in Mycology 60: 1–66. https://doi.org/10.3114/sim.2008.60.01

Chen MJ, Wang T, Lin Y, Huang B (2021a) *Gibellula flava* sp. nov. (Cordycipitaceae, Hypocreales), a new pathogen of spider from China. Phytotaxa 527(2): 125–133. https://doi.org/10.11646/phytotaxa.527.2.5

Chen WH, Han YF, Liang JD, Tian WY, Liang ZQ (2021b) Multi-gene phylogenetic evidence indicates that *Pleurodesmospora* belongs in Cordycipitaceae (Hypocreales, Hypocreomycetidae) and *Pleurodesmospora lepidopterorum* sp. nov. on pupa from China. MycoKeys 80: 45–55. https://doi.org/10.3897/mycokeys.80.66794

Chiriví J, Danies G, Sierra R, Schauer N, Trenkamp S, Restrepo S, Sanjuan T (2017) Metabolomic profile and nucleoside composition of *Cordyceps nidus* sp. nov. (Cordycipitaceae): A new source of active compounds. PLoS ONE 12(6): e0179428. https://doi.org/10.1371/journal.pone.0179428

Costa PP (2014) *Gibellula* spp. associadas a aranhas da Mata do Paraíso, Viçosa-MG (M.Sc.), Minas Gerais, Brazil, Universidade Federal de Viçosaans.

Crous PW, Wingfield MJ, Lombard L, Roets F, Swart WJ, Alvarado P, Carnegie AJ, Moreno G, Luangsa-ard J, Thangavel R, Alexandrova AV, Baseia IG, Bellanger JM, Bessette AE, Bessette AR, Delapeña-Lastra S, García D, Gené J, Pham THG, Heykoop M, Malysheva E, Malysheva V, Martín MP, Morozova OV, Noisripoom W, Overton BE, Rea AE, Sewall BJ, Smith ME, Smyth CW, Tasanathai K, Visagie CM, Adamík S, Alves A, Andrade JP, Aninat MJ, Araújo RVB, Bordallo JJ, Boufleur T, Baroncelli R, Barreto RW, Bolin J, Cabero J, Cabo M, Cafà G, Caffot MLH, Cai L, Carlavilla JR, Chávez R, Decastro RRL,

Delgat L, Deschuyteneer D, Dios MM, Domínguez LS, Evans HC, Eyssartier G, Ferreira BW, Figueiredo CN, Liu F, Fournier J, Galli-Terasawa LV, Gil-Durán C, Glienke C, Gonçalves MFM, Gryta H, Guarro J, Himaman W, Hywel-Jones N, Iturrieta-González I, Ivanushkina NE, Jargeat P, Khalid AN, Khan J, Kiran M, Kiss L, Kochkina GA, Kolaík M, Kubátová A, Lodge DJ, Loizides M, Luque D, Manjón JL, Marbach PAS, Massolajr NS, Mata M, Miller AN, Mongkolsamrit S, Moreau P-A, Morte A, Mujic A, Navarro-Ródenas A, Németh MZ, Nóbrega TF, Nováková A, Olariaga I, Ozerskaya SM, Palma MA, Petters-Vandresen DAL, Piontelli E, Popov ES, Rodríguez A, Requejo Ó, Rodrigues ACM, Rong IH, Roux J, Seifert KA, Silva BDB, Sklená F, Smith JA, Sousa JO, Souza HG, Desouza JT, Vec K, Tanchaud P, Tanney JB, Terasawa F, Thanakitpipattana D, Torres-Garcia D, Vaca I, Vaghefi N, Vaniperen AL, Vasilenko OV, Verbeken A, Yilmaz N, Zamora JC, Zapata M, Jurjević Ž, Groenewald JZ (2019) Fungal Planet description sheets: 951–1041. Persoonia 43(1): 223–425. https://doi.org/10.3767/persoonia.2019.43.06

Deeleman-Reinhold CL (2001) Forest spiders of South East Asia: with a revision of the sac and ground spiders (Araneae: Clubionidae, Corinnidae, Liocranidae, Gnaphosidae, Prodidomidae and Trochanterriidae. Brill, Leiden, 591 pp. https://doi.org/10.1163/9789004475588

Eriksson O (1982) *Cordyceps bifusispora* spec. nov. Mycotaxon 15: 185–188.

Hall T (1999) BioEdit: A user-friendly biological sequence alignment editor and analysis program for windows 95/98/NT. Nucleic Acids Symposium Series 41: 95–98.

Hsieh L, Tzean S, Wu WJ (1997) The Genus *Akanthomyces* on Spiders from Taiwan. Mycologia 89(2): 319–324. https://doi.org/10.1080/00275514.1997.12026788

Huang B, Wang S, Fan M, Li Z (2000) Two species of *Akanthomyces* from Dabieshan mountains. Junwu Xuebao 19: 172–174.

Hywel-Jones NL (1996) *Akanthomyces* on spiders in Thailand. Mycological Research 100(9): 1065–1070. https://doi.org/10.1016/S0953-7562(96)80214-0

Johnson D, Sung GH, Hywel-Jones NL, Luangsa-Ard JJ, Bischoff JF, Kepler RM, Spatafora JW (2009) Systematics and evolution of the genus *Torrubiella* (Hypocreales, Ascomycota). Mycological Research 113(3): 279–289. https://doi.org/10.1016/j.mycres.2008.09.008

Kepler RM, Sung GH, Ban S, Nakagiri A, Chen MJ, Huang B, Li Z, Spatafora JW (2012) New teleomorph combinations in the entomopathogenic genus *Metacordyceps*. Mycologia 104(1): 182–197. https://doi.org/10.3852/11-070

Kepler RM, Luangsa-ard JJ, Hywel-Jones NL, Quandt CA, Sung GH, Rehner SA, Aime MC, Henkel TW, Sanjuan T, Zare R, Chen M, Li Z, Rossman AY, Spatafora JW, Shrestha B (2017) A phylogenetically-based nomenclature for Cordycipitaceae (Hypocreales). IMA Fungus 8(2): 335–353. https://doi.org/10.5598/imafungus.2017.08.02.08

Kobayasi Y, Shimizu D (1977) Some species of *Cordyceps* and its allies on spiders. Kew Bulletin 31(3): 557–566. https://doi.org/10.2307/4119402

Kobayasi Y, Shimizu D (1982) Monograph of the genus *Torrubiella*. Bulletin of the National Science Museum, Tokyo 8: 43–78.

Kuephadungphan W, Macabeo APG, Luangsa-ard JJ, Tasanathai K, Thanakitpipattana D, Phongpaichit S, Yuyama K, Stadler M (2019) Studies on the biologically active secondary metabolites of the new spider parasitic fungus *Gibellula gamsii*. Mycological Progress 18(1–2): 135–146. https://doi.org/10.1007/s11557-018-1431-4

Kuephadungphan W, Tasanathai K, Petcharad B, Khonsanit A, Stadler M, Luangsa-ard JJ (2020) Phylogeny- and morphology-based recognition of new species in the spider-parasitic genus *Gibellula* (Hypocreales, Cordycipitaceae) from Thailand. MycoKeys 72: 17–42. https://doi.org/10.3897/mycokeys.72.55088

Kuephadungphan W, Petcharad B, Tasanathai K, Thanakitpipattana D, Kobmoo N, Khonsanit A, Samson RA, Luangsaard JJ (2022) Multi-locus phylogeny unmasks hidden species within the specialised spider parasitic fungus, *Gibellula* (Hypocreales, Cordycipitaceae). Studies in Mycology 101(1): 245–286. https://doi.org/10.3114/sim.2022.101.04

Liu YJ, Whelen S, Hall BD (1999) Phylogenetic relationships among Ascomycetes: Evidence from an RNA polymerse II subunit. Molecular Biology and Evolution 16(12): 1799–1808. https://doi.org/10.1093/oxfordjournals.molbev.a026092

Luangsa-ard J, Tasanathai K, Thanakitpipattana D, Khonsanit A, Stadler M (2018) Novel and interesting *Ophiocordyceps* spp. (Ophiocordycipitaceae, Hypocreales) with superficial perithecia from Thailand. Studies in Mycology 89(1): 125–142. https://doi.org/10.1016/j.simyco.2018.02.001

Mains EB (1958) North American Entomogenous Species of *Cordyceps*. Mycologia 50(2): 169–222. https://doi.org/10.1080/00275514.1958.12024722

Mongkolsamrit S, Luangsa-ard JJ, Spatafora JW, Sung GH, Hywel-Jones NL (2009) A combined ITS rDNA and beta-tubulin phylogeny of Thai species of *Hypocrella* with nonfragmenting ascospores. Mycological Research 113(6–7): 684–699. https://doi.org/10.1016/j.mycres.2009.02.004

Mongkolsamrit S, Noisripoom W, Thanakitpipattana D, Wutikhun T, Spatafora JW, Luangsa-ard J (2018) Disentangling cryptic species with isaria-like morphs in Cordycipitaceae. Mycologia 110(1): 230–257. https://doi.org/10.1080/00275514.2018.1446651

Mongkolsamrit S, Khonsanit A, Thanakitpipattana D, Tasanathai K, Noisripoom W, Lamlertthon S, Himaman W, Houbraken J, Samson RA, Luangsa-ard J (2020a) Revisiting *Metarhizium* and the description of new species from Thailand. Studies in Mycology 95: 171–251. https://doi.org/10.1016/j.simyco.2020.04.001

Mongkolsamrit S, Noisripoom W, Tasanathai K, Khonsanit A, Thanakitpipattana D, Himaman W, Kobmoo N, Luangsa-ard JJ (2020b) Molecular phylogeny and morphology reveal cryptic species in *Blackwellomyces* and *Cordyceps* (Cordycipitaceae) from Thailand. Mycological Progress 19(9): 957–983. https://doi.org/10.1007/s11557-020-01615-2

Mongkolsamrit S, Noisripoom W, Pumiputikul S, Boonlarppradab C, Samson RA, Stadler M, Becker K, Luangsa-ard JJ (2021) *Ophiocordyceps flavida* sp. nov. (Ophiocordycipitaceae), a new species from Thailand associated with *Pseudogibellula formicarum* (Cordycipitaceae), and their bioactive secondary metabolites. Mycological Progress 20(4): 477–492. https://doi.org/10.1007/s11557-021-01683-y

Nylander JAA (2004) MrModeltest 2.0. Program distributed by the author. Evolutionary Biology Centre, Uppsala University, Uppsala.

O'Donnell K, Sarver BA, Brandt M, Chang DC, Noble-Wang J, Park BJ, Sutton DA, Benjamin L, Lindsley M, Padhye A, Geiser DM, Ward TJ (2007) Phylogenetic diversity and microsphere array-based genotyping of human pathogenic Fusaria, including isolates from the multistate contact lens-associated U.S. keratitis outbreaks of 2005 and 2006. Journal of Clinical Microbiology 45(7): 2235–2248. https://doi.org/10.1128/JCM.00533-07

Page RD (1996) TreeView: An application to display phylogenetic trees on personal computers. Computer Applications in the Biosciences 12: 357–358. https://doi.org/10.1093/bioinformatics/12.4.357

Petch T (1944) Notes on entomogenous fungi. Transactions of the British Mycological Society 27(1–2): 81–93. https://doi.org/10.1016/S0007-1536(44)80014-6

Rehner SA, Buckley E (2005) A beauveria phylogeny inferred from nuclear ITS and EF1-α sequences: Evidence for cryptic diversification and links to *Cordyceps* teleomorphs. Mycologia 97(1): 84–98. https://doi.org/10.3852/mycologia.97.1.84

Rehner SA, Samuels GJ (1994) Taxonomy and phylogeny of *Gliocladium* analysed from nuclear large subunit ribosomal DNA sequences. Mycological Research 98(6): 625–634. https://doi.org/10.1016/S0953-7562(09)80409-7

Rehner SA, Minnis AM, Sung GH, Luangsa-ard JJ, Devotto L, Humber RA (2011) Phylogeny and systematics of the anamorphic, entomopathogenic genus *Beauveria*. Mycologia 103(5): 1055–1073. https://doi.org/10.3852/10-302

Ronquist F, Teslenko M, Mark P, Ayres D, Darling A, Höhna S, Larget B, Liu L, Suchard M, Huelsenbeck J (2012) MrBayes 3.2: Efficient Bayesian phylogenetic inference and model choice across a large model space. Systematic Biology 61(3): 539–542. https://doi.org/10.1093/sysbio/sys029

Royal Horticultural Society (RHS) (2015) Colour Chart 6th edn. Royal Horticultural Society: London, UK.

Samson RA, Brady BL (1982) *Akanthomyces novoguineensis* sp. nov. Transactions of the British Mycological Society 79(3): 571–572. https://doi.org/10.1016/S0007-1536(82)80065-X

Samson RA, Evans HC (1974) Note on entomopathogenous fungi from Ghana. II. The genus *Akanthomyces*. Acta Botanica Neerlandica 23(1): 28–35. https://doi.org/10.1111/j.1438-8677.1974.tb00913.x

Samson RA, Evans HC (1992) New species of *Gibellula* on spiders (Araneida) from South America. Mycologia 84(3): 300–314. https://doi.org/10.1080/00275514.1992.12026143

Sanjuan T, Tabima J, Restrepo S, Læssøe T, Spatafora J, Molano A (2014) Entomopathogens of Amazonian stick insects and locusts are members of the *Beauveria* species complex (*Cordyceps sensu stricto*). Mycologia 106(2): 260–275. https://doi.org/10.3852/13-020

Shimizu D (1994) Color iconography of vegetable wasps and plant worms (in Japanese). Seibundo Shinkosha, Tokyo.

Shrestha B, Tanaka E, Hyun MW, Han JG, Kim CS, Jo JW, Han SK, Oh J, Sung GH (2016) Coleopteran and Lepidopteran Hosts of the Entomopathogenic Genus *Cordyceps sensu lato*. Journal of Mycology 7648219: 1–14. https://doi.org/10.1155/2016/7648219

Shrestha B, Kubátová A, Tanaka E, Oh J, Yoon DH, Sung JM, Sung GH (2019) Spider-pathogenic fungi within Hypocreales (Ascomycota): Their current nomenclature, diversity, and distribution. Mycological Progress 18(8): 983–1003. https://doi.org/10.1007/s11557-019-01512-3

Spatafora JW, Sung GH, Sung JM, Hywel-Jones NL, White Jr JF (2007) Phylogenetic evidence for an animal pathogen origin of ergot and the grass endophytes. Molecular Ecology 16(8): 1701–1711. https://doi.org/10.1111/j.1365-294X.2007.03225.x

Stamatakis A (2014) RAxML version 8: A tool for phylogenetic analysis and post-analysis of large phylogenies. Bioinformatics (Oxford, England) 30(9): 1312–1313. https://doi.org/10.1093/bioinformatics/btu033

Su CH, Wang HH (1986) *Phytocordyceps*, a new genus of the Clavicipitaceae. Mycotaxon 26: 337–344.

Sullivan RF, Bills GF, Hywel-Jones NL, White Jr JF (2000) *Hyperdermium*: A new clavicipitalean genus for some tropical epibionts of dicotyledonous plants. Mycologia 92(5): 908–918. https://doi.org/10.1080/00275514.2000.12061236

Sun T, Shen Z, Shaukat M, Du C, Ali S (2020) Endophytic isolates of *Cordyceps fumosorosea* to enhance the growth of *Solanum melongena* and reduce the survival of Whitefly (*Bemisia tabaci*). Insects 11(2): 78. https://doi.org/10.3390/insects11020078

Sung GH, Spatafora JW (2004) *Cordyceps cardinalis* sp. nov., a new species of *Cordyceps* with an east Asian-eastern North American distribution. Mycologia 96(3): 658–666. https://doi.org/10.1080/15572536.2005.11832962

Sung GH, Spatafora JW, Zare R, Hodge KT, Gams W (2001) A revision of *Verticillium* sect. Prostrata. II. Phylogenetic analyses of SSU and LSU nuclear rDNA sequences from anamorphs and teleomorphs of the Clavicipitaceae. Nova Hedwigia 72(3–4): 311–328. https://doi.org/10.1127/nova.hedwigia/72/2001/311

Sung GH, Hywel-Jones NL, Sung JM, Luangsa-ard JJ, Shrestha B, Spatafora JW (2007) Phylogenetic classification of *Cordyceps* and the clavicipitaceous fungi. Studies in Mycology 57: 5–59. https://doi.org/10.3114/sim.2007.57.01

Tasanathai K, Thanakitpipattana D, Noisripoom W, Khonsanit A, Kumsao J, Luangsa-ard JJ (2016) Two new *Cordyceps* species from a community forest in Thailand. Mycological Progress 15(3): e28. https://doi.org/10.1007/s11557-016-1170-3

Thanakitpipattana D, Tasanathai K, Mongkolsamrit S, Khonsanit A, Lamlertthon S, Luangsa-ard J (2020) Fungal pathogens occurring on *Orthopterida* in Thailand. Persoonia 44(1): 140–160. https://doi.org/10.3767/persoonia.2020.44.06

Vilgalys R, Hester M (1990) Rapid genetic identification and mapping of enzymatically amplified ribosomal DNA from several *Cryptococcus* species. Journal of Bacteriology 172(8): 4238–4246. https://doi.org/10.1128/jb.172.8.4238-4246.1990

Vu D, Groenewald M, de Vries M, Gehrmann T, Stielow B, Eberhardt U, Al-Hatmi A, Groenewald JZ, Cardinali G, Houbraken J, Boekhout T, Crous PW, Robert V, Verkley GJM (2019) Large-scale generation and analysis of filamentous fungal DNA barcodes boosts coverage for kingdom fungi and reveals thresholds for fungal species and higher taxon delimitation. Studies in Mycology 92(1): 135–154. https://doi.org/10.1016/j.simyco.2018.05.001

Wang X, Xu J, Wang X, Qiu B, Cuthbertson AGS, Du C, Wu J, Ali S (2019) *Isaria fumosorosea*-based zero-valent iron nanoparticles affect the growth and survival of sweet potato whitefly, *Bemisia tabaci* (Gennadius). Pest Management Science 75(8): 2174–2181. https://doi.org/10.1002/ps.5340

Wang YB, Wang Y, Fan Q, Duan DE, Zhang GD, Dai RQ, Dai YD, Zeng WB, Chen ZH, Li DD, Tang DX, Xu ZH, Sun T, Nguyen TT, Tran NL, Dao VM, Zhang CM, Huang LD, Liu YJ, Zhang XM, Yang DR, Sanjuan T, Liu XZ, Yang ZL, Yu H (2020) Multigene phylogeny of the family Cordycipitaceae (Hypocreales): New taxa and the new systematic

position of the Chinese cordycipitoid fungus *Paecilomyces hepiali*. Fungal Diversity 103(1): 1–46. https://doi.org/10.1007/s13225-020-00457-3

White TJ, Bruns T, Lee S (1990) Amplification and direct sequencing of fungal ribosomal RNA genes for phylogenetics. In: Innis MA, Gelfand DH, Sninsky JJ (Eds) PCR protocols: a guide to methods and applications. Academic Press Inc, New York, 315–322. https://doi.org/10.1016/B978-0-12-372180-8.50042-1

Wu X, Wu T, Huang A, Shen Y, Zhang X, Song W, Wang S, Ruan H (2021) New insights into the biosynthesis of typical bioactive components in the traditional Chinese medicinal fungus *Cordyceps militaris*. Frontiers in Bioengineering and Biotechnology 9: e801721. https://doi.org/10.3389/fbioe.2021.801721

Zare R, Gams W (2016) More white verticillium-like anamorphs with erect conidiophores. Mycological Progress 15(10–11): 993–1030. https://doi.org/10.1007/s11557-016-1214-8

Zhang ZF, Zhou SY, Eurwilaichitr L, Ingsriswang S, Raza M, Chen Q, Zhao P, Liu F, Cai L (2020) Culturable mycobiota from Karst caves in China II, with descriptions of 33 new species. Fungal Diversity 106(1): 29–136. https://doi.org/10.1007/s13225-020-00453-7

Supplementary material 1

Figures S1–S5

Authors: Suchada Mongkolsamrit, Wasana Noisripoom, Kanoksri Tasanathai, Noppol Kobmoo, Donnaya Thanakitpipattana, Artit Khonsanit, Booppa Petcharad, Baramee Sakolrak, Winanda Himaman

Data type: Pdf file

Explanation note: RAxML trees of *Hevansia*, *Jenniferia*, *Parahevansia*, *Polystromomyces* and related genera in the Cordycipitaceae from different molecular markers.

Link: https://doi.org/10.3897/mycokeys.91.83091.suppl1

MycoKeys 91: 151–168 (2022)
doi: 10.3897/mycokeys.91.87841
https://mycokeys.pensoft.net

RESEARCH ARTICLE

A peer-reviewed open-access journal
MycoKeys
Launched to accelerate biodiversity research

Cladosporium spp. (Cladosporiaceae) isolated from *Eucommia ulmoides* in China

Si-Yao Wang[1,2,3], Yong Wang[3], Yan Li[1,2]

1 *Key Laboratory of Plant Resources Conservation and Germplasm Innovation in Mountainous Region (Ministry of Education), Guiyang 550025, Guizhou Province, China* **2** *College of Life Sciences/Institute of Agro-Bioengineering, Guizhou University, Guiyang 550025, Guizhou Province, China* **3** *Department of Plant Pathology, Agriculture College, Guizhou University, Guiyang, Guizhou Province, 550025, China*

Corresponding authors: Yong Wang (yongwangbis@aliyun.com), Yan Li (yli@gzu.edu.cn)

Academic editor: Thorsten Lumbsch | Received 15 June 2022 | Accepted 4 July 2022 | Published 26 July 2022

Citation: Wang S-Y, Wang Y, Li Y (2022) *Cladosporium* spp. (Cladosporiaceae) isolated from *Eucommia ulmoides* in China. MycoKeys 91: 151–168. https://doi.org/10.3897/mycokeys.91.87841

Abstract

Eucommia ulmoides is a rare tree species in China with high medicinal and gum value. Nine strains of hyphomycetous fungi were isolated from the leaf litter of *E. ulmoides* in Guizhou Province. Preliminary identifications based on ITS indicated that they belong to the genus *Cladosporium*. Morphology and phylogenetic analyses based on the internal transcribed spacer regions (ITS) of the nrDNA, the partial translation elongation factor 1-α (*tef1*) gene and partial of actin (*act*) gene confirmed that the strains represent four species, including two novel taxa, viz., *Cladosporium eucommiae* and *C. guizhouense* and two new substrate records for known species.

Keywords

Asexual morphs, new species, phylogeny, taxonomy

Introduction

Eucommia ulmoides Oliver ('du-zhong' in Chinese), the single extant species of *Eucommiaceae* (related to *Ulmaceae*), is a dioecious, wind-pollinated tree evenly distributed in mixed mesophytic forest habitats of valleys, hills, and low mountains in central and eastern China (Cronquist 1981; Zhang 2016). *E. ulmoides* is widely cultivated in China and other countries owing to its high medicinal and gum value.

The fungal genus *Cladosporium* was established by Link (1816). *Cladosporium* (*Cladosporiaceae*) is a ubiquitous genus in *Dothideomycetes* (Abdollahzadeh et al. 2020). This genus is widely distributed throughout the world and isolated from various sources such as air, soil, plants, food, debris, cloth, paint and other organic materials (Ellis 1977; Bensch et al. 2010, 2012, 2018; Temperini et al. 2018; Chung et al. 2019). Most *Cladosporium* species are saprobic (Bensch et al. 2010), and they occur on various senescing and dead leaves and stems of herbaceous and woody plants (Brown et al. 1998; El-Morsy 2000). The morphology of *Cladosporium* is mainly characterized by its asexual morph, which comprises differentiated conidiophores producing acropetal chains of conidia from mono- or polyblastic conidiogenous cells (Isabel et al. 2021). Both the conidiogenous cells and conidia show conidiogenous loci (scars) with a distinctive coronal structure, which is composed of a central convex dome surrounded by a raised periphery, usually thickened, refractive and dark (David 1997; Isabel et al. 2021). A molecular approach combined with morphological features has recognized more than 230 species in *Cladosporium*, which are grouped into three species complexes, i.e., the *C. cladosporioides*, *C. herbarum* and *C. sphaerospermum* complex (Schubert et al. 2007; Bensch et al. 2010, 2012, 2015, 2018; Sandoval-Denis et al. 2016; Marin-Felix et al. 2017).

In a recent research program, we have carried out a survey of micro-fungi associated with *E. ulmoides* in a forest in China. In this study, four *Cladosporium* taxa were isolated from fallen leaves of this plant species in Guizhou Province, including two new species, namely *C. eucommiae* and *C. guizhouense* spp. nov., which are introduced based on morphology and phylogenetic analyses. Newly generated molecular data, descriptions and illustrations of *C. tenuissimum* and *C. perangustum* are also provided herein.

Materials and methods

Sample collection and fungal strains isolation

Fallen leaves of *E. ulmoides* were collected in a forest plantation of Guizhou University, Guiyang, Guizhou Province, China, in January 2021. The samples were stored in envelopes and several topsoil samples from the forest were stored in self-sealing bags, then taken back to the laboratory and photographed. Before isolation, collected leaves samples were sprayed two to three times with 75% ethanol to disinfect the leaf surface. Pure cultures of the fungi were obtained by single spore isolation (Chomnunti et al. 2014). Fungi in the soil samples were isolated by the dilution plate method (Zhang et al. 2015). A small amount of soil (1 g) per sample was collected and added to 9 mL of sterile water in a 15 mL sterile glass test tube. It was manually mixed and then the suspension was diluted to a series of concentrations (10^{-1}, 10^{-2}, 10^{-3}, 10^{-4}, 10^{-5} and 10^{-6}), and 100 μL from each concentration was spread onto 90-mm-diam

Petri dishes containing Synthesis of low nutrient Agar (SNA), Potato Dextrose Agar (PDA), Malt Extract Agar (MEA) and Oatmeal Agar (OA) (Zhang et al. 2017). These SNA, PDA, MEA and OA plates were incubated at constant temperature (25 °C) in a controlled temperature light incubator. Holotype specimens of the new species were conserved in the Herbarium of the Department of Plant Pathology, Agricultural College, Guizhou University (**HGUP**). Ex-type cultures were conserved in the Culture Collection at the Department of Plant Pathology, Agriculture College, Guizhou University, P.R. China (**GUCC**).

Morphological description

Pure cultures were grown on SNA, PDA, MEA and OA media in a constant temperature incubator (25 °C). Culture characteristics were recorded and examined using a dissecting microscope (LEICA S9i, Germany). The morphological observations and measurements on SNA were made using a Zeiss Scope 5 compound microscope (Axioscope 5, China) with an attached camera AxioCam 208 color (ZEN 3.0) and measurements were made using ZEN 3.0. Taxonomic information for the two new taxa were deposited in MycoBank (www.mycobank.org).

DNA extraction, PCR amplification and sequencing

Fresh mycelia were scraped from the PDA plates with a sterilized scalpel. Genomic DNA was extracted using Fungal gDNA Kit (Biomiga #GD2416, San Diego, California, USA) in accordance with the manufacturer's instructions. PCR amplification was performed in a 25 μL reaction volume following Liang et al. (2018). Primer pairs ITS4/ITS5 (White et al. 1990), EF1-728F/EF1-986R (Carbone and Kohn 1999) and ACT-512F/ACT-783R (Carbone and Kohn 1999) were used for ITS, *tef1* and *act*, respectively. The amplification procedures were performed using the method described by Halo et al. (2019). Purification and sequencing of these three gene loci were carried out by the SinoGenoMax company (Beijing, China).

Phylogeny

Sequences used in this study (Table 1) were assembled based on the closest matches from the BLASTn search results (https://blast.ncbi.nlm.nih.gov/Blast.cgi) and previous publications (Sandoval-Denis et al. 2016; Bensch et al. 2018; Halo et al. 2019). Alignments were conducted with the online version of MAFFT v. 7.307 (Katoh and Standley 2016), checked visually and improved manually where necessary using BioEdit v. 7.1.3.0 (Hall 1999). SequenceMatrix v. 1.7.8 (Vaidya et al. 2011) was used to concatenate the aligned sequences of the different loci. Ambiguous areas were excluded from the analysis using AliView (Larsson 2014) and gaps were coded as missing data.

Table 1. Taxa used for molecular phylogenetic analyses and their GenBank accession numbers. Newly generated sequences are in bold. ([T]) = ex-holotype strain, ([ET]) = ex-epitype strain, ([NT]) = ex-neotype strain.

Species	Strain number	Host	Country	GenBank Accession number		
				ITS	*tef1*	*act*
Cladosporium angulosum	CBS 140692[T]	Man, bronchoalveolar lavage fluid	USA	LN834425	LN834521	LN834609
C. angulosum	CPC 11526	Acacia mangium	Thailand	HM148127	HM148371	HM148616
C. anthropophilum	CBS 140685[T]	Man, bronchoalveolar lavage fluid	USA	LN834437	LN834533	LN834621
C. anthropophilum	CBS 117483	–	USA	HM148007	HM148248	HM148494
C. anthropophilum	CPC 22272	Indoor air sample, ship	USA	MF574171	MF574173	MF574175
C. cladosporioides	CBS 101367	Soil	Brazil	HM148002	HM148243	HM148489
C. cladosporioides	CBS 112388	Air, indoor environment	Germany	HM148003	HM148244	HM148490
C. cladosporioides	CBS 113738	*Grape bud*	USA	HM148004	HM148245	HM148491
C. colocasiae	CBS 386.64T	*Colocasia esculenta*	Taiwan	HM148067	HM148310	HM148555
C. colocasiae	CBS 119542	*Colocasia esculenta*	Japan	HM148066	HM148309	HM148554
***C. eucommiae* sp. nov.**	**GUCC 401.1[T]**	**Fallen leaves of *Eucommia ulmoide*s**	**China**	**OL587465**	**OL504966**	**OL519775**
***C. eucommiae* sp. nov.**	**GUCC 401.9**	**Fallen leaves of Eucommia ulmoides**	**China**	**ON334729**	**–**	**ON383337**
***C. guizhouense* sp. nov.**	**GUCC 401.7[T]**	**Fallen leaves of *Eucommia ulmoides***	**China**	**OL579741**	**OL504965**	**OL519780**
***C. guizhouense* sp. nov.**	**GUCC 401.8**	**Fallen leaves of *Eucommia ulmoides***	**China**	**ON334728**	**ON383470**	**ON383338**
C. magnoliigena	MFLUCC 18-1559[T]	*Magnolia grandiflora*	China	MK347813	MK340864	–
C. magnoliigena	MFLUCC 18-1557	*Magnolia grandiflora*	China	MK347811	MK340862	–
C. oxysporum	CBS 125991[T]	Soil, near the terracotta army	China	HM148118	HM148362	HM148607
C. oxysporum	CBS 126351	Indoor air	Venezuela	HM148119	HM148363	HM148608
C. perangustum	**GUCC 401.6**	**Fallen leaves of *Eucommia ulmoides***	**China**	**OL579742**	**OL581726**	**OL519779**
C. perangustum	CBS 125996[T]	*Cussonia sp.*	South Africa	HM148121	HM148365	HM148610
C. perangustum	CPC 12216	*Morus rubra*	Germany	HM148135	HM148379	HM148624
C. perangustum	CPC 14247	*Magnolia sp.*	USA	HM148145	HM148389	HM148634
C. perangustum	CPC 13870	*Teratosphaeria fibrillosa*	South Africa	HM148142	HM148386	HM148631
C. perangustum	DTO 323-E4	Indoor air	China	MF473180	MF473602	MF474028
C. perangustum	CPC 22297	Indoor air sample	USA	MF473172	MF473595	MF474020
C. rectoides	CBS 125994[T]	*Vitis flexuosa*	South Korea	HM148193	HM148438	HM148683
C. tenuissimum	**GUCC 401.2**	**Fallen leaves of *Eucommia ulmoides***	**China**	**OL579746**	**OL504967**	**OL519776**
C. tenuissimum	**GUCC 401.3**	**Fallen leaves of *Eucommia ulmoides***	**China**	**OL579745**	**OL505077**	**–**
C. tenuissimum	**GUCC 401.4**	**Fallen leaves of *Eucommia ulmoides***	**China**	**OL579744**	**OL581724**	**OL519777**
C. tenuissimum	**GUCC 401.5**	**Fallen leaves of *Eucommia ulmoides***	**China**	**OL579743**	**OL581725**	**OL519778**
C. tenuissimum	CBS 125995[ET]	*Lagerstroemia sp.*	USA	HM148197	HM148442	HM148687
C. tenuissimum	CPC 12795	*Musa sp.*	Polynesia	HM148209	HM148454	HM148699
C. tenuissimum	CBS 126359	*Musa sp.*	USA	HM148198	HM148443	HM148688
C. tenuissimum	CPC 10882	*Gnaphalium affine*	South Korea	HM148204	HM148449	HM148694
C. tenuissimum	CPC 10538	*Musa sp.*	Mozambique	HM148202	HM148447	HM148692
C. tenuissimum	DTO 323-C5	Indoor air	China	MF473289	MF473712	MF474139
C. tenuissimum	CPC 13252	Rock	Australia	HM148216	HM148461	HM148706

Species	Strain number	Host	Country	GenBank Accession number		
				ITS	*tef1*	*act*
C. tenuissimum	CPC 13732	*Shorea siamensis*	Laos	HM148217	HM148462	HM148707
C. tenuissimum	CPC 14196	*Basella alba*, leaves	Laos	HM148218	HM148463	HM148708
C. xanthochromaticum	CPC 11609[T]	Man, bronchoalveolar lavage fluid	USA	EF679356	EF679431	EF679508
C. xanthochromaticum	CBS 126364	*Erythrophleum chlorostachys*	Australia	HM148122	HM148366	HM148611
C. xylophilum	CBS 125997[T]	*Picea abies*, dead wood	Russia	HM148230	HM148476	HM148721
C. langeronii	CBS 189.54[T]	Man, mycosis	Brazil	DQ780379	JN906990	EF101357
C. neolangeronii	CBS 797.97[T]	Indoor environment	Netherlands	MF473143	MF473576	MF473992

The Maximum Likelihood (ML) analyses were carried out at the CIPRES web portal (Miller et al. 2010) using RAxML (Stamatakis 2006). The tree search included 1,000 non-parametric bootstrap replicates and the best scoring tree was selected from suboptimal trees under the GTRGAMMA substitution model. The resulting replicates were plotted on to the best scoring tree obtained previously. Non-parametric bootstrap analysis was implemented with 1,000 duplicates. Maximum Parsimony (MP) analyses were performed with PAUP v. 4.0a (Swofford 2003), using the heuristic search option with 1,000 random sequence addition replicates and tree bisection-reconnection (TBR) with reconnection limit (=8) as the branch swapping algorithm. Max-trees was set at 5,000. Branches collapsed (creating polytomies) if maximum branch length is zero. The Tree Length (TL), Consistency Indices (CI), Retention Indices (RI), Rescaled Consistency Indices (RC) and Homoplasy Index (HI) were calculated for each tree generated. Bayesian Inference (BI) analyses were performed in MrBayes v. 3.2.7a (Ronquist et al. 2012). Six Markov chain Monte Carlo runs were started, and the random start trees were calculated for 50,000,000 generations and sampled every 1,000 generations. 25% of the trees initially produced were discarded as burn-in. ML bootstrap support (MLBS) and MP bootstrap support (PBS) equal or greater than 70% (Hillis and Bull 1993) and Bayesian posterior probabilities (PP) equal or greater than 0.95 (Hespanhol et al. 2019) are displayed on the edited phylogenetic tree. The phylogenetic tree was drawn with FigTree v. 1.4.4 (Rambaut 2009).

Genealogical Phylogenetic Species Recognition (GCPSR) analysis

Morphological and phylogenetically related species were analyzed using the genealogical consistency phylogenetic species identification (GCPSR) model as described by Taylor et al. (2000) by pin-pair homogeneity index test (PHI) (Bruen et al. 2006). The PHI tests were performed in SplitsTree v. 4.17.1 (Huson 1998; Huson and Bryant 2006) as described by Quaedvlieg et al. (2014) to determine the level of recombination within phylogenetically closely related species. The results can be visualized by constructing a split graph using LogDet conversion and the Splits options. The hypothesis of this analysis is if the PHI value is below 0.05 ($\Phi w < 0.05$), there is significant evidence for the presence of recombination.

Results

Phylogenetic analysis

DNA sequences used in this study (Table 1) were selected to obtain phylogenetic trees based on the closest matches by the BLASTn search with strain GUCC 401.6 and eight strains (GUCC 401.1–401.5 to GUCC 401.7–401.9), respectively, with outgroup *C. neolangeronii* (CBS 797.97) and *C. langeronii* (CBS 189.54). The final alignment (GUCC 401.6) of ITS, *tef1* and *act* comprised 1,033 characters, viz. ITS: 1–543, *act*: 544–770 and *tef1*: 771–1033, which included 843 constant characters, 38 variable characters and 152 parsimony-informative characters, and the alignment (GUCC 401.1–GUCC 401.9 except for GUCC 401.6) comprised 1,040 characters, viz., ITS: 1–544, *act*: 545–780 and *tef1*: 781–1040; which included 813 constant characters, 46 variable characters and 181 parsimony-informative characters. The RAxML results were selected to show the topology (Fig. 1 for GUCC 401.6 and Fig. 2 for GUCC 401.1–GUCC 401.9 except for GUCC 401.6), because the MP and Bayesian analyses resulted in similar topologies. The parameter settings that were used are shown in Table 3.

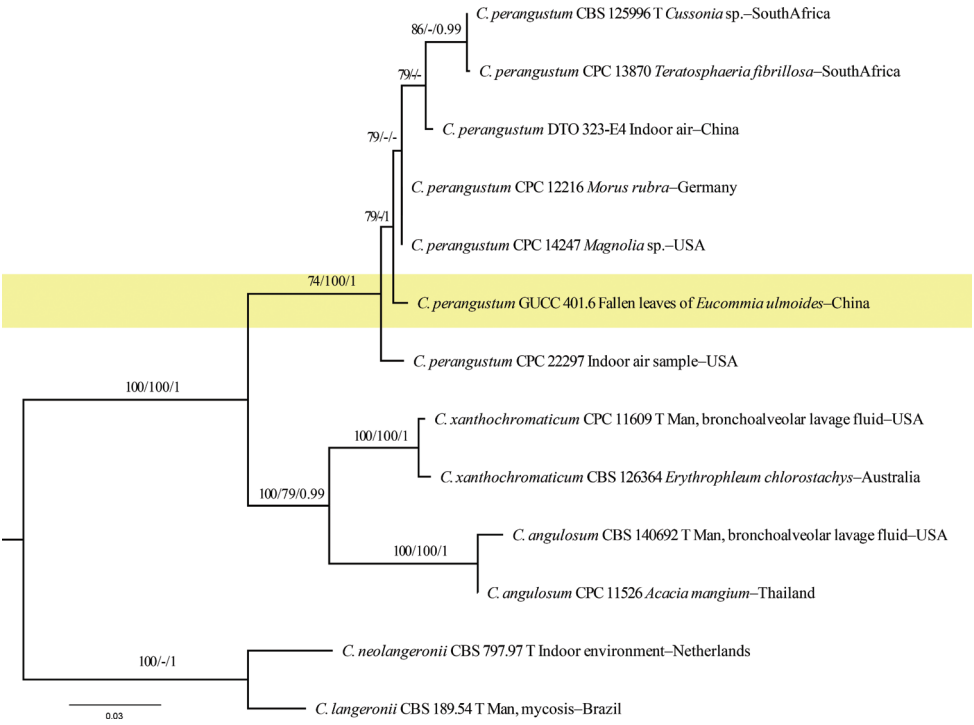

Figure 1. Maximum Likelihood (RAxML) tree from the combined analysis of ITS, *tef1* and *act* sequences of *Cladosporium*, which includes our strain GUCC 401.6. The tree was rooted with *C. neolangeronii* (CBS 797.97) and *C. langeronii* (CBS 189.54). ML and MP bootstrap values (≥ 70%) and Bayesian posterior probability (≥ 0.95) are indicated along branches (ML/MP/PP). Our species is highlighted with a yellow background. T = ex-holotype strain.

GUCC 401.6 clustered very close to *C. perangustum* (CBS 125996 = ex-holotype strain) with relatively high statistical support (79% MLBS/1 PP) (Fig. 1). Strains GUCC 401.2, GUCC 401.3, GUCC 401.4 and GUCC 401.5 had a very close relationship to *C. tenuissimum* (CBS 125995), variedly supported by MLBS (93%), PBS (70%) and PP (1) (Fig. 2). The comparison of DNA bases (Table 2) showed that our strains cluster with the ex-type strain of *C. tenuissimum* (CBS 125995, ex-epitype strain) with only one base pair difference in the ITS, two to fifteen base pair difference in the *tef1*, and one to five base pair difference in the *act*. *Cladosporium eucommiae* (GUCC 401.1) is a sister

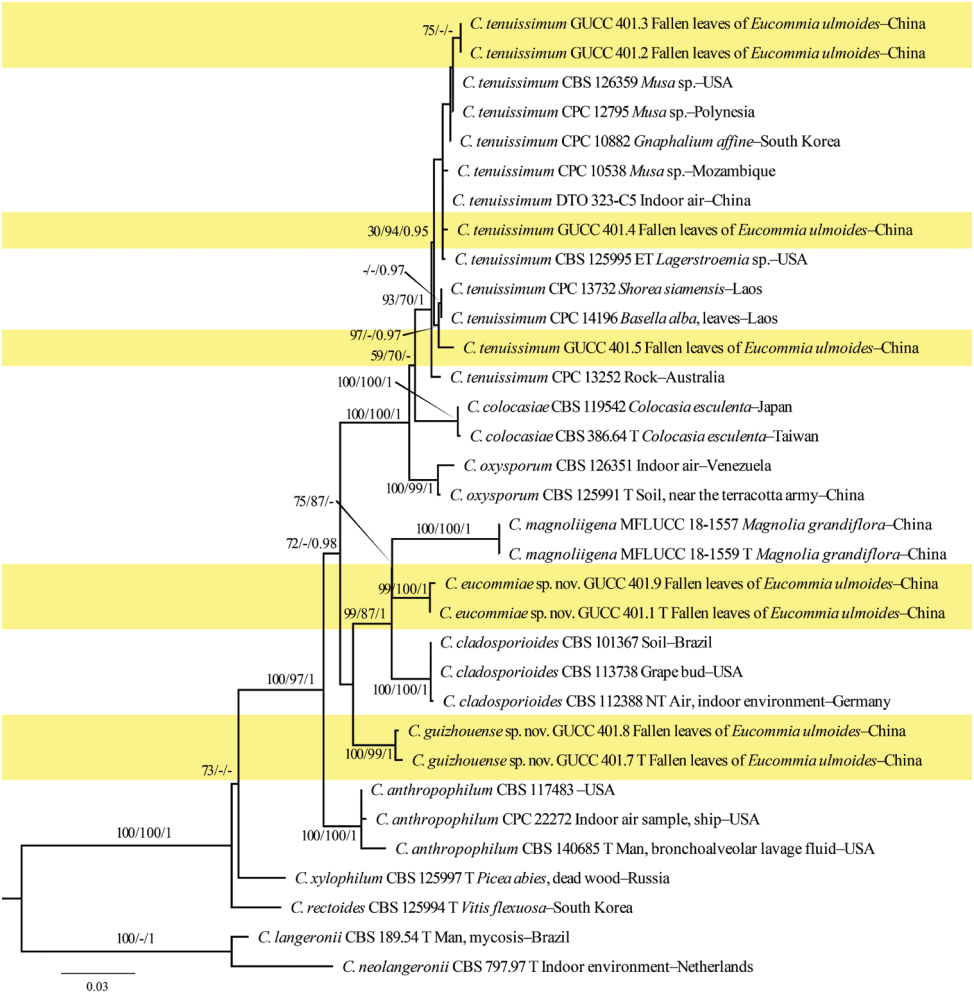

Figure 2. Maximum Likelihood (RAxML) tree from the combined analysis of ITS, *tef1* and *act* sequences of *Cladosporium*, which includes our strains GUCC 401.1–GUCC 401.9 (except for GUCC 401.6). The tree was rooted with *C. neolangeronii* (CBS 797.97) and *C. langeronii* (CBS 189.54). ML and MP bootstrap values (≥ 70%) and Bayesian posterior probability (≥ 0.95) are indicated along branches (ML/MP/PP). Our species are emphasized with a yellow background. T = ex-holotype strain, ET = ex-epitype strain, NT = ex-neotype strain.

to *C. magnoliigena* (MFLUCC 18-1559) and *C. cladosporioides* (CBS 101367) with high statistical support (75% MLBS / 87% MPBS)/(99 MLBS / 87% MPBS / 1 PP) (Fig. 2). The comparison of DNA bases composition (Table 2) indicated that, between *C. eucommiae* (GUCC 401.1) and *C. magnoliigena*, there were identical sequences in the ITS region, but 29 bases different in the *tef1* region. Unfortunately, *Cladosporium magnoliigena* did not have *act* sequence data for comparison. The comparison of DNA bases composition (Table 2) indicated that, between *C. eucommiae* (GUCC 401.1) and *C. cladosporioides* (CBS 112388, ex-neotype strain), there were 18 bp differences in the *tef1* region, and 13 in the *act* region, but without difference in the ITS sequences. GUCC 401.7 was closer to *C. cladosporioides* (CBS 112388, ex-neotype strain) with high support in their respective branches (100% MLBS / 99% MPBS / 1 PP)/(100% MLBS / 100% MPBS / 1 PP) (Fig. 2). The comparison of DNA bases (Table 2) reveals 29 bp difference on *tef1* and 14 bp difference in *act* between *C. guizhouense* and *C. cladosporioides* (CBS 112388, ex-neotype strain), but only 1 bp difference in ITS sequences.

The pairwise homoplasy index (PHI) test revealed that there was no significant recombination (Φw = 0.4589) between *C. eucommiae* (GUCC 401.1 and GUCC 401.9) and the related taxa *C. magnoliigena*, *C. cladosporioides*, *C. guizhouense* (GUCC

Table 2. The DNA base differences between our strains and related taxa in the three gene regions. Asterisks (*) denote our material.

Species	Strain number	Gene region and alignment positions		
		ITS (1–489 characters)	***tef1* (490–718 characters)**	***act* (719–1008 characters)**
C. eucommiae sp. nov.*	GUCC 401.1^{T}	–	–	–
C. eucommiae sp. nov.*	GUCC 401.9	0	3	0
C. magnoliigena	MFLUCC 18-1559^{T}	0	29	n/a
C. magnoliigena	MFLUCC 18-1557	0	29	n/a
*C. cladosporioide*s	CBS 112388	0	18	13
C. cladosporioides	CBS 113738	0	16	13
C. cladosporioides	CBS 101367	1	16	13
		ITS (1–542 characters)	***tef1* (543–796 characters)**	***act* (797–1029 characters)**
C. tenuissimum	CBS 125995^{ET}	–	–	–
*C. tenuissimum**	GUCC 401.2	0	3	5
*C. tenuissimum**	GUCC 401.3	0	15	n/a
*C. tenuissimum**	GUCC 401.4	0	2	1
*C. tenuissimum**	GUCC 401.5	1	9	3
		ITS (1–507 characters)	***tef1* (508–743 characters)**	***act* (744–948 characters)**
*C. perangustum**	GUCC 401.6	–	–	–
C. perangustum	CBS 12599^{6}T	0	26	7
C. perangustum	CPC 13870	0	22	7
C. perangustum	DTO 323-E4	0	13	5
C. perangustum	CPC 12216	0	2	5
C. perangustum	CPC 14247	0	2	5
		ITS (1–480 characters)	***tef1* (481–728 characters)**	***act* (729–933 characters)**
C. guizhouense sp. nov.*	GUCC 401.7^{T}	–	–	–
C. guizhouense sp. nov.*	GUCC 401.8	0	3	2
C. cladosporioides	CBS 112388	1	29	14
C. cladosporioides	CBS 113738	1	27	14
C. cladosporioides	CBS 101367	2	27	14

Table 3. The parameters of MP and Bayesian methods in this study.

Strain number	MP						Bayesian		
	TL	PT	CI	RI	RC	HI	Model	Unique site patterns	ASDSF
GUCC 401.1 –GUCC 401.9 (except for GUCC 401.6)	400	300	0.7475	0.8648	0.6464	0.2525	ITS: JC+I; *tef1*: GTR+G; *act*: HKY+G	Division 1 = 54 Division 2 = 99 Division 3 = 154	0.009875
GUCC 401.6	281	2	0.8505	0.8817	0.7499	0.1495	ITS: SYM; *tef1*: GTR+G; *act*: GTR+G	Division 1 = 30 Division 2 = 75 Division 3 = 128	0.009961

TL: Tree length; PT: Parsimonious tree; CI: Consistency Indices; RI: Retention Indices; RC: Rescaled Consistency Indices HI: Homoplasy Index; Model: the models used for the different partitions; ASDSF: average standard deviation of split frequencies.

401.7 and GUCC 401.8). The PHI test did not find any statistically significant evidence for recombination (Φw = 0.02487) between our four strains (GUCC 401.2, GUCC 401.3, GUCC 401.4 and GUCC 401.5) and the related taxon *C. tenuissimum* (CBS 126359, ex-epitype strain, CPC 12795, CPC 10882, CPC 10538, DTO 323-C5, CBS 125995, CPC 13732, CPC 14196 and CPC 13252). Based on the PHI test, there was a statistically significant recombination (Φw = 0.0104) between GUCC 401.6 and the related taxon *C. perangustum* (CBS 125996, = ex-holotype strain, CPC 13870, DTO 323-E4, CPC 12216, CPC 14247 and CPC 22297).

Taxonomy

In this section, we introduced two new species and report two new substrate records.

Cladosporium eucommiae **S.Y. Wang, Yong Wang bis & Y. Li, sp. nov.**
MycoBank No: 842406
Fig. 3a–h

Etymology. *eucommiae*, in reference to the genus name of the host plant (*Eucommia ulmoides*), from which the fungus was isolated.

Type. China, Guizhou Province, Guiyang, Huaxi district, plantation forest of *E. ulmoides*, Guizhou University (26°24'16"N, 106°40'29"E), on fallen leaves of *E. ulmoides*, S.Y. Wang, Y. Wang & Y. Li, 13 January 2021 (HGUP 401.1, ***holotype***; ex-type living culture GUCC 401.1; additional living culture GUCC 401.9).

Description. Saprobic on fallen leaves of *Eucommia ulmoides*. **Sexual morph:** Not developed. **Asexual morph**: Hyphomycetous. ***Mycelium*** abundant, superficially and submerged, overgrowing whole culture dishes, thin to dense, hyphae straight to slightly sinuous, branched, light olive-green to olive-brown, 1.5–5 µm wide, thin-walled, smooth. ***Conidiophores*** (7–)22–198 × 2.5–4.5 µm ($\bar{x}$ = 77.2 × 3.3 µm; n = 20), erect, branching, slightly attenuated towards the apex, light olive-green, smooth and thick-walled. ***Conidia*** 3–9 × 2.5–4.5 µm ($\bar{x}$ = 5.6 × 3.3 µm; n = 30), in simple and branched acropetal chains, mostly light olive, aseptate, smooth-walled and thin-walled, variable in size and shape, subglobose, ellipsoid-ovoid, obovoid, fusiform, subcylindrical.

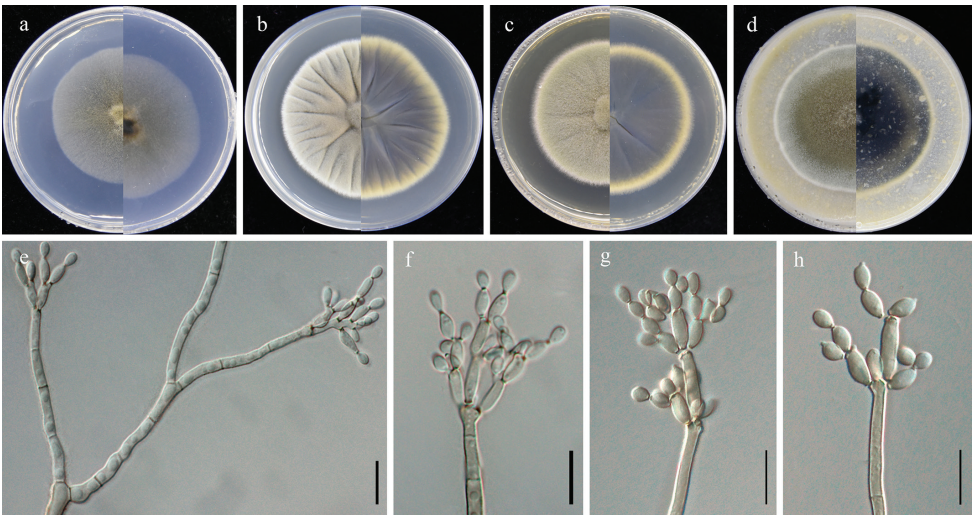

Figure 3. *Cladosporium eucommiae* (GUCC 401.1, ex holotype strain). **a–d** colonies on SNA, PDA, MEA and OA (left: above, right: reverse) **e** branching conidiophore, secondary ramoconidia and conidia on SNA **f–h** conidiogenous cells, secondary ramoconidia and conidia on SNA. Scale bars: 10 μm (**e–h**).

Secondary ramoconidia 5–25 × 2.5–4.0 μm ($\overline{x}$ = 11.9 × 3.4 μm; n = 30), olive-green, ellipsoid-ovoid, obovoid, fusiform, subcylindrical, aseptate, smooth-walled and thin-walled, rarely thick-walled.

Culture characteristics. ***Colonies*** on SNA 35–45 mm diam, after 2 weeks at 25 °C, pale olive, flat, velvety, with a regular edge, reverse light olive. ***Colonies*** on PDA 30–45 mm diam, after 2 weeks at 25 °C, olive-brown to gray-olive to iron-gray, with a regular white edge, irregularly folded, slightly depressed at the center, thatched, and often forming a bulge in the colony kernel, reverse olive to dark olive, with a whitish final edge. ***Colonies*** on MEA 35–45 mm diam, after 2 weeks at 25 °C, gray-green to olive, less radially furrowed, velvety, with an even gray white edge, reverse olive to dark olive, with an even gray-green final edge. ***Colonies*** on OA 35–40 mm diam, after 2 weeks at 25 °C, olive to gray-green, white at the final edge, flat, velvety, margin regular; reverse dark green to black, with a whitish final edge.

GenBank numbers. ITS: OL587465, *tef1*: OL504966, *act*: OL519775 (GUCC 401.1); ITS: ON334729, *act*: ON383337 (GUCC 401.9).

Cladosporium guizhouense **S.Y. Wang, Yong Wang bis & Y. Li, sp. nov.**
MycoBank No: 842407
Fig. 4a–h

Etymology. guizhouense, in reference to the type location (Guizhou Province), where the fungus was isolated.

Type. China, Guizhou Province, Guiyang, Huaxi district, plantation forest of *Eucommia ulmoides*, Guizhou University (26°24'16"N, 106°40'29"E), on fallen leaves of *E. ulmoides*, S.Y. Wang, Y. Wang & Y. Li, 13 January 2021 (HGUP 401.6, ***holotype***; living culture GUCC 401.7; additional living culture GUCC 401.8).

Description. Saprobic on fallen leaves of *Eucommia ulmoides*. **Sexual morph**: Not developed. **Asexual morph**: Hyphomycetous. ***Mycelium*** abundant, submerged, overgrowing whole culture dishes, hyphae straight to slightly sinuous, septate, branching, light olive-green to olive-brown, mostly smooth- and thin-walled, 1.5–6 µm wide. ***Conidiophores*** 13–100 × 3–4.5 µm ($\bar{x}$ = 60.8 × 3.5 µm; n = 10), erect, branching, light olive-green, smooth- and thin-walled. ***Conidia*** 3–7.5 × 2.5–4 µm ($\bar{x}$ = 4.8 × 3.1 µm; n = 30), in simple and branched acropetal chains, mostly light olive, aseptate, mostly smooth- and thin-walled, variable in size and shape, ellipsoid-ovoid, obovoid, fusiform. ***Secondary ramoconidia*** 6.5–23 × 3–5.5 µm ($\bar{x}$ = 11.3 × 4.1 µm; n = 30), pale olive-green, narrowly ellipsoid to cylindrical-oblong, subcylindrical, aseptate, smooth- and thin-walled.

Culture characteristics: ***Colonies*** on SNA 45–55 mm diam, after 2 weeks at 25 °C, pale olive, flat, velvety, margin regularly, reverse light olive. ***Colonies*** on PDA 40–50 mm diam, after 2 weeks at 25 °C, smoke-gray to light olive-gray, reverse leaden-gray, gray-olive at edge both surface and reverse, woolly or felty, broad edge, regular, growth low convex, without protuberant exudates, reverse formed cracks in the middle small circle. ***Colonies*** on MEA 30–40 mm diam, after 2 weeks at 25 °C, smoke-gray to light olive-gray, woolly or felty, fluffy, with a whitish narrow final edge; reverse olive-yellow or olive-brown, radially furrowed, irregularly folded, with

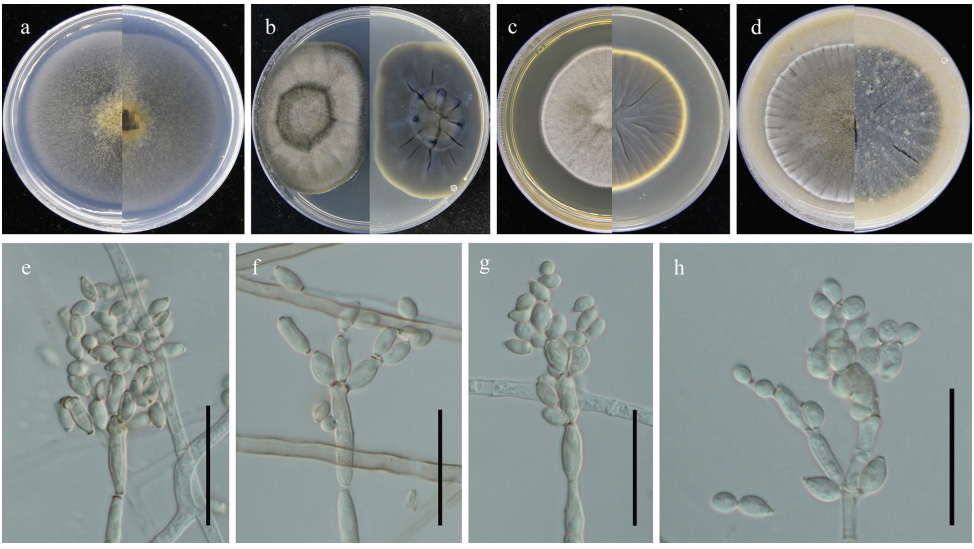

Figure 4. *Cladosporium guizhouense* (GUCC 401.7). **a–d** colony on SNA, PDA, MEA and OA (left: above, right: reverse) **e–h** conidiogenous cells, secondary ramoconidia and conidia on SNA. Scale bars: 10 µm (**e–h**).

a whitish narrow final edge. ***Colonies*** on OA 30–45 mm diam, after 2 weeks at 25 °C, gray-green or olive, granular and fluffy mycelium, woolly and felty edge, with an irregularly folded whitish and olive final edge; reverse olive-yellow or olive-brown, with a whitish narrow final edge.

GenBank numbers. ITS: OL579741, *tef1*: OL504965, *act*: OL519780 (GUCC 401.7); ITS: ON334728, *tef1*: ON383470, *act*: ON383338 (GUCC 401.8).

Cladosporium perangustum **Bensch, Crous & U. Braun, Studies in Mycology 67: 65 (2010)**

MycoBank No: 517085

Fig. 5a–h

Material examined. China, Guizhou Province, Guiyang, Huaxi district, plantation forest of *E. ulmoides*, Guizhou University (26°24'16"N, 106°40'29"E), on fallen leaves of *E. ulmoides*, S.Y. Wang, Y. Wang & Y. Li, 13 January 2021 (HGUP 401.6, living culture GUCC 401.6) (new substrate record).

Description. Saprobic on fallen leaves of *Eucommia ulmoides*. **Sexual morph**: Not developed. **Asexual morph**: Hyphomycetous. ***Mycelium*** superficial, hyphae branched, hyaline to subhyaline, 2.5–5 µm wide, usually slightly constricted at the septa and some-

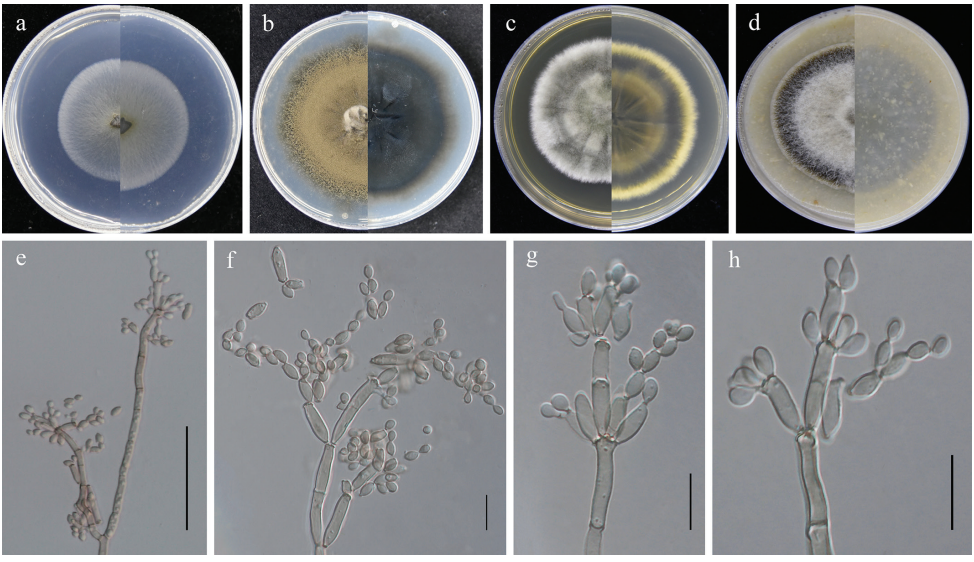

Figure 5. *Cladosporium perangustum* (GUCC 401.6, new substrate record from Guizhou Province). **a–d** colonies on SNA, PDA, MEA and OA (left: above, right: reverse) **e** branching conidiophore, secondary ramoconidia and conidia on SNA **f–h** conidiogenous cells, secondary ramoconidia and conidia on SNA. Scale bars: 50 µm (**e**); 10 µm (**f–h**).

what swollen, smooth to somewhat verruculose or irregularly rough-walled. ***Conidiophores*** macro- and micronematous, 14–167 × 2.5–4.5 µm ($\bar{x}$ = 65.4 × 3.4 µm; n = 20), erect, branched, slightly attenuated towards the apex, light olive-green, smooth and thick-walled. ***Conidia*** in acropetal chains, 2–9.5 × 2–4 µm ($\bar{x}$ = 5.6 × 3.3 µm; n = 30) mostly light olive-green, aseptate, mostly smooth-walled and thin-walled, variable in size and shape, subglobose, ellipsoid-ovoid, obovoid, fusiform. ***Secondary ramoconidia*** 6–24 × 2–5.5 µm ($\bar{x}$ = 11.2 × 3.3 µm; n = 30), olive-green, narrowly ellipsoid to cylindrical-oblong, subcylindrical, aseptate, rarely 1-septate, mostly smooth-walled and thick-walled.

Culture characteristics. ***Colonies*** on SNA 30–40 mm diam, after 2 weeks at 25 °C, pale olive to pale whitish, flat, velvety, with a regular edge, reverse light olive to light white. ***Colonies*** on PDA 30–40 mm diam, after 2 weeks at 25 °C, olive-gray to olive-green or olive-brown, powdery or flocculent, fluffy, regular, radially furrowed, lacerated or feathery, and often forming a gray-white or olive bulge in the colony kernel; reverse dark olive or dull green to black. ***Colonies*** on MEA 35–45 mm diam, after 2 weeks at 25 °C, gray-green to white or gray-white, fluffy, radially furrowed, with a whitish final edge; reverse olive-yellow to olive-gray to olive-green, with a whitish final edge. ***Colonies*** on OA 35–45 mm diam, after 2 weeks at 25°C, white to olive-green, with a pale gray final edge, velvety or fluffy, margins colorless or pale gray, glabrous, regular; reverse olive-green to dark green.

GenBank numbers. ITS: OL579742, *tef1*: OL581726, *act*: OL519779.

Cladosporium tenuissimum **Cooke, Grevillea 6: 140 (1878)**
MycoBank No: 145672
Fig. 6a–i

Materials examined. China, Guizhou Province, Guiyang, Huaxi district, plantation forest of *E. ulmoides*, Guizhou University (26°24'16"N, 106°40'29"E), on fallen leaves of *E. ulmoides*, S.Y. Wang, Y. Wang & Y. Li, 13 January 2021, (HGUP 401.1; HGUP 401.2; HGUP 401.3 and HGUP 401.4, living cultures GUCC 401.2; GUCC 401.3; GUCC 401.4 and GUCC 401.5) (new substrate record).

Description. Saprobic on fallen leaves of *Eucommia ulmoides*. **Sexual morph**: Not developed. **Asexual morph**: Hyphomycetous. ***Mycelium*** abundant, superficial and submerged, overgrowing whole culture dishes, hyphae straight to slightly sinuous, septate, branching, light olive-green to olive-brown, smooth-walled, 1.5–6 µm wide. ***Conidiophores*** 13–100 × 2.5–4.5 µm ($\bar{x}$ = 60.8 × 3.6 µm; n = 10), erect, branching, light olive-green, smooth and thin walled. ***Conidia*** 2.5–7.5 × 2–4 µm ($\bar{x}$ = 4.9 × 3.2 µm; n = 30), in simple and branched acropetal chains, mostly light olive-green, aseptate, mostly smooth- and thin-walled, variable in size and shape, subglobose, ellipsoid-ovoid, obovoid, fusiform. ***Secondary ramoconidia*** 5.5–23 × 2.5–5.5 µm ($\bar{x}$ = 0.9 × 3.8 µm; n = 30), pale olive-green, narrowly ellipsoid to cylindrical-oblong or subcylindrical, sometimes septate and sometimes aspetate (1-septate appear at maturity), smooth- and thin-walled.

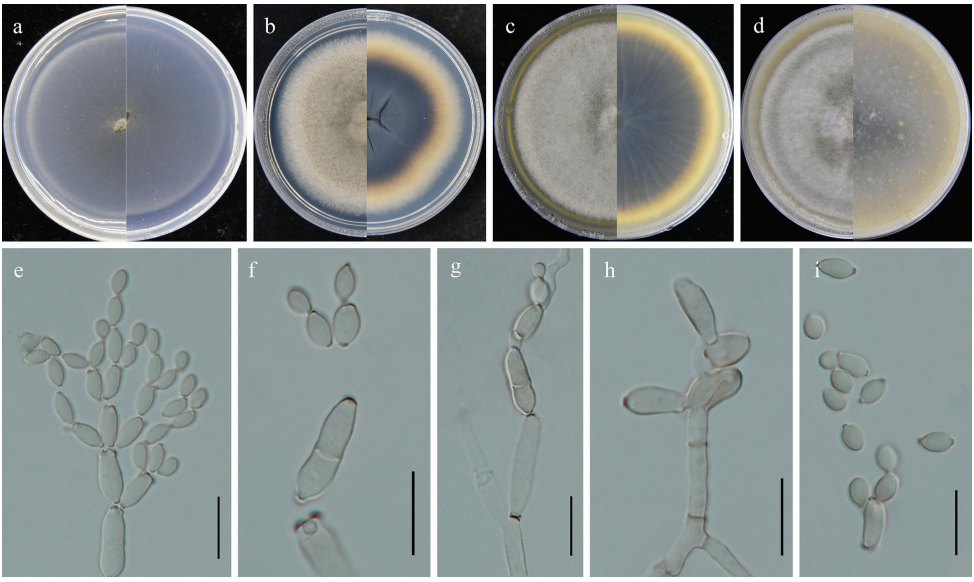

Figure 6. *Cladosporium tenuissimum* (GUCC 401.2, new substrate record from Guizhou Province). **a–d** colonies on SNA, PDA, MEA and OA (left: above, right: reverse) **e–h** secondary ramoconidia and conidia on SNA **i** conidia on SNA. Scale bars: 10 μm (**e–i**).

Culture characteristics: ***Colonies*** on SNA 50–55 mm diam, after 2 weeks at 25 °C, pale olive to pale white, flat, velvety, with a regular edge, reverse light olive to light white. ***Colonies*** on PDA 40–55 mm diam, after 2 weeks at 25 °C, smoke-gray to light olive-gray or olive to light olive-gray, reverse leaden-gray, gray-olive at edge both surface and reverse, woolly or felty, broad edge, regular, growth low convex, without protuberant exudates, occasionally reverse formed a sunflower like shape in the middle. ***Colonies*** on MEA 40–50 mm diam, after 2 weeks at 25 °C, olive-gray or gray, fluffy; reverse olive-green to dark olive, with an olive-yellow to gray-white edge, radially furrowed. ***Colonies*** on OA 40–60 mm diam, after 2 weeks at 25 °C, gray-white or iron-gray to gray-olive, fluffy to felty; reverse olive-brown to olive.

GenBank numbers. ITS: OL579746, *tef1*: OL504967, *act*: OL519776 (GUCC 401.2); ITS: OL579745, *tef1*: OL505077 (GUCC 401.3); ITS: OL579744, *tef1*: OL581724, *act*: OL519777 (GUCC 401.4); ITS: OL579743, *tef1*: OL581725, *act*: OL519778 (GUCC 401.5).

Discussion

In this paper, we revealed four *Cladosporium* taxa on fallen leaves of *E. ulmoides*, two of which are described here as new to science. Phylogenetic analyses showed that *C. eucommiae* is different from *C. magnoliigena* (Jayasiri et al. 2019), although

act sequences are not available for the latter species. Conidia of *C. eucommiae* (3–9 × 2.5–4.5 μm) are usually narrower and longer than those of *C. magnoliigena* (4.2–5.5 × 2–5 μm), while secondary ramoconidia of *C. eucommiae* are usually aseptate and longer than those of *C. magnoliigena* (5–25 × 2.5–4.0 μm *vs* 9.5–18 × 2.7–4.2 μm and 0–3-septate). Thus, the two species are clearly distinct in morphology as well as DNA sequence data. Phylogenetic analyses showed that sequences retrieved from GUCC 401.7 and GUCC 401.8 are different from those obtained from *C. cladosporioides* (CBS 112388, ex-neotype strain) (Bensch et al. 2010) by phylogenetic analyses (Fig. 2). Conidia of GUCC 401.7 and *C. cladosporioides* show no significant differences in size, color and shape, but secondary ramoconidia of GUCC 401.7 were usually shorter than those of *C. cladosporioides* (6.5–23 × 3–5.5 μm *vs* 15–50 × (2.5–)3–5 μm), and conidiophores of GUCC 401.7 (13–100 × 3–4.5 μm) were shorter than in *C. cladosporioides* (40–300(–350) × (2.5–)3–4(–5.5) μm). Therefore, there are significant differences in the morphology and DNA sequence data between the two species. The combination of morphology, phylogenetic analyses, comparison of DNA base composition and GCPSR analysis support our proposal that *C. eucommiae* and *C. guizhouense* represent two novel taxa.

Sequences retrieved from GUCC 401.6 clustered among six sequences obtained from *C. perangustum* strains (Fig. 1), but conidia of GUCC 401.6 (2–9.5 × 2–4 μm) were usually somewhat narrower and longer than CBS 125996 (Bensch et al. 2010) (2–4(–5) × (1.5–)2–2.5 μm), and secondary ramoconidia of GUCC 401.6 (6–24 × 2–5.5 μm) were wider than those of *C. perangustum* (6–30(–34) × 2–3(–3.5) μm). In addition, GUCC 401.6 can be well distinguished from *C. perangustum* by its slower growing colonies in PDA, MEA and OA (30–40, 35–45 and 35–45 mm diam/14 d), whereas CBS 125996 grew 33–76, 40–72 and 40–75 mm diam/14 d. Although morphology and phylogeny showed minor differences, GCPSR analysis supported statistically significant recombination, after careful consideration, GUCC 401.6 was identified as *C. perangustum.* The differences may be caused by different substrates or geographical regions, which needs further investigation. Conidiophores of GUCC 401.2–GUCC 401.5 were shorter than in CBS 125995 (13–100 × 2.5–4.5 μm *vs* 49–542(–800) × (3–)4–7 μm), but secondary ramoconidia and conidia (5.5–23 × 2.5–5.5 μm; 2.5–7.5 × 2–4 μm) were similar to those of *C. tenuissimum* (15–31 × 4–5 μm; 3–13 × 2–6 μm) (Cooke 1878). Sequences retrieved from our four strains cluster with sequences obtained from *C. tenuissimum* strains (Fig. 2) with minor DNA base differences. Thus, our four strains were identified as *C. tenuissimum.*

Our five strains pertain to two known species, viz., *C. perangustum* and *C. tenuissimum*, but with *E. ulmoides* as new substrate records for these species. The main focus of this study was the exploration of the diversity of microfungi associated with a *E. ulmoides* plantation forest. In previous studies, *Cladosporium parapenidielloides* was found on *Eucalyptus* sp. in Australia, *C. perangustum* on *Magnolia* sp. in the USA, and *C. pini-ponderosae* on *Pinus ponderosa* in Argentina. So far, *Cladosporium* species have never been isolated from fallen leaves of *E. ulmoides*, the only species of the genus *Eucommia*.

Acknowledgements

This research was supported by the following sources: The Open Project of Key Laboratory of Plant Resources Conservation and Germplasm Innovation in Mountainous Region (Ministry of Education) (MOELP-201801), and Postgraduate Education Innovation Program in Guizhou Province (YJSKYJJ [2021] 058). We thank Profs. Mohammed Amin Uddin Mridha and Eric HC McKenzie for improving the quality of our manuscript.

References

Abdollahzadeh J, Groenewald JZ, Coetzee M, Wingfield MJ, Crous PW (2020) Evolution of lifestyles in Capnodiales. Studies in Mycology 95: 381–414. https://doi.org/10.1016/j.simyco.2020.02.004

Bensch K, Groenewald JZ, Dijksterhuis J, Starink-Willemse M, Andersen B, Summerell BA, Shin H-D, Dugan FM, Schroers H-J, Braun U, Crous PW (2010) Species and ecological diversity within the *Cladosporium cladosporioides* complex (Davidiellaceae, Capnodiales). Studies in Mycology 67: 1–94. https://doi.org/10.3114/sim.2010.67.01

Bensch K, Braun U, Groenewald JZ, Crous PW (2012) The genus *Cladosporium*. Studies in Mycology 72: 1–401. https://doi.org/10.3114/sim0003

Bensch K, Groenewald JZ, Braun U, Dijksterhuis J, Yanez-Morales M, Crous PW (2015) Common but different: The expanding realm of *Cladosporium*. Studies in Mycology 82(1): 23–74. https://doi.org/10.1016/j.simyco.2015.10.001

Bensch K, Groenewald JZ, Meijer M, Dijksterhuis J, Jurjevic Z, Andersen B, Houbraken J, Crous PW, Samson RA (2018) *Cladosporium* species in indoor environments. Studies in Mycology 89(1): 177–301. https://doi.org/10.1016/j.simyco.2018.03.002

Brown KB, Hyde KD, Guest DI (1998) Preliminary studies on endophytic fungal communities of *Musa acuminata* species complex in Hong Kong and Australia. Fungal Diversity 1: 27–51.

Bruen TC, Philippe H, Bryant D (2006) A simple and robust statistical test for detecting the presence of recombination. Genetics 172(4): 2665–2681. https://doi.org/10.1534/genetics.105.048975

Carbone I, Kohn LM (1999) A method for designing primer sets for speciation studies in filamentous Ascomycetes. Mycologia 91(3): 553–556. https://doi.org/10.1080/00275514.1999.12061051

Chomnunti P, Hongsanan S, Aguirre-Hudson B, Tian Q, Persoh D, Dhami MK, Alias AS, Xu JC, Liu XZ, Stadler M, Hyde KD (2014) The sooty moulds. Fungal Diversity 66(1): 1–36. https://doi.org/10.1007/s13225-014-0278-5

Chung D, Kim H, Choi HS (2019) Fungi in salterns. Journal of Microbiology 57(9): 717–724. https://doi.org/10.1007/s12275-019-9195-3

Cooke MC (1878) Ravenel's American fungi. Grevillea 6: 129–146.

Cronquist A (1981) An integrated system of classification of flowering plants. Columbia University Press, New York. https://doi.org/10.2307/2806386

David JC (1997) A contribution to the systematics of *Cladosporium*. Revision of the fungi previously referred to *Heterosporium*. Mycological Papers 172: 1–157.

El-Morsy EM (2000) Fungi isolated from the endorhizosphere of halophytic plants from the Red Sea Coast of Egypt. Fungal Diversity 5: 43–54.

Ellis M (1977) More Dematiaceous Hyphomycetes. Commonwealth Mycological Institute, Kew, Surrey, England. https://doi.org/10.2307/3758674

Hall TA (1999) BioEdit: A user-friendly biological sequence alignment editor and analysis program for Windows 95/98/NT. Nucleic Acids Symposium Series 41: 95–98. https://doi.org/10.1021/bk-1999-0734.ch008

Halo BA, Maharachchikumbura SS, Al-Yahyai RA, Al-Sadi AM (2019) *Cladosporium omanense*, a new endophytic species from *Zygophyllum coccineum* in Oman. Phytotaxa 388(1): 145–154. https://doi.org/10.11646/phytotaxa.388.1.8

Hespanhol L, Vallio CS, Costa LM, Saragiotto BT (2019) Understanding and interpreting confidence and credible intervals around effect estimates. Brazilian Journal of Physical Therapy 23(4): 290–301. https://doi.org/10.1016/j.bjpt.2018.12.006

Hillis DM, Bull JJ (1993) An empirical test of bootstrapping as a method for assessing confidence in phylogenetic analysis. Systematic Biology 42(2): 182–192. https://doi.org/10.1093/sysbio/42.2.182

Huson DH (1998) SplitsTree: Analyzing and visualizing evolutionary data. Bioinformatics 14(1): 68–73. https://doi.org/10.1093/bioinformatics/14.1.68

Huson DH, Bryant D (2006) Application of phylogenetic networks in evolutionary studies. Molecular Biology and Evolution 23(2): 254–267. https://doi.org/10.1093/molbev/msj030

Isabel IG, Dania G, Josepa G (2021) Novel species of *Cladosporium* from environmental sources in Spain. MycoKeys 77: 1–25. https://doi.org/10.3897/mycokeys.77.60862

Jayasiri SC, Hyde KD, Jones EBG, Mckenzie E, Karunarathna SC (2019) Diversity, morphology and molecular phylogeny of Dothideomycetes on decaying wild seed pods and fruits. Mycosphere 10(1): 1–186. https://doi.org/10.5943/mycosphere/10/1/1

Katoh K, Standley DM (2016) A simple method to control over-alignment in the MAFFT multiple sequence alignment program. Bioinformatics 32(13): 1933–1942. https://doi.org/10.1093/bioinformatics/btw108

Larsson A (2014) AliView: A fast and lightweight alignment viewer and editor for large datasets. Bioinformatics 22(22): 3276–3278. https://doi.org/10.1093/bioinformatics/btu531

Liang Y, Ran SF, Bhat J, Hyde KD, Wang Y, Zhao DG (2018) *Curvularia microspora* sp. nov. associated with leaf diseases of *Hippeastrum striatum* in China. MycoKeys 29: 49–61. https://doi.org/10.3897/mycokeys.29.21122

Link HF (1816) Observationes in ordines plantarum naturales. 2. Magazin der Gesellschaft Naturforschenden Freunde Berlin 8: 25–45.

Marin-Felix Y, Groenewald JZ, Cai L, Chen Q, Marincowitz S, Barnes I, Bensch K, Braun U, Camporesi E, Damm U, de Beer ZW, Dissanayake A, Edwards J, Giraldo A, Hernandez-Restrepo M, Hyde KD, Jayawardena RS, Lombard L, Crous PW (2017) Genera of phytopathogenic fungi: GOPHY 1. Studies in Mycology 86(1): 99–216. https://doi.org/10.1016/j.simyco.2017.04.002

Miller MA, Pfeiffer W, Schwartz T (2010) Creating the CIPRES Science Gateway for inference of large phylogenetic trees. Proceeding of the 2010 gateway computing environments workshop (GCE), New Orleans, Louisiana, 1–8. https://doi.org/10.1109/GCE.2010.5676129

Quaedvlieg W, Binder M, Groenewald JZ, Summerell BA, Carnegie AJ, Burgess TI, Crous PW (2014) Introducing the consolidated species concept to resolve species in the Teratosphaeriaceae. Persoonia 33(1): 1–40. https://doi.org/10.3767/003158514X681981

Rambaut A (2009) FigTree, a graphical viewer of phylogenetic trees.

Ronquist F, Teslenko M, Van Der Mark P, Ayres DL, Darling A, Hohna S, Larget B, Liu L, Suchard MA, Huelsenbeck JP (2012) MrBayes 3.2: Efficient Bayesian phylogenetic inference and model choice across a large model space. Systematic Biology 61(3): 539–542. https://doi.org/10.1093/sysbio/sys029

Sandoval-Denis M, Gene J, Sutton DA, Wiederhold NP, Cano-Lira JF, Guarro J (2016) New species of *Cladosporium* associated with human and animal infections. Persoonia 36(1): 281–298. https://doi.org/10.3767/003158516X691951

Schubert K, Groenewald JZ, Braun U, Dijksterhuis J, Starink M, Hill CF, Zalar P, de Hoog GS, Crous PW (2007) Biodiversity in the C*ladosporium herbarum* complex (Davidiellaceae, Capnodiales), with standardisation of methods for *Cladosporium* taxonomy and diagnostics. Studies in Mycology 58: 105–156. https://doi.org/10.3114/sim.2007.58.05

Stamatakis A (2006) RAxML-VI-HPC: Maximum likelihood-based phylogenetic analyses with thousands of taxa and mixed models. Bioinformatics 22(21): 2688–2690. https://doi.org/10.1093/bioinformatics/btl446

Swofford DL (2003) PAUP*: Phylogenetic analysis using parsimony (and other methods), version 4.0 b10. Sinauer Associates. https://doi.org/10.1111/j.0014-3820.2002.tb00191.x

Taylor JW, Jacobson DJ, Kroken S, Kasuga T, Geiser DM, Hibbett DS, Fisher MC (2000) Phylogenetic species recognition and species concepts in fungi. Fungal Genetics and Biology 31(1): 21–32. https://doi.org/10.1006/fgbi.2000.1228

Temperini CV, Pardo AG, Pose GN (2018) Diversity of airborne *Cladosporium* species isolated from agricultural environments of northern Argentinean Patagonia: Molecular characterization and plant pathogenicity. Aerobiologia 34(2): 227–239. https://doi.org/10.1007/s10453-018-9509-7

Vaidya G, Lohman DJ, Meier R (2011) SequenceMatrix: Concatenation software for the fast assembly of multi-gene datasets with character set and codon information. Cladistics 27(2): 171–180. https://doi.org/10.1111/j.1096-0031.2010.00329.x

White T, Bruns T, Lee S, Taylor JW (1990) Amplification and direct sequencing of fungal ribosomal RNA genes for phylogenetics. In: Innis M, Gelfand D, Shinsky J, White T (Eds) PCR protocols: a guide to methods and applications 18(1): 315–322. https://doi.org/10.1016/B978-0-12-372180-8.50042-1

Zhang LB (2016) Eucommiaceae. Springer International Publishing, 193–196. https://doi.org/10.1007/978-3-319-28534-4_15

Zhang Y, Liu F, Wu W, Cai L (2015) A phylogenetic assessment and taxonomic revision of the thermotolerant hyphomycete genera *Acrophialophora* and *Taifanglania.* Mycologia 107(4): 768–779. https://doi.org/10.3852/14-173

Zhang ZF, Liu F, Zhou X, Liu XZ, Liu SJ, Cai L (2017) Culturable mycobiota from Karst caves in China, with descriptions of 20 new species. Persoonia 39(1): 1–31. https://doi.org/10.3767/persoonia.2017.39.01

MycoKeys 91: 169–197 (2022)
doi: 10.3897/mycokeys.91.84896
https://mycokeys.pensoft.net

RESEARCH ARTICLE

A peer-reviewed open-access journal
MycoKeys
Launched to accelerate biodiversity research

Two new species of *Calonectria* (Hypocreales, Nectriaceae) causing *Eucalyptus* leaf blight in Brazil

Enrique I. Sanchez-Gonzalez[1], Thaissa de Paula Farias Soares[2], Talyta Galafassi Zarpelon[2], Edival Angelo Valverde Zauza[2], Reginaldo Gonçalves Mafia[2], Maria Alves Ferreira[1]

1 *Universidade Federal de Lavras, Departamento de Fitopatologia, Lavras, MG, 37200-900, Brasil* **2** *Suzano Papel e Celulose S. A. Centro de Tecnologia, Aracruz, ES, 29197-900, Brasil*

Corresponding author: Maria Alves Ferreira (mariaferreira@ufla.br)

Academic editor: Nalin Wijayawardene | Received 5 April 2022 | Accepted 29 June 2022 | Published 29 July 2022

Citation: Sanchez-Gonzalez EI, Farias Soares TdP, Galafassi Zarpelon T, Valverde Zauza EA, Gonçalves Mafia R, Alves Ferreira M (2022) Two new species of *Calonectria* (Hypocreales, Nectriaceae) causing *Eucalyptus* leaf blight in Brazil. MycoKeys 91: 169–197. https://doi.org/10.3897/mycokeys.91.84896

Abstract

In recent decades, commercial *Eucalyptus* plantations have expanded toward the warm and humid regions of northern and northeastern Brazil, where *Calonectria* leaf blight (CLB) has become the primary fungal leaf disease of this crop. CLB can be caused by different *Calonectria* species, and previous studies have indicated that *Calonectria* might have high species diversity in Brazil. During a disease survey conducted in three commercial plantations of *Eucalyptus* in northeastern Brazil, diseased leaves from *Eucalyptus* trees with typical symptoms of CLB were collected, and *Calonectria* fungi were isolated. Based on phylogenetic analyses of six gene regions (*act*, *cmdA*, *his3*, *rpb2*, *tef1*, and *tub2*) and morphological characteristics, two new species of *Calonectria* were identified. Five isolates were named as *C. paragominensis* **sp. nov.** and four were named as *C. imperata* **sp. nov.** The pathogenicity to *Eucalyptus* of both species was confirmed by fulfilling the Koch's postulates.

Keywords

Cylindrocladium, GCPSR, phylogenetic network analysis, phylogeny

Introduction

Calonectria species are widely distributed around the world and cause diseases in more than 335 plant species, distributed among nearly 100 plant families, including forestry, agricultural and horticultural crops (Crous 2002; Lombard et al. 2010c; Vitale et al. 2013; Lombard et al. 2016; Li et al. 2021). Most reports of *Calonectria* from Brazil are focused on forestry crops, such as *Acacia*, *Eucalyptus*, and *Pinus* trees (Alfenas et al. 2015), and mainly evaluate the epidemiology and disease control of *Calonectria*-associated diseases such as *Calonectria* leaf blight (CLB), damping-off, cutting rot and root rot in commercial plantations and nurseries of *Eucalyptus* (Soares et al. 2018).

Currently, 130 *Calonectria* species have been identified based on DNA phylogenetic analyses and morphological comparisons (Crous et al. 2018, 2019, 2021a, 2021b; Wang et al. 2019; Liu et al. 2020; Mohali and Stewart 2021; Pham et al. 2022). These species are accommodated in eleven species complexes, which are divided into two main phylogenetic groups based on their morphological features: the Prolate Group (*C. brassicae*, *C. candelabrum*, *C. colhounii*, *C. cylindrospora*, *C. gracilipes*, *C. mexicana*, *C. pteridis*, *C. reteaudii* and *C. spathiphylli* species complexes), and the Sphaero-Naviculate Group (*C. kyotensis* and *C. naviculata* species complexes) (Lombard et al. 2016; Liu et al. 2020).

In Brazil, a total of 35 species have been described: eleven species isolated from diseased tissues of *Eucalyptus*, ten species isolated from soil samples of *Eucalyptus* plantations, seven species isolated from different plant species, six species isolated from soil samples of tropical rainforests, and one mycoparasite species (Crous et al. 2018, 2019; Liu et al. 2020); they belong in the species complexes of *C. candelabrum*, *C. brassicae*, *C. cylindrospora*, *C. pteridis*, *C. gracilipes*, and *C. naviculata* (Crous et al. 2018, 2019; Liu et al. 2020). The results from a previous study indicated high species diversity of *Calonectria* in Brazil (Alfenas et al. 2015).

Brazil is one of the main producers of pulp, paper, and wood panels in the world, mainly due to the genus *Eucalyptus*; its hybrids are the most grown trees in the country for these purposes (IBÁ, 2021). In 2020, the total area of *Eucalyptus* plantations was 7.47 million hectares, with an average productivity of 36.8 m^3/ha per year (IBÁ, 2021). However, in recent decades, commercial *Eucalyptus* plantations have expanded toward the warm and humid regions of northern and northeastern Brazil, where CLB has become the primary fungal leaf disease of this crop (Alfenas et al. 2015). CLB can be caused by different *Calonectria* species, is widely distributed throughout the country, and affects *Eucalyptus* plants most severely from six months to 2–3 years after planting (Graça et al. 2009). This disease starts from spores or microsclerotia present in soil or diseased plant debris on the ground and disseminates to lower branches of the tree canopy; lesions start at the base, apex or margins of leaves and can reach a large area of the leaf blade, resulting in leaf drop and, in some cases, severe defoliation in the basal, middle, and apical thirds of the canopy (Alfenas et al. 2009). The defoliation may decrease timber volume as a result of the reduced photosynthetic area and facilitates weed growth due to the increased entrance of light through the subcanopy, leading to competition for nutrients between *Eucalyptus* and understory plants (Graça et al. 2009; Alfenas et al. 2015).

CLB can be controlled by integrated cultivation and chemical methods as well as by the selection and cultivation of resistant genotypes, which is a much more effective approach (Soares et al. 2018). The demand for new strategies to control this disease requires proper identification of the pathogen species. Additionally, this information may be useful for breeding programs, leading to the development of *Eucalyptus* genotypes resistant to CLB. Recently, during a disease survey conducted in three commercial plantations of *Eucalyptus* in northeastern Brazil, diseased leaves from *Eucalyptus* trees with typical symptoms of CLB were collected, and *Calonectria* fungi were isolated. Thus, the aims of this study were to identify these isolates based on phylogenetic analyses and morphological characteristics and to confirm their pathogenicity to *Eucalyptus*.

Materials and methods

Sample collection and fungal isolation

In February 2020, during a disease survey conducted in three commercial plantations of *Eucalyptus* on six-month-old to one-year-old trees, diseased leaves with typical symptoms of CLB (small, circular or elongated pale grey to pale brown to dark brown spots, that extend throughout the leaf blade), were observed and collected for fungal isolation and species characterization. On average, 50 diseased leaves were sampled from each *Eucalyptus* genotype, one leaf per tree, depending on the planted areas. The sampled *Eucalyptus* genotypes corresponded to *E. urophylla*, localized in the municipalities of Cidelândia (5°09'24"S, 47°46'26"W) and Itinga do Maranhão (4°34'43"S, 47°29'48"W), in the state of Maranhão, and to the *E. grandis* × *E. brassiana* hybrid genotype, in the microregion of Paragominas (3°10'51"S, 47°18'49"W), in the state of Pará, Brazil.

Samples were stored in paper bags and transported to the Laboratory of Forest Pathology at the Universidade Federal de Lavras. From each leaf, small segments of 1 cm^2 from the transition section between healthy and diseased tissue were cut and the surface was disinfected by washing with 1% sodium hypochlorite for 1 min, with 70% ethanol for 30 s and with sterilized water three times before culture on 2% malt extract agar (MEA; malt extract 20 $g{\cdot}L^{-1}$, agar 20 $g{\cdot}L^{-1}$, yeast extract 2 $g{\cdot}L^{-1}$, sucrose 5 $g{\cdot}L^{-1}$) plates at 25 °C. After 48 h of incubation, *Calonectria*-like mycelial plugs, 5 mm in diameter, were transferred to a fresh MEA plate and incubated at 25 °C until the fungus covered the plate completely. Induction of sporulation on MEA plates and single spore cultures was obtained following the procedures described by Alfenas et al. (2013). Each single spore culture was stored and maintained in a metabolically inactive state in dry culture and sterile water following Castellani's method (Castellani 1939). Holotypes were deposited as herbaria in the Coleção Micológica do Herbário da Universidade de Brasília (UB). Ex-types were deposited as pure cultures in the Coleção de Culturas de Microrganismos do Departamento de Ciência dos Alimentos/UFLA (CCDCA) at Universidade Federal de Lavras (UFLA), Minas Gerais, Brazil. Ex-paratypes were deposited as pure cultures in the Laboratory of Forest Pathology (PFC) at UFLA.

DNA extraction, PCR amplification, and sequencing

Total genomic DNA was extracted from fresh mycelia of single spore cultures grown on malt extract broth (MEB; malt extract 20 $g \cdot L^{-1}$, yeast extract 2 $g \cdot L^{-1}$, sucrose 5 $g \cdot L^{-1}$) for ten days at 25 °C in the dark. The protocol described by Lee and Taylor (1990) was followed with slight modifications; by adding 1.5 M NaCl and 2% polyvinylpyrrolidone (MW: 40000) to the lysis buffer; the DNA was precipitated directly with isopropanol without the use of 3 M NaOAc, and the DNA pellet was dried at room temperature overnight. A NanoDrop 1,000 spectrometer (Thermo Fisher Scientific, Waltham, MA, USA) was used to quantify its concentration.

Based on a previous study (Liu et al. 2020), actine (*act*), calmodulin (*cmdA*), histone H3 (*his3*), RNA polymerase II (*rpb2*), translation elongation factor 1-alpha (*tef1*), and β-tubulin (*tub2*) genes were used as DNA barcodes due to provide a stable and reliable resolution to distinguish all *Calonectria* species. The primers ACT-512F and ACT-783R (Carbone and Kohn 1999) were used to amplify the *act* gene region; CAL-228F and CAL-2Rd (Carbone and Kohn 1999; Quaedvlieg et al. 2011) for the *cmdA* gene region; CYLH3F and CYLH3R (Crous et al. 2004) for the *his3* gene region; fRpb2-5F and fRpb2-7cR (Liu et al. 1999; Reeb et al. 2004) for the *rpb2* gene region; EF1-728F (Carbone and Kohn 1999) and EF2 (O'Donnell et al. 1998) for the *tef1* gene region and the primer pairs T1 (O'Donnell and Cigelnik 1997) and CYLTUB1R (Crous et al. 2004) for the *tub2* gene region.

The PCRs were carried out in a 25 μL final volume containing molecular biology-grade water (Sigma–Aldrich, St. Louis, MO, USA) 1X PCR buffer (Promega, Madison, WI, USA), 2.5 mM $MgCl_2$, 0.2 mM deoxyribonucleotide triphosphate (dNTP) mix (Promega, Madison, WI, USA), 1 U GoTaq Flexi DNA Polymerase (Promega, Madison, WI, USA), 0.2 mM each primer, and 30 ng DNA template. DNA amplifications were conducted in a thermal cycler (5 PRIME G gradient Thermal Cycler, Techne, Staffordshire, UK). The PCR conditions for the *act*, *cmdA*, *his3*, *tef1*, and *tub2* gene regions were as follows: an initial denaturation step at 95 °C for 5 min; then 35 amplification cycles at [94 °C for 30 s; 52 °C for 1 min; 72 °C for 2 min], and a final extension step at 72 °C for 5 min. For the *rpb2* gene region, a touchdown PCR protocol was used: an initial denaturation step at 95 °C for 5 min, then (95 °C for 30 s, 57 °C for 30 s, 72 °C for 90 s) × 10 cycles, (95 °C for 30 s, 57 °C for 45 s, 72 °C for 90 s + 5 s/cycle increase) × 30 cycles, and a final extension step at 72 °C for 10 min.

PCR products were separated by electrophoresis at 120 V for 1 h in a 1.2% agarose gel, stained with Diamond Nucleic Acid Dye (Promega, Madison, WI, USA), and visualized using an ultraviolet light transilluminator. Successful PCR products were purified and sequenced in both directions using the same primer pairs used for amplification by Macrogen Inc. (Macrogen, Seoul, Korea). Raw sequences from each gene region were edited, consensus sequences were generated using SeqAssem software ver. 07/2008 (Hepperle 2004), and the sequences generated in this study were deposited in the NCBI/GenBank database (http://www.ncbi.nlm.nih.gov).

Phylogenetic analyses

The generated sequences were aligned with other sequences of closely related *Calonectria* spp. obtained from GenBank (Table 1), using the online interface of MAFFT v. 7.0 (Katoh et al. 2019, http://mafft.cbrc.jp/alignment/server) with the alignment strategy FFT-NS-i (Slow; interactive refinement method). Alignments were manually corrected using MEGA7 (Kumar et al. 2016).

The partition homogeneity test (PHT) described by Farris et al. (1995) was conducted to determine if data for six genes could be combined using PAUP 4.0b10 (Swofford 2003). To determine the phylogenetic relationships among species, phylogenetic analyses based on maximum parsimony (MP), maximum likelihood (ML), and bayesian inference (BI) were conducted on the individual gene regions and their concatenated dataset, depending on the sequence availability.

Maximum parsimony analysis was performed using PAUP 4.0b10 (Swofford 2003), with phylogenetic relationships estimated by heuristic searches, random stepwise addition sequences, and tree bisection and reconnection (TBR) branch swapping. Gaps were treated as missing data, and all characters were unordered and weighted equally. The measures calculated for parsimony included the tree length (TL), consistency index (CI), homoplasy index (HI), retention index (RI), and rescaled consistency index (RC). Statistical support for branch nodes was assessed with 1,000 bootstrap replicates.

The best evolutionary model of nucleotide substitution for each gene region was selected according to the Akaike Information Criterion (AIC) using MODELTEST v. 3.4 (Posada and Crandall 1998) for ML analyses and MRMODELTEST v. 2 (Nylander 2004) for BI analyses.

ML analyses for individual gene regions were performed using PAUP 4.0b10 (Swofford 2003). The ML models used were K80 + G (*act*), TVM + G (*cmdA*), TrN + G (*his3*), SYM + G (*rpb2*), TVM + I + G (*tef1*) and HKY + I (*tub2*). Statistical support for branch nodes was assessed with 1,000 bootstrap replicates. A partitioned ML analysis was performed using IQ-TREE (Nguyen et al. 2015) as implemented in the IQ-TREE web server (http://iqtree.cibiv.univie.ac.at, Trifinopoulos et al. 2016) by using partition models (Chernomor et al. 2016). Branch support values were evaluated based on 10,000 replicates for ultrafast bootstrapping (UFBoot2) (Hoang et al. 2018).

Individual and partitioned BI analyses were performed using MRBAYES v.3.2.7a (Ronquist et al. 2012) on XSEDE at the CIPRES Science Gateway v.3.3 (http://www.phylo.org/). The BI models used were K80 + G (*act*), GTR + G (*cmdA* and *his3*), SYM + G (*rpb2*), GTR + I + G (*tef1*) and HKY + I (*tub2*). A Markov Chain Monte Carlo (MCMC) algorithm was employed, and two independent runs of four MCMC chains (three hot and one cold) were run in parallel simultaneously starting from random trees for 10^7 generations (individual gene regions) and 30^7 generations (concatenated dataset), sampling trees every 1,000 generations. The distribution of log-likelihood scores was examined with TRACER v.1.5 (Rambaut and Drummond 2007) to determine the whether the stationary phase of each search was reached and whether chains

Table 1. *Calonectria* species and GenBank accession numbers of DNA sequences used in this study.

Species complex	Species	Isolate representing the species[‡,§]	Other isolate numbers	Host/ Substrate	Country	Genbank accession numbers					
						act[|]	*cmdA*	*his3*	*rpb2*	*tef1*	*tub2*
Calonectria spathiphylli species complex	*C. densa*	**CMW 31182**		Soil	Ecuador	GQ280525	GQ267444	GQ267281	N/A	GQ267352	GQ267232
		CMW 31184		Soil	Ecuador	GQ280523	GQ267442	GQ267279	N/A	GQ267350	GQ267230
		CMW 31185		Soil	Ecuador	GQ280524	GQ267443	GQ267280	N/A	GQ267351	GQ267231
	C. humicola	**CMW 31183**		Soil	Ecuador	GQ280526	GQ267445	GQ267282	N/A	GQ267353	GQ267233
		CMW 31186		Soil	Ecuador	GQ280527	GQ267446	GQ267283	N/A	GQ267354	GQ267234
		CMW 31187		Soil	Ecuador	GQ280528	GQ267447	GQ267284	N/A	GQ267355	GQ267235
	***C. paragominensis* sp. nov.** [†]	**CCDCA 11648**		*E. grandis* × *E. brassiana*	Brazil	**ON009346**	**OM974325**	**OM974334**	**OM974343**	**OM974352**	**OM974361**
		PFC2		*E. grandis* × *E. brassiana*	Brazil	**ON009347**	**OM974326**	**OM974335**	**OM974344**	**OM974353**	**OM974362**
		PFC3		*E. grandis* × *E. brassiana*	Brazil	**ON009348**	**OM974327**	**OM974336**	**OM974345**	**OM974354**	**OM974363**
		PFC4		*E. grandis* × *E. brassiana*	Brazil	**ON009349**	**OM974328**	**OM974337**	**OM974346**	**OM974355**	**OM974364**
		PFC5		*E. grandis* × *E. brassiana*	Brazil	**ON009350**	**OM974329**	**OM974338**	**OM974347**	**OM974356**	**OM974365**
	C. pseudospathiphylli	**CBS 109165**	CPC 1623	Soil	Ecuador	GQ280493	GQ267412	AF348241	KY653435	FJ918562	AF348225
		CPC 1641		Soil	Ecuador	N/A	N/A	AF348233	N/A	N/A	AF348217
	C. spathiphylli	**CBS 114540**	ATCC44730, CSF11330	*Spathiphyllum* sp.	USA	GQ280505	GQ267424	AF348230	MT412666	GQ267330	AF348214
		CBS 116168	CSF 11401	*Spathiphyllum* sp.	Switzerland	GQ280506	GQ267425	FJ918530	MT412667	FJ918561	FJ918512
Calonectria candelabrum species complex	*C. brasiliana*	**CBS 111484**	CSF 11249	Soil	Brazil	MT334968	MT335198	MT335438	MT412502	MT412729	MT412951
		CBS 111485	CSF 11250	Soil	Brazil	MT334969	MT335199	MT335439	MT412503	MT412730	MT412952
	C. brassiana	**CBS 134855**		Soil	Brazil	N/A	KM396056	KM396139	N/A	KM395882	KM395969
		CBS 134856		Soil	Brazil	N/A	KM396057	KM396140	N/A	KM395883	KM395970
	C. brevistipitata	**CBS 115671**	CSF 11288	Soil	Mexico	MT334973	MT335203	MT335443	MT412507	MT412734	MT412956
		CBS 110928	CSF 11235	Soil	Mexico	MT334974	MT335204	MT335444	MT412508	MT412735	MT412957
	C. candelabrum	**CMW 31000**	CSF 11404	*Eucalyptus* sp.	Brazil	MT334977	MT335207	MT335447	MT412511	MT412738	MT412959
		CMW 31001	CSF 11405	*Eucalyptus* sp.	Brazil	MT334978	MT335208	MT335448	MT412512	MT412739	MT412960
	C. colombiana	**CBS 115127**		Soil	Colombia	GQ280538	GQ267455	FJ972442	N/A	FJ972492	FJ972423
		CBS 115638		Soil	Colombia	GQ280539	GQ267456	FJ972441	N/A	FJ972491	FJ972422
	C. eucalypticola	**CBS 134847**		*Eucalyptus* sp.	Brazil	N/A	KM396051	KM396134	N/A	KM395877	KM395964
		CBS 134846		*Eucalyptus* sp.	Brazil	N/A	KM396050	KM396133	N/A	KM395876	KM395963
	C. fragariae	**CBS 133607**		*Fragaria* × *ananassa*	Brazil	N/A	KM998966	KM998964	N/A	KM998963	KM998965
		LPF141.1		*Fragaria* × *ananassa*	Brazil	N/A	KX500191	KX500194	N/A	KX500197	KX500195
	C. glaebicola	**CBS 134852**		Soil	Brazil	N/A	KM396053	KM396136	N/A	KM395879	KM395966
		CBS 134853		*Eucalyptus* sp.	Brazil	N/A	KM396054	KM396137	N/A	KM395880	KM395967
	C. hemileiae	**COAD 2544**		*Hemileia vastatrix*	Brazil	N/A	MK037392	MK006026	N/A	MK006027	MK037391

Species complex	Species	Isolate representing the species[‡,§]	Other isolate numbers	Host/ Substrate	Country	Genbank accession numbers					
						act[|]	*cmdA*	*his3*	*rpb2*	*tef1*	*tub2*
Calonectria candelabrum species complex	***C. imperata* sp. nov.**[†]	**CCDCA 11649**		*E. urophylla*	Brazil	**ON009351**	**OM974330**	**OM974339**	**OM974348**	**OM974357**	**OM974366**
		PFC7		*E. urophylla*	Brazil	**ON009352**	**OM974331**	**OM974340**	**OM974349**	**OM974358**	**OM974367**
		PFC8		*E. urophylla*	Brazil	**ON009353**	**OM974332**	**OM974341**	**OM974350**	**OM974359**	**OM974368**
		PFC9		*E. urophylla*	Brazil	**ON009354**	**OM974333**	**OM974342**	**OM974351**	**OM974360**	**OM974369**
	C. matogrossensis	**GFP 006**		*E. urophylla*	Brazil	N/A	MH837653	MH837648	N/A	MH837659	MH837664
		GFP 018		*E. urophylla*	Brazil	N/A	MH837657	MH837652	N/A	MH837663	MH837668
	C. metrosideri	**CBS 133603**		*Metrosideros polymorpha*	Brazil	N/A	KC294304	KC294307	N/A	KC294310	KC294313
		CBS 133604	CSF 11309	*Metrosideros polymorpha*	Brazil	MT335056	MT335288	MT335528	MT412585	MT412819	MT413033
	C. nemoricola	**CBS 134837**		Soil	Brazil	N/A	KM396066	KM396149	N/A	KM395892	KM395979
		CBS 134838		Soil	Brazil	N/A	KM396067	KM396150	N/A	KM395893	KM395980
	C. pauciramosa	**CBS 138824**	CSF 16461	Soil	South Africa	MT335093	MT335325	MT335565	MT412618	MT412856	MT413068
		CMW 31474	CSF 11422	*E. urophylla* × *E. grandis*	China	MT335104	MT335336	MT335576	MT412629	MT412867	MT413079
	C. piauiensis	**CBS 134850**		Soil	Brazil	N/A	KM396060	KM396143	N/A	KM395886	KM395973
		CBS 134851		Soil	Brazil	N/A	KM396061	KM396144	N/A	KM395887	KM395974
	C. pseudometrosideri	**CBS 134845**		Soil	Brazil	N/A	KM395995	KM396083	N/A	KM395821	KM395909
		CBS 134843		*Metrosideros polymorpha*	Brazil	N/A	KM395993	KM396081	N/A	KM395819	KM395907
	C. pseudospathulata	**CBS 134841**		Soil	Brazil	N/A	KM396070	KM396153	N/A	KM395896	KM395983
		CBS 134840		Soil	Brazil	N/A	KM396069	KM396152	N/A	KM395895	KM395982
	C. putriramosa	**CBS 111449**	CSF 11246	*Eucalyptus* cutting	Brazil	MT335129	MT335364	MT335604	MT412657	MT412895	MT413105
		CBS 111470	CSF 11247	Soil	Brazil	MT335130	MT335365	MT335605	MT412658	MT412896	MT413106
	C. silvicola	**CBS 135237**	LPF081	Soil	Brazil	N/A	KM396065	KM396148	N/A	KM395891	KM395978
		CBS 134836		Soil	Brazil	N/A	KM396062	KM396145	N/A	KM395888	KM395975
	C. spathulata	**CMW 16744**	CSF 11331	*E. viminalis*	Brazil	MT335139	MT335376	MT335616	MT412668	MT412907	MT413117
		CBS 112513	CSF 11259	*Eucalyptus* sp.	Colombia	MT335140	MT335377	MT335617	MT412669	MT412908	MT413118
	C. venezuelana	**CBS 111052**	CSF 11238	Soil	Venezuela	MT335155	MT335394	MT335634	MT412685	MT412925	MT413132
Calonectria gracilipes species complex	*C. gracilipes*	**CBS 115674**	CSF 11289	Soil	Colombia	MT335022	MT335252	MT335492	MT412554	MT412783	MT413001
		CBS 111141	CSF11239	Soil	Colombia	MT335023	MT335253	MT335493	MT412555	MT412784	MT413002

† New *Calonectria* species reported in the present study.

‡ Ex-type isolates of the *Calonectria* species are marked in bold.

§ ATCC: American Type Culture Collection, Virginia, USA; CBS: Westerdijk Fungal Biodiversity Institute, Utrecht, The Netherlands; CCDCA: Coleção de Culturas de Microrganismos do Departamento de Ciência dos Alimentos/UFLA, Lavras, Brazil; CMW: Culture collection of the Forestry and Agricultural Biotechnology Institute (FABI), University of Pretoria, Pretoria, South Africa; COAD: Coleção Octávio de Almeida Drumond, Universidade Federal de Viçosa, Viçosa, Brazil; CPC: Pedro Crous working collection housed at Westerdijk Fungal Biodiversity Institute; CSF: Culture Collection located at China Eucalypt Research Centre (CERC), Chinese Academy of Forestry, ZhanJiang, GuangDong Province, China; GFP: Universidade Federal de Brasilia, Brasilia, Brazil; LPF: Laboratorio de Patologia Florestal, Universidade Federal de Viçosa, Viçosa, Brazil; PFC: Laboratorio de Patologia Florestal, Universidade Federal de Lavras, Lavras, Brazil.

| *act*: actin; *cmdA*: calmodulin; *his3*: histone H3; *rpb2*: the second largest subunit of RNA polymerase; *tef1*: translation elongation factor 1-alpha; *tub2*: β-tubulin. GenBank accession number obtained in this study are marked in bold.

had achieved convergence. The convergence of the chains was also assessed by the convergent diagnostics of the effective sampling site (ESS), the potential scale reduction factor (PSRF), and the average standard deviation of split frequencies (ASDSF) (Ronquist et al. 2019). The first 25% of saved trees were discarded as the "burn-in" phase, and posterior probabilities (PP) were computed using the remaining trees. Trees were visualized in FIGTREE v. 1.4.4 (Rambaut 2009) and edited in INKSCAPE v. 1.0 (https://inkscape.org).

Pairwise homoplasy index (PHI) test and phylogenetic network analysis

Phylogenetically closely related species were analyzed using the Genealogical Concordance Phylogenetic Species Recognition (GCPSR) model (as described by Taylor et al. 2000) by performing a pairwise homoplasy index (Φw) test (PHI) (Bruen et al. 2006). The PHI test was performed in SPLIT TREE4 v.4.16.1. (https://uni-tuebingen.de) (Huson and Bryant 2006) to determine the recombination level within phylogenetically closely related species. Only the gene regions that were available for all compared individuals were used. Gaps' sites were excluded. Significant recombination was considered at a PHI index below 0.05 ($\Phi w < 0.05$). The relationships between closely related taxa were visualized by constructing a phylogenetic network from the concatenated datasets using the LogDet transformation and the NeighborNet method; the resultant networks were displayed with the EqualAngle algorithm (Dress and Huson 2004). Bootstrap analysis was then conducted with 1,000 replicates.

Mating type and sexual compatibility test

The mating-type idiomorph of each *Calonectria* species isolate was determined through PCR by using the primer pairs Cal_MAT111_F/Cal_MAT111_R and Cal_MAT121_F/Cal_MAT121_R, which amplify the MAT1-1-1 and MAT1-2-1 genes using the protocol described by Li et al. (2020). Additionally, sexual compatibility tests were performed for all the single-spore isolates of both species on minimal salt agar (MSA; Guerber and Correll 2001) by crossing them in all possible combinations, following the procedure described by Lombard et al. (2010a). The plates were stacked in plastic bags and incubated at 25 °C for 12 weeks.

Morphology

Morphological characterization of representative isolates of each *Calonectria* species identified by phylogenetic analyses was performed as described by Liu and Chen (2017). Optimal growth temperatures were determined by incubating the representative isolate at temperatures ranging from 5 °C to 30 °C at 5 °C intervals in the dark on MEA plates (three replicates per isolate were used). Colonial characteristics (diameter, color, and texture of colonies) were determined by inoculating the isolates on MEA plates at 25 °C in the dark after seven days of incubation.

Pathogenicity tests

One representative isolate of each *Calonectria* species was selected for inoculation. Healthy leaves of three short cut branches from an approximately eleven-month-old *Eucalyptus* plants were inoculated with suspensions of 1×10^4 conidia·mL^{-1} obtained from single spore cultures. The conidia suspensions for each isolate were prepared using the method described by Graça et al. (2009). *Calonectria paragominensis* was inoculated on *E. grandis* × *E. brassiana* hybrid genotype and *C. imperata* on *E. urophylla* genotype. The inoculation consisted of spraying the conidia suspension until the suspension run off the leaves. Sterile water was sprayed onto healthy leaves as the negative control. The branches with inoculated leaves were covered with plastic bags to maintain high humidity and kept at 25 °C under a photoperiod of 12 h for 72 h. After that time, the plastic bags were removed, and necrotic symptoms were observed.

Results

Fungal isolates

A total of 34 isolates with the typical morphology of *Calonectria* species were obtained from infected leaves of the *Eucalyptus* genotypes sampled. Based on preliminary phylogenetic analyses of the *tef1* and *tub2* gene regions (data not shown), nine isolates were selected for further studies (Table 1).

Phylogenetic analyses

Sequences from 50 isolates corresponding to 25 *Calonectria* species closely related to the isolates obtained in this study were downloaded from GenBank (Table 1). For the nine isolates selected in this study, five resided in the *Calonectria spathiphylli* species complex (CSSC), and four resided in the *Calonectria candelabrum* species complex (CCSC). Both *Calonectria* complexes belong to the Prolate Group, whose species are characterized by their clavate to pyriform to ellipsoidal vesicles (Liu et al. 2020). Therefore, both complexes were combined into a single sequence dataset for phylogenetic analyses, including two strains of *Calonectria gracilipes* as the outgroup taxa.

Alignments for each gene region and the concatenated dataset were as follows: *act* (36 isolates, 267 characters), *cmdA* (58 isolates, 485 characters), *his3* (59 isolates, 439 characters), *rpb2* (28 isolates, 863 characters), *tef1* (58 isolates, 496 characters), *tub2* (59 isolates, 511 characters) and concatenated (59 isolates, 3061 characters). The PHT generated a *p* value of 0.01 for the concatenated dataset, suggesting some incongruence in the datasets for the six regions and the accuracy of the combined data could have suffered relative to the individual partitions (Cunningham 1997). Although the *p* value was low, the different gene regions were combined because the significance threshold

of 0.05 may be too conservative and it has been shown that combining incongruent datasets improves phylogenetic accuracy (Sullivan 1996; Cunningham 1997); moreover, this approach was followed by several previous studies (Lombard et al. 2016; Pham et al. 2019; Liu et al. 2020, 2021).

Tree topologies derived from the MP, ML, and BI analyses of the individual gene regions were similar overall, but the relative positions of some *Calonectria* species slightly differed. Moreover, the concatenated dataset formed well-supported lineages in the MP, ML, and BI analyses. Only the ML trees are presented in this study (Fig. 1, Suppl. material 1: Figs S1–S6). The concatenated dataset had 466 parsimony-informative characters, 67 parsimony-uninformative characters, and 2,528 constant characters. Analysis of the 466 parsimony-informative characters yielded 2 equally parsimonious trees, with TL = 862, CI = 0.7042, HI = 0.2958, RI = 0.9192, RC = 0.6472. For the partitioned BI analysis, the convergence of the chains was confirmed by an ESS > 200, a PSRF approaching 1, and an ASDSF equal to 0.000793. The aligned sequences were deposited in TreeBASE (http://treebase.org; No. 29573).

Phylogenetic analyses of the six individual gene regions showed that the five isolates from the CSSC were clustered in an independent clade (Suppl. material 1: Figs S1–S6). Based on the concatenated dataset of the six genes, the five isolates formed a new, strongly defined phylogenetic clade that was distinct from the other *Calonectria* species of the CSSC and was supported by high bootstrap values (MP = 100%, ML = 100%) and high values of posterior probability (1.0) (Fig. 1). A total of 41 fixed unique single nucleotide polymorphisms (SNPs) were identified in the new phylogenetic clade of the five isolates in comparison with their phylogenetically closely related *Calonectria* species in the six-gene concatenated dataset (Table 2). The results of these phylogenetic and SNP analyses indicate that the five isolates in the CSSC represent a distinct, undescribed species, which we named *C. paragominesis*.

Table 2. Single nucleotide polymorphisms unique to *C. paragominensis* in comparison with their phylogenetically closely related species in the six gene regions.

Species	*act*†										*cmdA*									
	188‡	189	190	191	192	193	194	195	196	197	142	144	170	185	217	270	437	444	455	483
C. paragominensis CCDCA 11648	a	g	a	a	a	a	a	g	a	a	t	a	c	c	t	c	a	a	g	a
C. densa CMW 31182	t	-	-	-	-	-	-	-	-	-	a	c	t	t	c	t	g	g	a	c
C. humicola CMW 31183	t	-	-	-	-	-	-	-	-	-	a	c	t	t	c	t	g	g	a	c
C. pseudospathiphylli CBS 109165	t	-	-	-	-	-	-	-	-	-	a	c	t	t	c	t	g	g	a	c
C. spathiphylli CBS 114540	t	-	-	-	-	-	-	-	-	-	a	c	t	t	c	t	g	g	a	c

Species	*his3*										*rpb2*						*tef1*					*tub2*
	6	43	47	52	53	54	247	259	274	81	141	315	474	630	735	32	123	208	434	459	15
C. paragominensis CCDCA 11648	c	t	t	-	-	-	a	g	a	t	c	t	t	a	g	c	t	g	g	c	a
C. densa CMW 31182	t	a	c	c	t	c	t	a	g							-	-	a	t	t	t
C. humicola CMW 31183	t	a	c	c	t	c	t	a	g							-	-	a	t	t	t
C. pseudospathiphylli CBS 109165	-	a	c	c	a	c	c	a	g	c	t	c	c	g	a	-	-	a	a	t	t
C. spathiphylli CBS 114540	-	a	c	c	c	c	c	a	g	c	t	c	c	g	a	-	-	a	t	t	t

† Only polymorphic nucleotides occurring in all the isolates are shown, not alleles that partially occur in individuals per phylogenetic group. ‡ Numerical positions of the nucleotides in the DNA sequence alignments.

Phylogenetic analyses of the individual gene regions of *act*, *cmdA*, *his3*, *rpb2*, and *tub2* showed that the four isolates that resided in the CCSC were clustered in an independent clade (Suppl. material 1: Figs S1–S4, S6). However, the phylogenetic tree based on *tef1* showed that three of those isolates formed an independent clade, while one isolate was closely related to *C. metrosideri*, *C. pseudometrosideri*, and *C. candelabrum* (Suppl. material 1: Fig. S5). Based on the concatenated dataset of the six genes, the four isolates formed a new, strongly defined phylogenetic clade that was distinct from other *Calonectria* species in the CSSC and was supported by high bootstrap values (MP = 91%, ML = 99%) and high values of posterior probability (1.0) (Fig. 1). The four isolates of the new phylogenetic clade were distinguished from their phylogenetically closely related *Calonectria* species using SNP analyses for the six-gene concatenated dataset, by presenting eight unique SNPs from a total of 78 SNPs (Table 3). The results of these phylogenetic and SNP analyses indicate that the four isolates in the CCSC represent a distinct, undescribed species, which we named *C. imperata*.

Table 3. Single nucleotide polymorphisms found in *Calonectria imperata* and its phylogenetically closely related species in the six gene regions.

Species	*act*†						*cmdA*										*his3*					
	57‡	62	71	121	171	187	210	319	376	403	405	418	444	8	44	46	53	56	60	66
C. imperata CCDCA 11649	**c**	a	c	c	g	g	c	c	t	**t**	c	**t**	t	c	c	t	c	c	g	a
C. brassiana CBS 134855		c	g	t	g	g	c	c	c	c	c	a	t	t	c	t	c	c	g	a
C. glaebicola CBS 134852		a	c	c	g	g	c	g	t	c	c	a	t	c	t	c	c	c	g	a
C. piauiensis CBS 134850		a	g	c	c	a	c	c	c	c	c	a	c	c	c	-	a	c	a	c
C. venezuelana CBS 111052	t	a	c	c	g	g	a	g	t	c	t	a	t	c	c	t	c	t	g	a

Species	*his3*																			
	93	99	105	114	156	189	234	235	238	244	245	250	251	252	254	255	257	262	275	276
C. imperata CCDCA 11649	c	c	c	a	t	t	t	t	c	c	a	c	c	a	g	c	a	a	t	g
C. brassiana CBS 134855	c	c	c	t	t	t	t	t	c	c	a	c	c	a	g	c	a	a	t	g
C. glaebicola CBS 134852	c	c	c	a	t	t	t	t	c	a	a	c	c	a	g	c	a	a	t	g
C. piauiensis CBS 134850	t	t	c	a	c	t	c	g	t	g	g	t	a	g	a	t	g	g	c	a
C. venezuelana CBS 111052	c	c	a	a	t	c	t	t	c	c	a	c	c	a	g	c	a	a	t	g

Species	*his3*						*rpb2*						*tef1*							
	277	278	333	336	351	405	420	105	603	624	693	840	47	81	110	112	135	220	239	357
C. imperata CCDCA 11649	c	t	t	c	g	c	t	**g**	**a**	**c**	**t**	**a**	c	g	a	t	t	c	c	c
C. brassiana CBS 134855	c	t	t	c	g	t	t						c	g	t	t	t	c	c	c
C. glaebicola CBS 134852	c	t	t	c	a	c	t						c	a	a	t	t	c	c	c
C. piauiensis CBS 134850	t	t	c	t	g	c	g						t	g	a	a	c	a	t	c
C. venezuelana CBS 111052	c	c	t	c	g	c	t	t	g	t	c	t	c	g	a	t	t	c	c	t

Species	*tef1a*								*tub2*									
	417	421	422	425	453	50	99	120	132	174	175	188	191	220	377	398	408	409
C. imperata CCDCA 11649	c	c	c	a	a	c	a	g	t	c	c	g	c	t	t	t	-	-
C. brassiana CBS 134855	c	t	t	a	a	c	a	g	t	c	c	g	c	t	t	t	a	c
C. glaebicola CBS 134852	c	t	t	a	a	c	a	g	t	c	c	g	c	t	t	t	a	c
C. piauiensis CBS 134850	t	c	c	a	a	g	g	a	c	t	t	a	a	c	c	g	a	c
C. venezuelana CBS 111052	c	c	c	c	g	c	a	g	t	c	c	g	c	t	t	t	a	c

† Only polymorphic nucleotides occurring in all the isolates are shown, not alleles that partially occur in individuals per phylogenetic group. ‡ Numerical positions of the nucleotides in the DNA sequence alignments.

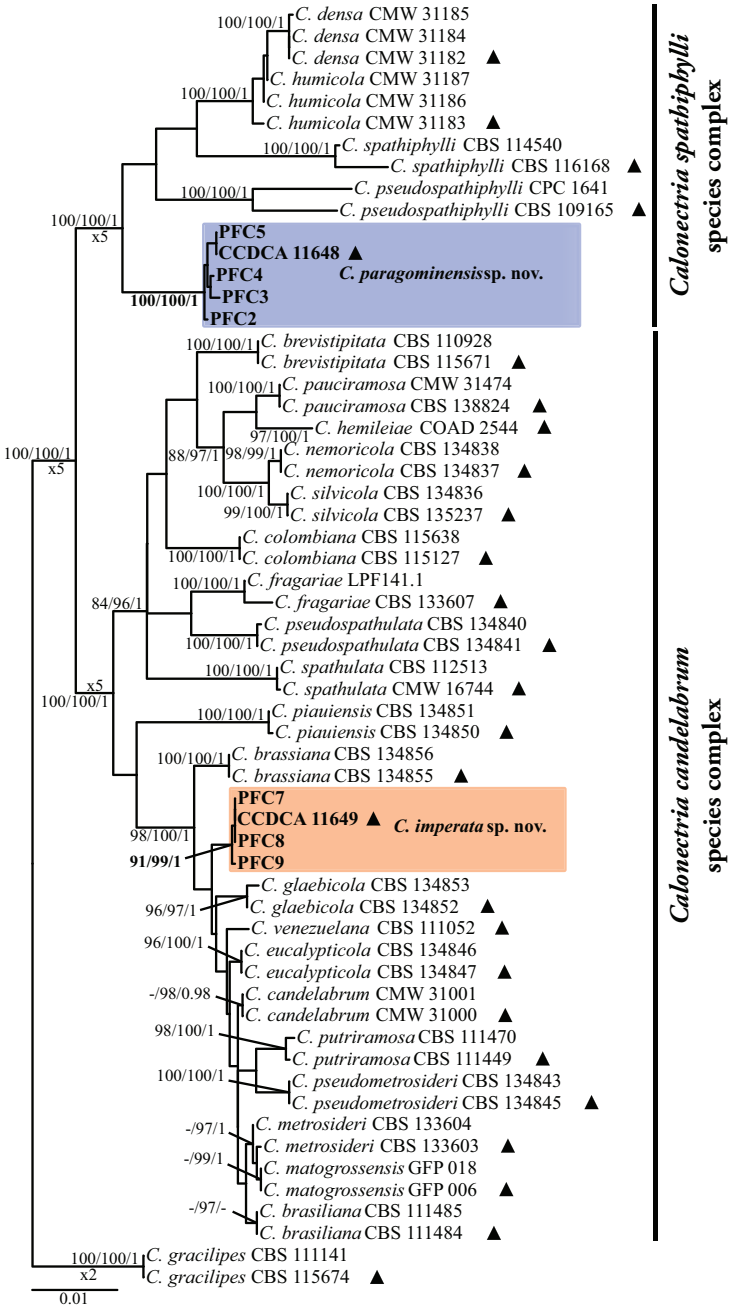

Figure 1. Phylogenetic tree based on maximum likelihood analysis of concatenated *act*, *cmdA*, *his3*, *rpb2*, *tef1* and *tub2* gene regions. Bootstrap support values ≥ 80% for maximum parsimony (MP), Ultrafast bootstrap support values ≥ 95% for maximum likelihood (ML), and posterior probability (PP) values ≥ 0.95 from BI analyses are presented at the nodes (MP/ML/PP). Bootstrap values below 80% (MP), 95% (ML) and posterior probabilities below 0.80 are marked with "-". Ex-type isolates are indicated by "▲", isolates highlighted in bold were sequenced in this study, and novel species are in blue and orange. *C. gracilipes* was used as outgroup. The scale bar indicates the number of nucleotide substitutions per site.

Species delimitation by GCPSR analysis

A PHI test using a five-locus concatenated dataset (*act*, *cmdA*, *his3*, *tef1*, *tub2*) was performed to determine the recombination level among *C. paragominensis* and its phylogenetically closely related species, *C. densa*, *C. humicola*, *C. spathiphylli* and *C. pseudospathiphylli*. A value of Φw = 0.2879 revealed no significant genetic recombination events, and this relationship was supported with a high bootstrap value (100%) in the phylogenetic network analysis, indicating that they are different species (Fig. 2A).

A PHI test using a four-locus concatenated dataset (*cmdA*, *his3*, *tef1*, *tub2*) was performed to determine the recombination level among *C. imperata* and its

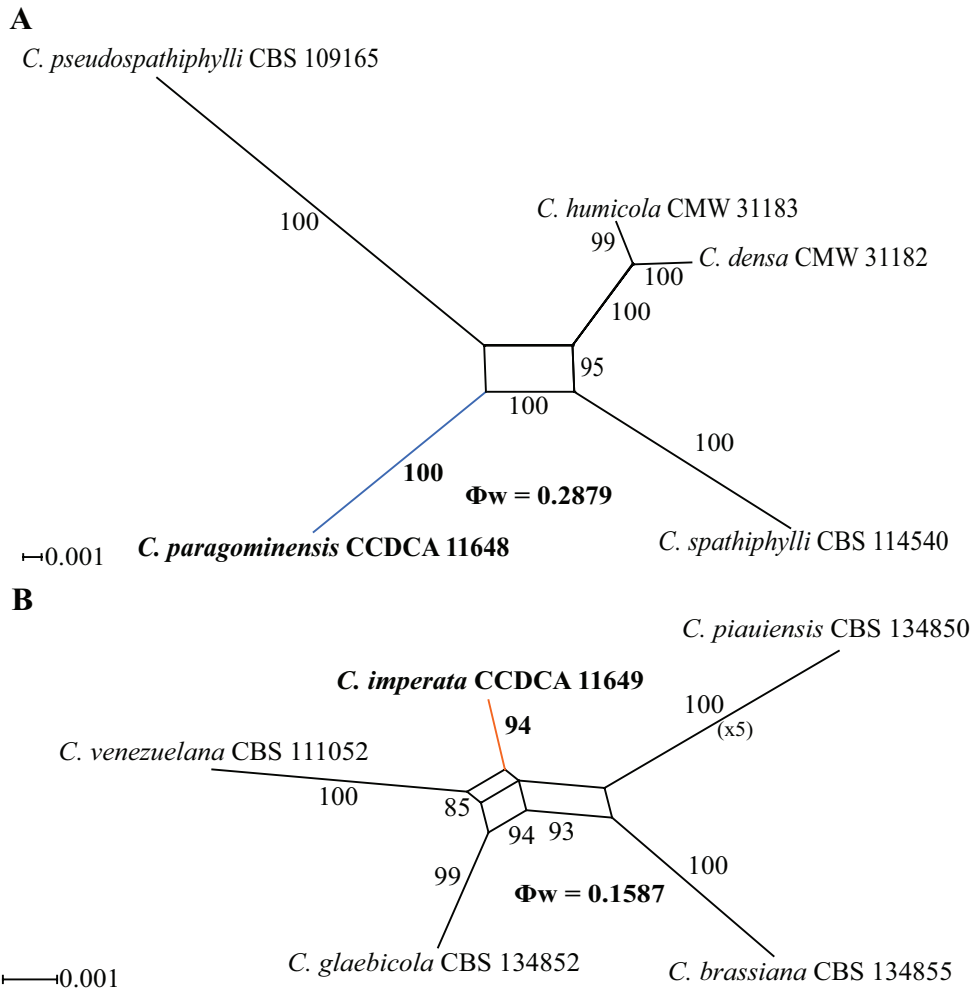

Figure 2. Results of the pairwise homoplasy index (PHI) test for *C. paragominensis* and *C. imperata*. Phylogenetic networks constructed using the LogDet transformation and the NeighborNet method and displayed with the EqualAngle algorithm. Bootstrap support values > 80% are shown. Φw < 0.05 indicate significant recombination. New species described in this study are highlighted in bold, with blue (**A**) and orange (**B**) lines.

phylogenetically closely related species, *C. brassiana*, *C. glabeicola*, *C. piauiensis*, and *C. venezuelana*. A value of Φw = 0.1587 revealed no significant genetic recombination events, and this relationship was supported with a high bootstrap value (94%) in the phylogenetic network analysis, indicating that they are different species (Fig. 2B).

Mating-type and sexual compatibility test

MAT1-1-1 and MAT1-2-1 genes were amplified in all isolates of each identified species, indicating that they are putatively homothallic. However, after a twelve-week mating test on MSA, all isolates failed to yield sexual structures, indicating that they have lost the ability to be self-fertile or have retained the ability to favor outcrossing rather than selfing.

Taxonomy

Based on phylogenetic analyses, GCPSR, and network analyses, the nine isolates presented two strongly defined phylogenetic clades in both the *Calonectria spathiphylli* species complex and the *Calonectria candelabrum* species complex. Morphological differences, especially in the macroconidia and stipe dimensions, were observed between each phylogenetic clade and its phylogenetically closely related species (Table 4). Thus, the fungi isolated in this study represent two new species of *Calonectria* and are described as follows:

Calonectria paragominensis **E.I.Sanchez, T.P.F.Soares & M.A.Ferreira, sp. nov.**
MycoBank No: 843460
Fig. 3

Etymology. The term "*paragominensis*" refers to the microregion of Paragominas, Brazil, which is the place where the fungus was collected.

Diagnosis. *Calonectria paragominensis* differs from the phylogenetically closely related species *C. densa*, *C. humicola*, *C. spathiphylli* and *C. pseudospathiphylli* with respect to its macroconidia dimensions.

Type. Brazil,• Pará state, Paragominas microregion; 3°10'51"S, 47°18'49"W; From infected leaves of *E. grandis* × *E. brassiana*; 20 Feb. 2020; M.A. Ferreira; **holotype**: UB24349, **ex-type**: CCDCA 11648 = PFC1. GenBank: *act* = ON009346; *cmdA* = OM974325; *his3* = OM974334; *rpb2* = OM974343; *tef1* = OM974352; *tub2* = OM974361.

Description. Sexual morph unknown. Macroconidiophores consisted of a stipe, a suite of penicillate arrangements of fertile branches, a stipe extension, and a terminal vesicle; stipe septate, hyaline, smooth, (112–)135–207(–281) × (2–)2.6–3.5(–4) μm; stipe extension septate, straight to flexuous, (123–)147–220(–295) μm long, (1.5–)1.9–2.4(–3) μm wide at the apical septum, terminating in a globose to

Table 4. Morphological characteristics of two new *Calonectria* species and their phylogenetically closely related species.

Species complex	Species	Conidiogenus apparatus		Stipe		Macroconidia			Vesicle		Reference
		Size (L × W)†,‡,§	Branches	Size (L × W)†,‡,§	Extension (L × W)†,‡,§	Size (L × W)†,‡,§,|	Average (L × W)†,‡,§	Septa	Diameter†,§	Shape	
***Calonectria spathiphylli* species complex**	***C. paragominensis***	40–113 × 45–129	(–4)	112–281 × 2–4	123–295 × 1.5–3	(47–)56–66(–71) × (4–)4.8–5.9(–7)	61 × 5	1(–3)	8–12	globoid to sphaeropedunculate	This study
	C. densa	49–78 × 63–123	(–4)	54–90 × 6–10	149–192 × 5–6	(47–)50–58(–62) × (5–)6	54 × 6	1	10–12	ovoid to ellipsoid to sphaeropedunculate	Lombard et al. 2010b
	C. humicola	43–71 × 42–49	3	44–90 × 6–8	126–157 × 4–5	(45–)48–54(–56) × (4–)5	51 × 5	1	10–12	globoid to ovoid to sphaeropedunculate	Lombard et al. 2010b
	C. pseudospathiphylli	70–100 × 25–70	4	100–350 × 5–6	100–250 × 2.5–3.5	(40–)47–55(–60) × 4–5	52 × 4	1(–3)	8–12	sphaeropedunculate to ellipsoid	Kang et al. 2001; Crous 2002
	C. spathiphylli	60–150 × 40–90	4	120–150 × 6–8	170–260 × 3–4	(45–)65–80(–120) × (5–)6(–7)¶	70 × 6	1(–3)	8–15	globoid or ellipsoid to obpyriform	Crous 2002
***Calonectria candelabrum* species complex**	***C. imperata***	50–127 × 41–110	(–3)	135–227 × 2–4	151–254 × 1.5–3	(38–)43–49(–52) × (2–)2.7–3.2(–4)	46 × 3	(–1)	3–6	ellipsoid to narrowly obpyriform	This study
	C. piauiensis	20–60 × 35–80	2	50–110 × 4–6	95–130 × 2–3	(38–)47–52(–60) × 3–5	49 × 4.5	1	3–7	ellipsoid to narrowly obpyriform	Alfenas et al. 2015
	C. brassiana	50–80 × 50–135	3	55–155 × 5–8	90–172 × 2–3	(35–)50–56(–65) × 3–5	53 × 4	1	3–7	ellipsoid to narrowly obpyriform	Alfenas et al. 2015
	C. glaebicola	27–45 × 25–40	2	50–130 × 5–7	100–165 × 2–4	(45–)50–52(–55) × 3–5	50 × 4	1	3–5	ellipsoid to narrowly obpyriform	Alfenas et al. 2015
	C. venezuelana	25–65 × 25–60	3	35–100 × 4–8	85–190 × 3–6	(48–)54–62(–65) × (4–)4.5–5.5(–7)	58 × 5	1	5–9	fusiform to ovoid to ellipsoid	Lombard et al. 2016

† All measurements are in µm. ‡ L × W = length × width. § Minimum–maximum. | Measurements are presented in the format [(minimum–) (average – standard deviation) – (average + standard deviation) (–maximum)]. ¶ Measurements are presented in the format [(minimum–) (average) (–maximum)].

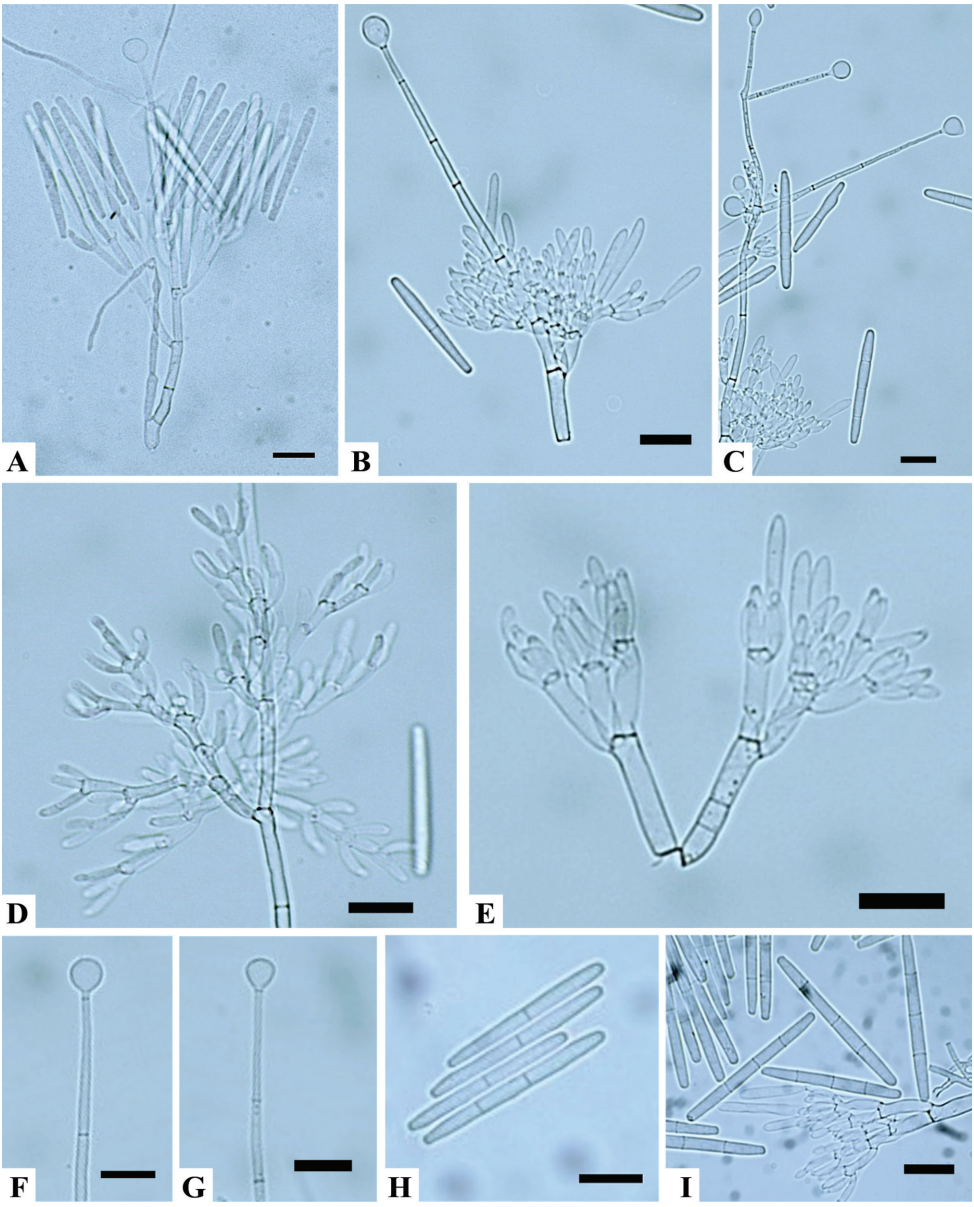

Figure 3. *Calonectria paragominensis* **A, B** macroconidiophore **C** lateral stipe extensions **D, E** conidiogenous apparatus with conidiophore branches and doliiform to reniform phialides **F, G** globose to sphaeropedunculate vesicles **H, I** one, two, and three-septate macroconidia. Scale bars: 20 µm.

sphaeropedunculate vesicle, (8–)8.5–10.5(–12) µm diam; lateral stipe extensions (90° to the axis) also present. Conidiogenous apparatus was (40–)56–88(–113) µm long, (45–)67–107(–129) µm wide; primary branches aseptate or 1-septate, (15.7–)18.4–25.9(–30.6) × (3.3–)4–6(–6.5) µm; secondary branches aseptate, (12.7–)14.3–

19.6(–22.1) × (3–)3.5–5(–6) µm; tertiary branches aseptate, (9.9–)11.6–15.3(–17.9) × (2.8–)3.6–5.3(–6.4) µm; additional branches (–4), aseptate, (10.3–)11–13.2(–14) × (3–)3.2–4.4(–5) µm; each terminal branch produced 2–4 phialides; phialides doliiform to reniform, hyaline, aseptate, (8–)9.1–11.8(–14) × (2–)2.7–4.1(–6) µm, apex with minute periclinal thickening and inconspicuous collarette. Macroconidia were cylindrical, rounded at both ends, straight, (47–)56–66(–71) × (4–)4.8–5.9(–7) µm (av. = 61 × 5 µm), (1–3) septate, lacking a visible abscission scar, held in parallel cylindrical clusters by colorless slime. Megaconidia and microconidia were not observed.

Culture characteristics. Colonies formed abundant white aerial mycelium on MEA at 25 °C after seven days, with irregular margins and moderate sporulation. The surface had white to buff outer margins, and sienna to amber in reverse with abundant chlamydospores throughout the medium, forming microsclerotia. The optimal growth temperature was 23.8 °C, with no growth at 5 °C; after seven days, colonies at 10 °C, 15 °C, 20 °C, 25 °C, and 30 °C reached 7 mm, 23 mm, 38.3 mm, 36.1 mm, and 31.8 mm, respectively.

Substratum. Leaves of *E. grandis* × *E. brassiana*.

Distribution. Northeast Brazil.

Other specimens examined. Brazil,• Pará state, Paragominas microregion; From infected leaves of *E. grandis* × *E. brassiana*; 20 Feb. 2020; M.A. Ferreira; cultures PFC2, PFC3, PFC4, PFC5.

Notes. *C. paragominensis* is a new species in the *C. spathiphylli* species complex (Liu et al., 2020). Morphologically, *C. paragominensis* is very similar to *C. densa*, since both form lateral stipe extensions, which have not been reported for the other three species in the complex. However, the macroconidia of *C. paragominensis* (av. 61 × 5 µm) are longer than those of *C. densa* (av. 54 × 6 µm), *C. humicola* (av. 51 × 5 µm) and *C. pseudospathiphylli* (av. 52 × 4 µm) but smaller than those of *C. spathiphylli* (av. 70 × 6 µm).

Calonectria imperata **E.I.Sanchez, T.P.F.Soares & M.A.Ferreira, sp. nov.**
MycoBank No: 843461
Fig. 4

Etymology. The term "*imperata*" is in honor of the city of Imperatriz, Brazil, which was close to the place where the fungus was collected.

Diagnosis. *Calonectria imperata* differs from the phylogenetically closely related species *C. brassiana*, *C. glaebicola*, *C. piauiensis* and *C. venezuelana* with respect to the number of unique alleles and stipe dimensions.

Type. Brazil,• Maranhão state, Cidelândia municipality; 5°09'24"S, 47°46'26"W; From infected leaves of *E. urophylla*; 20 Feb. 2020; M.A. Ferreira; **holotype**: UB24350, **ex-type**: CCDCA 11649 = PFC6. GenBank: *act* = ON009351; *cmdA* = OM974330; *his3* = OM974339; *rpb2* = OM974348; *tef1* = OM974357; *tub2* = OM974366.

Description. Sexual morph unknown. Macroconidiophores consisted of a stipe, a suite of penicillate arrangements of fertile branches, a stipe extension, and a terminal vesicle; stipe septate, hyaline, smooth, (135–)151–198(–227) × (2–)2.6–3.4(–4) µm; stipe extension

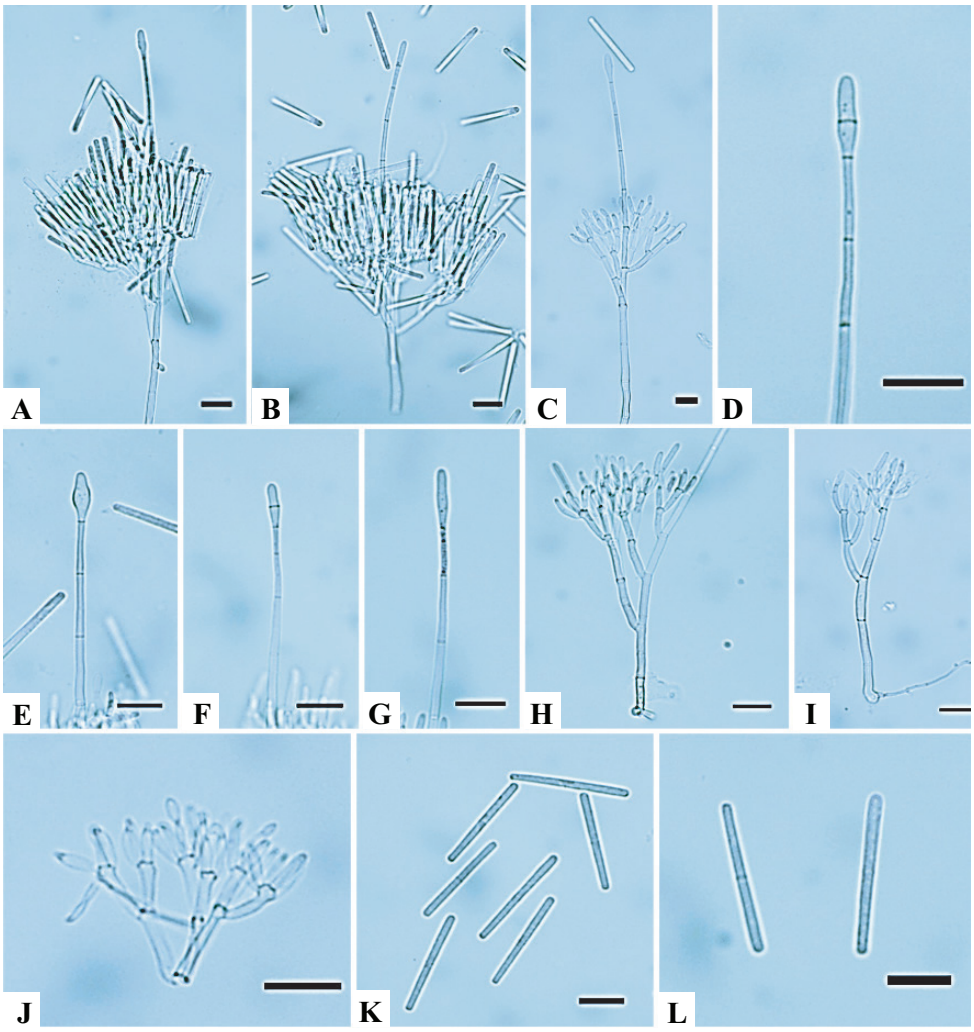

Figure 4. *Calonectria imperata* **A–C** macroconidiophore **D–G** ellipsoidal to narrowly obpyriform vesicles **H–J** conidiogenous apparatus with conidiophore branches and doliiform to reniform phialides **K, L** macroconidia. Scale bars: 20 µm.

septate, straight to flexuous, (151–)169–220(–254) µm long, (1.5–)1.9–2.7(–3) µm wide at the apical septum, terminating in an ellipsoidal to narrowly obpyriform vesicle (3–)3.1–4.6(–6) µm diam. Conidiogenous apparatus was (50–)66–100(–127) µm long, (41–)62–89(–110) µm wide; primary branches aseptate, (14.6–)19–24.8(–28.5) × (2.5–)3.2–4(–4.5) µm; secondary branches aseptate, (12.1–)13.5–18.2(–24.2) × (2.3–)2.8–3.7(–4) µm; tertiary branches aseptate, (10.1–)11–15(–18.1) × (1.9–)2.3–3.2(–4.1) µm; each terminal branch producing 2–4 phialides; phialides doliiform to reniform, hyaline, aseptate, (8–)9.1–13(–15) × (2–)2.7–3.3(–4) µm, apex with minute periclinal thickening and inconspicuous collarette. Macroconidia were cylindrical, rounded at both ends,

straight, (38–)43–49(–52) × (2–)2.7–3.2(–4) µm (av. = 46 × 3 µm), (–1) septate, lacking a visible abscission scar, held in parallel cylindrical clusters by colorless slime. Megaconidia and microconidia were not observed.

Culture characteristics. Colonies formed moderate aerial mycelium on MEA at 25 °C after seven days, with moderate sporulation. The surface had white to buff outer margins, and sepia to umber in reverse with abundant chlamydospores throughout the medium, forming microsclerotia. The optimal growth temperature was 25 °C, with no growth at 5 °C; after seven days, colonies at 10 °C, 15 °C, 20 °C, 25 °C, and 30 °C reached 10.1 mm, 25.5 mm, 29.1 mm, 44.5 mm, and 40.6 mm, respectively.

Substratum. Leaves of *E. urophylla*.

Distribution. Northeast Brazil.

Other specimens examined. Brazil,• Maranhão state, Cidelândia municipality; 5°09'24"S, 47°46'26"W; From infected leaves of *E. urophylla*; 20 Feb. 2020; M.A. Ferreira; cultures PFC7, PFC8, PFC9. Brazil• Maranhão state, Itinga do Maranhão; 4°34'43"S, 47°29'48"W; from infected leaves of *E. urophylla*; 20 Feb. 2020; M.A. Ferreira; culture PFC9.

Notes. *C. imperata* is a new species in the *C. candelabrum* species complex (Liu et al., 2020). Morphologically, *C. imperata* is very similar to its closest relatives, from which it can be distinguished based on stipe dimensions and phylogenetic inference. Stipe of *C. imperata* (135–227 × 2–4 µm) is larger than those of *C. piauiensis* (50–110 × 4–6 µm), *C. glaebicola* (50–130 × 5–7 µm), and *C. venezuelana* (35–100 × 4–8 µm) but narrower than those of *C. brassiana* (55–155 × 5–8 µm). Additionally, *C. imperata* lacks lateral stipe extensions, which are present in *C. piauiensis*.

Pathogenicity tests

The conidia suspensions of the representative isolates of *C. paragominensis* and *C. imperata* produced lesion symptoms on leaves (Fig. 5E, F, I, J), but no lesions were observed on the negative control inoculations (Fig. 5G, H, K). The pathogens were reisolated from inoculated leaves but not from the negative controls and identified by the same morphological characteristics as the originally inoculated species, thus, fulfilling the requirements of Koch's postulates.

Discussion

Two new species of *Calonectria* isolated from diseased *Eucalyptus* leaves were identified based on phylogenetic analyses of six gene regions and on morphological comparisons. These two species were named *C. paragominensis* and *C. imperata*.

Calonectria paragominensis is a new species in the *C. spathiphylli* complex. The five species identified and described in *C. spathiphylli* complex are *C. densa*, *C. humicola*, *C. spathiphylli*, *C. pseudospathiphylli*, and *C. paragominensis*, where *C. paragominensis* can be differentiated morphologically with respect to the macroconidia dimensions

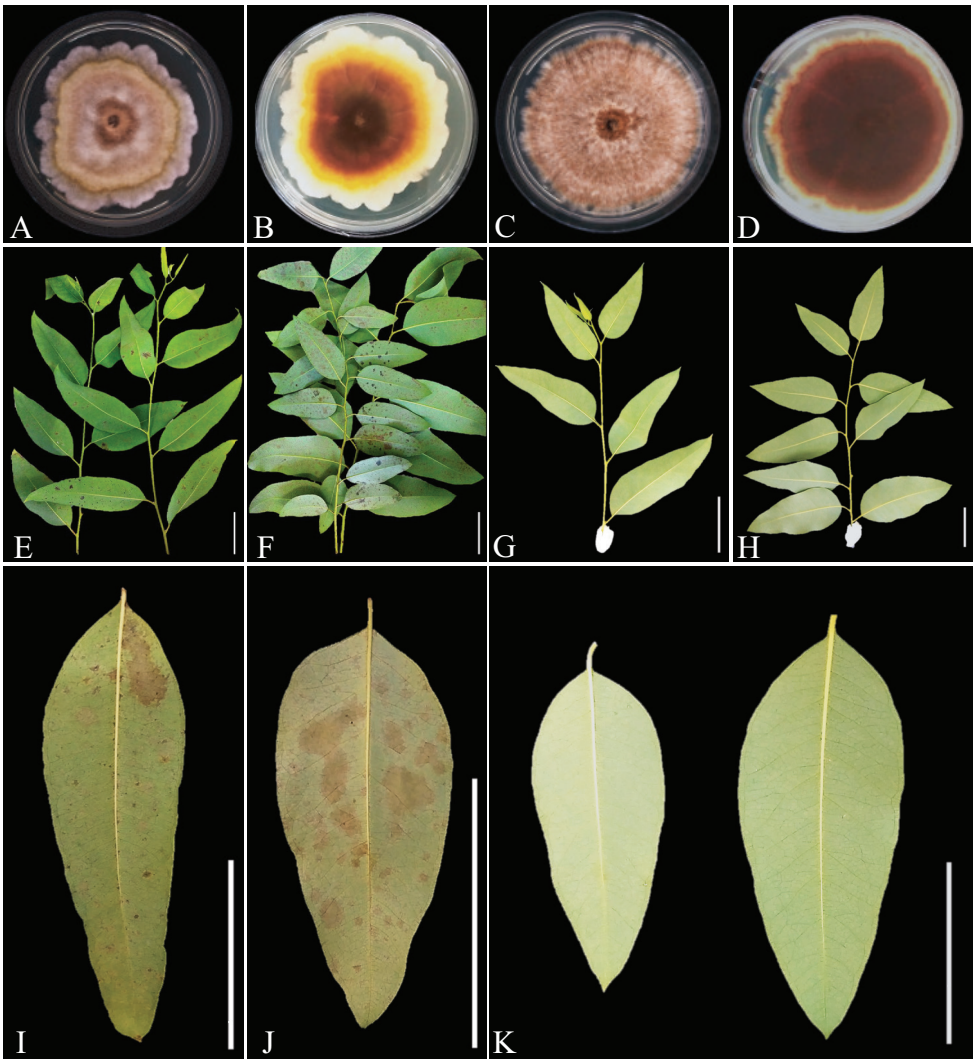

Figure 5. Pathogenicity tests on leaves of *Eucalyptus* genotypes **A, B** surface and reverse of *C. paragominensis* on MEA plates after 14 days grown at 25 °C **C, D** surface and reverse of *C. imperata* on MEA plates after 14 days grown at 25 °C **E, I** lesions on leaves of *E. grandis* × *E. brassiana* induced by *C. paragominensis* 72 h after inoculation **F, J** lesions on leaves of *E. urophylla* induced by *C. imperata* 72 h after inoculation **G, H, K** no disease symptoms on leaves inoculated with sterile water (negative controls). Scale bars: 5 cm (**E–K**).

(El-Gholl et al. 1992; Kang et al. 2001; Crous 2002; Lombard et al. 2010b). These species are characterized by presenting globoid to ovoid to sphaeropedunculate terminal vesicles (Kang et al. 2001; Crous 2002; Lombard et al. 2010b). *Calonectria spathiphylli* is described as heterothallic (El-Gholl et al. 1992), *C. densa* as putatively heterothallic (Li et al. 2020) and *C. pseudospatiphilly* as homothallic (Kang et al. 2001). The *C. humicola* mating type has not been indicated (Lombard et al. 2010b). Here,

C. paragominensis is described as putatively homothallic based on PCR amplification of the mating-type genes. Regarding pathogenicity, *C. paragominensis* is pathogenic to *Eucalyptus* sp., *C. spathiphylli* is pathogenic to *Sapthiphyllum* sp. *Heliconia* sp. *Ludwigia* sp. *Strelitzia* sp. and *Eugenia* sp. (El-Gholl et al. 1992; Poltronieri et al. 2011). *Calonectria densa*, *C. humicola*, and *C. pesudospathiphylli* were isolated from soil, and their pathogenicity has not been indicated (Kang et al. 2001; Lombard et al. 2010b). In addition to *C. paragominensis*, only *C. spathiphylli* has been indicated to be present in Brazil (Reis et al. 2004; Poltronieri et al. 2011).

Calonectria imperata is a new species in the *C. candelabrum* complex. Species in this complex are characterized by presenting ellipsoidal to obpyriform terminal vesicles, in both heterothallic and homothallic species, and occur in Africa, Asia, Europe, North and South America, and Oceania (Liu et al. 2020). Of the 21 species in the *C. candelabrum* complex (Crous et al. 2018, 2019; Liu et al. 2020), 17 have been found in Brazil (Schoch et al. 1999; Crous et al. 2018, 2019; Liu et al. 2020). *Calonectria imperata* is phylogenetically closely related to *C. brassiana*, *C. glaebicola*, *C. piauiensis* and *C. venezuelana*, which can be differentiated with respect to the number of unique alleles and stipe dimensions (Alfenas et al. 2015; Lombard et al. 2016). *Calonectria brassiana*, *C. glaebicola*, and *C. piauiensis* were found in Brazil, isolated from soil samples of *Eucalyptus* plantations, but only *C. glaebicola* has been confirmed to be pathogenic to *Eucalyptus* sp. (Alfenas et al. 2015). *Calonectria venezuelana* was reported in Venezuela, similarly, isolated from soil samples, but its pathogenicity has not been indicated (Lombard et al. 2016). The mating-type for *C. brassiana*, *C. glaebicola*, *C. piauiensis* and *C. venezuelana* has not been determined (Liu et al. 2020).

Pathogenicity tests showed that *C. paragominensis* and *C. imperata* are pathogenic to *E. grandis* × *E. brassiana* hybrid genotype and *E. urophylla* genotype, respectively. Although the death of *Eucalyptus* trees due to CLB is not common, it affects *Eucalyptus* plants most severely from six months to 2–3 years after planting (Graça et al. 2009). Although the economic loss due to defoliation caused by CLB has not been quantified directly, according to artificial pruning studies conducted by Pulrolnik et al. (2005) and Pires (2000), when the loss of branches is equal to or greater than 75% of *E. grandis* seedlings of one year of age, the volumetric productivity has decreased by 45% by the time they reach seven years old. Therefore, it has been inferred that in susceptible clones, the pathogen can cause economic losses, since under favorable conditions, infection by *Calonectria* can result in severe defoliation (Soares et al. 2018). Additionally, Miranda et al. (2021) indicated a potential growth loss of 19.8 to 39.6% due to CLB, and by using the estimates of growth reduction from Pires (2000) as a baseline, concluded that a reduction in the volumetric increment to the order of 39.6% may result in an economic loss of R$ 4291.00 per ha, considering a price of *Eucalyptus* wood as R$ 38.70 per m^3 (IEA 2020) and a production of 280 $m^3 \cdot ha^{-1}$ in the first 7-year rotation. Therefore, accurate diagnoses of plant diseases and identification of their casual agents are fundamental in promoting the development of effective disease management strategies (Wingfield et al. 2015; Liu and Chen 2017).

In this study, we described two new *Calonectria* species, both isolated from diseased *Eucalyptus* leaves from commercial plantations localized in a tropical zone. These results suggest that there are still more *Calonectria* species to be discovered in Brazil, and that they require careful monitoring, since this knowledge could facilitate the development of resistant *Eucalyptus* clones.

Acknowledgements

We thank Heitor S. Dallapiccola and Francisco J. A. Gomes for their help during sample collection. We thank the laboratories of Molecular Biology, Plant Virology, and Nematology at Universidade Federal de Lavras (UFLA) for the facilities granted during the completion of this study. The first author thanks the "Coordenação de Aperfeiçoamento de Pessoal de Nível Superior (CAPES)" for the doctorate scholarship assigned through Brazil's PAEC OAS-GCUB Scholarships Program.

References

Alfenas AC, Zauza EAV, Mafia RG, de Assis TF (2009) Clonagem e doenças do eucalipto. 2nd ed., Editora UFV, Viçosa, MG, Brazil, 500 pp.

Alfenas RF, Pereira OL, Freitas RG, Freitas CS, Dita MA, Alfenas AC (2013) Mass spore production and inoculation of *Calonectria pteridis* on *Eucalyptus* spp. under different environmental conditions. Tropical Plant Pathology 38(5): 406–413. https://doi.org/10.1590/S1982-56762013000500005

Alfenas RF, Lombard L, Pereira OL, Alfenas AC, Crous PW (2015) Diversity and potential impact of *Calonectria* species in *Eucalyptus* plantations in Brazil. Studies in Mycology 80(1): 89–130. https://doi.org/10.1016/j.simyco.2014.11.002

Bruen TC, Philippe H, Bryant D (2006) A simple and robust statistical test for detecting the presence of recombination. Genetics 172(4): 2665–2681. https://doi.org/10.1534/genetics.105.048975

Carbone I, Kohn LM (1999) A method for designing primer sets for speciation studies in filamentous ascomycetes. Mycologia 91(3): 553–556. https://doi.org/10.1080/00275514.1999.12061051

Castellani A (1939) Viability of some pathogenic fungi in distilled water. The Journal of Tropical Medicine and Hygiene 42: 225–226.

Chernomor O, Von Haeseler A, Minh BQ (2016) Terrace aware data structure for phylogenomic inference from supermatrices. Systematic Biology 65(6): 997–1008. https://doi.org/10.1093/sysbio/syw037

Crous PW (2002) Taxonomy and pathology of *Cylindrocladium* (*Calonectria*) and allied genera. APS Press, St. Paul, Minnesota, USA, 278 pp.

Crous PW, Groenewald JZ, Risède JM, Simoneau P, Hywel-Jones NL (2004) *Calonectria* species and their *Cylindrocladium* anamorphs: Species with sphaeropedunculate vesicles. Studies in Mycology 50: 415–430. https://doi.org/10.3114/sim.55.1.213

Crous PW, Luangsa-ard JJ, Wingfield MJ, Carnegie AJ, Hernández-Restrepo M, Lombard L, Roux J, Barreto RW, Baseia IG, Cano-Lira JF, Martín MP, Morozova OV, Stchigel AM, Summerell BA, Brandrud TE, Dima B, García D, Giraldo A, Guarro J, Gusmão LFP, Khamsuntorn P, Noordeloos ME, Nuankaew S, Pinruan U, Rodríguez-Andrade E, Souza-Motta CM, Thangavel R, van Iperen AL, Abreu VP, Accioly T, Alves JL, Andrade JP, Bahram M, Baral H-O, Barbier E, Barnes CW, Bendiksen E, Bernard E, Bezerra JDP, Bezerra JL, Bizio E, Blair JE, Bulyonkova TM, Cabral TS, Caiafa MV, Cantillo T, Colmán AA, Conceição LB, Cruz S, Cunha AOB, Darveaux BA, da Silva AL, da Silva GA, da Silva GM, da Silva RMF, de Oliveira RJV, Oliveira RL, De Souza JT, Dueñas M, Evans HC, Epifani F, Felipe MTC, Fernández-López J, Ferreira BW, Figueiredo CN, Filippova NV, Flores JA, Gené J, Ghorbani G, Gibertoni TB, Glushakova AM, Healy R, Huhndorf SM, Iturrieta-González I, Javan-Nikkhah M, Juciano RF, Jurjević Ž, Kachalkin AV, Keochanpheng K, Krisai-Greilhuber I, Li Y-C, Lima AA, Machado AR, Madrid H, Magalhães OMC, Marbach PAS, Melanda GCS, Miller AN, Mongkolsamrit S, Nascimento RP, Oliveira TGL, Ordoñez ME, Orzes R, Palma MA, Pearce CJ, Pereira OL, Perrone G, Peterson SW, Pham THG, Piontelli E, Pordel A, Quijada L, Raja HA, Rosas de Paz E, Ryvarden L, Saitta A, Salcedo SS, Sandoval-Denis M, Santos TAB, Seifert KA, Silva BDB, Smith ME, Soares AM, Sommai S, Sousa JO, Suetrong S, Susca A, Tedersoo L, Telleria MT, Thanakitpipattana D, Valenzuela-Lopez N, Visagie CM, Zapata M, Groenewald JZ (2018) Fungal Planet description sheets: 785–867. Persoonia: Molecular Phylogeny and Evolution of Fungi 41(1): 238–417. https://doi.org/10.3767/persoonia.2018.41.12

Crous PW, Carnegie AJ, Wingfield MJ, Sharma R, Mughini G, Noordeloos ME, Santini A, Shouche YS, Bezerra JDP, Dima B, Guarnaccia V, Imrefi I, Jurjević Ž, Knapp DG, Kovács GM, Magistà D, Perrone G, Rämä T, Rebriev YA, Shivas RG, Singh SM, Souza-Motta CM, Thangavel R, Adhapure NN, Alexandrova AV, Alfenas AC, Alfenas RF, Alvarado P, Alves AL, Andrade DA, Andrade JP, Barbosa RN, Barili A, Barnes CW, Baseia IG, Bellanger J-M, Berlanas C, Bessette AE, Bessette AR, Biketova AYu, Bomfim FS, Brandrud TE, Bransgrove K, Brito ACQ, Cano-Lira JF, Cantillo T, Cavalcanti AD, Cheewangkoon R, Chikowski RS, Conforto C, Cordeiro TRL, Craine JD, Cruz R, Damm U, de Oliveira RJV, de Souza JT, de Souza HG, Dearnaley JDW, Dimitrov RA, Dovana F, Erhard A, Esteve-Raventós F, Félix CR, Ferisin G, Fernandes RA, Ferreira RJ, Ferro LO, Figueiredo CN, Frank JL, Freire KTLS, García D, Gené J, Gęsiorska A, Gibertoni TB, Gondra RAG, Gouliamova DE, Gramaje D, Guard F, Gusmão LFP, Haitook S, Hirooka Y, Houbraken J, Hubka V, Inamdar A, Iturriaga T, Iturrieta-González I, Jadan M, Jiang N, Justo A, Kachalkin AV, Kapitonov VI, Karadelev M, Karakehian J, Kasuya T, Kautmanová I, Kruse J, Kušan I, Kuznetsova TA, Landell MF, Larsson K-H, Lee HB, Lima DX, Lira CRS, Machado AR, Madrid H, Magalhães OMC, Majerova H, Malysheva EF, Mapperson RR, Marbach PAS, Martín MP, Martín-Sanz A, Matočec N, McTaggart AR, Mello JF, Melo RFR, Mešič A, Michereff SJ, Miller AN, Minoshima A, Molinero-Ruiz L, Morozova OV, Mosoh D, Nabe M, Naik R, Nara K, Nascimento SS, Neves RP, Olariaga I, Oliveira RL, Oliveira TGL, Ono T, Ordoñez ME, de M Ottoni A, Paiva LM, Pancorbo F, Pant B, Pawłowska J, Peterson SW, Raudabaugh DB, Rodríguez-Andrade E, Rubio E, Rusevska K, Santiago ALCMA, Santos ACS, Santos C, Sazanova NA, Shah S, Sharma J, Silva BDB, Siquier JL, Sonawane MS, Stchigel AM, Svetasheva T, Tamakeaw N, Telleria MT, Tiago PV, Tian

CM, Tkalčec Z, Tomashevskaya MA, Truong HH, Vecherskii MV, Visagie CM, Vizzini A, Yilmaz N, Zmitrovich IV, Zvyagina EA, Boekhout T, Kehlet T, Læssøe T, Groenewald JZ (2019) Fungal Planet description sheets: 868–950. Persoonia: Molecular Phylogeny and Evolution of Fungi 42: 291–473. https://doi.org/10.3767/persoonia.2019.42.11

Crous PW, Hernández-Restrepo M, Schumacher RK, Cowan DA, Maggs-Kölling G, Marais E, Wingfield MJ, Yilmaz N, Adan OCG, Akulov A, Duarte E, Berraf-Tebbal A, Bulgakov TS, Carnegie AJ, de Beer ZW, Decock C, Dijksterhuis J, Duong TA, Eichmeier A, Hien LT, Houbraken JAMP, Khanh TN, Liem NV, Lombard L, Lutzoni FM, Miadlikowska JM, Nel WJ, Pascoe IG, Roets F, Roux J, Samson RA, Shen M, Spetik M, Thangavel R, Thanh HM, Thao LD, van Nieuwenhuijzen EJ, Zhang JQ, Zhang Y, Zhao LL, Groenewald JZ (2021a) New and Interesting Fungi 4. Fungal Systematics and Evolution 7(1): 255–343. https://doi.org/10.3114/fuse.2021.07.13

Crous PW, Cowan DA, Maggs-Kölling G, Yilmaz N, Thangavel R, Wingfield MJ, Noordeloos ME, Dima B, Brandrud TE, Jansen GM, Morozova OV, Vila J, Shivas RG, Tan YP, Bishop-Hurley S, Lacey E, Marney TS, Larsson E, Le Floch G, Lombard L, Nodet P, Hubka V, Alvarado P, Berraf-Tebbal A, Reyes JD, Delgado G, Eichmeier A, Jordal JB, Kachalkin AV, Kubátová A, Maciá-Vicente JG, Malysheva EF, Papp V, Rajeshkumar KC, Sharma A, Spetik M, Szabóová D, Tomashevskaya MA, Abad JA, Abad ZG, Alexandrova AV, Anand G, Arenas F, Ashtekar N, Balashov S, Bañares Á, Baroncelli R, Bera I, Biketova AYu, Blomquist CL, Boekhout T, Boertmann D, Bulyonkova TM, Burgess TI, Carnegie AJ, Cobo-Diaz JF, Corriol G, Cunnington JH, da Cruz MO, Damm U, Davoodian N, de A Santiago ALCM, Dearnaley J, de Freitas LWS, Dhileepan K, Dimitrov R, Di Piazza S, Fatima S, Fuljer F, Galera H, Ghosh A, Giraldo A, Glushakova AM, Gorczak M, Gouliamova DE, Gramaje D, Groenewald M, Gunsch CK, Gutiérrez A, Holdom D, Houbraken J, Ismailov AB, Istel Ł, Iturriaga T, Jeppson M, Jurjević Ž, Kalinina LB, Kapitonov VI, Kautmanova I, Khalid AN, Kiran M, Kiss L, Kovács Á, Kurose D, Kusan I, Lad S, Læssøe T, Lee HB, Luangsa-ard JJ, Lynch M, Mahamedi AE, Malysheva VF, Mateos A, Matočec N, Mešić A, Miller AN, Mongkolsamrit S, Moreno G, Morte A, Mostowfizadeh-Ghalamfarsa R, Naseer A, Navarro-Ródenas A, Nguyen TTT, Noisripoom W, Ntandu JE, Nuytinck J, Ostrý V, Pankratov TA, Pawłowska J, Pecenka J, Pham THG, Polhorský A, Posta A, Raudabaugh DB, Reschke K, Rodríguez A, Romero M, Rooney-Latham S, Roux J, Sandoval-Denis M, Smith MTh, Steinrucken TV, Svetasheva TY, Tkalčec Z, van der Linde EJ, vd Vegte M, Vauras J, Verbeken A, Visagie CM, Vitelli JS, Volobuev SV, Weill A, Wrzosek M, Zmitrovich IV, Zvyagina EA, Groenewald JZ (2021b) Fungal planet description sheets: 1182–1283. Persoonia: Molecular Phylogeny and Evolution of Fungi 46: 313–528. https://doi.org/10.3767/persoonia.2021.46.11

Cunningham CW (1997) Can three incongruence tests predict when data should be combined? Molecular Biology and Evolution 14(7): 733–740. https://doi.org/10.1093/oxfordjournals.molbev.a025813

Dress AW, Huson DH (2004) Constructing splits graphs. IEEE/ACM Transactions on Computational Biology and Bioinformatics 1(3): 109–115. https://doi.org/10.1109/TCBB.2004.27

El-Gholl NE, Uchida JY, Alfenas AC, Schubert TS, Alfieri SA (1992) Induction and description of perithecia of *Calonectria spathiphylli* sp. nov. Mycotaxon 45: 285–300.

Farris JS, Kallersjo M, Kluge AG, Bult C (1995) Testing significance of incongruence. Cladistics 10(3): 315–319. https://doi.org/10.1111/j.1096-0031.1994.tb00181.x

Graça RN, Alfenas AC, Maffia LA, Titon M, Alfenas RF, Lau D, Rocabado JMA (2009) Factors influencing infection of eucalypts by *Cylindrocladium pteridis*. Plant Pathology 58(5): 971–981. https://doi.org/10.1111/j.1365-3059.2009.02094.x

Guerber JC, Correll JC (2001) Characterization of *Glomerella acutata*, the teleomorph of *Colletotrichum acutatum*. Mycologia 93(1): 216–229. https://doi.org/10.1080/00275514.2001.12063151

Hepperle D (2004) SeqAssem. Win32–Version. A sequence analysis tool contig assembler and trace data visualization tool for molecular sequences. Win32-Version. [Distributed by the author via:] http://www.sequentix.de

Hoang DT, Chernomor O, Von Haeseler A, Minh BQ, Vinh LS (2018) UFBoot2: Improving the ultrafast bootstrap approximation. Molecular Biology and Evolution 35(2): 518–522. https://doi.org/10.1093/molbev/msx281

Huson DH, Bryant D (2006) Application of phylogenetic networks in evolutionary studies. Molecular Biology and Evolution 23(2): 254–267. https://doi.org/10.1093/molbev/msj030

IBÁ (2021) IBÁ–Indústria Brasileira de Árvores. Relatório 2020. https://iba.org/datafiles/publicacoes/relatorios/relatorio-iba-2020.pdf

IEA (2020) IEA–Instituto de Economia Agrícola. https://www.noticiasagricolas.com.br/cotacoes/silvicultura/preco-eucalipto

Kang JC, Crous PW, Schoch CL (2001) Species concepts in the *Cylindrocladium floridanum* and *Cy. spathiphylli* complexes (Hypocreaceae) based on multi-allelic sequence data, sexual compatibility and morphology. Systematic and Applied Microbiology 24(2): 206–217. https://doi.org/10.1078/0723-2020-00026

Katoh K, Rozewicki J, Yamada KD (2019) MAFFT online service: Multiple sequence alignment, interactive sequence choice and visualization. Briefings in Bioinformatics 20(4): 1160–1166. https://doi.org/10.1093/bib/bbx108

Kumar S, Stecher G, Tamura K (2016) MEGA7: Molecular evolutionary genetics analysis version 7.0 for bigger datasets. Molecular Biology and Evolution 33(7): 1870–1874. https://doi.org/10.1093/molbev/msw054

Lee SB, Taylor JW (1990) Isolation of DNA from fungal mycelia and single spores. In: Innis MA, Gelfand DV, Sninsky JJ, White TJ (Eds) PCR protocols: a guide to methods and applications. Academic Press, New York, 282–287. https://doi.org/10.1016/B978-0-12-372180-8.50038-X

Li JQ, Wingfield BD, Wingfield MJ, Barnes I, Fourie A, Crous PW, Chen SF (2020) Mating genes in *Calonectria* and evidence for a heterothallic ancestral state. Persoonia. Molecular Phylogeny and Evolution of Fungi 45(1): 163–176. https://doi.org/10.3767/persoonia.2020.45.06

Li JQ, Barnes I, Liu FF, Wingfield MJ, Chen SF (2021) Global genetic diversity and mating type distribution of *Calonectria pauciramosa*: An important wide host-range plant pathogen. Plant Disease 105(6): 1648–1656. https://doi.org/10.1094/PDIS-05-20-1050-RE

Liu Q, Chen S (2017) Two novel species of *Calonectria* isolated from soil in a natural forest in China. MycoKeys 26: 25–60. https://doi.org/10.3897/mycokeys.26.14688

Liu YJ, Whelen S, Hall BD (1999) Phylogenetic relationships among ascomycetes: Evidence from an RNA polymerse II subunit. Molecular Biology and Evolution 16(12): 1799–1808. https://doi.org/10.1093/oxfordjournals.molbev.a026092

Liu QL, Li JQ, Wingfield MJ, Duong TA, Wingfield BD, Crous PW, Chen SF (2020) Reconsideration of species boundaries and proposed DNA barcodes for *Calonectria*. Studies in Mycology 97: e100106. [71 pp.] https://doi.org/10.1016/j.simyco.2020.08.001

Liu L, Wu W, Chen S (2021) Species diversity and distribution characteristics of *Calonectria* in five soil layers in a eucalyptus plantation. Journal of Fungi (Basel, Switzerland) 7(10): e857. https://doi.org/10.3390/jof7100857

Lombard L, Crous PW, Wingfield BD, Wingfield MJ (2010a) Multigene phylogeny and mating tests reveal three cryptic species related to *Calonectria pauciramosa*. Studies in Mycology 66: 15–30. https://doi.org/10.3114/sim.2010.66.02

Lombard L, Crous PW, Wingfield BD, Wingfield MJ (2010b) Phylogeny and systematics of the genus *Calonectria*. Studies in Mycology 66: 31–69. https://doi.org/10.3114/sim.2010.66.03

Lombard L, Crous PW, Wingfield BD, Wingfield MJ (2010c) Species concepts in *Calonectria* (*Cylindrocladium*). Studies in Mycology 66: 1–13. https://doi.org/10.3114/sim.2010.66.01

Lombard L, Wingfield MJ, Alfenas AC, Crous PW (2016) The forgotten *Calonectria* collection: Pouring old wine into new bags. Studies in Mycology 85(1): 159–198. https://doi.org/10.1016/j.simyco.2016.11.004

Miranda IDS, Auer CG, dos Santos ÁF, Ferreira MA, Tambarussi EV, da Silva RAF, Rezende EH (2021) Occurrence of *Calonectria* leaf blight in *Eucalyptus benthamii* progenies and potential for disease resistance. Tropical Plant Pathology 46(3): 254–264. https://doi.org/10.1007/s40858-021-00426-4

Mohali SR, Stewart JE (2021) *Calonectria vigiensis* sp. nov. (Hypocreales, Nectriaceae) associated with dieback and sudden-death symptoms of *Theobroma cacao* from Mérida state, Venezuela. Botany 99(11): 683–693. https://doi.org/10.1139/cjb-2021-0050

Nguyen LT, Schmidt HA, Von Haeseler A, Minh BQ (2015) IQ-TREE: A fast and effective stochastic algorithm for estimating maximum-likelihood phylogenies. Molecular Biology and Evolution 32(1): 268–274. https://doi.org/10.1093/molbev/msu300

Nylander JAA (2004) MrModeltest v2. Program distributed by the author. Evolutionary Biology Centre, Uppsala University.

O'Donnell K, Cigelnik E (1997) Two divergent intragenomic rDNA ITS2 types within a monophyletic lineage of the fungus *Fusarium* are nonorthologous. Molecular Phylogenetics and Evolution 7(1): 103–116. https://doi.org/10.1006/mpev.1996.0376

O'Donnell K, Kistler HC, Cigelnik E, Ploetz RC (1998) Multiple evolutionary origins of the fungus causing Panama disease of banana: Concordant evidence from nuclear and mitochondrial gene genealogies. Proceedings of the National Academy of Sciences of the United States of America 95(5): 2044–2049. https://doi.org/10.1073/pnas.95.5.2044

Pham NQ, Barnes I, Chen S, Liu F, Dang QN, Pham TQ, Lombard L, Crous PW, Wingfield MJ (2019) Ten new species of *Calonectria* from Indonesia and Vietnam. Mycologia 111(1): 78–102. https://doi.org/10.1080/00275514.2018.1522179

Pham NQ, Marincowitz S, Chen S, Yaparudin Y, Wingfield MJ (2022) *Calonectria* species, including four novel taxa, associated with *Eucalyptus* in Malaysia. Mycological Progress 21(1): 181–197. https://doi.org/10.1007/s11557-021-01768-8

Pires BM (2000) Efeito da desrama artificial no crescimento e qualidade da madeira de *Eucalyptus grandis* para serraria. MSc Dissertation, Universidade Federal de Viçosa, Viçosa, Brasil. https://locus.ufv.br//handle/123456789/11170

Poltronieri LS, Alfenas RF, Verzignassi JR, Alfenas AC, Benchimol RL, Poltronieri TPDS (2011) Leaf blight and defoliation of *Eugenia* spp. caused by *Cylindrocladium candelabrum* and *C. spathiphylli* in Brazil. Summa Phytopathologica 37(2): 147–149. https://doi.org/10.1590/S0100-54052011000200011

Posada D, Crandall KA (1998) Modeltest: Testing the model of DNA substitution. Bioinformatics (Oxford, England) 14(9): 817–818. https://doi.org/10.1093/bioinformatics/14.9.817

Pulrolnik K, Reis GGD, Reis MDGF, Monte MA, Fontan IDCI (2005) Crescimento de plantas de clones de *Eucalyptus grandis* [Hill ex Maiden] submetidas a diferentes tratamentos de desrama artificial, na região do cerrado. Revista Árvore 29(4): 495–505. https://doi.org/10.1590/S0100-67622005000400001

Quaedvlieg W, Kema GHJ, Groenewald JZ, Verkley GJM, Seifbarghi S, Razavi M, Gohari AM, Mehrabi R, Crous PW (2011) *Zymoseptoria* gen. nov.: A new genus to accommodate *Septoria*-like species occurring on graminicolous hosts. Persoonia. Molecular Phylogeny and Evolution of Fungi 26(1): 57–69. https://doi.org/10.3767/003158511X571841

Rambaut A (2009) FigTree, a graphical viewer of phylogenetic trees. http://tree.bio.ed.ac.uk/software/figtree/

Rambaut A, Drummond AJ (2007) Tracer v1.5. http://tree.bio.ed.ac.uk/software/tracer/

Reeb V, Lutzoni F, Roux C (2004) Contribution of RPB2 to multilocus phylogenetic studies of the euascomycetes (Pezizomycotina, Fungi) with special emphasis on the lichen-forming Acarosporaceae and evolution of polyspory. Molecular Phylogenetics and Evolution 32(3): 1036–1060. https://doi.org/10.1016/j.ympev.2004.04.012

Reis A, Mafia RG, Silva PP, Lopes CA, Alfenas AC (2004) *Cylindrocladium spathiphylli*, causal agent of *Spathiphyllum* root and collar rot in the Federal District-Brazil. Fitopatologia Brasileira 29(1): 102–102. https://doi.org/10.1590/S0100-41582004000100017

Ronquist F, Teslenko M, Van Der Mark P, Ayres DL, Darling A, Höhna S, Larget B, Liu L, Suchard MA, Huelsenbeck JP (2012) MrBayes 3.2: Efficient Bayesian phylogenetic inference and model choice across a large model space. Systematic Biology 61(3): 539–542. https://doi.org/10.1093/sysbio/sys029

Ronquist F, Huelsenbeck J, Teslenko M, Nylander JAA (2019) MrBayes version 3.2 manual: tutorials and model summaries. https://nbisweden.github.io/MrBayes/manual.html

Schoch CL, Crous PW, Wingfield BD, Wingfield MJ (1999) The *Cylindrocladium candelabrum* species complex includes four distinct mating populations. Mycologia 91(2): 286–298. https://doi.org/10.1080/00275514.1999.12061019

Soares TP, Pozza EA, Pozza AA, Mafia RG, Ferreira MA (2018) Calcium and potassium imbalance favours leaf blight and defoliation caused by *Calonectria pteridis* in *Eucalyptus* plants. Forests 9(12): e782. https://doi.org/10.3390/f9120782

Sullivan J (1996) Combining data with different distributions of among-site rate variation. Systematic Biology 45(3): 375–380. https://doi.org/10.1093/sysbio/45.3.375

Swofford DL (2003) PAUP*. Phylogenetic analysis using parsimony (*and other methods). V. 4.0b10. Sinauer Associates, Sunderland, Massachusetts, USA.

Taylor JW, Jacobson DJ, Kroken S, Kasuga T, Geiser DM, Hibbett DS, Fisher MC (2000) Phylogenetic species recognition and species concepts in fungi. Fungal Genetics and Biology 31(1): 21–32. https://doi.org/10.1006/fgbi.2000.1228

Trifinopoulos J, Nguyen LT, von Haeseler A, Minh BQ (2016) W-IQ-TREE: A fast online phylogenetic tool for maximum likelihood analysis. Nucleic Acids Research 44(W1): W232–W235. https://doi.org/10.1093/nar/gkw256

Vitale A, Crous PW, Lombard L, Polizzi G (2013) *Calonectria* diseases on ornamental plants in Europe and the Mediterranean basin: An overview. Journal of Plant Pathology 95(3): 463–476. https://doi.org/10.4454/JPP.V95I3.007

Wang QC, Liu QL, Chen SF (2019) Novel species of *Calonectria* isolated from soil near *Eucalyptus* plantations in southern China. Mycologia 111(6): 1028–1040. https://doi.org/10.1080/00275514.2019.1666597

Wingfield MJ, Brockerhoff EG, Wingfield BD, Slippers B (2015) Planted forest health: The need for a global strategy. Science 349(6250): 832–836. https://doi.org/10.1126/science.aac6674

Supplementary material 1

Figures S1–S6

Authors: Enrique I. Sanchez-Gonzalez, Thaissa de Paula Farias Soares, Talyta Galafassi Zarpelon, Edival Angelo Valverde Zauza, Reginaldo Gonçalves Mafia, Maria Alves Ferreira

Data type: Phylogenetic trees (pdf file)

Explanation note: **Figure S1.** Phylogenetic tree based on maximum likelihood analysis of *act* gene region. Bootstrap support values ≥ 80% for maximum parsimony (MP), Ultrafast bootstrap support values ≥ 95% for maximum likelihood (ML), and posterior probability (PP) values ≥ 0.95 from BI analyses are presented at the nodes (MP/ML/PP). Bootstrap values below 80% (MP), 95% (ML) and posterior probabilities below 0.80 are marked with "-". Ex-type isolates are indicated by "▲", isolates highlighted in bold were sequenced in this study, and novel species are in blue and orange. *C. gracilipes* was used as outgroup. The scale bar indicates the number of nucleotide substitutions per site. **Figure S2.** Phylogenetic tree based on maximum likelihood analysis of *cmdA* gene region. Bootstrap support values ≥ 80% for maximum parsimony (MP), Ultrafast bootstrap support values ≥ 95% for maximum likelihood (ML), and posterior probability (PP) values ≥ 0.95 from BI analyses are presented at the nodes (MP/ML/PP). Bootstrap values below 80% (MP), 95% (ML) and posterior probabilities below 0.80 are marked with "-". Ex-type isolates are indicated by "▲", isolates highlighted in bold were sequenced

in this study, and novel species are in blue and orange. *C. gracilipes* was used as outgroup. The scale bar indicates the number of nucleotide substitutions per site. **Figure S3.** Phylogenetic tree based on maximum likelihood analysis of *his3* gene region. Bootstrap support values ≥ 80% for maximum parsimony (MP), Ultrafast bootstrap support values ≥ 95% for maximum likelihood (ML), and posterior probability (PP) values ≥ 0.95 from BI analyses are presented at the nodes (MP/ML/PP). Bootstrap values below 80% (MP), 95% (ML) and posterior probabilities below 0.80 are marked with "-". Ex-type isolates are indicated by "▲", isolates highlighted in bold were sequenced in this study, and novel species are in blue and orange. *C. gracilipes* was used as outgroup. The scale bar indicates the number of nucleotide substitutions per site. **Figure S4.** Phylogenetic tree based on maximum likelihood analysis of *rpb2* gene region. Bootstrap support values ≥ 80% for maximum parsimony (MP), Ultrafast bootstrap support values ≥ 95% for maximum likelihood (ML), and posterior probability (PP) values ≥ 0.95 from BI analyses are presented at the nodes (MP/ML/PP). Bootstrap values below 80% (MP), 95% (ML) and posterior probabilities below 0.80 are marked with "-". Ex-type isolates are indicated by "▲", isolates highlighted in bold were sequenced in this study, and novel species are in blue and orange. *C. gracilipes* was used as outgroup. The scale bar indicates the number of nucleotide substitutions per site. **Figure S5.** Phylogenetic tree based on maximum likelihood analysis of *tef1* gene region. Bootstrap support values ≥ 80% for maximum parsimony (MP), Ultrafast bootstrap support values ≥ 95% for maximum likelihood (ML), and posterior probability (PP) values ≥ 0.95 from BI analyses are presented at the nodes (MP/ML/PP). Bootstrap values below 80% (MP), 95% (ML) and posterior probabilities below 0.80 are marked with "-". Ex-type isolates are indicated by "▲", isolates highlighted in bold were sequenced in this study, and novel species are in blue and orange. *C. gracilipes* was used as outgroup. The scale bar indicates the number of nucleotide substitutions per site. **Figure S6.** Phylogenetic tree based on maximum likelihood analysis of *tub2* gene region. Bootstrap support values ≥ 80% for maximum parsimony (MP), Ultrafast bootstrap support values ≥ 95% for maximum likelihood (ML), and posterior probability (PP) values ≥ 0.95 from BI analyses are presented at the nodes (MP/ML/PP). Bootstrap values below 80% (MP), 95% (ML) and posterior probabilities below 0.80 are marked with "-". Ex-type isolates are indicated by "▲", isolates highlighted in bold were sequenced in this study, and novel species are in blue and orange. *C. gracilipes* was used as outgroup. The scale bar indicates the number of nucleotide substitutions per site.

Link: https://doi.org/10.3897/mycokeys.91.84896.suppl1